The design and evaluation of components for low heat loss diesel engines

Alexander, W. D.

Award date:
1989

Awarding institution:
University of Bath

THE DESIGN AND EVALUATION OF COMPONENTS FOR LOW HEAT LOSS DIESEL ENGINES

Submitted by : -
W.D. Alexander
for the degree of PhD
September 1989

ProQuest LLC
789 East Eisenhower Parkway
P.O. Box 1346
Ann Arbor, MI 48106-1346

THESIS INDEX

ACKNOWLEDGEMENTS

This thesis is a summary of work which has taken place over a number of years and, as such, has involved the collaboration of numerous persons.

As head of the projects, which this thesis covers, Professor F.J. Wallace deserves special mention, as without his help, and endeavours, the research would not have taken place.

Many thanks to Mr. D. Rushton, the long sufferring technician who has ably assisted me with all aspects of the test rig builds.

Thanks also to my fellow researchers, Dr. D. Howard, with whom I have had many discussions into the "wee" small hours, and who had to share an office with me, and to Mr. I. Marsh and Dr. J. Hall, who have provided useful comments in general.

On the theoretical side I would like to thank Dr. M. Wilson, Mr. N. Cambell, Dr. C. White, research officers and colleagues within the Department of Mechanical Engineering.

The contribution from the Materials Science Department has been critical over the last five years of the project, and special thanks go to Mr. H. Reiter who has supervised the work over there. Thanks also to N. Gathercole, M. Hobbs, and R. Russel-Floyd.

I also wish to thank those members of the technical staff who have helped with the machining of numerous items, over the years. Mr. A. Elley and Mr. K. Britton from the Wolfson Laboratory. Mr. K. Pepler, Mr. R. Weston and Mr. H. Simmons, from the main workshop. Mr. R. Pepler, from the Production Laboratory, for help with NC machining and surface quality determination. Thanks also to those not mentioned who have helped out when it has been necessary to "beg, borrow, or temporarily steal" equipment.

Thanks to Mr. P. Prest and Mr. D. Barker for their help with both the slow and high speed data acquisition systems.

Mrs. J. Thomas and Mrs. H. Ford deserve thanks for their assistance when it was necessary to use their machines in the

School Office.

Grateful thanks to those at Pilkingtons R&D and those at the Ford Motor Co.(U.K.) who have ensured that the DTI/Industry sponsored project was a successful collaborative venture.

At Pilkingtons :-

Dr. B. Proctor, Dr. B. Tilley, Dr. J. Bradshaw and Dr. A. Gerrard. With special thanks to Dr. B. Proctor, without whose efforts, the project would not have taken place.

At the Ford Motor Co. (U.K.) :-

Dr. G. Cooke and Dr. W. Shepard

Last, but by no means least, thanks to all of the students who I have supervised, or collaborated with, over the years. Hopefully, the relationships have been mutually beneficial, and that we have all learned something about engineering and the communication of ideas.

Thesis Synopsis

This thesis covers work carried at Bath University on the Low Heat Loss Diesel Engine, particularily with respect to ceramic piston crown design and to the development of a novel method of thermal shock testing of ceramic materials, in relation to Diesel engine applications. This test facility was designed, built and operated successfully, its purpose being to test a variety of monolithic ceramic and some ceramic coated specimens under thermal loadings similar to those which might pertain in the combustion chamber of a diesel engine. Other test rigs completed and described in this thesis include the modified Petter single cylinder I.D.I. Diesel engine and an engine simulation rig, as well as special instrumentation designed for these rigs.

Although the final outcome of the work was unsatisfactory in the sense that the glass ceramic piston crowns displayed a high failure rate, much fundamental information of permanent value was gathered.

CHAPTER 1 - INTRODUCTION

Work on low heat rejection diesel engines has been carried out at the University of Bath over the past nine years. Initial research concentrated on the use of air gaps for insulation of piston crowns and details of this work may be found in Kao's MSc and PhD theses (**Refs. 1** and **2**) and in Cole's PhD thesis (**Ref. 3**). Further work involved the use of plasma spray coatings particularily with respect to the residual stresses present in the coatings as a result of the deposition process. Detailed accounts of the experimental and theoretical work is to be found in Manton's PhD thesis (**Ref. 4**) and Hobb's PhD thesis (**Ref. 5**) The most recent work has been concerned with the use of monolithic ceramic inserts for the purposes of insulating the piston crown, and on the testing of such ceramic materials for their resistance to thermal shock. The writer has been involved in all aspects of the research work from the outset, but for the sake of brevity this thesis will only consider this latter phase of work on low heat rejection engines. It should be mentioned that this work has been carried out, in collaboration with Pilkington Brothers p.l.c., and Ford (U.K.), under the heading "CERAMICS IN ENGINES".

1.1 General

Heat engines may be loosely defined as those machines which involve a flow of thermal energy and some form of other energy flow. More specifically for the case of heat engines used for prime mover applications, the conversion of a flow of thermal energy into some form of motive power (see **Figure 1.1**). Thus it is readily accepted that spark ignition, Diesel, gas turbine, and Stirling engines are covered by this definition. **Figure 1.2** shows the common forms of heat engine already used, or proposed, for prime mover applications. However, this general description may be extended to cover other machines which convert other forms of energy into translational or rotational power, such as fuel cells. The

theoretical limitations of each type of heat engine may be appreciated when the Carnot efficiency for each type of machine is considered. The Carnot efficiency is the maximum possible thermal efficiency which a heat engine may attain. Theoretically, this efficiency may be described by an equation which relates the maximum and minimum cycle temperatures to the
Carnot efficiency : -

$$\text{Efficiency(Carnot)} = \frac{T_{max} - T_{min}}{T_{max}} (x100)\ \%$$

where T_{max} and T_{min} are the cycle maximum and minimum temperatures.
The traditional forms of heat engine rely on the conversion of chemical energy into heat usually by oxidising a hydrocarbon fuel. Either liquid or gaseous fuels may be used although to a large extent this depends upon the particular cycle utilised in the heat engine and on the application for which the heat engine is intended. Specialised heat engines exist which do not rely on the oxidisation of a hydrocarbon as their heat source, indeed the external combustion engines such as the Stirling, Rankine and Brayton cycle engines may obtain their heat input from any of a number of sources. A number of electricity power generating stations have the capability of burning either oil or coal. From the operation of the external cycle heat engines it is evident that only a source of heat is required and that whether it should come from solar heating, geothermal heating or the oxidation of hydrogen, for instance, is largely an economic decision. **Figure 1.3** lists a number of chemical sources from which thermal energy may be derived.
The internal combustion heat engines tend to be much more fuel specific, this results simply from the operation of the particular cycle in use. In spite of this inflexibility, internal heat engines are in widespread use and will no doubt continue to be so for some time to come. The explanation for this is addressed in the next section on heat engines for transport use.

Fuel cells are not generally considered as heat engines,

however if a temperature equivalent of energy level change is adopted, then this type of energy converter may also be considered as a heat engine. As stated earlier, the usual definition of a heat engine involves temperatures which arise from the oxidation of liquid or gaseous fuels, this normally involves a change from chemical potential energy into thermal energy in the form of rotational, vibrational and translational molecular motion, which is evident as increased pressure and temperature of the working fluid. Maximum stoichiometric temperatures attainable in such reactions are limited to bulk temperatures of around 2300 K. In a fuel cell the chemical potential energy is directly converted to electrical energy, without the degree of enthalpy increase involved in a highly disordered preocess such as those already described. The energy level changes when oxidation of a chemical species results, are of the order of one electron volt. The temperature equivalent of one electron volt is 11600 K. Consideration of the equation for Carnot efficiency immediately suggests that high energy conversion efficiencies should be possible. Indeed, this is the case for a typical oxygen/hydrogen fuel cell, efficiencies in excess of 90% are possible, and although less efficient, air/methane cells have been run at efficiencies in excess of 80%. However, the bulk of such fuel cell systems, together with their intolerance of impurities in their fuel supply, have limited their use to only very specialist applications so far.

1.2 Heat Engines for Transport

One of the basic requirements which a heat engine for transport use must fulfill, is that of high specific power output, both in terms of power to weight, and of power to volume. This requirement must hold not only for the heat engine itself, but also for the on board storage of the fuel. This latter point is probably the major reason for most transport heat engines opting for liquid rather than gaseous fuels, the choice being based on the requirement of high energy content per unit volume. Factors affecting the choice of fuel include low toxicity, the ability to store the fuel

safely, non-toxic combustion products, and of course, low cost.

Considering an ideal prime mover for automotive use, the engine would have maximum efficiency over its entire output shaft power and speed ranges. In reality this is not possible, and indeed power plants for automotive use are always associated with some form of gearbox/transmission system which endeavours to allow the heat engine to operate over a restricted speed range. This restriction on the output shaft speed is necessary largely because of mechanical constraints. The diesel engine has a restriction on its output shaft speed for a number of reasons : - inertial stresses on the connecting rods between the pistons and the crankshaft; friction between the piston and liner; sealing of the combustion gases; valve gear speed limitations; the rate of fuel injection; and fuel-air mixing and heat release. In a gas turbine the operating temperature of the power turbine limits the stresses which this component may be exposed to, and hence imposes a maximum shaft speed. At low speed, a turbine's efficiency drops, this is due mainly to operation away from the design point in terms of the blade angle and its relative rotational speed. Large incidence losses result from operation away from the design point as a result of the non-aligned velocity vectors. Generally the gas turbine is designed for a fixed operating shaft speed and is less tolerant than a diesel engine in this respect.

Varying the output power of a heat engine, while maintaining high efficiency, although desirable, results in inevitable comprimises. Diesel engine maximum output power is usually limited by the peak pressure which the cylinder and head deck may withstand, assuming that an unlimited supply of air is made available to the engine. Obviously an unlimited supply is never available to the engine for combustion, and furthermore this air supply has to be furnished by the engine itself. As the power output required diminishes, the air supply required also diminishes, this usually means that a parasitic loss burden is paid at low power levels, in the air supply system. In a naturally aspirated diesel engine, the

motion of the piston supplies the air for combustion, however, at low power output levels, the amount of air ingested by the engine is virtually the same as at high output power levels, while the amount of heat released per engine cycle is much reduced. This in turn reduces the maximum cycle temperature attainable and so reduces the efficiency of the engine.

The ideal form of a prime mover has been outlined and the reasons for the failure to reach such ideals have been given, nevertheless, useful improvements in the performance and efficiency of the three major heat engines used for transport purposes (spark ignition, diesel and gas turbine) have been made since their inception. One of the principal motivations for improvements in engine efficiency has been simply one of engine running costs. The fuel consumption of engines received considerable attention during the oil crisis in the mid 1970's , largely due to the reduction of fuel supplies available and due to the price of fuel which was subsequently demanded. The effort in more recent years has been towards reducing levels of carbon monoxide, unburnt hyrocarbons, and nitrogen oxides, however, the recent concern with the generation of greenhouse gases, such as carbon dioxide will no doubt draw attention once again to engine efficiency, simply because one product of completely burning a hydrocarbon in air is carbon dioxide. The more efficiently hydrocarbon fuel is utilised in a heat engine, the lower the output of pollutants, such as carbon dioxide, for a given power output.

1.3 Major Targets for Future Engine Development

Obviously, one of the main targets for future engine development will continue to be increased engine efficiency, however, the reduction in pollutants such as those already mentioned will also be of prime concern. Other developments which might improve the overall fuel consumption of vehicles on the roads are improvments in automotive aerodynamics, regenerative braking systems, and improvements in continuously variable transmission systems. It may well be argued that the basic concepts of transport systems in general may have to be reconsidered in the future, particularily with

respect to public transport, which if properly organised could have a profound influence on the amount of fuel consumed for transport purposes. However this thesis, which is a summary of research carried out mainly for the purposes of improving engine efficiency, will not address such contentious issues and will instead confine itelf to investigating one means by which improved efficiency of diesel engines might be achieved, namely through insulation.

1.4 Diesel Engine Efficiency and Heat Loss

Diesel engines are the most efficient form of automotive prime mover at the present time and have been so for many years. Spark ignition engines continue to compete with diesel engines largely on the basis of initial cost and engine flexibility. These two advantages of spark ignition engines may well be eroded in the next few years by improvement in diesel engine production techniques and by improvements in gearbox/transmission systems for diesels in the car market.

The heat loss to coolant in a diesel engine largely results from the high in-cylinder temperatures and heat transfer conditions which exist during the combustion phase. This heat loss, as for the spark ignition engine may be utilised for vehicle heating under conditions where this is required, but is largely rejected as a waste product of engine operation. It would obviously be more desirable if this waste heat could be utilised to improve engine efficiency. A reduction in the heat lost to the coolant would have further benefits in terms of the overall engine package efficiency, by virtue of the reduction in parasitic losses such as cooling fan, and water pump power. The elimination or reduction in size, of the coolant radiator, would bestow benefits such as reduced costs, improved reliability (30% of truck engine failures in the U.S.A. are as a result of coolant system failure) and through the reduction or elimination of the radiator, lower required frontal area for vehicles, which should have aerodynamic benefits. **Figure 1.4** lists the potential benefits resulting from the insulation of diesel

engines.

Initial research on low heat loss diesel engines around the end of the 1970's was based on claims that a reduction in heat loss to coolant would appear directly as increased shaft efficiency (**Ref. 6**). However, subsequent, more detailed, cycle simulation work showed that these claims were somewhat optimistic. The detailed cycle simulation work which was carried out by a number of research teams worldwide (**Refs. 7, 8** and **9**) showed that insulation of the combustion chamber of diesels resulted in two major effects. These effects were : - a reduction in the volumetric efficiency of the engine, due to the higher, cycle mean, wall temperatures within the combustion chamber , and an increase in the exhaust enthalpy. It was further found that there was a small potential increase in the thermal efficiency of the engine, but of only one or two percentage points. To utilise the increased exhaust enthalpy it was proposed to introduce bottoming cycle machines into the exhaust duct to recover the excess exhaust enthalpy. However, the introduction of further complexity, and the potential reliability problems which such bottoming cycle machines would introduce, was not well received by the diesel engine manufacturing community. At about the same time, the oil crisis abated somewhat, and the push for high efficiency engine systems was reduced, and more effort was expended on the reduction of pollutants from engine systems. Nevertheless, the application of new engineering materials for insulation had sparked off interest in these materials for other uses within the diesel engine. Ceramics in particular had received a great deal of attention for the purposes of insulation, but had also been proposed for such things as wear components, as well as components which would benefit from reductions in mass which the lower density ceramics could bring about. Turbocharger rotors and lightweight valve train components were among those items which were considered as deriving some benefit from being manufactured in ceramic materials. The use of ceramics for applications other than for insulation are not limited to the diesel engine and indeed spark ignition engine and turbine engine manufacturers devoted funds to

investigating the use of ceramics in such engines. Research work on the use of ceramics is currently still being carried out and some success has been achieved through the use of this class of material. One example of this success is the use of plasma sprayed zirconia coatings for use on turbine engine combustor cans. The use of this material has considerably improved the life of such engines. This life increase has come about through two factors, one of which is the reduction in the flame side temperature of the metal combustor can, and the other is the protection against corrosion which the ceramic front face coating provides for this surface.

Returning to the use of ceramics for insulation purposes in engines, it has so far yet to be proven that the use of insulating layers of ceramic provides any direct benefit to engine performance. Certainly there are changes in the combustion characteristics of diesel engines, this is largely brought about by the reduction in the ignition delay which occurs, through a decrease in the physical preparation time of the fuel. However there also appear to be major changes in the mixing of fuel and air within the combustion chamber, and this has to be taken into account when operating the diesel under low heat loss conditions. A number of engine manufacturers have spent time looking into means by which the combustion of low heat loss engines may be reoptimised to take into account the changes in the heat release characteristics, with varying degrees of success. A further point regarding the operation of low heat loss diesel engines, associated with combustion, is that the general increase in both the cycle mean temperature and pressure which occurs when operating under low heat loss conditions is that the level of nitrogen oxide production tends to increase. This situation is undesirable and further research will have to be directed towards ways of reducing these pollutants if low heat loss engines are to meet the tight emissions specifications which are to be introduced in the early 1990's.

1.5 Potential for Ceramic Material use in Engines

The situation regarding the use of ceramics in

engines may be summarised as follows :- Ceramics are a class of materials which offer the potential to operate at high stress levels at high temperatures. This is already showing benefits to turbine manufacturers through the use of plasma sprayed coatings. Ceramics also have high hardness and apart from their accepted use as cutting materials, there is considerable scope for their development as bearing materials, particularily in situations where currently used materials have limited operating lives. However, the design route for ceramic materials is by no means straightforward, particularily for monolithic components, and advances in ceramic material characteristics, such as their variability and their fracture toughness will need to continue to receive attention for some time to come. Aerospace applications apart from engine use, are feasible, should such advances in material characteristics occur.

The high temperature strength characteristics of ceramic materials may find use in reciprocating engines, where they may be used for such things as piston crowns and combustion chamber components. The low density of ceramic materials against those of the ferrous alloys could improve the response of engines through reductions in the inertias. This implies the use of ceramics for such components as valve train gear and reciprocating members such as the piston and possibly the gudgeon pin. The reduction in heat loss which is feasible through the application of ceramics may be of considerable benefit for certain engine configurations, and indeed the exhaust ports of the Porsche engine are currently insulated using aluminium titanate liners. Reduction of heat loss from the combustion chamber of spark ignition engines is unlikely to be pursued because of the general increase in combustion chamber wall temperatures which is likely to adversely affect the combustion processes. Reduction of heat loss from the combustion chambers of diesel engines may reduce the parasitic losses in the cooling system but there may well be an optimum level of insulation which will allow worthwhile reductions in the cooling system, while at the same time not adversely affecting the combustion processes.

Finally it should be remarked that even if the use of ceramics for insulation purposes in heat engines is not pursued, then useful design guides will have been explored which will enable this extremely versatile class of materials to be more fully utilised in the future.

1.6 Structural Analysis Developments

The design of mechanical components in general has been greatly aided by the use of finite element techniques over the last few years. The use of such techniques which was once only available to those with large mainframe computers, is now available to most small engineering firms through rapid advances in the power of desktop computer systems. The design of ceramic components is undoubtedly more complex than for metallic components, largely because of the brittle nature of these materials and their poor tolerance to stress concentrations and errors in design. The design procedures needed for ceramics can be greatly aided by the use of computers, and thus it may well be argued that such developments in computers were necessary precursors to the more commonplace usage of ceramics.

Although computational power has helped to open up complex design tasks to the smaller companies, there is still a considerable amount of fundamental research work to be undertaken regarding the failure criteria to be used for ceramics. The situation regarding accurate and reliable databases for monolithic ceramic materials is also in need of attention. Ceramic coatings are still not well understood and the effects which govern the deposition of such coatings, are not yet fully explained. A better theoretical understanding of coatings, and the deposition processes involved, is required. The plasma spray deposition of ceramic coatings, for instance, involves numerous variables in the process itself, apart from the variables in the powder used for spraying. Studies are currently in progress to assess the effect of spraying parameters on the deposition efficiency, the internal residual stresses, the homogeneity and the anisotropy of the coatings produced.

1.7 Modelling of Engine Processes

Cycle simulation of diesel engines is well documented and achieves reasonable agreement with experiment. However, although present modelling is probably accurate enough for diesel engine and combined heat engine/bottoming engine cycle concept studies, they still require a considerable amount of empirical data.

The study of airflow within the inlet and exhaust manifolds, and of the air motion within the cylinder are presently being studied utilising computational fluid dynamics; however, these studies are presently in their infancy. Further advances in computer power will be required before these studies can be directly incorporated in cycle simulation packages to assess the effect of, for instance, changes in combustion chamber geometry. The injection of fuel into a diesel engine combustion chamber is also a complex problem to model and the method of characteristics which is capable of tackling the propagation of pressure waves within the fuel line, is again computer intensive. Other such phenomena which are also receiving attention and which require considerable computer power are the mixing of the air and fuel within the combustion chamber and of course the highly complex burning of the fuel. At the present moment two lines of attack may be used to overcome the difficulties associated with modelling some of the more complex phenomena which occur within a heat engine. The first of these is to study empirical data from engines and test rigs, and to supply the cycle simulation package with equations and coefficients which result from curve fitting. However, a degree of caution is necessary when using such correlations as they may only be valid over a limited range of operating conditions and engine specifications. With this method no attempt is made to understand the underlying principles which govern the form of the curves.

The second method is to produce a theoretical model (based on accepted physical principles), but to accept that the model is not a full representation of what is actually

occurring and then once again to use coefficients in the model equations to produce a good fit with empirical data. Where the process in question has been reasonably well modelled but proves to be too complex or time consuming to incorporate as a submodel then it may be possible to incorporate it in the main program in the form of a simplified formulation or map which is built up from the independent running of that process model.

Although the fully modelled solution would be the most desirable, it is presently not possible. Indeed, because of the statistical nature of many of the complex phenomena which occur within an engine, it is true to say that exact solutions are not possible, but will always have to incorporate some form of error estimate. This situation is typified by the cycle to cycle variations in heat release which are observed. The starting point for one cycle is the finishing point of the previous cycle. However, the effect of the variations in cycle starting and finishing points must be small, as the system does not diverge to a situation where the engine cannot function.

1.8 Interaction between Theoretical and Experimental Studies

1.8.a General

Figure 1.5 shows the relationships which exist between the various major activities within the "CERAMICS IN ENGINES" programme described in this thesis. It is evident from the number of activities together with their individual complexities, that several participants were involved. As may be seen from the schematic, each major activity relates to the others, and this interrelationship is an essential part of the programme.

1.8.b Theoretical work

i). Cycle Simulation

This work draws heavily on the existing program "SPICE" developed at the University of Bath. This program has been enhanced by Rassihan (**Ref. 23**) to incorporate refined thermal resistance models for the combustion chamber walls and has included new models for

convective and radiative heat transfer.

ii). F.E. Analysis

The writer has played a leading role in this section of the programme which is concerned with the thermal and stress analysis of engine and rig components. Analyses carried out include :- the piston/piston cap assembly ; the cylinder liner with and without insulating layers ; and the specimen for the thermal shock and conductivity rig. This work is reported in detail in **Chapter 6** .

1.8.c Experimental and Design Work

i).Materials Testing and Property Determination

This work was carried out primarily in the School of Materials Science and, again for the sake of brevity, will not be reported in this thesis except for the work on the Thermal Shock and Conductivity Rig which was one of the major contributions of the writer (see **Chapter 2**).

ii).Experimental Engine Tests

This work included tests both on the single cylinder Petter engine, as well as on the motored engine simulation rig. The systematic test programmes for both the simulation test rig and the firing engine test rig originally planned were severely curtailed by repeated failures of the ceramic cap. However, a full summary of relevant work undertaken is given in **Chapters 3** and **4** .

iii). Engine Component Design and Production

This work was concerned primarily with the design of glass ceramic piston crowns and with alternative methods of attachment of the crowns to the piston body. It is reported fully in **Chapter 5** .

1.8.d Analysis of Test Results

The two blocks in **Fig. 1.5** labelled respectively "Detailed Heat Balances" and "Analysis of P-Ø Results" apply primarily to engine test results. Such tests are currently being conducted, after the earlier repeated piston crown failures, by Shams (**Ref. 47**), who will be submitting a thesis at a later date. No further reference is made to this work in the present thesis. However, results obtained with the thermal shock rig are reported in **Chapter 7** .

Heat Engine Schematic

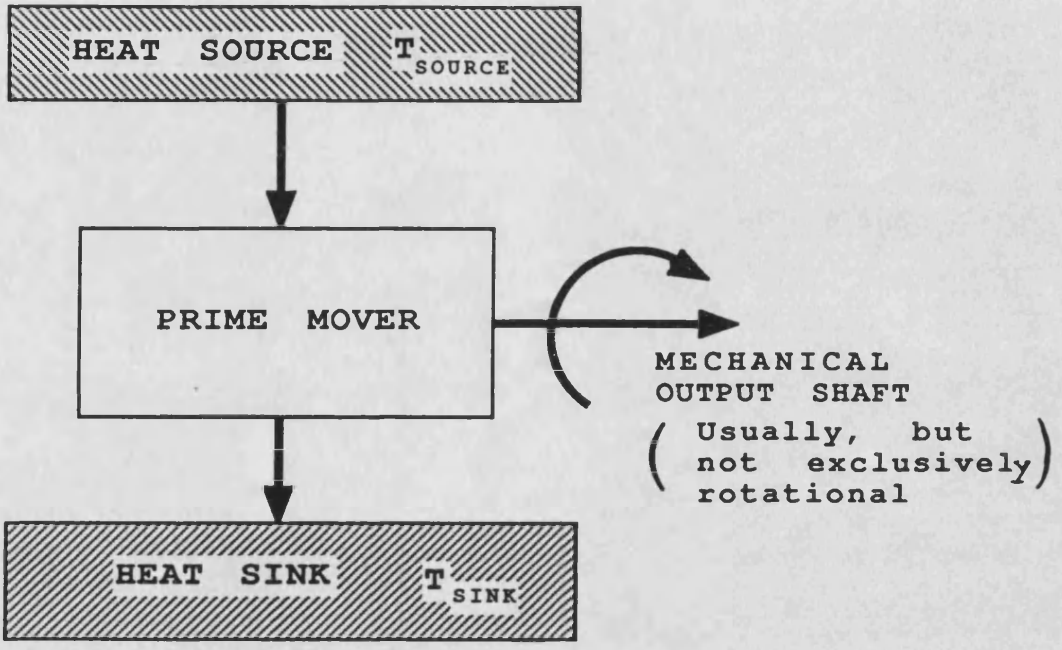

$$\eta_{CARNOT} = \frac{T_{SOURCE} - T_{SINK}}{T_{SOURCE}}$$

(in degrees Kelvin)

Figure 1.1

Examples of Heat Engines

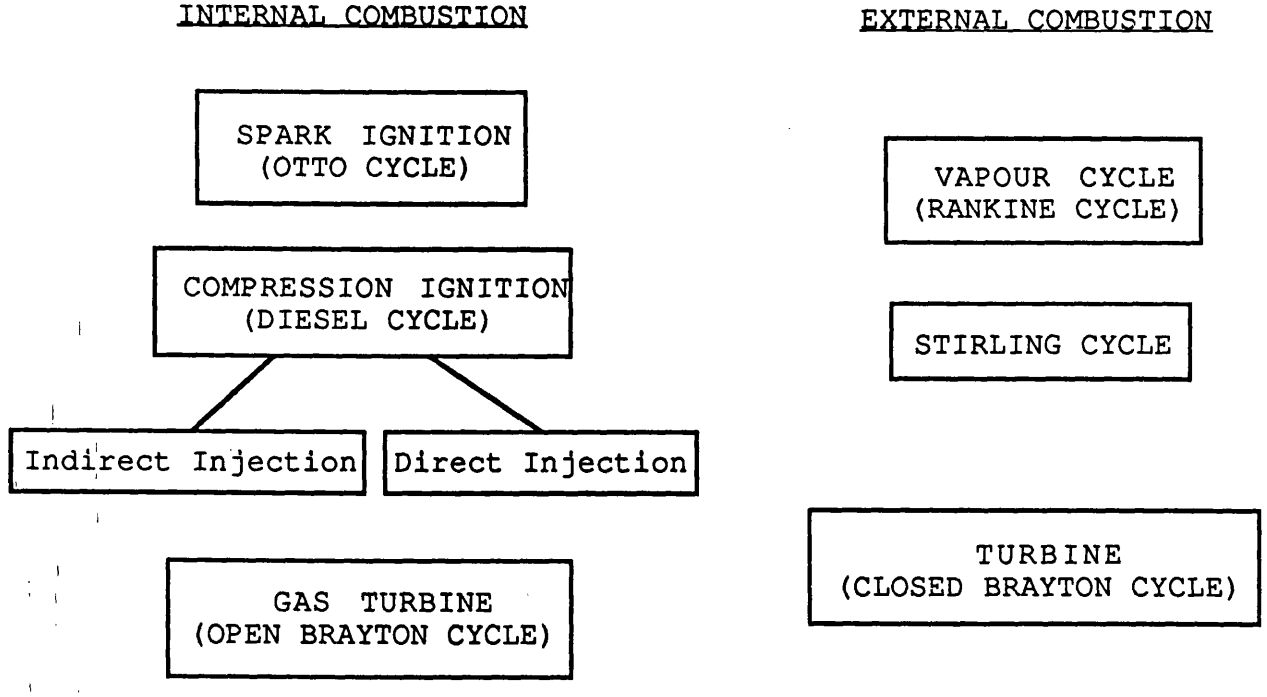

Figure 1.2

CHEMICAL THERMAL SOURCES

FUEL	OXIDANT
HYDROGEN	Air, Oxygen
HYDROCARBONS - ALKANES C_nH_{4n}	
ALKENES C_nH_{2n}	
ALKINES C_nH_n	
CARBOHYDRATES - ALCOHOLS R(OH)	
ETC.	
MIXED ORGANICS - PETROL	
DIESEL	
WOOD	
COAL	
HIGH MOLECULAR WEIGHT SOLIDS	
OTHER LIQUIDS HYDRAZINE	Hydrogen Peroxide (H_2O_2)
ORGANIC LIQUIDS AND SOLIDS	Nitric Acid (HNO_3)
ALKALI METALS (K, Na, Ca)	Oxygen, Acids, Water
OTHER METALS (Al, Mg)	Oxygen, Acids
Sulphur, Carbon	Alkali Nitrate

Trinitrobenzene ($C_6H_3(NO_3)_3$)

and other double and triple bonded organics

Unstable organics - no requirement for separate oxidant

Unstable inorganics - no requirement for separate oxidant

Figure 1.3

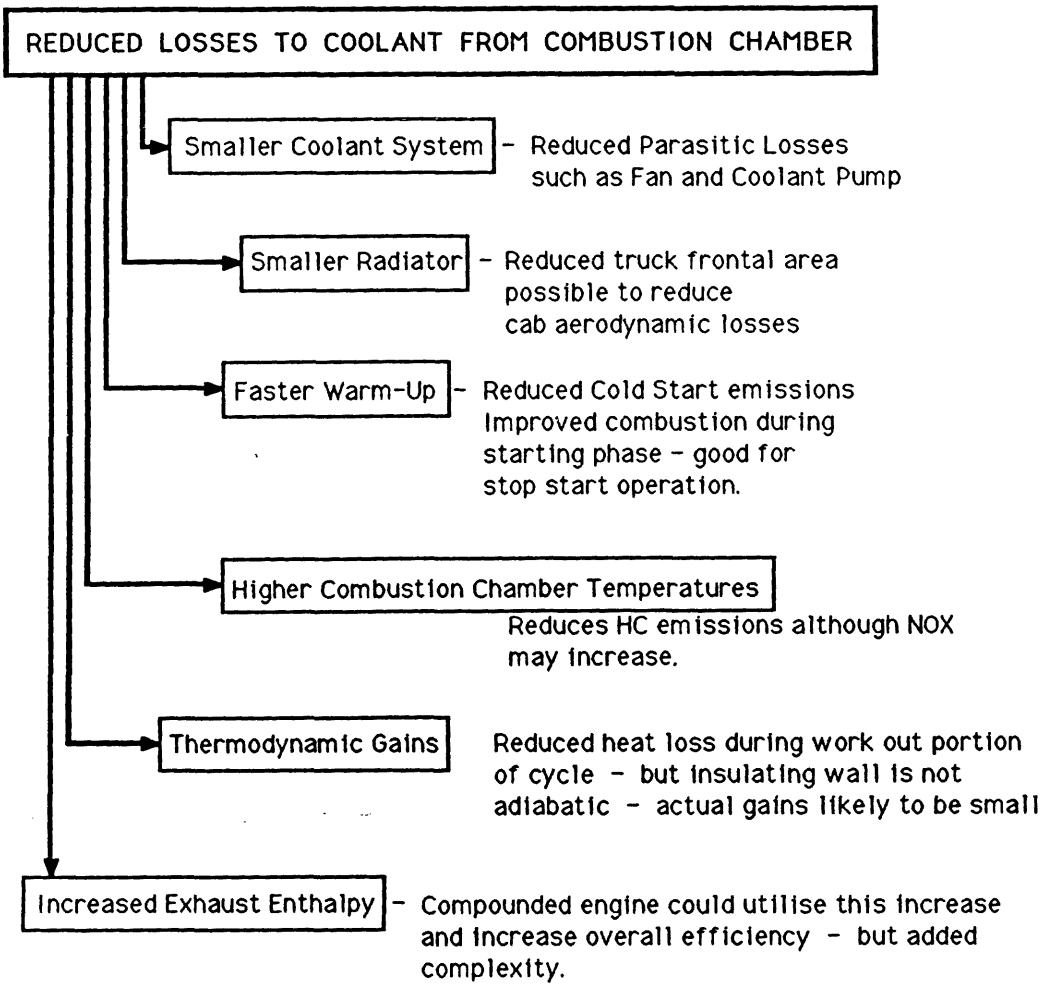
REDUCED LOSSES TO COOLANT FROM COMBUSTION CHAMBER
Smaller Coolant System
- Reduced Parasitic Losses such as Fan and Coolant Pump
Smaller Radiator
- Reduced truck frontal area possible to reduce cab aerodynamic losses
Faster Warm-Up
- Reduced Cold Start emissions Improved combustion during starting phase - good for stop start operation.
Higher Combustion Chamber Temperatures
Reduces HC emissions although NOX may increase.
Thermodynamic Gains
Reduced heat loss during work out portion of cycle - but insulating wall is not adiabatic - actual gains likely to be small
Increased Exhaust Enthalpy
- Compounded engine could utilise this increase and increase overall efficiency - but added complexity.

Figure 1.4

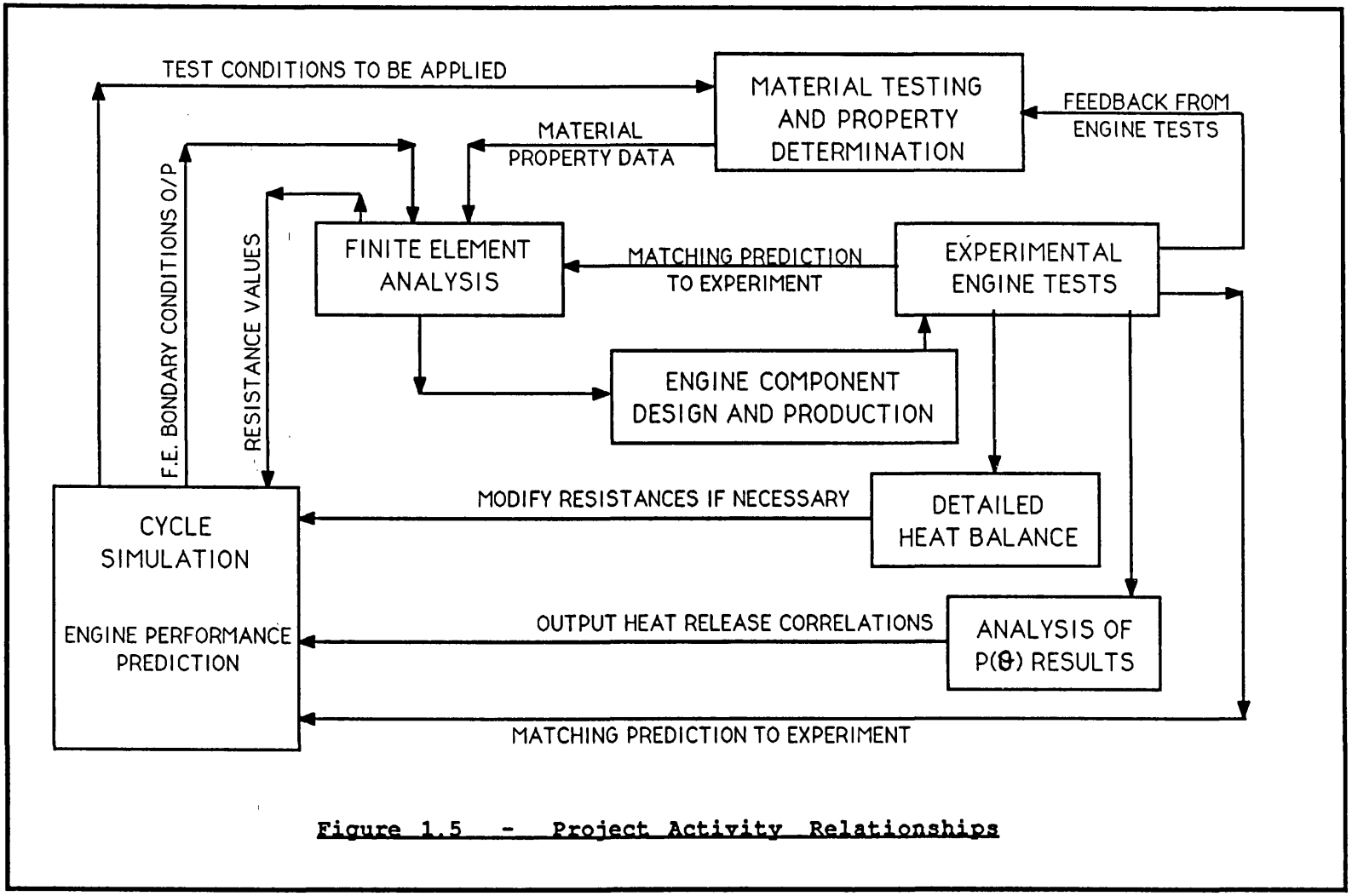

Figure 1.5 - Project Activity Relationships

CHAPTER 2 - THERMAL CONDUCTIVITY AND THERMAL SHOCK TEST RIG

2.1 Introduction

The original impetus for the development of a thermal conductivity/thermal shock rig, arose out of a need for an "in house" facility to measure the thermal conductivity of thin plasma sprayed coatings of ceramic produced in the School of Materials Science. This work was carried out under the auspices of the SERC who funded the three year collaborative project between the Schools of Mechanical Engineering and Materials Science. The purpose of the project was to look at the development of plasma sprayed zirconia ceramic coatings, both from an experimental and theoretical viewpoint, for use in Diesel engine combustion chambers. As the project was to be concerned with experimental aspects as well as theoretical modelling of plasma sprayed coatings it was necessary to obtain reliable property data for the materials which were sprayed down. Data available from the literature showed that a considerable variation in properties had been found. This appeared to be not only dependent on the percentage, and type of stabiliser used with the zirconia, but also on the starting powder, the spraying parameters, and the plasma spraying system used. With such information, it was decided, right from the outset of the research programme, that property determination rigs would be essential if progress was to be made.

Generally, the stresses in a component may be divided between those arising from mechanical sources such as pressure forces and clamping arrangements, and those originating from thermal expansion. Thermal expansion generated stresses may arise from within a body, due to temperature gradients, or may be due to differential thermal expansion resulting from a mismatch in the thermal expansion coefficients of two different materials in intimate contact.

In order to find the temperature distribution within a

component at thermal equilibrium, both the thermal conductivity of the body and its thermal boundary conditions are required. For the case of transient heating of a body, the specific heat and the density of the materials present in the model must also be known. It should be noted that the thermal boundary conditions may be affected by the strains which result in a body, either as a result of the thermal boundary conditions themselves, or as a result of imposed mechanical action. These strains may, for instance change the thermal coupling across interfaces, by opening up "gaps". This point arose in the ceramic crown/piston body analyses, and necessitated the use of special "gap" elements. These elements are available in the more sophisticated F.E. programs specifically to deal with such situations.

2.1.a Thermal Conductivity

Considering the importance of this particular material property, it was decided to embark upon a study of the available methods for the determination of thermal conductivity. An MSc student, P. Pappas, under the direction of the writer, was allocated the task of carrying out a literature search on the topic in question, this is detailed in **Ref. 10.** After discussion it was decided that the most appropriate test method was that of Lee's disc, where the temperature difference across a thin disc specimen is monitored together with the heat flow through the disc. This method, and adaptations of it, are commonly used for the measurement of the thermal conductivity of insulating materials. Detailed analyses of the errors which can arise from the practical application of this method have been carried out by a number of researchers, including Somers and Cypher, Dusinberre, and Pascal. These analyses are summarised in **Ref. 11** by Woodside.

Generaly, the method mentioned above, takes advantage of the solution for the simplest case of heat flow, where the flow is one dimensional and steady (equilibrium). Deviations from one dimensional heat flow will obviously introduce errors and it was for this reason that a finite element study of a

possible system configuration was undertaken by Pappas (**Ref.11**). The results of these analyses were compared with the analytical treatments for error determination mentioned earlier. A further point of note is that to drive any appreciable amount of heat through an insulating specimen, there has to be a reasonable temperature differential across the specimen. A number of insulating materials have a thermal conductivity which is dependent on temperature, this leads to some difficulty in extracting the thermal conductivity at a given temperature. However, **Appendix 1** shows that examination of the differential heat flow through the specimen with respect to temperature, gives the desired information.

2.1.b Thermal Shock

In addition to the property determination rigs there arose the need to provide a method of rapidly testing the plasma spray coatings produced, in order to determine whether a particular coating strategy was worth pursuing or not. Subsequent to the early work carried out, it became evident that it was necessary to examine the long term behaviour of coatings to thermal cycling. It was seen that by the addition of a number of components to the design of the basic thermal conductivity rig, thermal shock and thermal cycling could also be provided. Thus the thermal conductivity rig evolved to cater for all three testing modes :- thermal conductivity determination, single intense thermal shock and long term thermal cycling ; both for spray coated ceramics and for monoliths.

Manton (**Ref. 4**) developed a finite difference model to predict the magnitude of thermally generated stresses in a simple disc exposed to transient thermal conditions. The thermally generated stresses produced by both short, and long term, thermal cycling were examined. The short term cycling investigations were carried out to determine the likely level of stresses produced by the rapid changes in thermal conditions within the combustion chamber during the engine cycle. The longer term cycling runs were to examine the effect of load variations on the thermally induced stresses. The

result of such analyses suggested that it was the longer term engine load variations which produced by far the larger, and potentially more damaging, stresses. This view is supported by Huang and Borman (**Ref. 12**). However, it must be remarked that there is also recent evidence (**Ref. 13** and **14**) to suggest that the values of effective heat transfer coefficient used in the model by Manton are too small, and that further attention to this point should be made.

Regardless of the above, it was evident that the thermal cycling of ceramic components produced by engine load variations, was of great importance, and that a rig capable of producing such thermal loadings should be built.

2.2 Selection of Specimen Heating Source

As part of an MSc project, Pappas (**Ref. 11**) carried out finite element studies to aid design of a thermal conductivity apparatus. It was proposed that a simple electric resistance heater be used as the heat source. The particular design required a highly uniform, isothermal plate to be in contact with the specimen. At the time, a major concern was the non isothermal nature of the heating source, in the sense that the heating coil itself was comprised of a finite number of electric resistance wires embedded in a block of thermally conductive material. The finite element studies were used to examine the effect of coil spacing and the distance of the coils from the face of the block in which the coils were embedded. The application of these techniques allowed the spatial variations in temperature at the surface of the block to be minimised with reasonable thicknesses of metal.

The finite element design work assumed that the heating block face was in good thermal contact with the specimen. After completion of the MSc project more detailed design considerations by the author revealed that a potential problem might be that of specimen, and heating block distortion, with subsequent loss of uniform specimen heating. Previous researchers working on the determination of thermal conductivity have made use of compliant materials interposed

between the heating block and the specimen (**Ref. 15**). This method of ensuring good uniform specimen heating is, however, only available up to modest temperatures of around 300° - 400°C, this being the upper temperature limit for presently available compliant materials. Specimen surface roughness and high thermal stresses which result if the specimen is constrained from distorting are also problems which result from a solid face to face contact method of heating. As a result of these considerations it was decided to reconsider the methods available for specimen heating.

There are many potential sources which could be used for heating of the specimen, some of these are:-

a). gas or liquid fuel fired, flame heating
b). electric radiant heating
c). laser
d). hot air impingement
e). heat pipe
f). molten metal or salt bath
g). hot plate heating
h). microwave or dielectric methods

For the case of thermal conductivity measurements, it was essential that the flux available at the specimen front face be capable of raising the temperature to levels at which the thermal conductivity was to be determined. Estimates of the specimen thermal conductivity together with specimen thickness and the back face cooling conditions allowed equilibrium flux levels to be calculated. For the case of thermal shock it was possible to estimate the worst case flux level requirement from engine cycle simulation output data. As it was the load varying thermal shock which was required to be simulated, the cycle mean gas temperature and heat transfer coefficient were used for this calculation. Values of these obtained from cycle simulation programs were of the order of 500 to 1000 $Wm^{-2}K^{-1}$ for the cycle mean heat transfer coefficient and 1000 to 1300 K for the cycle mean gas temperature.

For the case of thermal conductivity determination, it was necessary to provide a controllable heat source. This requirement arises from the need to ensure rapid heating of the specimen front face and to ensure that the temperature was controlled within tight limits during the actual measurements of thermal conductivity. It was envisaged that more than one control strategy should be made available for the case of thermal shock, and this automatically required that a controllable source be made available.

The proposed method of thermal conductivity determination dictated a high degree of specimen front face heating uniformity. This arises from the one dimensional heat flow assumption on which the method is based. For the case of thermal shock evaluation it was considered that modelling of both the temperature and stress fields within the specimen would be simplified if one dimensional heat flow was assumed. Interpretation of the resultant acoustic emission data and specimen fracture analysis would also be simplified if one dimensional flow could be ensured.

Regarding the cost of the heating source, initial capital cost together with running costs for the proposed heating sources were considered, as the systems detailed below vary markedly in this respect.

Safe operation of the test rig was an important consideration. The flux levels anticipated at the specimen were such that serious injury to personnel might result if the rig were misused. Each heating source was examined to determine which of those available would be simplest to guard against accident and misuse.

A further aspect of the test rig operation is related to the basic purpose of the test rig, that is, to provide purely thermal stressing of the specimens. The failure of engine components, whether they be ceramic or metallic, depends upon a number of operational parameters. One of these parameters is the chemical environment in which they operate. It is well known that certain impurities present in liquid and gaseous fuels promote attack of both metallic and ceramic

components. For the purposes of this fundamental material assessment it was essential that failure be due to only one aspect of engine operation, namely that of thermal stress. The addition of chemical attack was considered to be an added complication which would only serve to confuse the origin of failure. This aspect necessitated the use of only chemically clean sources.

Although the list of heating sources included at the beginning of this section is not exhaustive each will now be examined with respect to the requirements outlined.

2.2.a Gas or Liquid Fuel fired, Flame Heating

This type of heating is capable of providing the fluxes necessary for both thermal conductivity and thermal shock investigations. Burner design is rather specialised but the system could be based on existing commercial high intensity burners. Uniformity of heat flux across the specimen front face could also be achieved. Although diesel, kerosene, petrol and similar fuels available in bulk contain appreciable quantities of impurities, natural gas available nationwide in the U.K. contains very low concentrations of impurities (sulphur content quoted as being of the order of fractions of ppm). Correct control and safety measures applicable to gas based systems are strict as would be expected from a fuel which is potentialy explosive. Added to this aspect of safety is the need to provide adequate venting of the exhaust and sealing of the flues, so that the attractiveness of the method is somewhat reduced.

2.2.b Electric Radiant Heating

This heading covers a number of possible configurations, although the only ones which are capable of meeting the flux requirements are arc lamp based systems and quartz-halogen tungsten filament systems. In terms of the maximum flux available, arc lamp based systems are superior to those based on tungsten filaments. Higher flux levels are available with arc lamps for two reasons i/. the source temperature of the arc lamp is higher and ii/. the source size is smaller. However, the control gear necessary for the

operation of this type of source is expensive, as are the arc lamps themselves. Tungsten halogen filament lamps available for photographic and theatre lighting can provide adequate flux levels with the correct design of reflector but have relatively short lives when run at full power. Control of filament lamps is simple, with commercial voltage controlled dimmer sets being available at low cost relative to the units necessary for arc lamp control. An hazard which is associated with both types of lamp is that of explosive failure of the lamp envelope. Under full power conditions, both types of lamp have internal pressures well above atmospheric. However, careful design of the reflector system around the lamps can overcome the problem of explosive lamp envelope failure.

2.2.c Laser Heating

Commercial CO2 lasers are easily capable of meeting the flux levels required but initial and running costs are high. Safety precautions are essential, particularily with this type of laser, as the radiation is invisible, being in the infra red (10.6μm) part of the spectrum.

2.2.d Hot Air Impingement

This system requires some heating source whether it be electric or flame to raise the temperature of air, which is then directed at the surface of the specimen. A low waste system could be designed by using recuperative or regenerative methods similar to those used in commercial air heaters, whereby the air exhausted from the heating chamber is used to preheat the incoming air. The overall package would be complex to design and the flux levels available might be on the low side, unless a pressurised system were used to raise the air to specimen surface heat transfer coefficient.

2.2.e Heat Pipe

Specialist design would be required especially at the power level required. Although such systems could easily provide the required heat fluxes, the required temperature range would result in control and safety problems.

2.2.f Molten Metal or Salt Bath Heating

These methods are restricted to rather narrower

ranges than those required, typically 20° to 800°C . Flux levels can be very high but the choice of melt would be extremely difficult to cover the wide range of potential ceramics to be tested without including chemical effects. Furthermore the melt would have to be non wetting when using porous ceramics to avoid problems on cooling. A number of potential hazards exist with this type of heating, particularily in the confines of the laboratory.

2.2.g Hot Plate Method

The uniform contact of the plate with the specimen at high temperatures has already been identified as a possible problem associated with this method. As the specimen is heated it will have a tendency to distort.

Two solutions are :-

a). to constrain the specimen to conform to the shape of the heating plate through the application of external pressure, or

b). to allow the heater to distort with the specimen

Solution a). may cause the specimen to fracture, which for the case of thermal conductivity may give rise to incorrect values due to the presence of cracks in the plane of the specimen. In the case of thermal shock it might be difficult to determine the exact causes of the failure due to the difficulties associated with modelling the interaction between two surfaces effectively in sliding contact.

Solution b). may allow the heating side to remain in full contact with the specimen but the same approach would also have to be taken with the cooling side, adding further complications. A further point is that most commercial heaters operating up to around 800°C are rather limited with respect to the heat flux available. This is simply because they are designed for long life with the heater core to surface temperature difference being relatively low.

The application of a hot plate contacting system for thermal shock, would require a low mass, low specific heat, high thermal conductivity plate, in order to comply with the

transient response required. This would not be a simple design task if the requirement for uniform heating was to be adhered to. This results from the discrete wire heater elements, and their associated spatial temperature ripple, unless a reasonable thickness of material is interposed between the wire sources and the specimen. It is possible that a monoblock, cermet heater could overcome this problem.

2.2.h Microwave or Dielectric Heating

For the power levels required, the cost of the installation of either of these methods would be expensive relative to some of the others. A number of the ceramic materials which were expected to be tested are almost transparent to microwave energy and have low dielectric loss coefficients. These facts imply that a reasonably thick coating of high loss tangent material be placed in contact with the specimen front face to absorb the radio frequency energy and thus the problem of uniform contact of the heat source with the specimen arises once more.

2.2.i Final Choice of Heating Source

Of the methods discussed above, the two major contenders were gas flame, and electric radiant heating. Safety considerations and the absence of exhaust systems necessary for the gas flame system favoured the choice of electric radiant heating. Purely on the basis of cost, the tungsten filament source was chosen in favour of the arc lamp. The control electronics were of the order of five times more expensive for the arc lamp than for the filament lamp systems. The reflector/collector assemblies for commercial units were on the order of two to three times more expensive for the arc based systems although the arc systems offered higher flux densities. The arc lamps were at least six times as expensive as the quartz halogen tungsten lamps but had the advantage of an estimated life of some 1500 - 2000 hours against typically 200 hours for the tungsten lamps.

In an attempt to improve on the flux levels, uniformity of heating and to reduce cost still further, the reflectors for the tungsten lamps were designed and built "in house", at

the university.

2.3 Control Strategy

The test rig was required to cater for thermal shock as well as thermal conductivity testing, and to this end it was necessary to provide appropriate control schemes for each application. For the case of thermal conductivity testing, the requirement is for as rapid an attainment of thermal equilibrium, at some fixed front face temperature, as is possible, to reduce settling time and thus overall testing time. For the case of the thermal shock testing, the choice of control scheme is not quite so simple. Several possible control options may be considered, and of these, three were identified as being most appropriate to cover the requirements. The control schemes chosen were :-

a). Simple fixed power output control

b). Specimen front face temperature control

c). Simulated convective heat transfer control

It is important to reconsider the reasons behind the design of the test rig for the case of thermal shock testing. The brittle behaviour shown by most ceramic materials can lead to catastrophic failure, brought about by the application of severe stress due to transient thermal conditions. In the past, a standard test applied to candidate materials was to heat a bar of the material up to a given temperature and then to immerse the bar in either an oil, or water bath. There are a number of objections to this testing method, one is that little or no control exists over the degree of thermal shock which is imposed on the test bar, another point is that materials with different thermal characteristics will undergo different degrees of transient stressing. Of course it could be argued that in a real working environment this is exactly what occurs. However, it is difficult to assess the conditions to which each material should be subjected in order adequately to test that material for a given application, using this method.

Essentially, the thermal shock capability of a material

should be amenable to analysis, having a knowledge of the thermal and mechanical properties of that material, and as such there should be no need for thermal shock testing. However, due to the variability of the materials in question, it is necessary to subject them to a stress test which is applied to a large volume of the material rather than the rather small volumes (with respect to the volume of the test sample as a whole) which are inspected in either the standard three or four point bending tests. This is done to test more rigourously the data available on that material.

2.3.a Fixed Output Power

The simple fixed output power control scheme assumes that with fixed output power from the lamps that a fixed input flux will exist at the front face of the specimen. If this assumption is correct, then the rate of rise in front face temperature and the level of transient thermal stress should be the same for materials with identical properties, but be dependent on those properties. Likewise the final, equilibrium, front face temperature will be dependent on the material thermal properties and on the back face cooling conditions. The control of the lamps is specimen independent, and it remains only to cater for electricity supply variations and long term lamp output variations which might occur through ageing of the lamps.

2.3.b Specimen Front Face Temperature Control

The specimen front face temperature control scheme automatically requires that the front face temperature of the specimens be monitored in some way, and the test becomes specimen dependent.

2.3.c Simulated Convective Heat Transfer Control

Simulated convective heat transfer control - this is the most complex of the control schemes in that both front face temperature and lamp power output must be monitored together with circuitry capable of simulating convective transfer from what is essentially a radiative source.

2.4 Control Electronics

2.4.a Simple Fixed Output Power Control

As previously stated, it was desirable to make available more than one control schedule for the heating of the specimens. Power control of the lamps was achieved by using an "off the shelf" phase angle controller, normally used for theatre lighting. **Figure 2.1** explains the operation of phase angle power control. A zero to 10V voltage control input signal is required for this controller. The output power is not, however, linear with respect to the input control voltage due to the circuit operation, which more closely approximates to a linear increase in phase angle with respect to control voltage. However, as a closed control loop was envisaged, this point was of secondary importance, and more related to the stability of the control system. Basically in a closed loop control system, a parameter demand is set, and a sensor system detects the error between that which is set and that which is observed. The error, or difference, signal is used to adjust the observed signal until it coincides with that demanded.

2.4.b Specimen Front Face Temperature Control

The main use for this control scheme was the rapid attainment of a set, specimen front face temperature, as is required for thermal conducitivity determinations. For this case, a front face thin film thermocouple is used as the sensor and after appropriate signal conditioning the signal obtained is compared with the set front face temperature required. The conditioning circuit incorporates both proportional and integral sections to enable rapid attainment of the desired specimen front face temperature. The non-linearity of the power control section does not cause any instabilities.

2.4.c Simulated Convective Heating Control

This type of control was considered for the simulation of load step transients, as might be found in the combustion chamber of diesel engines. For this case it was important to carefully monitor the output power from the lamps. First thoughts on this included the use of Hall effect probes or current transformers to monitor lamp current, and

the use of isolated stage voltage sensors for lamp voltage. Through the use of appropriate conditioning and a hardware multiplier the power into the lamp could be obtained. However, this route was ruled out simply because the output would be a measure of the power INPUT to the lamp and not the power OUTPUT, i.e. that which is required. As the major purpose of simulating convective heating was to produce a thermal transient, the source must respond transiently. It was considered that the transient response of the lamp was insufficient for it to be ignored (of the order of 0.5 - 1.5 seconds) and as such the assumption that lamp power input be equal to lamp power output was considered invalid for the purpose. An alternative method was sought which actually monitored lamp power output. A photodiode sensing the light from the lamp would certainly respond to variations in lamp power output but there was concern as to whether this response would be linear. To ascertain the response of the photodiode to variations in lamp power output it was necessary to obtain the spectral response curve of the photodiode and to compare this with the spectral distribution of the lamp for varations in power. For this study the lamp was assumed to behave as a black or grey body radiator. The spectral response curve was obtained from data sheets on the diodes to be used (see **Fig. 2.2**). The method used is outlined in **Fig. 2.3** and the result of the study is given in **Fig. 2.4.**

In terms of lamp power output variations required, the worst case was considered to be for that of a highly insulating specimen. Initially the specimen is at room temperature, while at the end of the heating period it will be much closer to the fluid temperature which is being simulated. This situation results in the widest power input level swing of the lamps, estimated to be from 100% lamp power down to around 20% . Inspection of the graph in **Figure 2.4,** shows that power measurement errors of less than ±5% will result.

Convective heat transfer to a surface is governed by three parameters, these are :- h - the heat transfer coefficient ; T_{gas} - the temperature of the medium in contact

with the specimen ; and T_{wall} - the temperature of the front face of the specimen. The thermal boundary conditions to be simulated, that is , h and T_{gas} , are manually dialled up, on the front panel of the instrument. The specimen front face temperature is monitored using a thin film, surface thermocouple. The circuit operation is as follows :-

The temperature of the specimen front face is compared with the set value of the gas temperature (input on the front panel). This temperature difference is then multiplied by the heat transfer coefficient (also input on the front panel), to give the required heat input to the sample. The power output from the lamps, which is monitored by the photodiodes, is then adjusted to give the required heat input at the specimen front face. As stated previously this method of control is based on the assumption that a fixed fraction of the lamp output power is intercepted by the specimen front face, for all lamp output powers. **Figures 2.5** and **2.6** are schematic circuit diagrams for the convective control.

2.5 Control System Commissioning

2.5.a Temperature Monitoring (for details of the thin film thermocouples see **Chapter 3 , section 3.2**)

The control systems for both the specimen front face temperature control and the convective heating control required that the thin film thermocouples on the front face of the specimens should respond correctly to variations in temperature. It was to this end that careful calibration of the thin film thermocouples was instigated. Correct calibration procedures for thin films are not simple tasks and some thought has been given to the geometry of the test specimens used for this purpose, as well as the method of calibration. Three such methods were considered. One of these utilises a medium power (5W maximum) argon ion laser, another utilised a small barrel furnace, and the third method was that of temperature controlled hot and cold pads, in contact with the surface of a ceramic test disc, onto which had been

deposited the thin films to be assessed.

The argon ion laser method (see **Fig. 2.7**) involves chopping the beam at a predetermined set of frequencies and observing the output from the thin film thermocouple. The test specimen in this instance is a piece of ceramic material of known thermal conductivity, specific heat, density and thickness. The actual junction is made small enough to be completely covered by the laser beam. The laser power and the chopping frequency is known and so a theoretical estimate of the temperature swing can be obtained. This estimate is compared with the actual value obtained. A problem with this method was that it proved difficult to obtain sufficiently high flux densities at the specimen while ensuring that the thermocouple junction was evenly illuminated. This problem arises from the size of the junction which it was feasible to fabricate reliably, together with the power ouput available from the laser. Tests which were carried out, showed that the response of the thin film thermocouples was as fast as had been expected but that the magnitude of the temperature swings recorded was extremely sensitive to positioning of the beam with respect to the junction.

The barrel furnace is used for steady state calibration of the thermocouples (see **Fig. 2.8**). Care was taken to isolate thermally the thin film to wire junction from the junction to be calibrated. This involved the production of a long set of thin film leadouts from the thin film junction, which proved to be a rather difficult task. The difficulty arose from the thin film deposition technique which was necessary with the equipment available. The length of the thin films dictated that each "leg" of the thermocouple be deposited in two stages. This procedure involved taking the vacuum system "down" to atmospheric pressure in order to reposition the specimen. The risk of contamination was therefore increased, and reliable thin films were not always produced. The substrate on which the thin film leads and junction were deposited was also long and thin, to minimise conduction of heat from the junction (to be calibrated) to the

wire/thin film interface. Alongside both the main junction and the wire/thin film junctions, thin foil thermocouples of known calibration were placed. This rather involved procedure for the steady state calibration was necessary, as it is relatively easy to make the mistake that what is being calibrated is not the main junction but rather that of the two wires connecting the thin films to the measuring apparatus. This point is more fully treated in **Appendix 2.**

The final method proved to be most amenable for the rapid assessment of the thin film thermocouples in service, as a check on performance. The apparatus is essentially comprised of a cold "finger", and a hot "finger", which are placed on the surface of a disc of ceramic, onto which thin film thermocouples are deposited. The cold "finger" is temperature controlled using a Peltier junction cooling device, and associated control circuit. The hot "finger" is simply a modified, temperature controlled, soldering iron. **Fig. 2.9** shows a schematic of the apparatus detailing its major features, and **Fig. 2.10** is a photograph of the calibrator and its associated control units. At the present moment the device is limited to clibrations of thin films between approximately 0°C and 400°C. The upper limit being set by the temperature controller on the hot "finger". **Fig. 2.11** is a circuit schematic of the temperature control used for the apparatus, and **Fig. 2.12** is a cross sectional view of the cooler attached to the Peltier device for the controlled clod junction.

2.5.b Flux Monitoring

Calibration of the flux present at full lamp power is necessary if the control circuits are to ensure correct simulation of thermal transients. A calibration system was therefore designed and built to monitor the flux at the specimen front face.

The flux calibrator comprises a thermally isolated cylinder of copper, one face of which is exposed to the combined lamp flux at the position normally taken up by the specimen front face. The block is thermally isolated from the

carrier block by ceramic or PTFE spacer rings and an air gap. The cylinder is bright nickel plated along its length and at one end face to reduce radiative losses. The exposed, front face is left unplated and is coated with a very thin layer of black, absorbing, high temperature paint. A 1/16" stainless steel sheathed thermocouple is used to monitor the temperature of the block. The calibration procedure simply comprises of running up the lamps to full power, with the calorimeter block removed and then to place the block in the position normally occupied by the specimen. A plot of block temperature versus time is then made, up to a maximum temperature of around 200°C. The mass of the copper block and its specific heat are known, thus the power absorbed by the block may be calculated, and, accurately knowing the front face area, the mean flux at the specimen front face. **Fig. 2.13** is a cross sectional view of the flux calibrator assembly, and **Fig. 2.14** is a photograph of its component parts. A typical recorder trace is shown in **Fig. 2.15** , showing the temperature of the calorimeter block versus time. The linearity of the trace at the higher temperatures, justifies the care taken in the design, to minimise conduction and radiation losses. The non-linear portion of the curve , at the start of the heating period, is probably due to the thermal resistance and inertia of the copper block, which although small, does have a finite value.

Although not directly connected to the control circuit calibration, another important parameter to measure is the distribution of flux across the specimen front face. A knowledge of this allows the uniformity of heat input to the specimen to be checked and hence justify the one dimensional heat flow assumption used in the analysis models. The flux distribution across the front face of the specimen was monitored by two methods, both utilising photodiodes. The first flux monitor produced, was comprised of a series of ten photodiodes distributed in the specimen front face plane, at known distances from the centreline. A map of the flux distribution was obtained by rotating the assembly around the

centreline. The lamps were operated at such a power level as to enable reasonable signal levels to be obtained, but not so high that temperature drift of the photodiodes became a problem. An assumption made was that the flux distribution was independent of lamp power. This assumption is reasonable as long as a). the reflectivity of the reflectors is wavelength independent and b). the geometry of the source does not change appreciably with power level. The photodiodes used had a temperature coefficient of around 0.3% per degree Centigrade, on sensitivity. As the lamp power is turned down, an increasing proportion of the radiation is in the infra red. In order to reduce the problem of sensor heating, and thus sensitivity changes, two plates of soda lime glass separated by an air gap were placed in front of the photodiode array. However some drift of the photodiodes was still noted. If the temperature drift of all of the photodiodes was identical then, as the readings taken are relative in nature and not absolute, then this would not present a problem. Checking for uniformity of photodiode temperature was accomplished by examining the dark current generated by each of the photodiodes, as this is also temperature sensitive. Of course it was necessary to have a plot of photodiode dark current for each of the photodiodes.

As an alternative to this method of measuring flux distribution, a single photodiode coupled to the specimen plane via an optic fibre was used. This is a much simpler piece of apparatus but has the disadvantage that the process of mapping the specimen plane for flux distribution is much slower. The method avoids the problem of sensor heating and subsequent drift, by isolating the diodes from the "hot" region, just as in the power measurement system. The photodiodes may be placed in a temperature controlled environment some distance from the specimen plane. However the drift of the photodiodes was not found to be a problem when they were placed in a simple die-cast enclosure with the amplifier. **Fig. 2.16** shows a photograph of the box containing the amplifier and photodiode together with the fibre optic

coupling. A specimen sized disc with holes at discrete intervals was used to fix the end of the optic fibre during the mapping process. The results of the flux mapping exercise with the second reflector system are given in **Chapter 7.**

The single photodiode/amplifier system was finally chosen as the preferred method of flux mapping due to the instabilities in response which were noted for the multidiode system. It appeared that even with the soda lime glass isolating plates, that some heating of the diodes was taking place, which in turn was causing shifts in their response.

2.6 Design of Heating System Utilising Quartz Halogen Lamps

2.6.a First Reflector System Design

The design of the reflector system had to take into account two major requirements, namely that the system should provide adequate flux levels at the specimen plane and also that the flux should be reasonably uniform at this plane. It was apparent that some form of analysis should be performed to enable the reflectors to be properly set up to ensure that these requirements were met. In order to simplify modelling, a well defined mirror form was chosen, that of the parabola. Of the three most basic mirror forms, the circular, the parabola and the elliptical, the parabola seemed to possess the most favourable features. With the circular mirror form, any light emitted from a source placed at the centre, will return to the centre. The resulting beam from such a source/mirror combination will have the same characteristics as a plain source but with double the intensity in the forward direction (away from the mirror). The ideal elliptical form mirror has the characteristic that a source placed at one of the foci will have its output directed to the other focus point within the ellipse. The parabola on the other hand has the feature that rays originating at the focus will leave the mirror parallel to the axis of the parabola. One advantage of using the parabolic mirror form is therefore that the focus to incident plane distance, is not critical due to the parallellism of the output beam.

Given the advantage of the parabolic mirror form as outlined above, it can be seen that, with no constraints on the lamp to specimen plane distance, it is feasible to have several sources and reflectors operating together to produce the required flux levels and uniformity of flux. However, unlike the circular (or spherical), or elliptical mirror forms, the parabolic form is never closed. As the parabolic mirror increases in size (assuming fixed focal point), an increasing proportion of the light emitted by the source is intercepted by the mirror and forced to travel parallel to the axis, and thus the proportion of light output which is not parallel to the axis decreases. Considering the equation for the parabola it became evident that in order to maximise the parallel portion of the output beam, while maintaining reasonable flux levels, that the focal distance should be minimised.

A study of available lamps (**Ref. 16**) showed that high output, photographic lamps seemed to have the required characteristics, in terms of output and dimensions. A further consideration which arose was that of lamp life. Two ratings are commonly available for photographic lamps, those for use with colour film balanced for 3200K, and those for film balanced for 3400K. Obviously the lamps rated for the higher temperature are shorter lived. Approximate lifetimes are around 15 hours for the 3400K lamps and from about 50 up to 400 hours for the 3200K lamps. Testing periods in excess of 320 minutes were estimated for the thermal conductivity tests proposed. A figure of approximately 2 minutes per cycle for the thermal cycling tests, with 1000 of such cycles, gave a total test period for this usage, of at least 2000 minutes (33.3 hours). The 3400K lamps would therefore only just execute the 1000 cycles before lamp lifetime became a problem. The increase in the loading of the lamp envelope would obviously decrease the life of the lamps and thus the 3400K lamps would not reliably execute the required number of cycles. The 3200K lamps were thus chosen. The lamps with the minimum envelope size, and of maximum output per unit filament

length were those of the P2/12 type (1250W power output lamps). The lamps have an envelope diameter of approximately 12mm. This implies a minimum focal distance of half of 12 mm , i.e. 6mm, if the lamp is not to touch the reflector and the true parabolic mirror shape is to be retained. **Figure 2.17** shows the calculated mirror efficiency and beam mean flux, which results from varying the focal point of the mirror. It should be noted that the calculation does not take into account such things as :- finite source size, source shadowing, reflection coefficient of mirror surface and non-parallel rays. A further point of note is that a full three dimensional axisymmetric mirror is assumed. This assumption is only valid for one plane, for the case of this type of lamp. While the lamp may be treated as approximating to a point source in one plane, it must be approximated to a linear, or line source, in the plane orthogonal to this.

A computer model was produced to examine the effects of combining more than one source and mirror, and the result that this has on the flux at a given specimen plane. This model takes into account the contribution from non parallel rays, but does not take into account the size of the source, nor the linear form which the chosen lamps have, in the plane which contains the axis of the filament. A more detailed description of the program and its results are given in **Appendix 3.**

Initially it was decided to fix the focal point of the mirrors at 10mm, with an aperture of 80mm. Heat transfer calculations showed that some form of mirror cooling was essential if an aluminium alloy was to be used for the mirror material. Water cooling was chosen to minimise noise, eliminate dust generation, and to be compatible with the specimen carrier coolant system. Four identical parabolic mirrors were produced from solid aluminium alloy blocks using a numerically controlled machine. After machining, the blocks were polished using graded grits and pastes and a male rubbing block of parabolic form. Final polishing with Brasso patented metal cleaner completed the mirrors. In addition to the parabolic mirrors, four barn door type reflectors were

produced to reduce the side losses from the mirror assembly. These mirrors were produced from flat aluminium alloy plate, into which cooling channels had been milled. Again the reflecting surfaces of these mirrors were finished to a high polish. **Figure 2.18** is a photograph of the first reflector assemblies and the barn door side reflectors in position.

2.6.b Second Reflector System Design

Initial calibration runs showed that the variation of flux across the specimen plane was around ± 5% , and indicated low flux levels of around 150 KWm^{-2} . As one of the aims of the system was to provide an even distribution of flux, the variation measured was encouraging. However, while the flux levels recorded were sufficient to allow thermal conductivity testing to be carried out, the level was insufficient to allow thermal shock simulation. At this point it was decided to reconsider the design of the lamp/reflector assembly for the case of thermal shock testing.

The low levels of flux obtained with the first reflector assembly were attributed to the linear nature of the sources and reflectors, together with the angle of the barn door side reflectors to the axis of the specimen. On detailed re-examination of the system as a whole, it became apparent that the high levels of flux required for thermal shock testing could not be achieved without changing the lamp/reflector assembly.

Two major factors which influenced the design of the second reflector assembly were :- the time constraint for design and build, and relaxation of the requirement for even distribution of flux at the specimen plane. The production of a fully three dimensional computer model of the lamp/reflector assembly, to accurately predict the flux distribution at the specimen plane, was considered to present too lengthy a task to be achieved in the available time, within the overall work schedule. Accepting that a complex model was out of the question, a simpler analysis scheme had to be found. However, it was desirable that some degree of accuracy should still be retained and for this it was considered that simple, manual,

ray tracing could produce the accuracy required.

Obviously, no ray tracing could commence until some ideas had been sketched out to examine the factors most likely to affect the flux at the specimen plane, and indeed what overall form the reflector should have. Starting from basic lamp considerations, it was evident from the lamp data sheets that the quartz envelopes had been designed to operate below some maximum flux throughput. This was presumably based on an assumed absorbtion factor for quartz for broadband blackbody radiation, on assumed external heat transfer coefficients likely to be prevailing under all lamp operating conditions, and the maximum envelope operating temperature considered to be sustainable for the life of the filament. These considerations led to the conclusion that increases in lamp envelope loading, through multiple passages of the beam, should be avoided, if the lamp life was not to be markedly reduced. A further point, noted on examination of the lamp data sheets was that the flux throughput, at the envelope was around 250 KWm^{-2} , which is below that which was required for thermal shock testing (above 400 KWm^{-2}). One lamp, on its own, without any reflector assembly would therefore be incapable of providing adequate flux at the specimen plane. Considerations such as :- lamp to specimen plane distance, envelope loading, specimen size to source size ratio, and reflector losses, also indicated that one lamp, even with a reflector, would be unlikely to provide the flux levels required. A number of possible lamp configurations were next examined, bearing in mind the specimen size preferred, together with the minimum acceptable distance between lamps (set by the lamp envelope diameter).

It has already been stated that the 1250W lamps had the highest power per unit length of the 12mm diameter types, however, the highest power per unit length available, was from the 2000W (P2/27)lamps, albeit with an envelope diameter of 30mm. The departure from a parabolic reflector form, and the relaxation of the uniform flux distribution requirement, meant that the large filament, source diameter of around 5mm for the

2000W lamps, was of lesser consequence. One, two, three and four lamp configurations were examined, in an attempt to maximise the specimen plane flux while keeping the envelope loadings down to reasonable levels. Treating the problem rather simplistically, it appeared that maximum flux levels could be obtained with a two lamp system (see sketches in **Fig. 2.19**) The next task was to examine the effects produced by varying the angle between the two reflector cavities in the plane perpendicular to the lamp axes, and to study the effect of varying the shape of the individual lamp cavities.

The ray tracing procedure was somewhat simplified by using a commercial computer aided design package, MACDRAFT, available on the Apple Macintosh computer. A similar procedure was carried out for the plane parallel to the lamp axes. A simplified calculation was carried out to estimate the loss due to passage through the lamp envelopes and a fixed reflection coefficient of 0.9 was used to estimate the incident power on the specimen plane for each of the orthogonal cases. The result for each of the orthogonal planes was multiplied together to give an overall efficiency figure for the transmission of power from the source to the specimen plane. **Figures 2.20** and **2.21** together with **Figure 2.22** outline the procedure and give estimates for the various parameters examined.

As stated above, each orthogonal plane was treated independently. Basically the procedure involved stepping round the source in small angular increments, and noting the number of reflections which occurred before the ray was incident on the specimen plane. The output from the source could thus be divided into that which underwent one, two or three and more reflections before hitting the target. Further, it was possible to estimate how many passes through the lamp envelope were made by each angular region and thus establish a figure for the additional loading which the lamp envelope would "see". **Table 2.1** is a summary of the results obtained, using this simple analysis.

2.7 Specimen Holders

2.7.a Electrical Connections

The use of thin film surface thermocouples would allow the transient surface temperature of the specimen to be accurately monitored. However, some method of attaching wires to the thin films had to be produced. The method had to give reliable, low resistance, low noise contact, but at the same time had to ensure that no damage to the ceramic specimen resulted from the fitting of such contacts. This ruled out any of the methods involving the application of heat, such as soldering, brazing, or spot welding. Further it was necessary to minimise any heat flow paths which might result from the incorporation of a wire to thin film contact on the front face of the specimen , as this would lead to deviations from the one dimensional heat flow which was intended. The solution chosen was to use a multi fingered system which comprised two semi-circular thermocouple metal contact rings with fingers. The fingers presented several contact points of minimal area to reduce radial heat flow away from the front face of the specimen, while at the same time ensuring that electrical contact took place at several positions on the periphery of the front face of the specimen (see **Fig. 2.23**).

Initially, there was some doubt as to whether or not the contact provided by the fingers would be good enough to ensure electrical continuity due to the build up of surface oxide films. There was also concern regarding the integrity of the thin film when subjected to point contacts bearing down on them. Initial results were encouraging and were obtained using chromel/alumel thin films. These tests were obtained at room temperature.

It became necessary to move to noble metal thermocouples as considerable difficulties had been experienced in producing consistent, base metal alloy ,thin films. Subsequent tests on gold and platinum thin films proved that the method was equally suitable for these materials. The long term integrity of this method of joining thin films to wires, has been shown with gold platinum films on disc specimens of ceramic

subjected to over 1000 heating and cooling cycles. However, it should be added that the contacts have since been moved to the side of the disc. This was necessary because of problems associated with the front face clamping disc, which distorted heavily under thermal cycling. The result of this was that the clamping plate would lift from the surface of the specimen and produce intermittent contact.

The method of producing an electrical contact between thin films and wires was used for both the thermal conductivity and the thermal shock specimens, although the geometry of the thin films was adapted for the particular application.

2.7.b Specimen Holder Bodies

Two distinct types of specimen holder were designed and built, one each for the thermal conductivity and thermal shock tests respectively. In both cases, attempts were made to ensure one dimensional heat flow. For the case of the thermal conductivity specimen holder this was essential and indeed was more readily realised. The thermal shock specimen holder presented the problem that an acoustic waveguide had to be fitted to the back face of the specimen which automatically ruled out truly one dimensional flow. However for the case of the plasma spray coated specimens, the presence of a highly thermally conductive substrate, between the insulating coating and the back plane, somewhat reduced the problem. The use of resistive modelling or finite element analyses shows that the presence of the conductive substrate on the cold side of the specimen serves to even out back face cooling boundary conditions on the back face of the specimen. Nonetheless, for the case of monolithic specimens the problem remains. As the initial tests were to be conducted on coatings, it was considered that this source of deviation from the desired situation should receive further attention at a later date when the monoliths were to be tested. Testing of monoliths has since been carried out with this apparatus, **Chapter 8** includes suggestions for improvements to the holder for thermal shock testing.

With reference to **Fig. 2.24** it may be seen that the thermal conductivity specimen holder essentially comprises an outer, water cooled jacket separated from an inner calorimeter section to which the specimen is attached by its back face. The inner and outer sections are connected by PTFE spacers with minimum contact area to reduce conductive side losses from the calorimeter. Radiative losses from the calorimeter, to the outer jacket via the air space created, are minimised by utilising aluminium alloy as the construction material for these items. Aluminium alloy has a low emmissivity, and coupled with the low temperature differential between inner and outer sections, results in low radiative losses.

The front face of the specimen holder comprises a stainless steel ring, behind which sits an electrically insulating ceramic ring. It is this ring which forces the two semicircular sections of thermocouple material down onto the thin film thermocouple.

The thermal shock specimen holder is similar to the holder for thermal conductivity except that there is no inner calorimeter and the back face of the specimen is in direct contact with the water cooled aluminium alloy housing. To accommodate the acoustic emission waveguide, a through hole runs from the back face of the specimen to the outside of the holder. A number of more complex designs were considered which allowed full back face cooling of the specimen in the thermal shock mode of operation. The decision to opt for this system was made in the absence of data relating to spurious noise generated elsewhere in the rig and the possibility that noise arising from the flow of the coolant might present a problem. It was considered prudent therefore to build a simpler holder to start with, in order to identify these problems, and then on the second build to eradicate such problems. A schematic of a possible, improved thermal shock specimen holder is shown in **Fig. 2.25.**

2.8 Specimen Motion

During the early stages of rig design it was

decided that with the chosen method of heating, it was going to be necessary to provide some form of mechanism to transport the specimen from the heating zone to the cooling zone, as it was not possible to easily provide heating and cooling in the same portion of the rig. As an alternative to moving the specimen, motion of the heating and cooling sections about a stationary specimen was considered. Although this layout would have conferred some desirable features, the general complexity of such a scheme outweighed its advantages. This was largely due to the expected masses of the heating and cooling sources.

Having made the decision to move the specimen, the next task was to decide on what form of motion was most appropriate to transport the specimen from the heating to the cooling zone. The major contenders were :- rotary motion - horizontally; linear motion - horizontally; and rotary motion - vertically. These are shown schematically in **Fig. 2.26.**

The high power quartz halogen lamps chosen for the heating source were of the linear variety, i.e. long filament, and it is essential that these lamps be operated close to the horizontal. If this requirement is not adhered to, overheating of the lamp envelope and end cap is likely to result. It was also considered to be easier to have an horizontally disposed array of lamps rather than a vertical one, on the grounds of mounting and adjustment. A further constraint was simply one of rig stability. An attempt was made to keep the centre of gravity of the rig as low as possible. The choice was therefore reduced to either the rotary - horizontal or the linear - horizontal forms. These have the added advantage that running coolant lines to the back face of the specimens becomes somewhat easier.

The deciding factors resulted from considerations of the actuator mechanisms available for providing specimen and water cooled carrier motion. Again, a number of possible choices existed, the major types being divided between those with electric drives and those with pneumatic drives. Hydraulic systems were ruled out on the basis that a separate power

pack would have to be provided, whereas, electricity and air supplies were readily available at no extra cost or complexity.

Actuator speed, force and length of travel specifications, together with ease of actuator control, led to the choice of a pneumatic device. The choice of a linear, rather than a rotational device, was made after considerations of rig layout, together with the wider choice of linear device specifications and availability. It had been previously noted that a recent development in linear pneumatic actuators was the rodless variety available from Origa Ltd. This type of actuator offers the advantage that the overall length of the actuator does not change with piston travel as with the traditional type. This automatically cuts the space requirement needed to accomodate the mechanism by approximately half, this is more evident when considering **Fig. 2.27** , and is ideal where space is at a premium. **Fig. 2.28** shows the air circuit for the pneumatic cylinder and **Fig. 2.29** is a general schematic of the electronic circuit used for the control of the cylinder. **Fig. 2.30** is the timing diagram for the control of the carriage, this figure indicates the edge triggering of the monostables as well as the actuation of the solenoid valves. **Fig. 2.31** is the electronic circuit for precision timing of the carriage control, the output from this circuit is carried over to the circuit in **Fig. 2.32** which contains the two monostables. Finally, **Fig. 2.33** shows the solid state relay circuit which provides the power interface to the air solenoids.

2.9 Test Rig Cooling

2.9.a General Comments on Cooling Systems

The main cooling system comprises two independent circuits, coupled thermally by a heat exchanger. The primary circuit comprises an electric circulating pump, of the centrifugal type, a reservoir for the coolant, and a conventional oil cooler as the heat exchanger. The secondary

circuit is completely isolated from the primary circuit to allow choice of coolant and appropriate additives in the primary circuit, for corrosion inhibition. Mains water is simply connected to the secondary circuit via a thermostatically controlled valve which monitors the temperature of the primary circuit reservoir through a volatile liquid, bulb sensor. Experience with this configuration showed that direct connection to the mains water supply results in large oscillations of the reservoir temperature due to the system thermal lag, it was necessary therefore to limit the flow of mains water to the secondary side of the heat exchanger by the use of a restriction.

For the case of the original, parabolic mirror configuration, there were three main flow paths. As may be seen from **Fig. 2.34** each of the flow paths is monitored for flow, and the output from these sensors connected to the automatic shutdown system. In the event that a pipe should develop a leak or that one of the flexible connecting tubes burst, then a level switch internal to the reservoir trips, and shuts the entire rig off.

To ensure that the reservoir is correctly filled with coolant, a second level sensor is installed which senses an upper, maximum fill level, this is independent of the main level sensor and does not communicate with the shutdown system, and is only used during reservoir filling. A further failure mode is that which might result if the secondary, mains water supply should be faulty. This situation might arise for a number of reasons, such as :- failure to turn the water supply on, before starting the rig, blockage in the pipework or heat exchanger, or simply failure of the mains water supply. As mentioned earlier, the flow through the secondary circuit is intermittent due to the action of the thermostatically controlled valve, this rules out the use of a flow sensor. A pressure sensor in the secondary circuit is also ruled out, as it is feasible that if a blockage is the cause of the failure then when flow is demanded it may not be capable of providing sufficient cooling. The solution to the

problem was to install a simple, bimetal snap switch temperature sensor on the reservoir. If the temperature of the reservoir should rise above a certain limit, for whatever reason, then the whole rig will shut down.

Ideally, the entire cooling system would have been constructed in the same metal, to avoid galvanic corrosion, however this was not feasible. The carrier was fabricated from mild steel, seamless tubing and mild steel blocks, largely on the basis of cost and machinability, although the stiffness of this component was also of importance. The carrier has to cope with very high thermal loadings when the specimen is in the cooling section of the rig, it was essential therefore to ensure adequate cooling of this component. Heat transfer calculations dictated the size of the coolant passages, and although the long sections of the carrier could have been machined from solid it was decided to opt for a simpler solution. Cold drawn seamless steel tubes are available to high tolerances and are less susceptible to damage prior to assembly than pure copper tubes of the same dimensions. The steel tubes also offer advantages in terms of stiffness/weight.

The new reflector assembly, specifically designed for maximising the flux at the specimen plane for thermal shock testing, only has two major flow paths, as the side and main reflectors are combined in one unit. However, the basic coolant system is similar to that for the original reflector assemblies (**Fig. 2.34**). The changeover from thermal conductivity to thermal shock testing, is simply achieved by diverting one of the flow paths to the parabolic reflectors, closing the other flow path off, and placing a shorting link across the flow switch for the path closed off. It is of course essential that this link be removed when reverting to the thermal conductivity test set up. **Fig. 2.35** shows the internal flow paths present in the new reflector assembly.

For both the case of thermal shock and thermal conductivity testing, a "tee" connection with taps on the carrier, provides a coolant path to the specimen holder. This

arrangement allows the coolant supply to the specimen holder to be controlled, or shut off completely should it be necessary to remove the holder from the rig.

2.9.b Thermal Conductivity Cooling System

The purpose of this independent cooling system is to provide a controlled flow of pure deionised water to the calorimeter section of the specimen holder. It was essential to ensure in the design, that the flow rate could be manually set and that this flow rate would remain fixed throughout the thermal conductivity test. **Fig. 2.36** shows this cooling system schematically. Reservoir "1" provides, together with its overflow pipe, a constant head to the manual flow control valve. This head is maintained to better than ± 2mm on a total head of 2000mm this implies an error of ± 0.1%, assuming fixed coolant temperature. However, the pressure head is actually a function of ρ(density) , g (gravitational accel'.) , and h (the pressure head), with ρ temperature dependent. Variations in temperature will also affect the viscosity of the fluid and hence the flow rate for a given head, the temperature of the fluid in the top tank is therefore controlled. Temperature control of the fluid is provided by a temperature sensor, electric fan and a water to air heat exchanger.

To obtain the highest possible accuracy for the measurement of heat flow through the specimen it was necessary to consider carefully the likely sources of error. The total error in the determination of thermal conductivity, using the chosen method, arise from several sources. Departure from one dimensional heat transfer through the specimen is one source of error. This may arise either from non isothermal heating and cooling surfaces on the disc specimen, or may result from side losses from the specimen. Side losses from the specimen were reduced as much as possible by including an air gap around the periphery of the disc, and by ensuring that the thickness to diameter ratio of the specimen was less than 0.2 . Somers and Cypher in **Ref. 17** give an analytical

expression to estimate the error due to this ratio taking into account the nature of the specimen peripheral section. A compliant layer on the back face of the specimen was allowed for in the design of the test apparatus and, as such, isothermal conditions on the cooling side of the specimen are a reasonable assumption. The errors due to non isothermal conditions pertaining at the hot side of the specimen were examined using finite element techniques. The boundary conditions were comprised of imposing a "cosine like" flux profile on the heating side of the specimen, with various amplitudes of the cosine profile. The cosine profile was added to some mean value, such that although the amplitude of the cosine section was varied, the area mean flux imposed on the specimen remained the same. This allowed variations in the surface temperature to be examined as the flux profile was altered, for the same heat throughput. Further details of this analysis are to be found in **Chapter 6 section 6.1.c**

Obviously, the measurement of heat flow through the specimen is critical in the determination of thermal conductivity using this method, this is monitored using the calorimeter system already described. As already mentioned, it is important to know accurately the coolant flow rate for the calorimeter, it is also necessary to monitor the temperature rise of the coolant on passing through the calorimeter, utilising either sheathed thermocouples, or platinum resistance thermometers. The absolute accuracy of thermocouples is not as high as may be obtained with platinum resistance thermometers. However, the differential accuracy of the two types is similar. The size of thermocouple temperature sensors may be smaller than that of platinum resistance types and thus less prone to conduction errors along the sheath. The matching of the thermocouple sensors is carried out by inserting the two sensors to be used, into an isothermal block and placing this in a well stirred water bath. The temperature of the bath is varied over the temperature range expected, and, allowing for settling time the differential output from the two sensors is examined using a high sensitivity

microvoltmeter. The particular unit used was a Ferranti auto-zeroing voltmeter chip (Type ZN 451) with a front end amplifier of gain 50 . This circuit allowed a resolution of 1μV which is equivalent to a temperature differential of approximately 0.025°C using type K thermocouples. The second system for differential temperature measurement was based on a commercially available platinum resistance differential panel meter, from ANCOM Ltd. The D6000 series meter is capable of a resolution to 0.001°C, although its absolute accuracy is somewhat lower, at around 0.03°C. This unit was used in conjunction with 1/10th DIN specification sheathed, platinum resitance probes, which have an absolute accuracy of 0.03°C. Unfortunately, this system was only capable of measuring a maximum differential of 20°C, or more precisely, 19.999°C. The flow restrictions which were present in the calorimeter circuit (largely as a result of the fine flow passages in the calorimeter itself) limited the flow rate with the gravity fed coolant supply. This in turn meant that differential temperatures above 20°C were found at the higher flux input levels. Suffice to say that both platinum resistance and thermocouple gauge techniques have ben used and provide a degree of cross checking on the values of differential temperature.

Mass flow of coolant through the calorimeter was measured using a simple weighing technique. This technique comprised of allowing the system to settle thermally, and then to weigh the coolant throughput over a known period of time. The error in the measurement of heat flow was estimated to be less than 0.3%, from the combined errors associated with :- coolant mass, time for the given mass to flow through the calorimeter, and the temperature rise of the coolant, and also the assumption that the specific heat remaining constant over the coolant temperature range. A plot of specific heat, viscosity and density, versus temperature, are given for water, in **Fig. 2.37** .

2.9.c Temperature Difference Across Specimen

This was another potential source of error in the

determination of thermal conductivity using this method. The back face temperature of the specimen was monitored using a standard type K sheathed thermocouple. The thermocouple was of small physical dimensions to minimise disturbances in the heat flow path, and being of standard type, simplified the conditioning of the signal, to provide an accurate value of back-face temperature. However, the front face thin film thermocouple was not constructed of standard materials and both calibration and stability testing of the gauge was necessary. The reproducibility of the thin film thermocouples used for thermal conductivity testing is more critical than for thermal shock testing; however, the test method adopted for the thermal conductivity test thermocouples is the same as used for the thermal shock test thermocouples but with more attention paid to departure from linearity, and reproducibility.

A detailed assessment of the error sources and their estimated magnitudes arising from a disc based system such as that just described, is to be found in Pappas' thesis **(Ref. 10)** . **Chapter 7** contains thermal conductivity results which have been obtained, together with additional comments.

2.10 Automatic Shutdown System

In either the thermal shock or thermal conductivity mode, the test rig was required to operate for long periods of time largely unattended. An automatic shutdown system was considered essential both on the grounds of safety and in the event of system failure. The original lamp/reflector system adopted for thermal conductivity testing consumed about 5KW maximum, whereas the later lamp/reflector system consumed about 4KW maximum. Of necessity, the flux at the specimen plane is high and so adequate cooling around this area was critical. For this reason several sensors were incorporated to monitor both coolant flow and temperature, to ensure that, should failure occur, then safe shutdown of the test rig would take place. Details of this instrumentation are given in the preceding section on rig cooling.

From the standpoint of safety it was necessary to consider the possibility of unsupervised use or tampering with the rig. The high flux densities present at the specimen plane are of the same order as those output by low to medium power lasers, it was therefore required to prevent personal injury which might be caused by exposure to such an intense source of radiation. Microswitches were fitted to the door which allows access to the heating chamber, such that if the door were inadvertantly opened with the rig operating, that the rig safely shut down. It was also necessary to incorporate a microswitch trip on the section of the carrier into which the specimen holder fits. This was to guard against removal of the specimen holder when the lamps are operating. Removal of the specimen holder would be sensed as a reduction in temperature on the front face of the specimen and the lamp control circuit would ramp the lamp power to maximum, unless a shutdown system was incorporated.

The pneumatic actuator is powerful enough to cause injury to hands or fingers should they be trapped between the carrier and the rig frame, when the carrier is in motion. This required adequate guarding and microswitches placed between the guards and the rig frame.

A further requirement was that if any of the following should fail, then the test was to be aborted, these are :-

i/. loss of air supply - this was monitored by a simple in-line pressure switch.

ii/. lamp failure - Hall effect current transducers mounted around the power lines to the lamps provided the necessary signal here. The transducers were powered from the ±15V supply contained within the control circuit box.

iii/. front face thermocouple failure - the custom circuit to condition the signal from this thermocouple was provided with a section similar to that found in commercial circuits for standard thermocouples - see below.

iv/. back face thermocouple failure - the

conditioning for this thermocouple incoporates a chip with on-board thermocouple failure sense. This comprises a high value bleed resistor such that if the thermocouple should fail then one of the inputs to the front end differential amplifier floats up to one of the supply rails. The output of the amplifier is sensed, and this failure condition produces a fail signal from the chip which may be used to shut the rig off.

v/. actuator malfunction due to excessive friction - failure to execute traverse of the carrier from heating to cooling zones within a predetermined time was detected. Monostable circuits in conjunction with simple switches and logic gates provided an error signal if correct operation was not maintained. The logic diagram for this is given in **Fig. 2.38**, with the electronic circuit details in **Fig. 2.39**. **Fig. 2.40** is the timing diagram showing the circuit operation.

It was necessary to provide shutdown of the rig when the predetermined number of thermal shock cycles had been executed. An electromechanical counter provided a non-volatile indicator for the total number of cycles, it also provided a relay output when the set value of cycles had been performed.

Whilst it was necessary to provide a number of inputs for shutdown, on the basis of safety and correct operation of the rig, it was also thought prudent to provide further channels to indicate the status of other functions which, while not critical to the operation of the rig, would nonetheless be useful. A total of 18 inputs were provided which would signal shutdown of the rig, and a further 6 channels to allow monitoring of non-critical functions. A schematic circuit diagram of the automatic shutdown system is given in **Fig. 2.41**. The logic of the circuit is arranged such that should failure of this circuit's power supply result, or if a wire feed should work loose, or break, then the system should fail safe. A non-volatile latching relay is present on the output of the circuit such that if a failure should occur, then the system will remain shutdown until the fault is

examined and the system manually cleared. This feature was incorporated for situations which might arise where a failure results, shutting down the rig, the fault clears and the rig supply is re-established, only for the rig to fail again. This circumstance might, for instance, take place if the coolant temperature sensor tripped, due to insufficient mains water supply to the heat exchanger. The rig would shutdown and the coolant temperature go down to below the trip point. A non-latching system would re-establish the rig supply, and the rig would fail again as the temperature trip operated. Undesirable cyclic behaviour, such as that described, was avoided by the use of a latching relay on the output with a manually operated reset.

All of the inputs to the automatic shutdown system are buffered. To avoid false triggerring of the system, each input is RC coupled to the buffers. The time constant of the RC coupling was chosen to ensure that reliable action of the trip would take place if the error signal was present for more than some predetermined time. This input configuration allowed for contact bounce which might occur on external relay contacts and noise on the unshielded lines. The logic which is connected to the monostables and the end of travel sensors, for the detection of failure on the carriage movement, will produce zero going spikes on every travel of the carriage. This condition may be seen by examining the timing diagram in **Fig. 2.40** , however, these spikes have a width of less than 200nSec and as such are filtered out by the input stage of the shutdown system.

2.11 Operational Problems related to the Quartz Halogen Lamps

Although some care had been exercised in the design of the reflector assembly to minimise overheating of the lamps, a problem arose with respect to the end seals. The lamp literature specifies that the temperature of the end seals/electrode cap should not exceed about 350°C . It was evident that this temperature was being exceeded when lamps from two separate sources both failed from this end seal

region. Inspection of the lamps showed evidence of some problem around this region. A detailed thermal analysis of the lamp was made in an attempt to identify solutions to this problem. The analysis and its conclusions are to be found in **Chapter 6 , section 6.4.b .**

2.12 Estimation of Errors in the Determination of Thermal Conductivity

An estimate of the errors which might arise from the use of the apparatus described, is given in **Ref.10 , Table 3.3** . Of the nine sources of error quoted in this table, none are greater than 1 % , with the overall error quoted as being 6.75 % . However, it should be remarked that these estimates were based on theoretical considerations, the basis of which was that any departure from one dimensionality was due purely from specimen side losses. Initially it was thought that the light sources could be arranged to provide a very uniform thermal input to the specimen, and indeed this was the case with the first lamp/reflector design. This first design gave typical specimen front face flux variations of less than ± 5 % (this gave the input for the original F.E. analyses which are shown in **Chapter 6 , section 6.1.c**). Unfortunately the flux levels were inadequate for thermal shock testing, hence the redesign of lamp/reflector assembly. One of the consequences of this which did not come to light until much later was the large variation in specimen front face flux, of the order of 300 - 800 KWm^{-2} . It is to be expected therefore that this source of non-uniformity will contribute the most to the error in the determination of thermal conductivity. Also it is considered that rather than quantify this error, it would be better to invest effort into devising a more uniform heat source for the thermal conductivity apparatus.

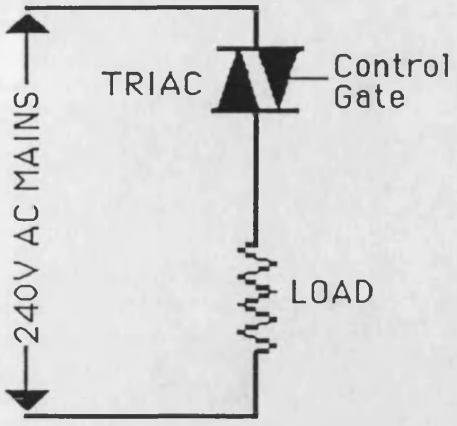

Basic Circuit for Power Control

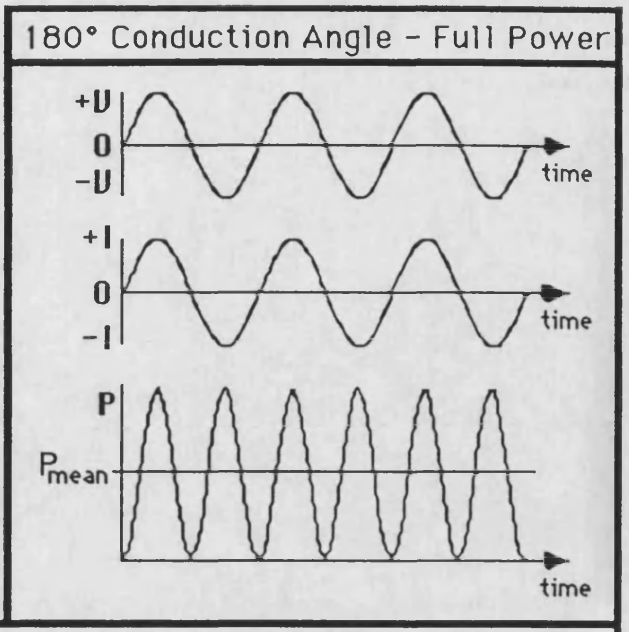

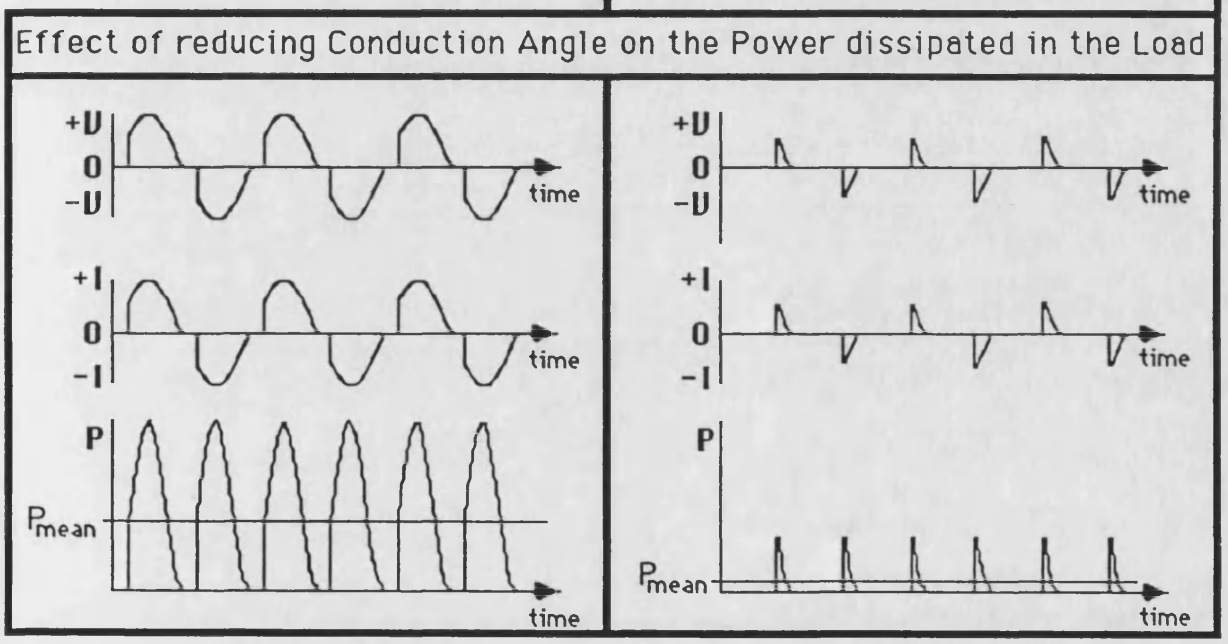

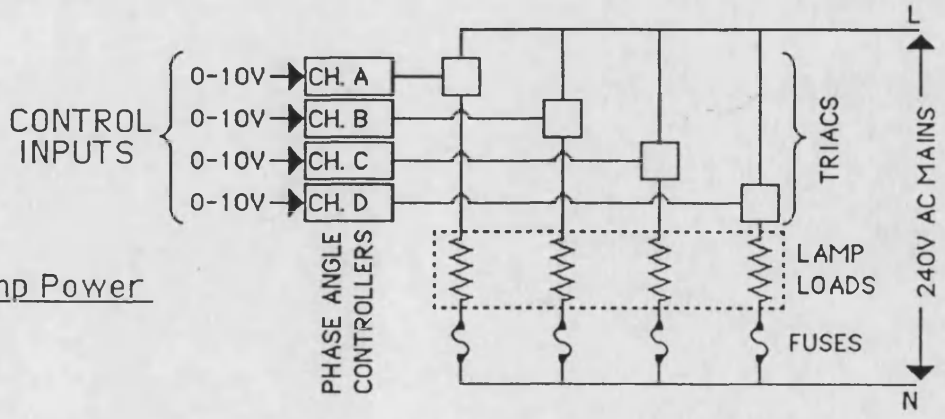

Four Channel Lamp Power Control System

Figure 2.1 - Phase Angle Power Control

Normalised Spectral Response of General Purpose
of General Purpose Photodiode RS 305-462

Extracted from R.S. Data Sheet
2135 Dec. 1981

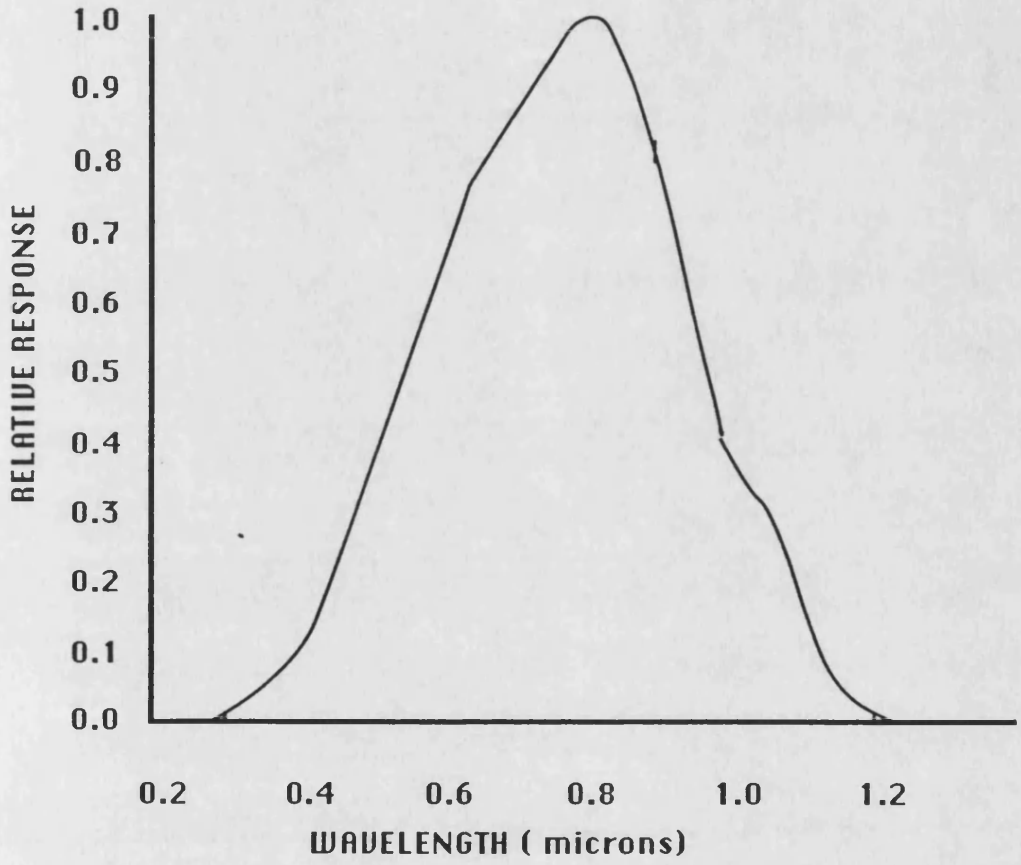

Figure 2.2

Calculation of Photodiode Response to Variation in Lamp Power

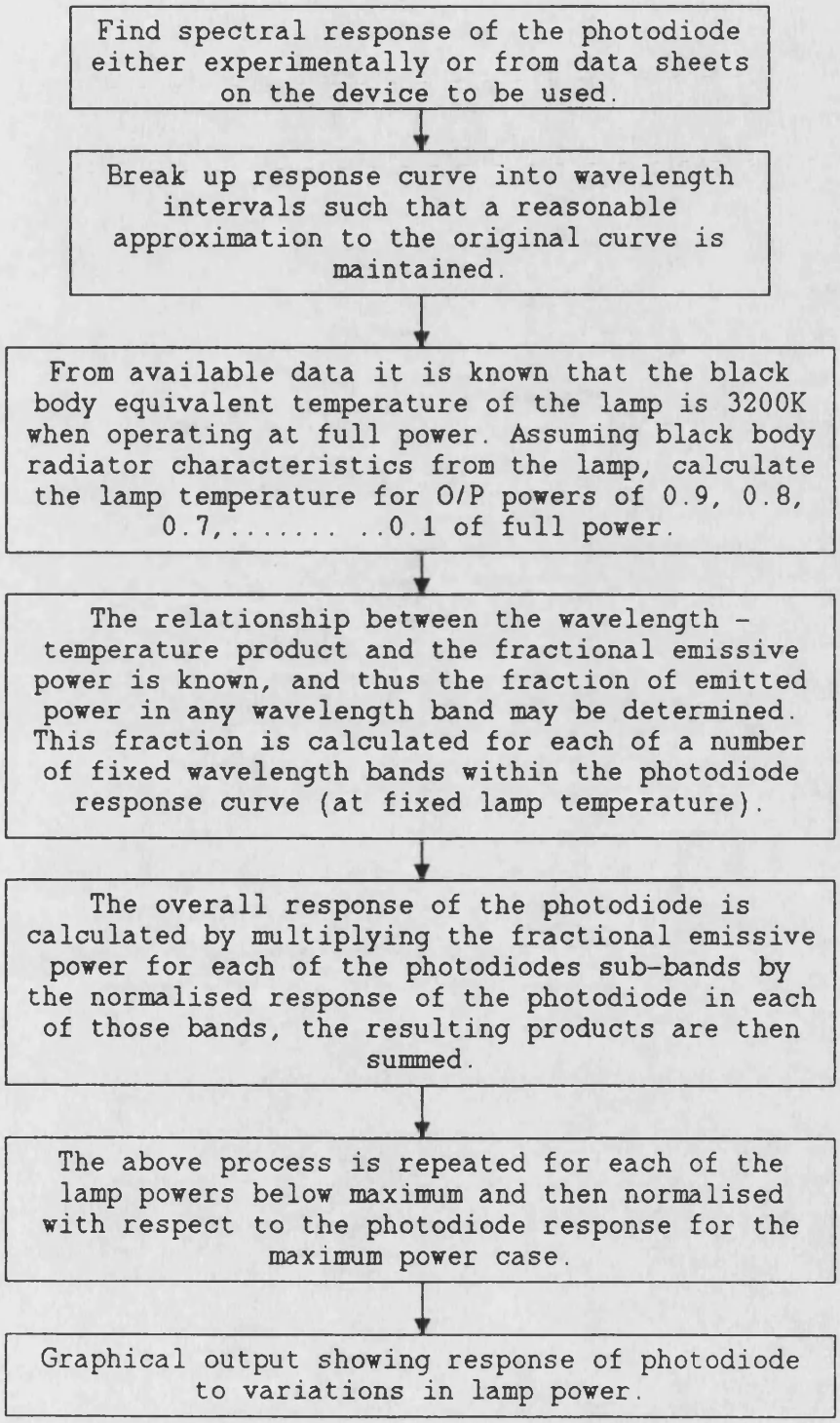

Figure 2.3

Calculated Photodiode Current vs. Lamp Power

Photodiode - General Purpose R.S. 305 - 462
Lamp - P2/12 1250W 3200K Assumed
Black Body Radiator

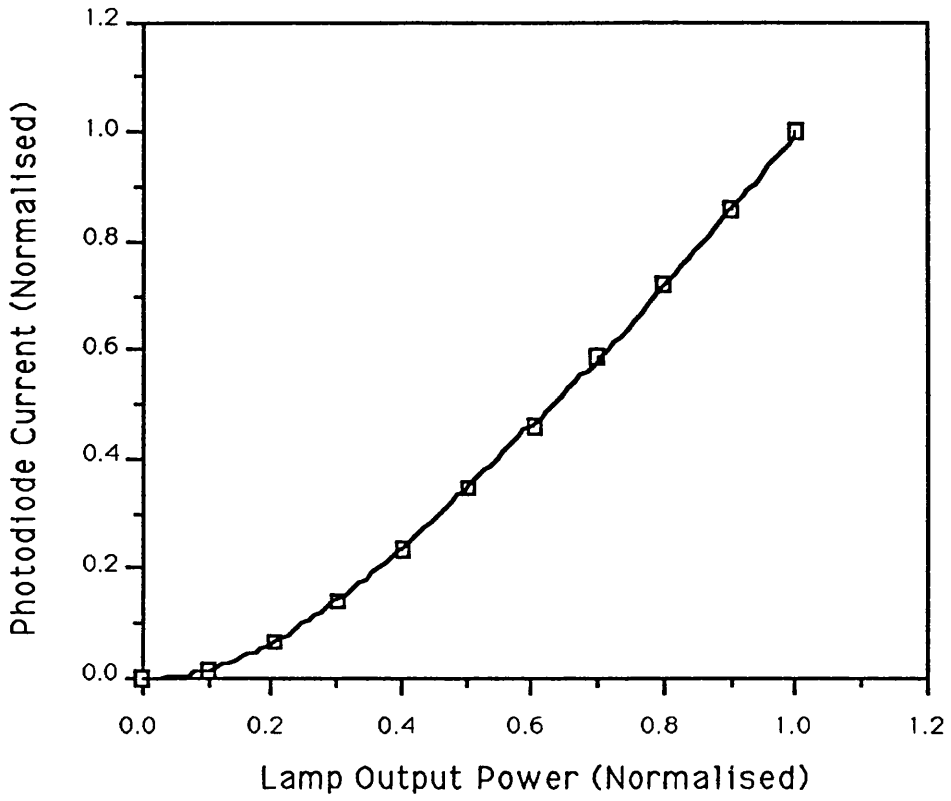

Figure 2.4

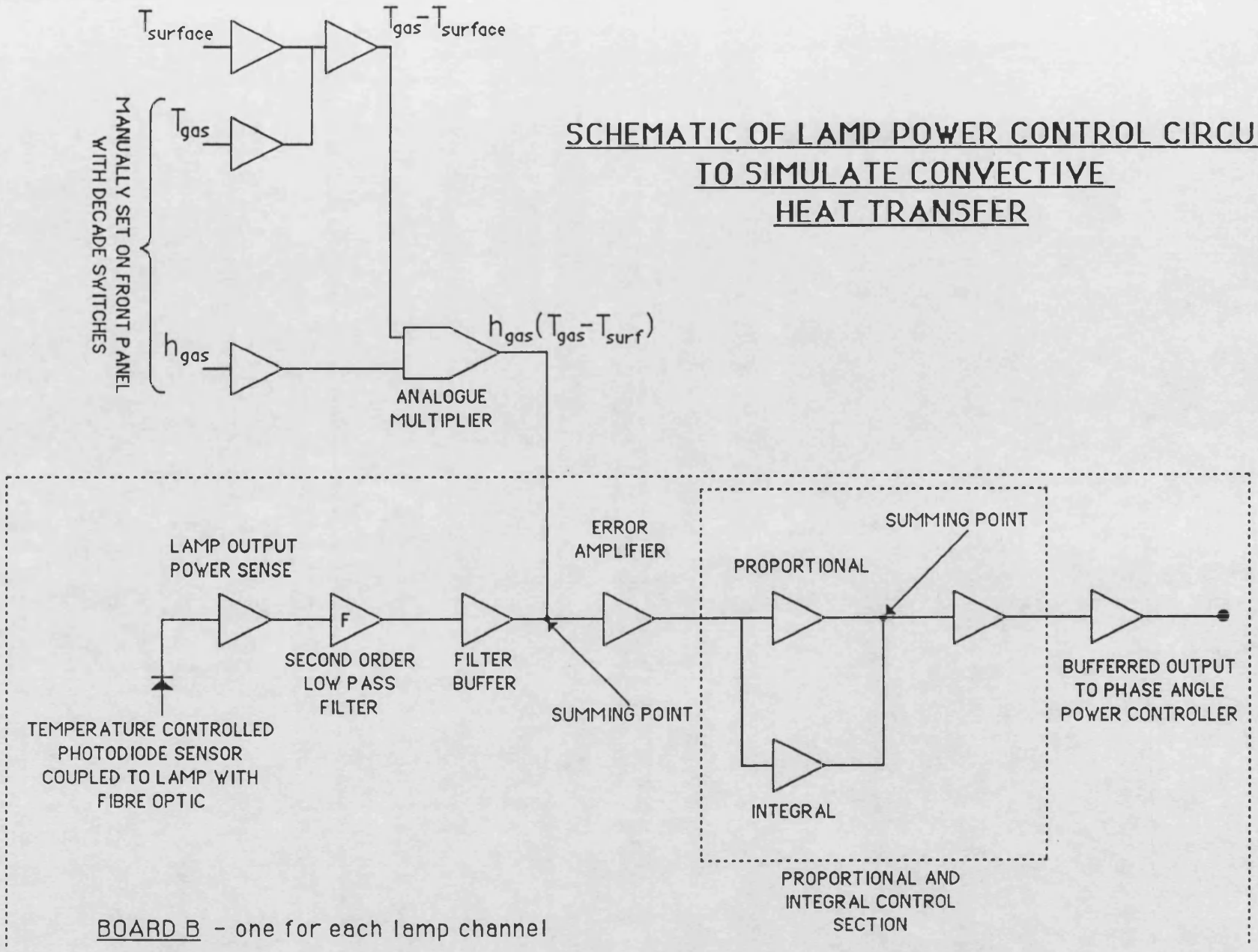
SCHEMATIC OF LAMP POWER CONTROL CIRCUIT
TO SIMULATE CONVECTIVE
HEAT TRANSFER
$T_{surface}$
$T_{gas}-T_{surface}$
T_{gas}
MANUALLY SET ON FRONT PANEL
WITH DECADE SWITCHES
h_{gas}
$h_{gas}(T_{gas}-T_{surf})$
ANALOGUE
MULTIPLIER
LAMP OUTPUT
POWER SENSE
F
SECOND ORDER
LOW PASS
FILTER
FILTER
BUFFER
ERROR
AMPLIFIER
SUMMING POINT
PROPORTIONAL
SUMMING POINT
BUFFERRED OUTPUT
TO PHASE ANGLE
POWER CONTROLLER
TEMPERATURE CONTROLLED
PHOTODIODE SENSOR
COUPLED TO LAMP WITH
FIBRE OPTIC
INTEGRAL
PROPORTIONAL AND
INTEGRAL CONTROL
SECTION
BOARD B - one for each lamp channel

Figure 2.5

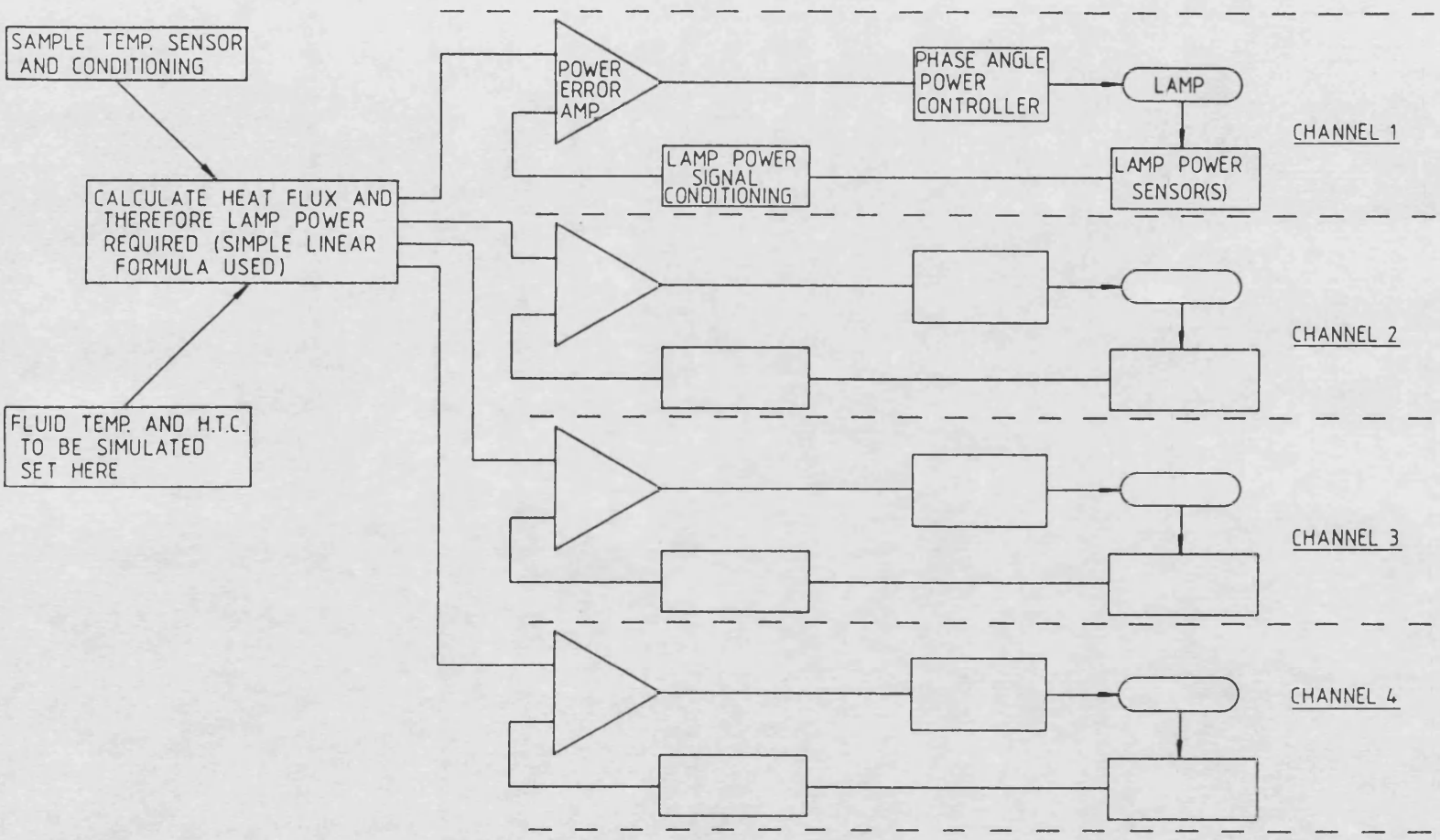

Figure 2.6 – THERMAL SHOCK RIG LAMP POWER CONTROL

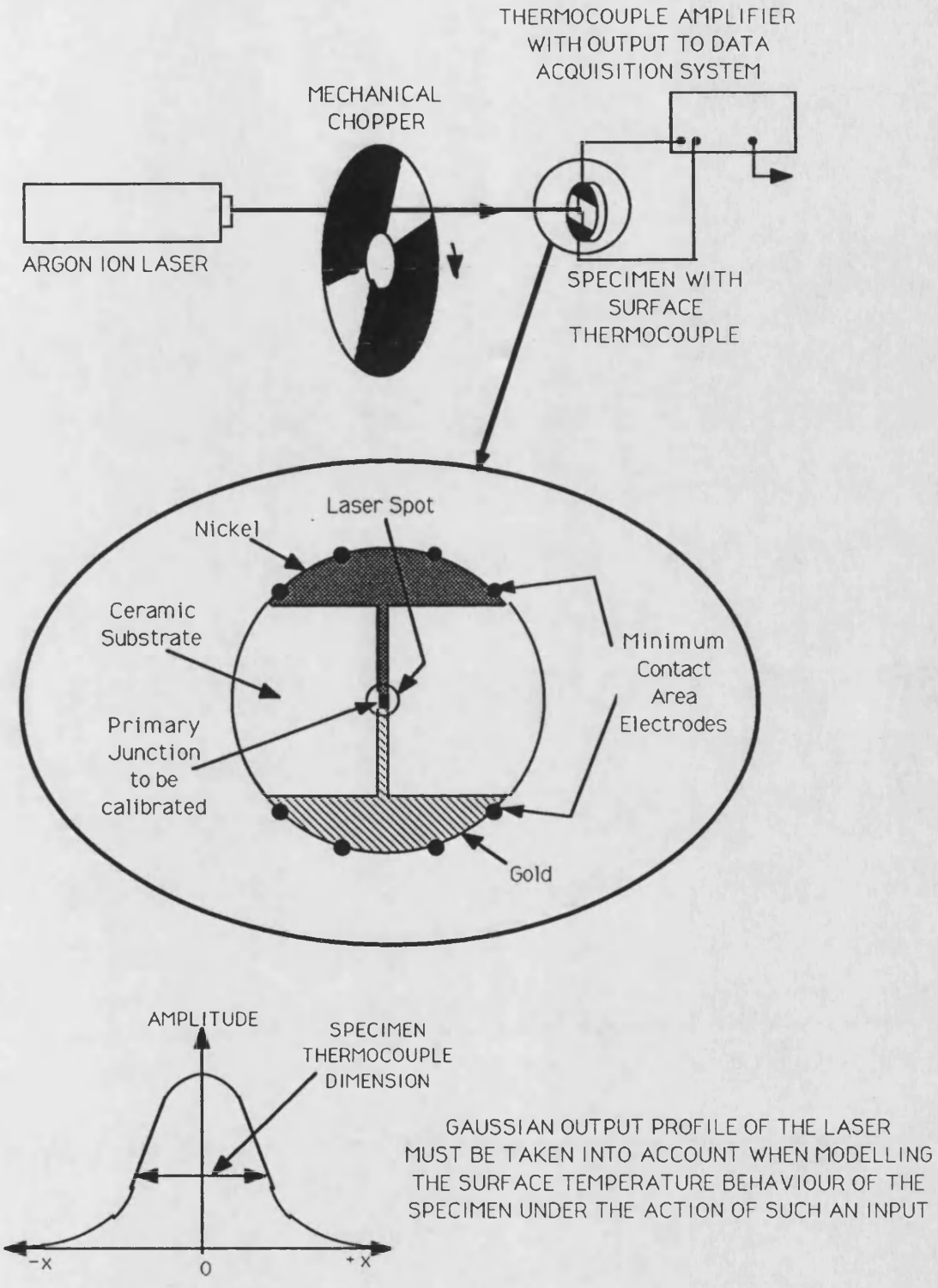

Figure 2.7 - Laser Calibration of Thin Film T/C Junction

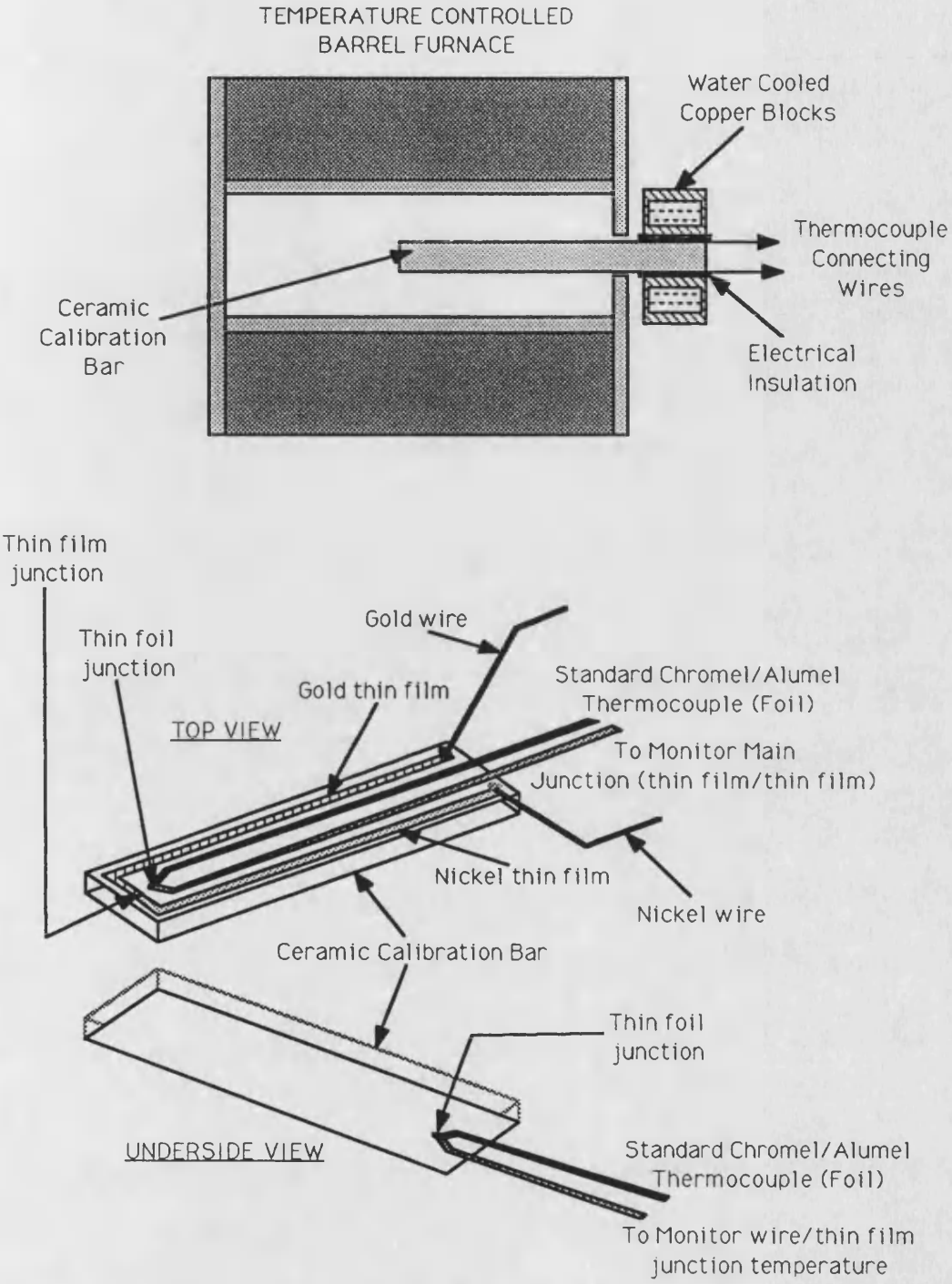

Figure 2.8 - Barrel Furnace Calibration of Thin Film Thermocouples

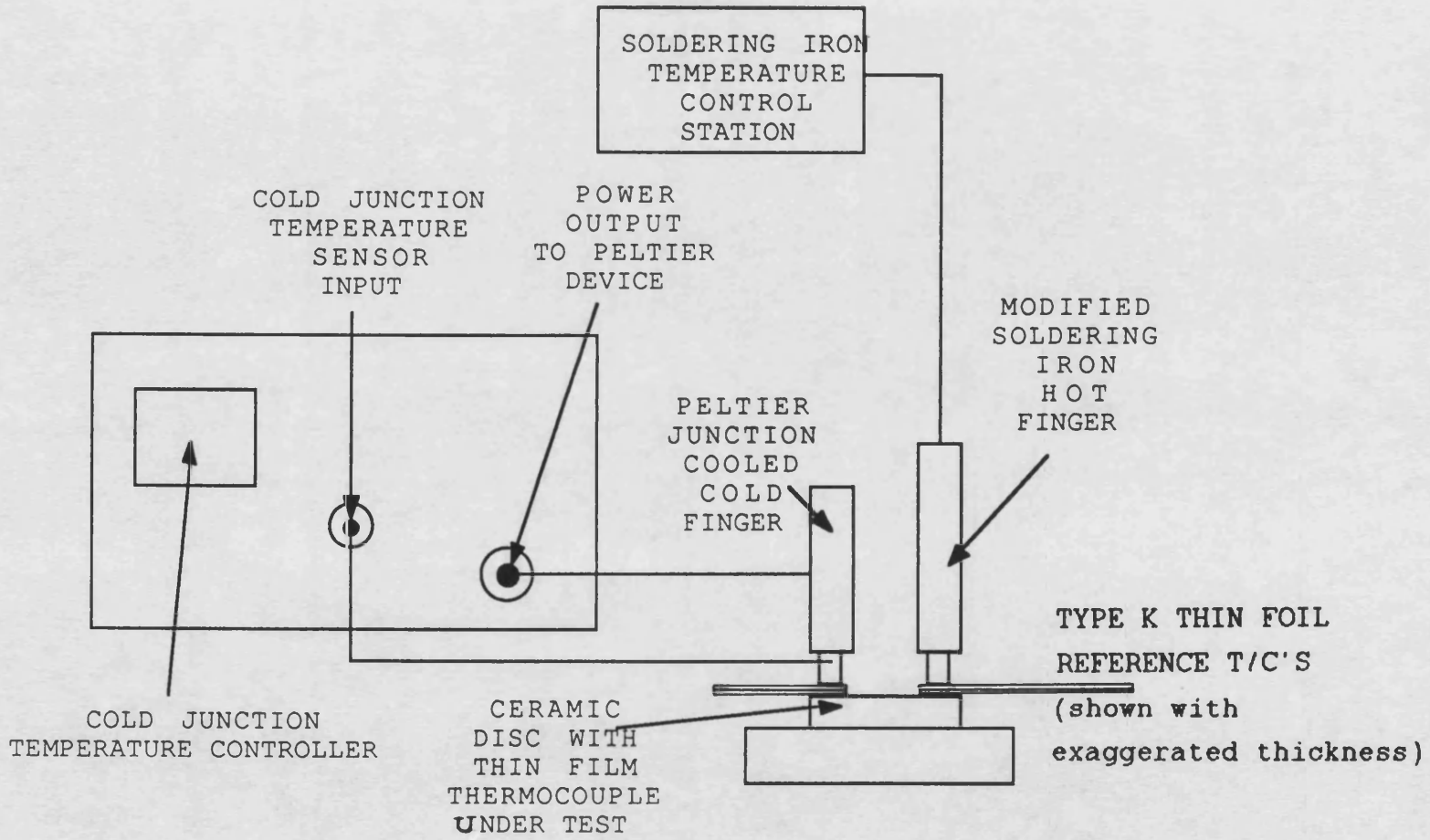

Figure 2.9 - Schematic of Thin Film Thermocouple Calibrator

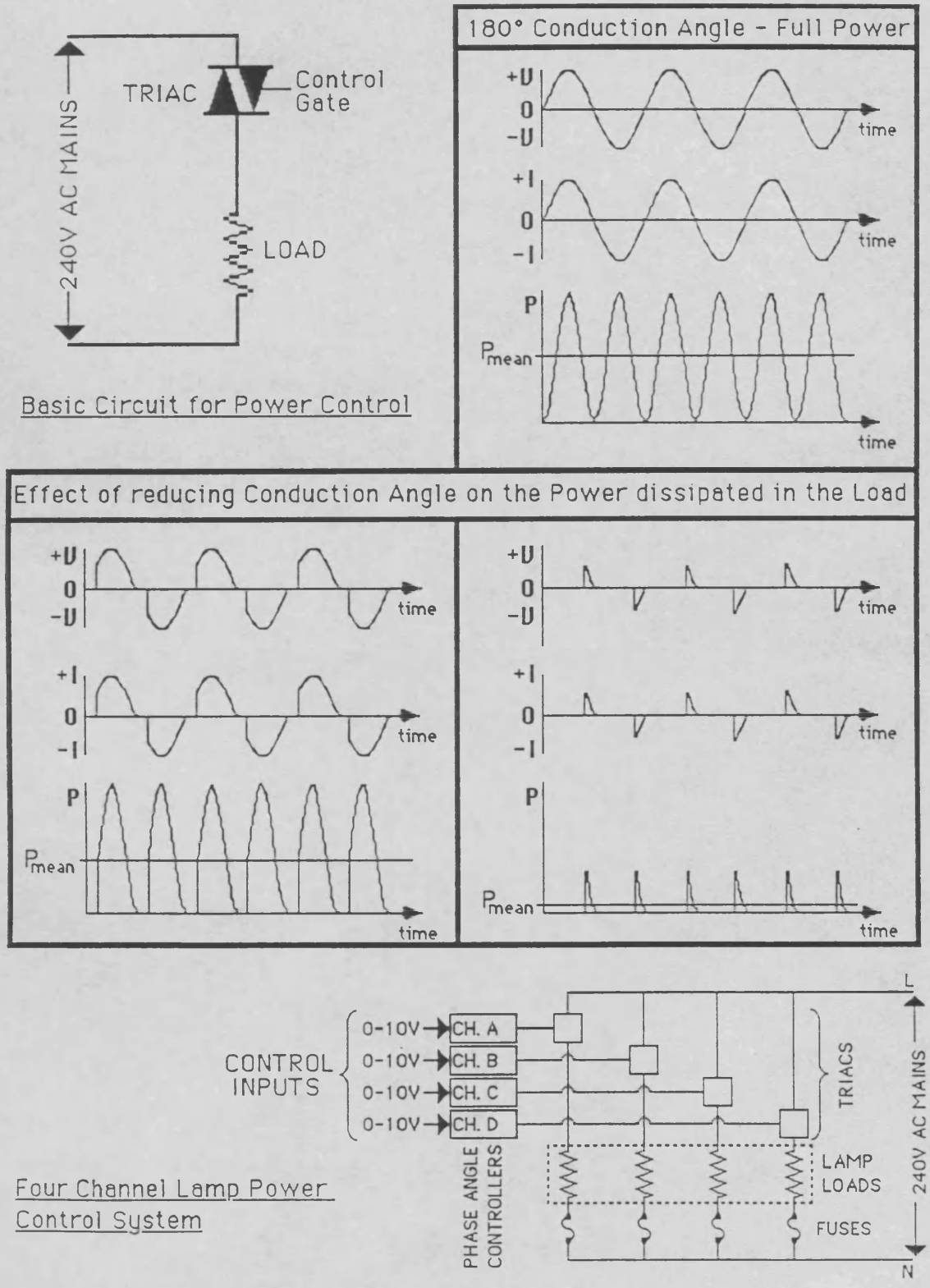

Figure 2.1 - Phase Angle Power Control

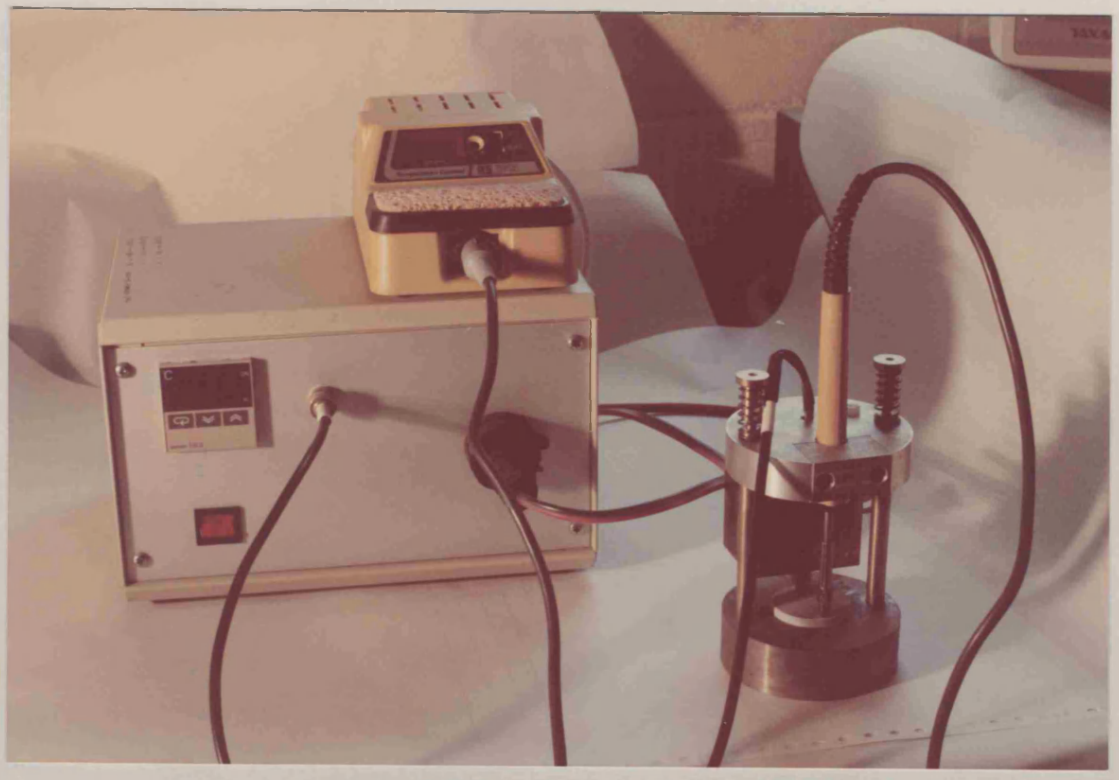

Overall View of Thermocouple Calibrator

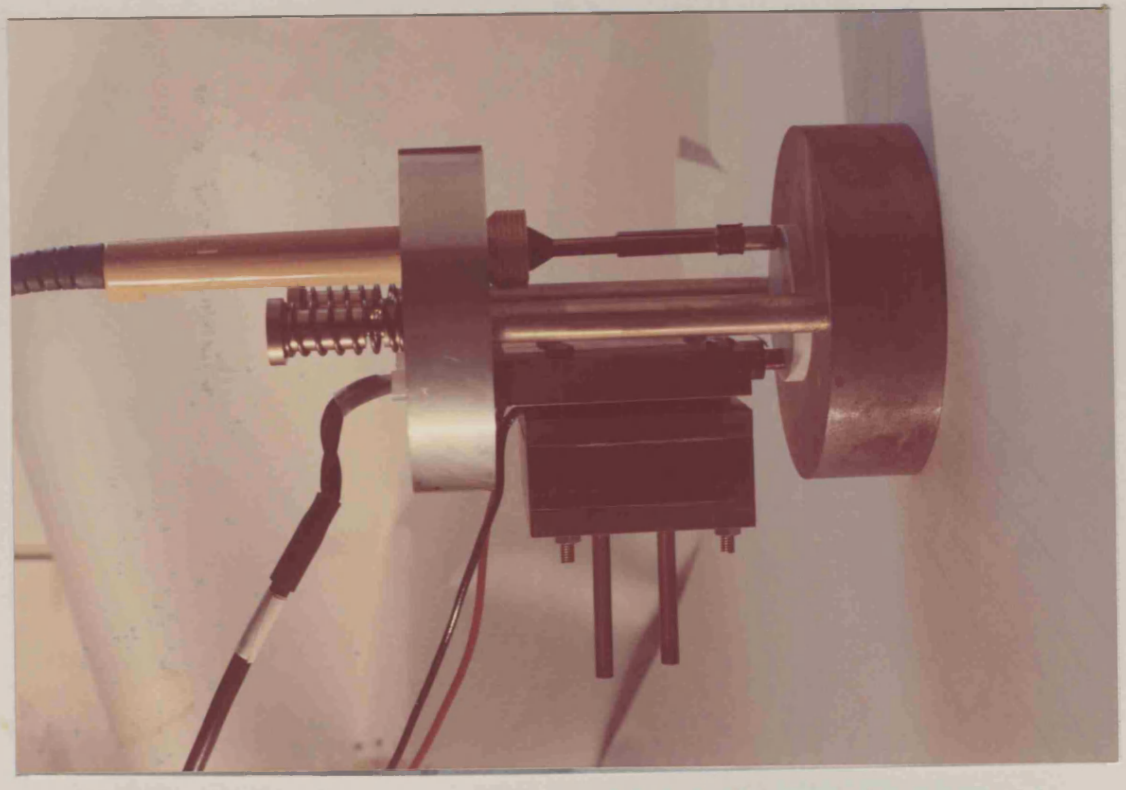

View of Specimen with Hot and Cold Fingers

Figure 2.10 - Thin Film Thermocouple Calibrator

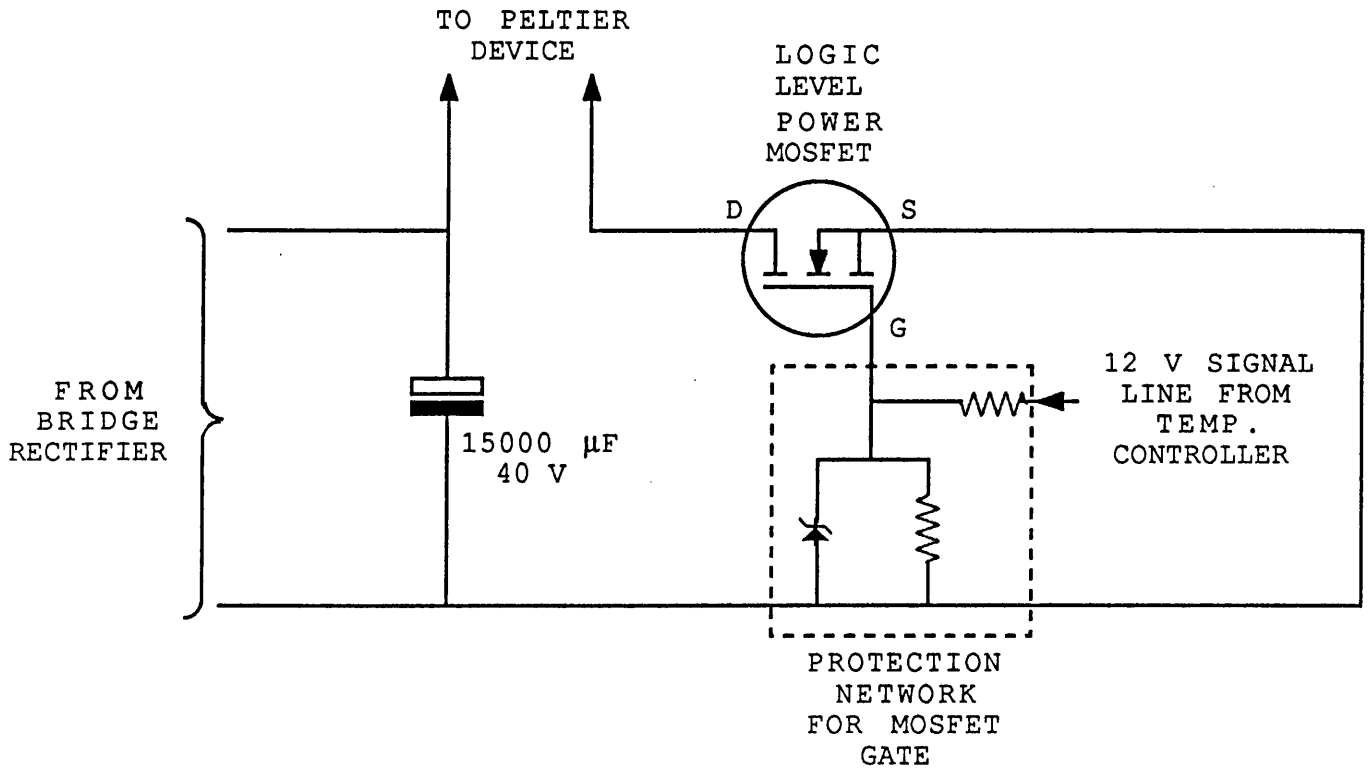

Figure 2.11 - Circuit Diagram for Peltier Cooling Power Supply

Cross Sectional View of Peltier Cooled Cold Probe for Thermocouple Calibration

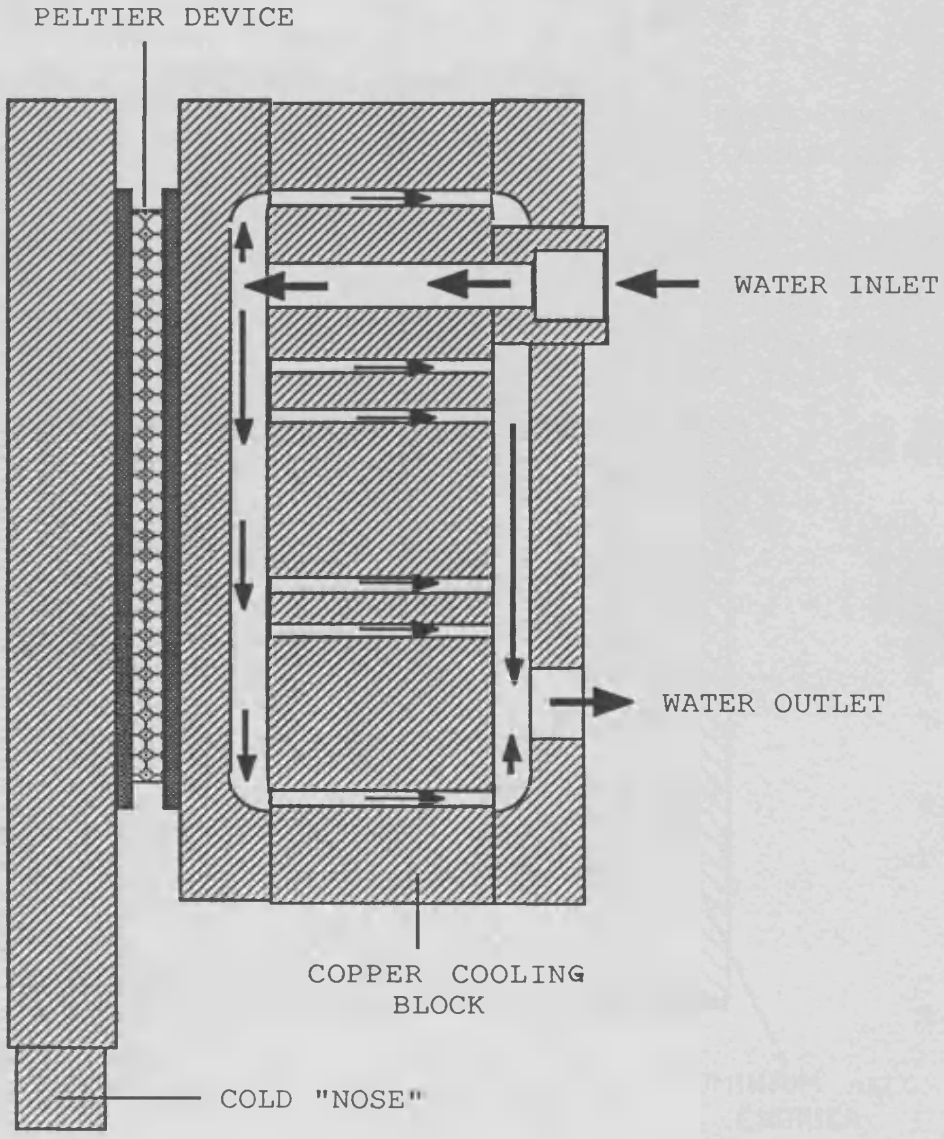

Figure 2.12

Final Scale Cutaway of Lamp Flux Calorimeter

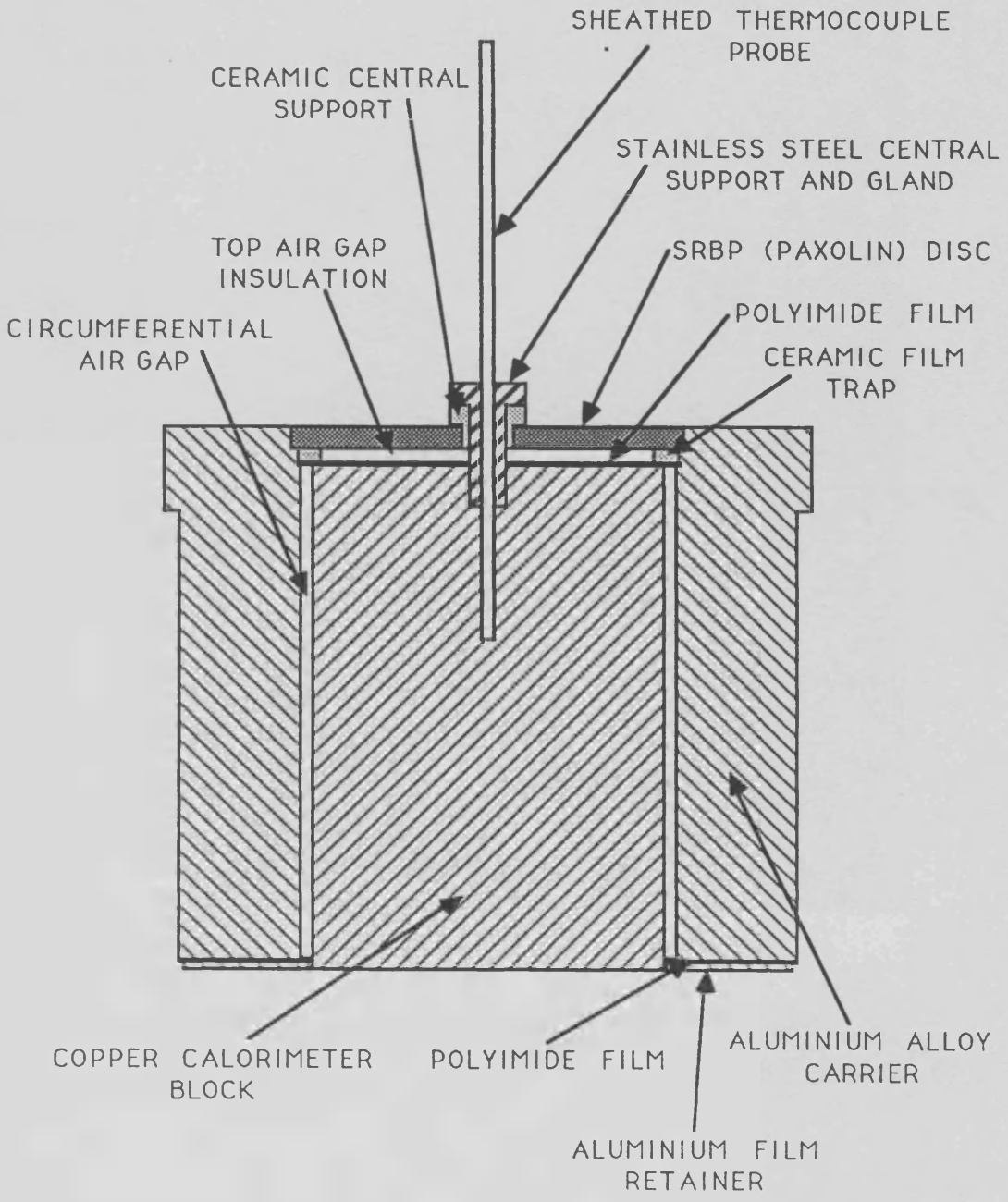

Figure 2.13

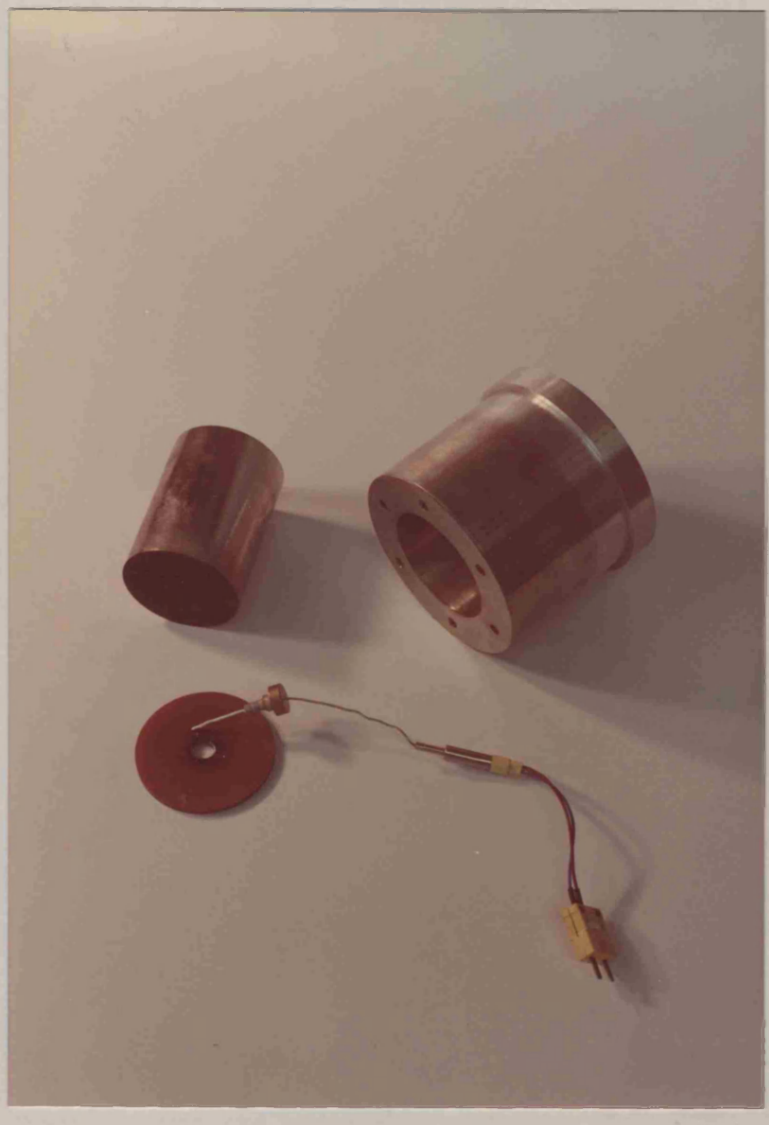

Figure 2.14 - Major Components of Flux Calibrator for Thermal Shock Rig

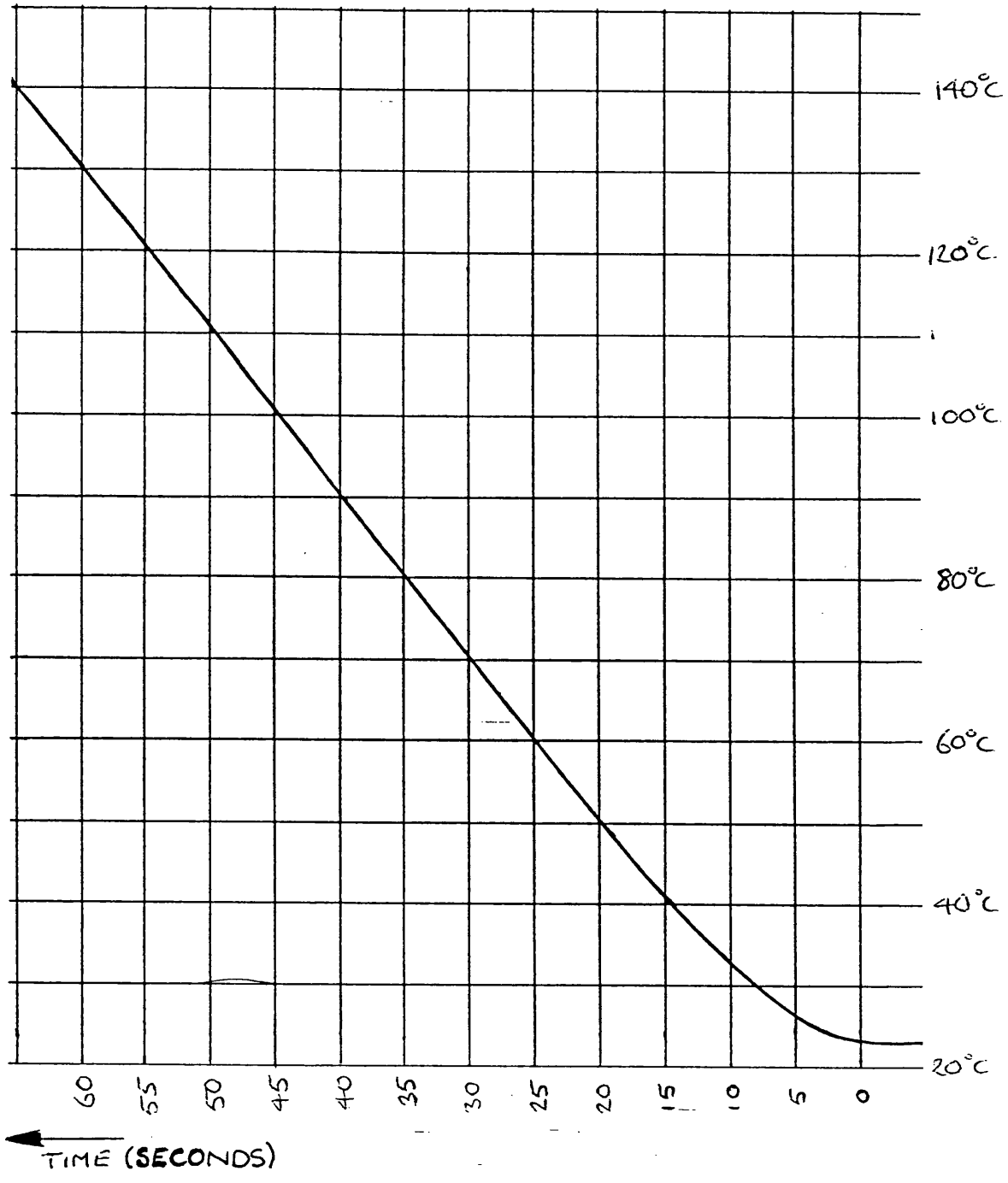

Figure 2.15 - Typical Chart Recorder Trace Obtained with Flux Calibrator

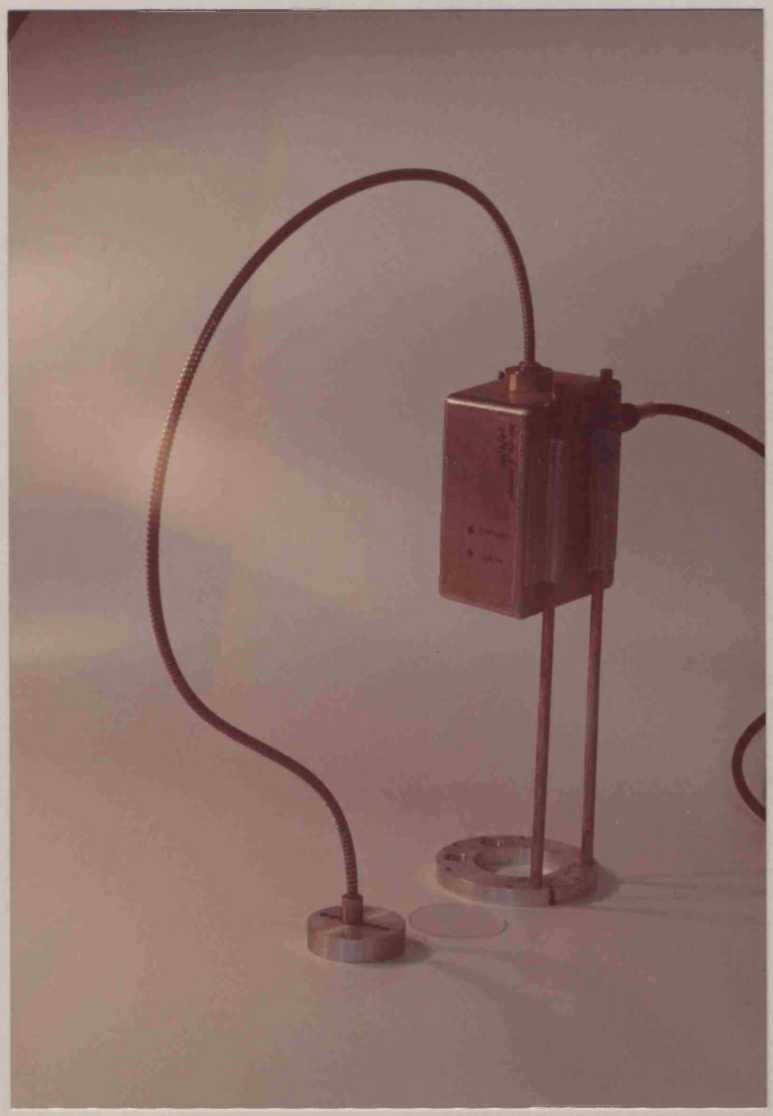

Figure 2.16 - Flux Distribution Monitor

Efficiency and Mean Flux from a Parabolic Mirror

as a function of mirror aperture (400W point source assumed)

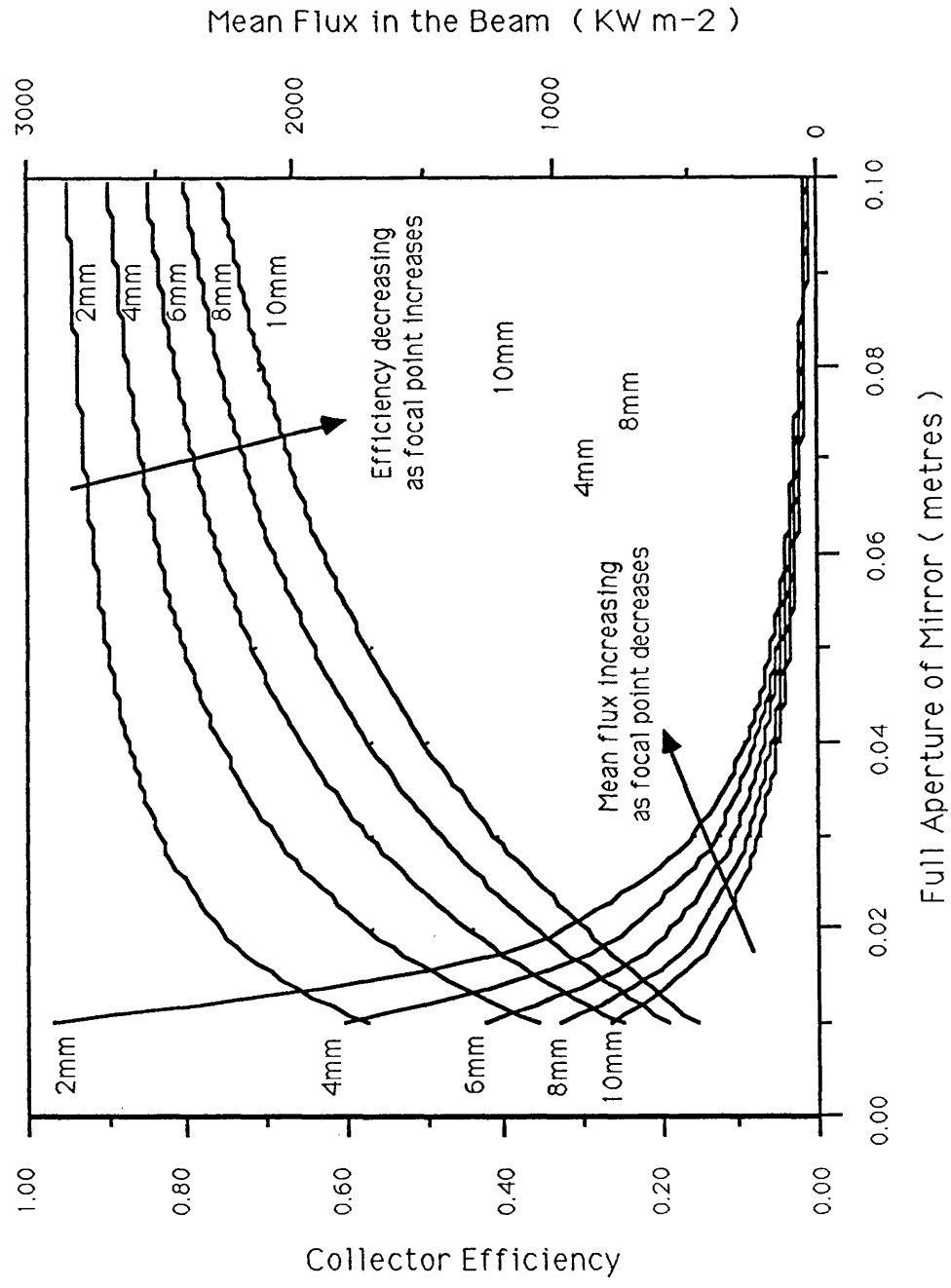

Figure 2.17

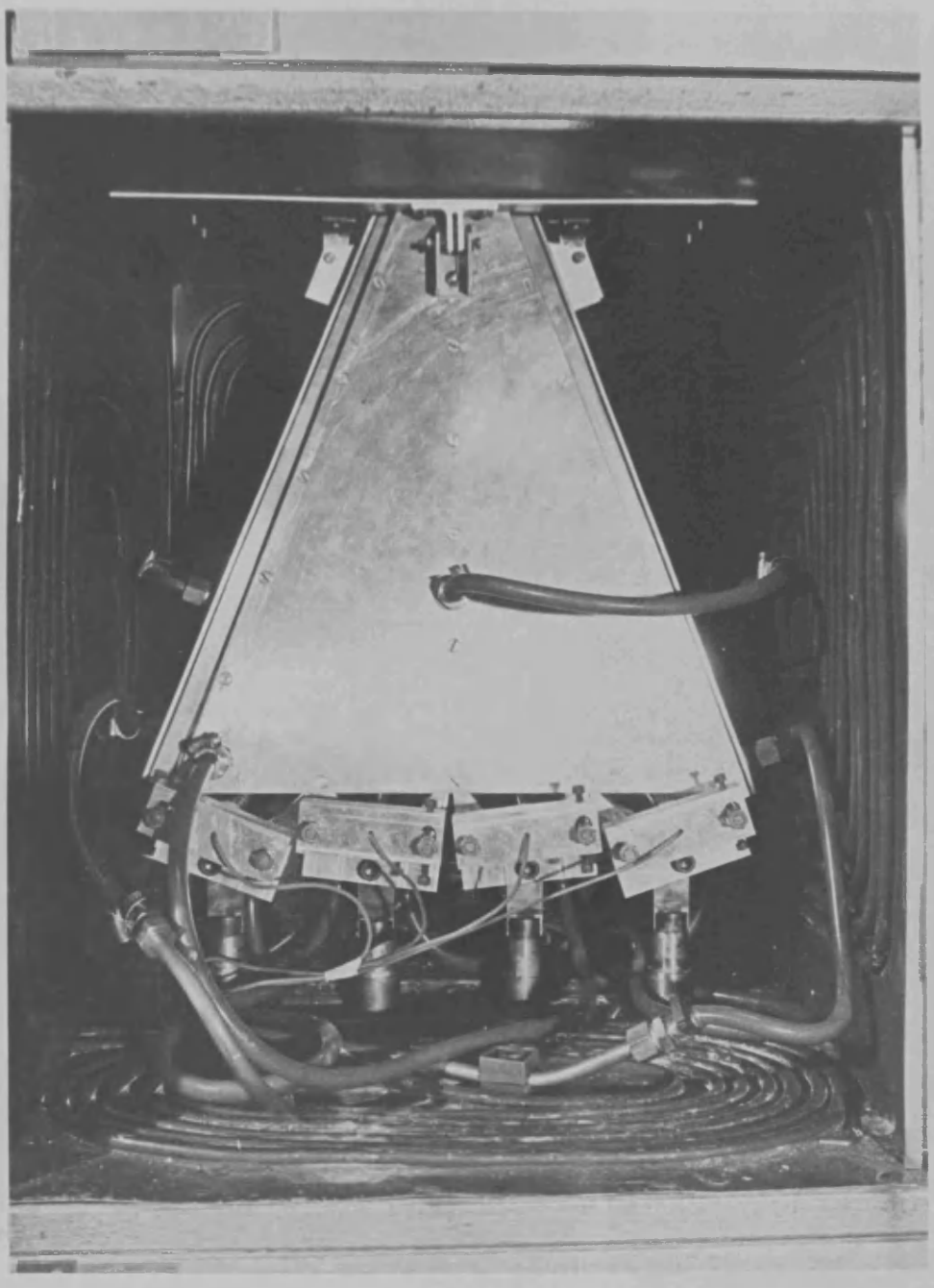

Figure 2.18 - First Reflector Assembly

The basic reflector, on which all the assemblies below are comprised, is formed from half an ellipse plus two sides with an included angle of 12°. The assemblies are arranged such that the source contained within any one reflector cannot directly "see" the envelope of the adjacent lamp. The source to specimen plane distance for all the assemblies is set to approximately 30mm. The resulting flux levels quoted for each assembly assumes a fixed out of plane dimension of 60mm.

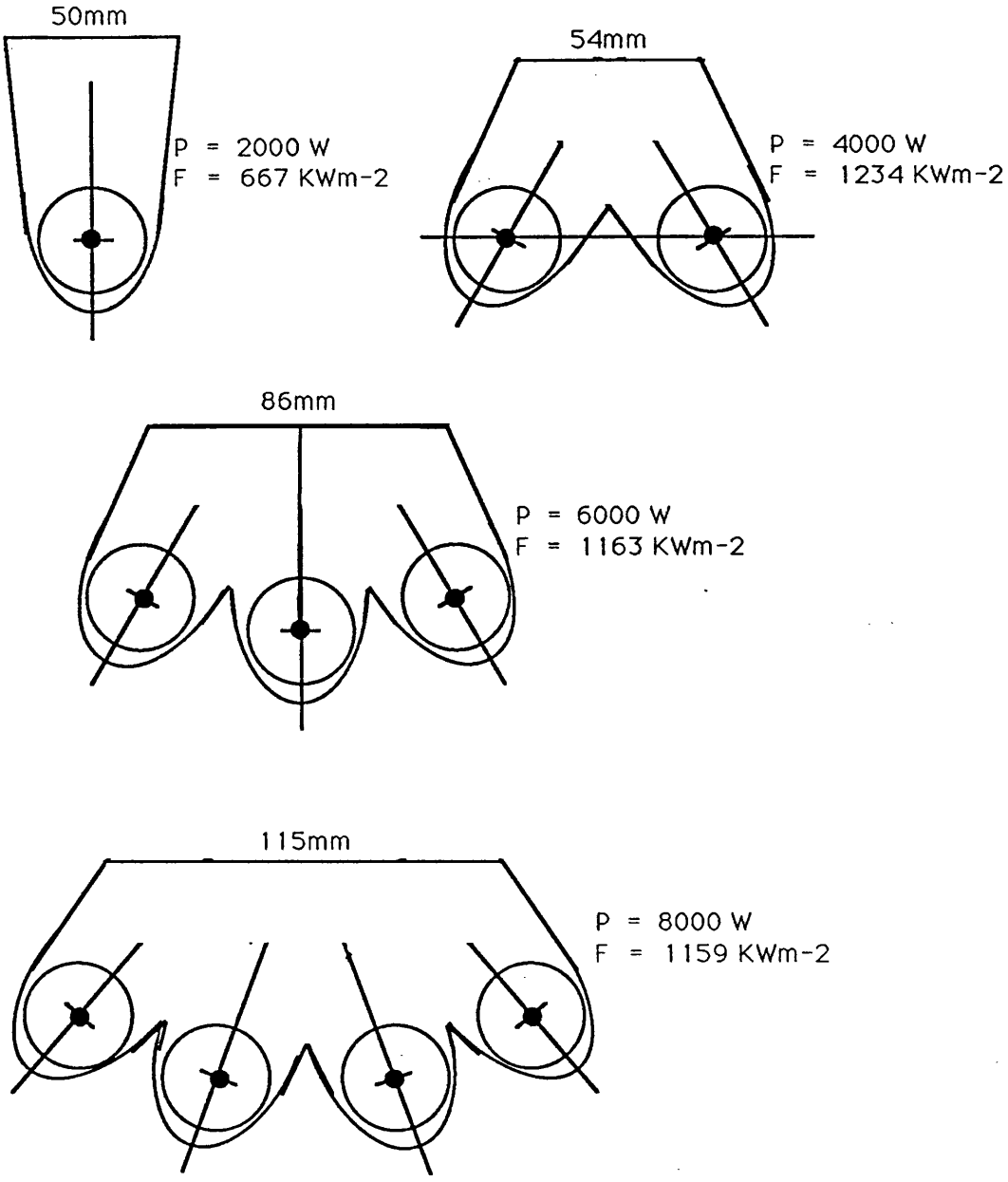

The flux levels quoted above are for completely loss free conditions and are only given as a guide to show one of the steps towards the final design of the thermal shock reflector assembly. The actual mean flux levels at the specimen plane will of course be much lower due to envelope and reflector losses.

Figure 2.19

Figure 2.20

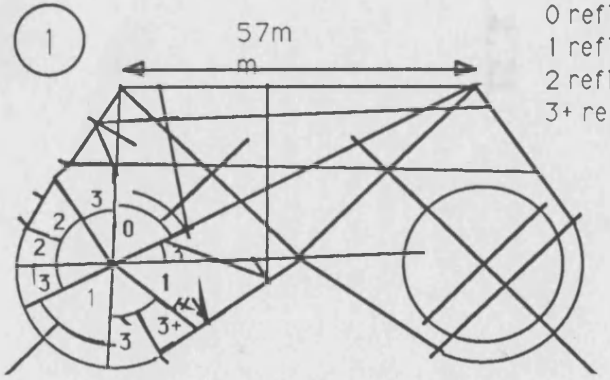

Included reflector angle = 24 degrees

0 reflections	60	proportion =	0.167
1 reflection	100	: =	0.278
2 reflections	60	: =	0.167
3+ reflections	140	: =	0.389

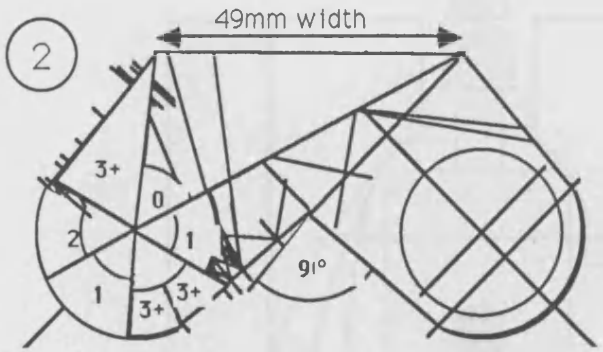

In this case the included reflector angle has been reduced from 24° to 10°

0 reflections	56	proportion =	0.156
1 reflection	119	: =	0.331
2 reflections	52	: =	0.144
3+ reflections	133	: =	0.369

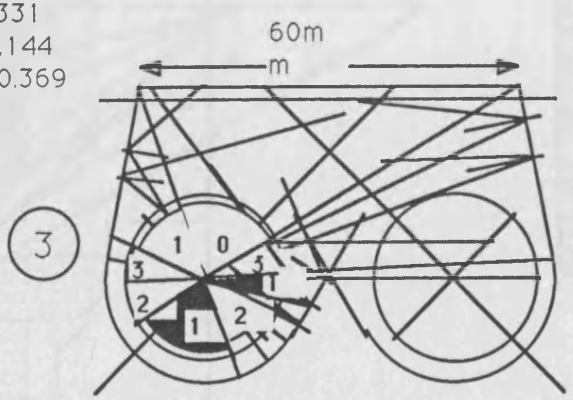

0 reflections	76	proportion =	0.211
1 reflection	145	: =	0.403
2 reflections	86	: =	0.239
3+ reflections	53	: =	0.147

Initial Raytracing of Side Elevation
of Second Reflector Design

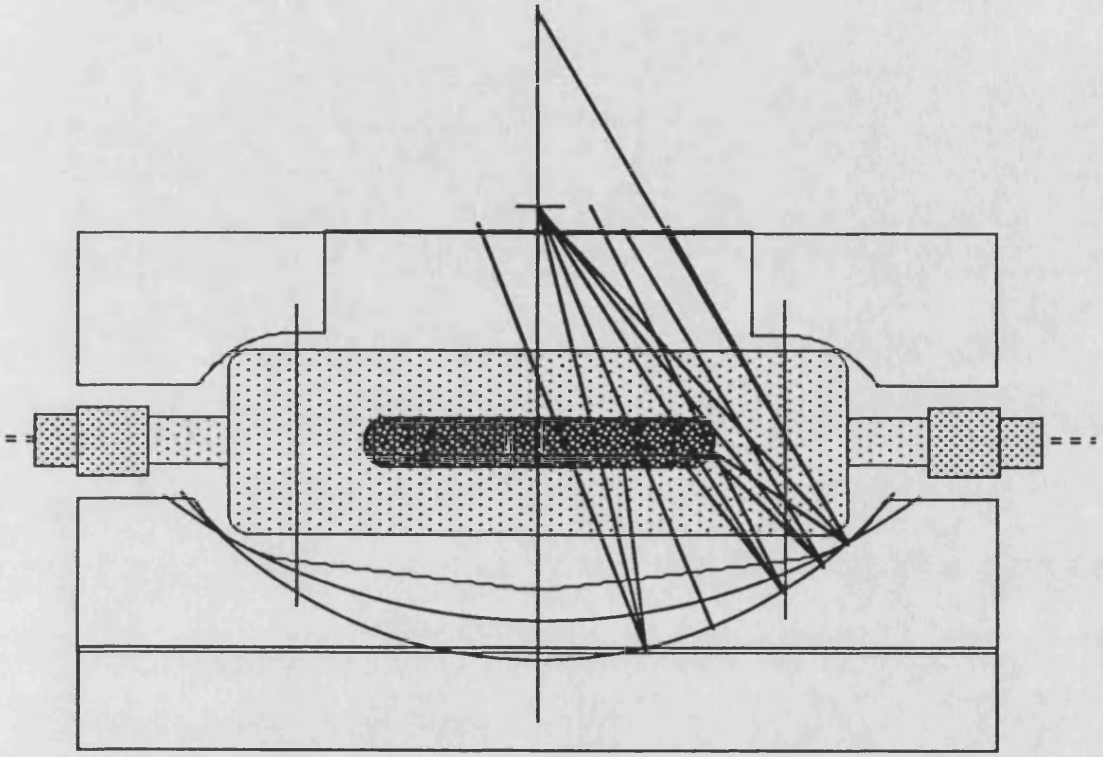

Figure 2.21

Method for the Determination of Specimen Flux and Envelope Losses

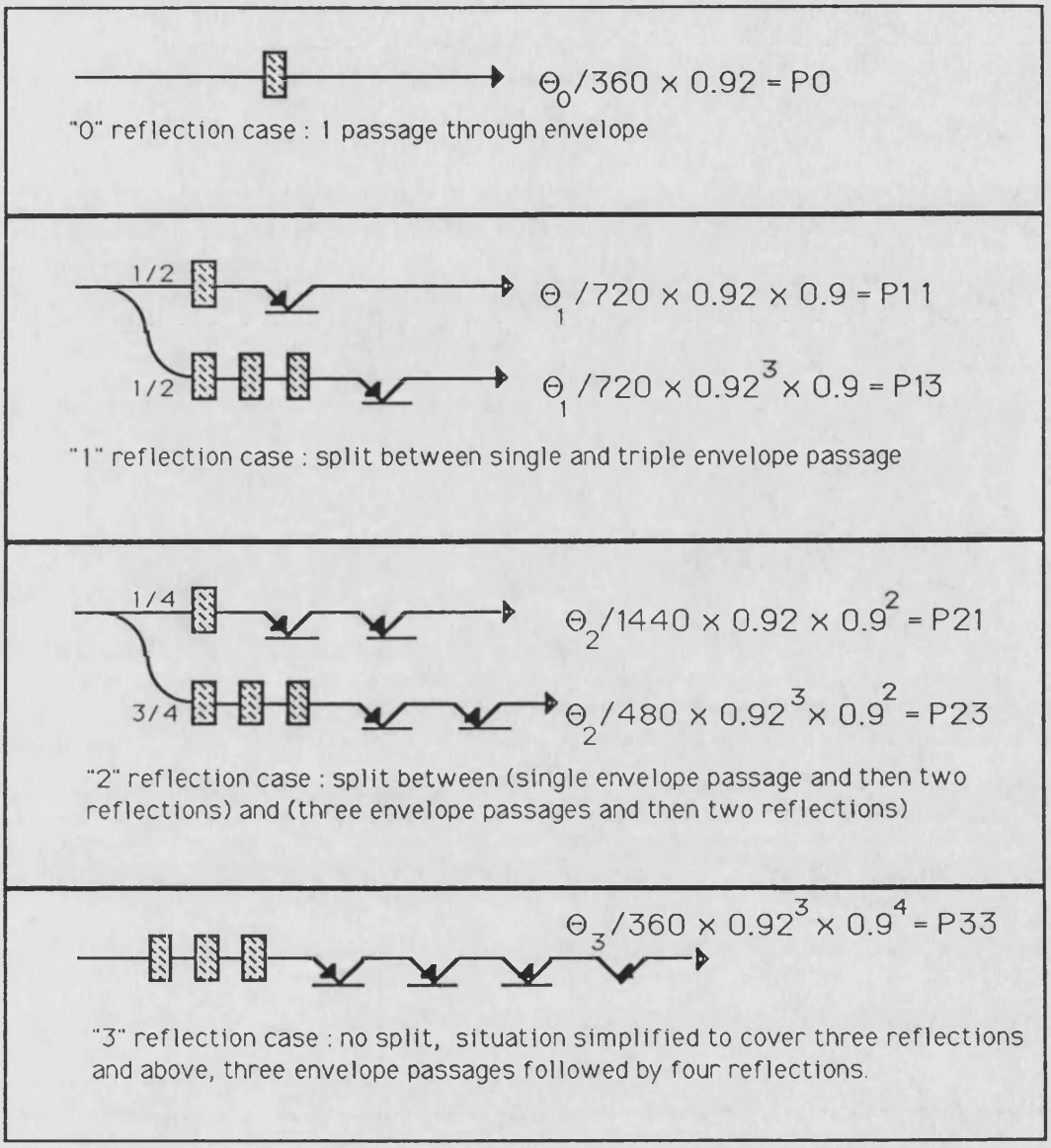

The figures above, indicate the four classes into which the rays from the source were divided, for the purpose of estimating the flux at the specimen plane and the losses incurred. The fractional splits involved for the cases of one and two reflections were arrived at by inspection of the ray traces for the particular reflectors in question.

The value of reflection coefficient has been estimated at 0.9 and the loss on passage through the envelope estimated at about 8% giving a transmission of 0.92 . The angles theta 0 to 3 are the estimates, from ray tracing, of the fraction of the source beam undergoing zero to three,or more reflections before reaching the specimen plane, for a particular reflector/lamp configuration.

Figure 2.22

Table 2.1 Reflector Effectiveness and Envelope Losses

	REFLECTIONS	0	1	2	3+	TOTALS
REFLECTOR No. 1	Included Angle	6	100	6	140	360
	w, x, y, z	0.167	0.278	0.167	0.389	1.001
	Envelope Absorbtion	0.01336	0.03992	0.02929	0.08609	0.169
	Power at Aperture	0.154	0.212	0.110	0.183	0.659
REFLECTOR No. 2	REFLECTIONS	0	1	2	3+	TOTALS
	Included Angle	5	119	5	133	360
	w, x, y, z	0.156	0.331	0.144	0.369	1.000
	Envelope Absorbtion	0.01248	0.04753	0.02526	0.08166	0.167
	Power at Aperture	0.144	0.253	0.095	0.173	0.665
REFLECTOR No. 3	REFLECTIONS	0	1	2	3+	TOTALS
	Included Angle	7	145	8	5	360
	w, x, y, z	0.211	0.403	0.239	0.147	1.000
	Envelope Absorbtion	0.01688	0.05787	0.04192	0.03253	0.149
	Power at Aperture	0.194	0.308	0.158	0.069	0.729

Where w, x, y, and z are the respective proportions of the lamp output undergoing 0, 1, 2 or 3+ reflections. The proportions w, x, y, and z are used as coefficients in the following equations to determine both the power absorbed in the envelope and the power incident at the aperture of the reflector assembly :-

Proportion absorbed by envelope =

$$0.08w + (0.08 + 0.0707R)x + (0.08 + 0.1060R)y + 0.2213z$$

Proportion incident at aperture =

$$0.92w + 0.849Rx + 0.814R^2y + 0.716R^4$$

R is the broadband reflection coefficient of the reflecting surfaces and has been taken as 0.9 for the above table.

The value in the last column for the Power at Aperture is the effectiveness of the reflector in the plane at right angles to the lamp axis and must be multiplied by the appropriate value for the other plane to give the full reflector "effectiveness".

SPUTTERED THIN FILM THERMOCOUPLE LAYOUT INDICATING MINIMAL CONTACT ELECTRODE AS USED FOR BOTH THERMAL CONDUCTIVITY AND THERMAL SHOCK TESTING

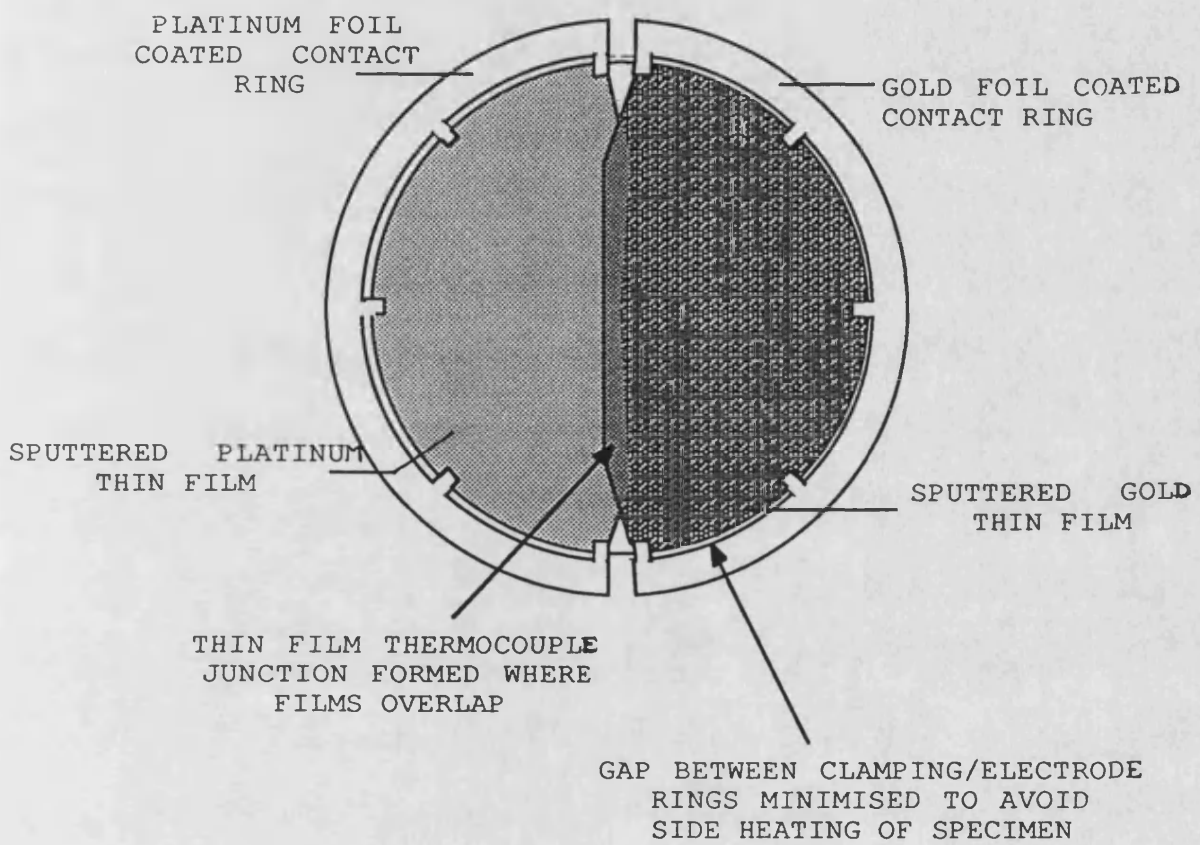

Figure 2.23

Cross Section of Assembled Thermal Conductivity Calorimeter

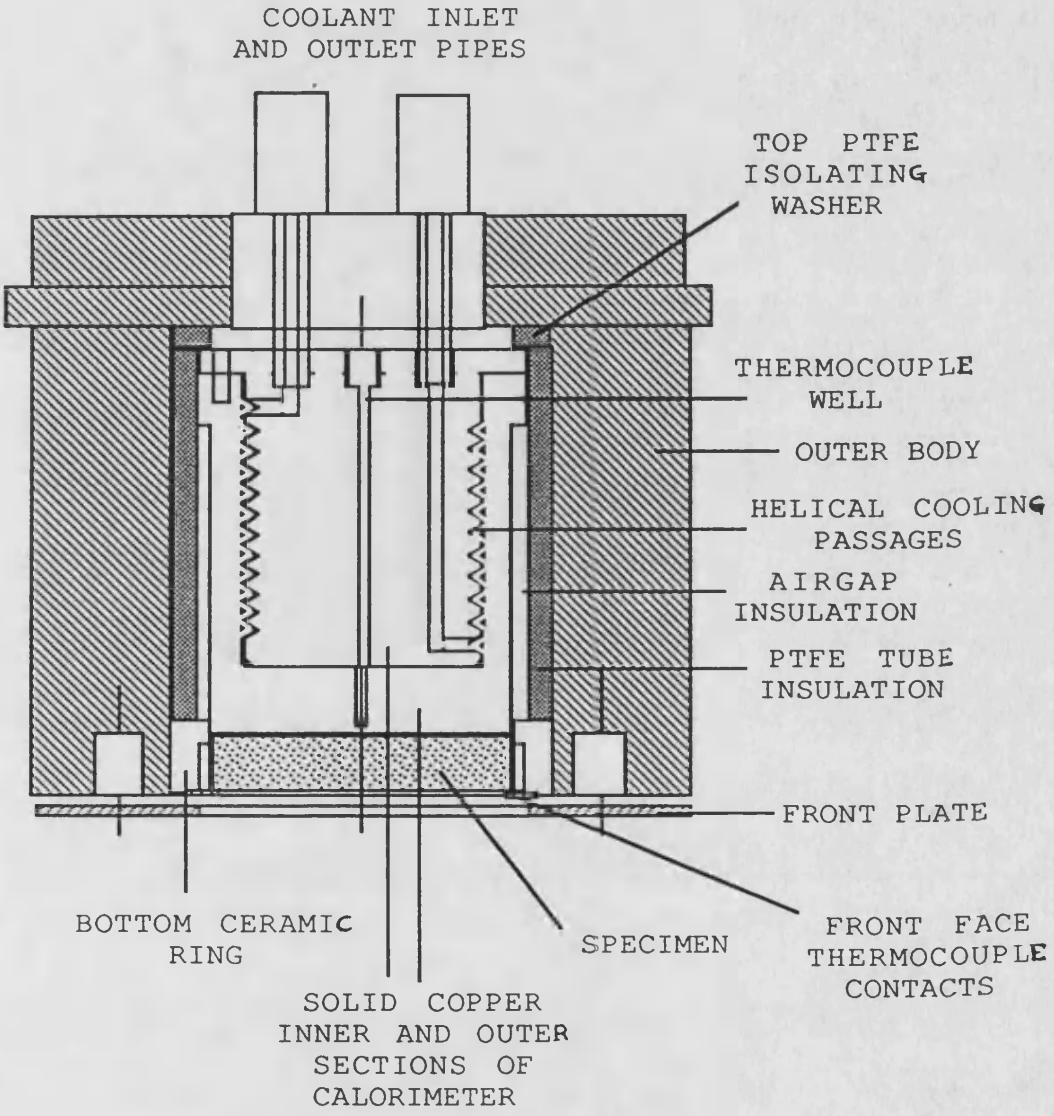

Figure 2.24

Improved Thermal Shock Specimen Holder for Acoustic Emission Monitoring

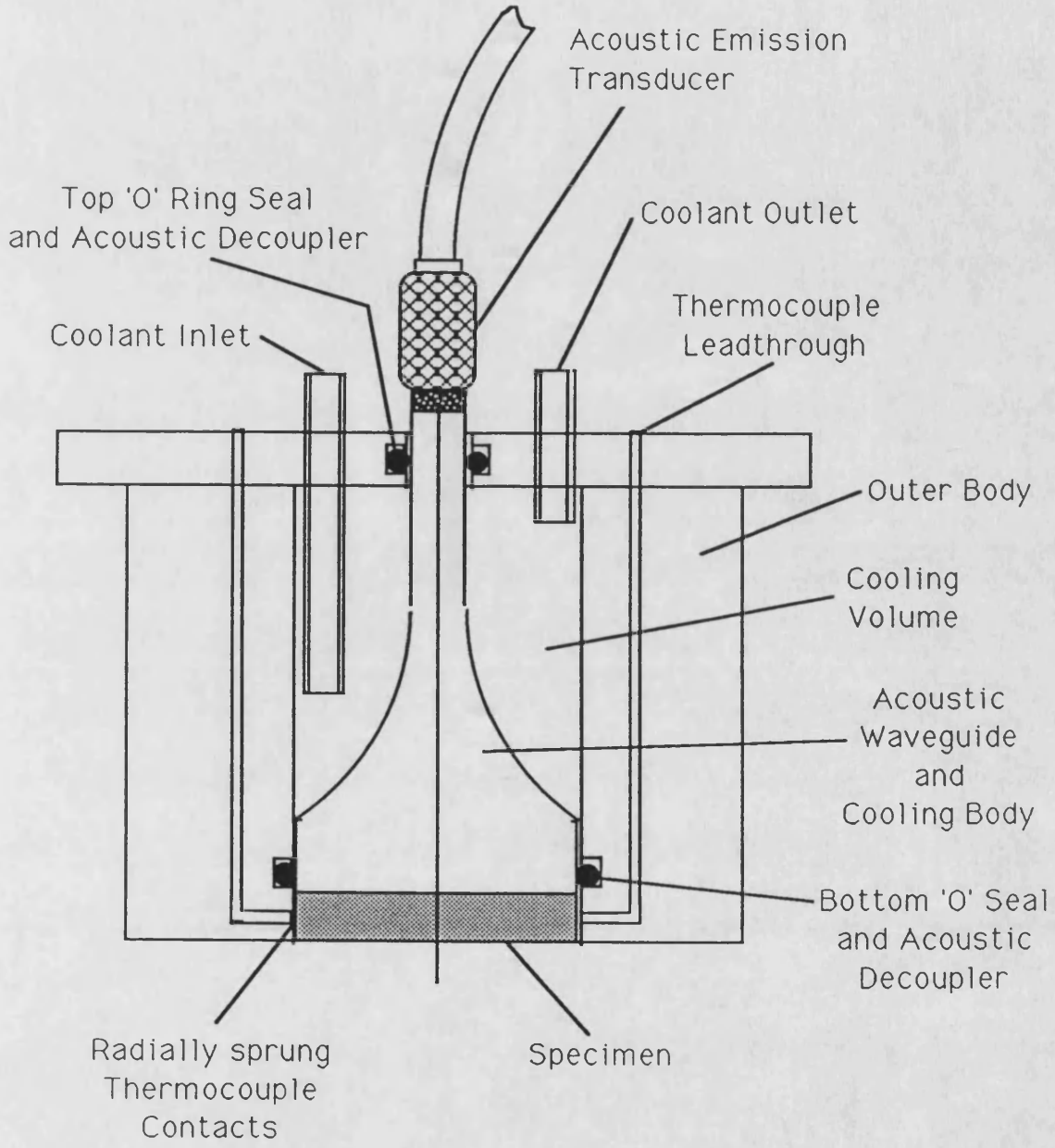

Figure 2.25

PREFERRED FORMS OF SPECIMEN MOTION

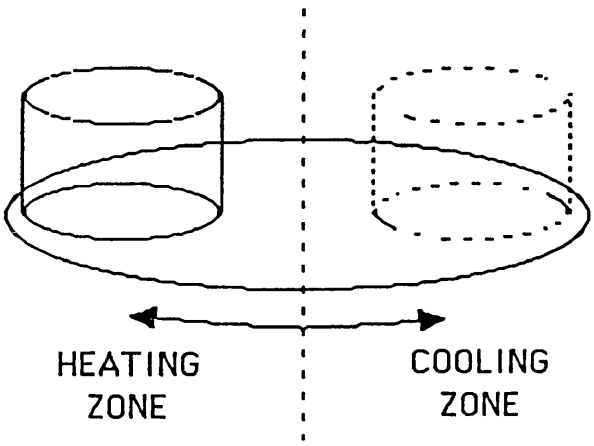

ROTARY - HORIZONTAL

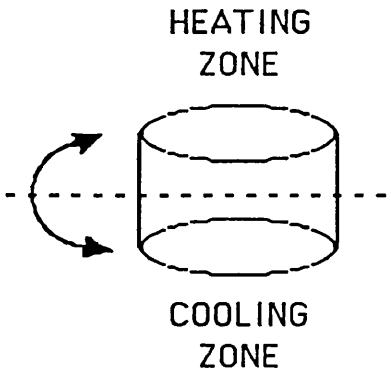

ROTARY - VERTICAL

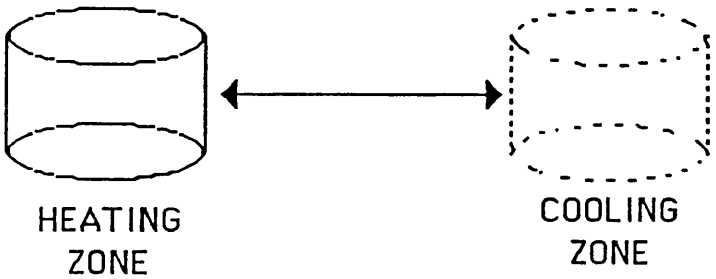

LINEAR - HORIZONTAL

Figure 2.26

Simple Comparison between Rod base and Rodless Pneumatic Actuation

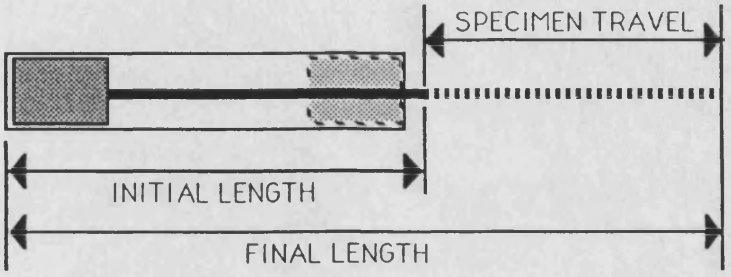

ROD BASED SYSTEM

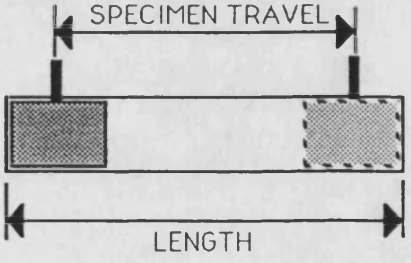

RODLESS SYSTEM

Figure 2.27

Air Circuit for Pneumatic Cylinder

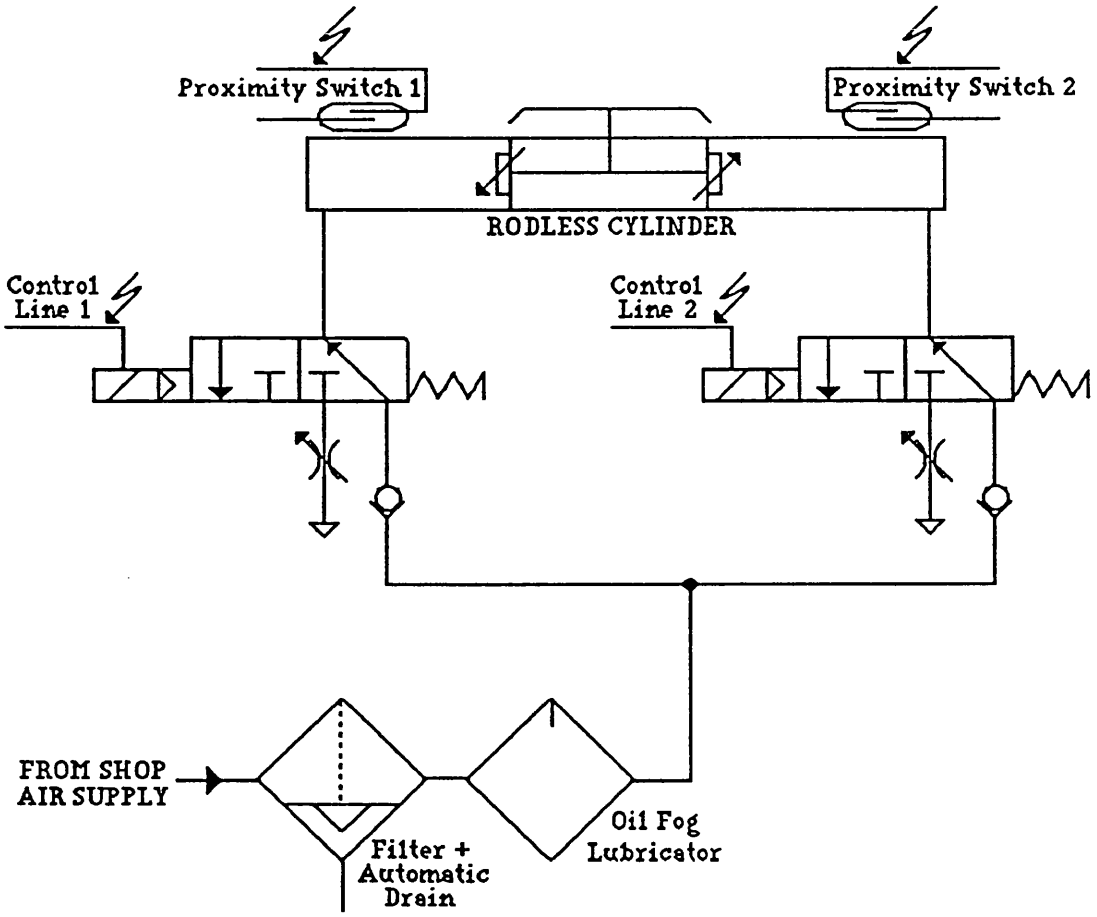

Figure 2.28

Circuit Schematic for Pneumatic Cylinder Control

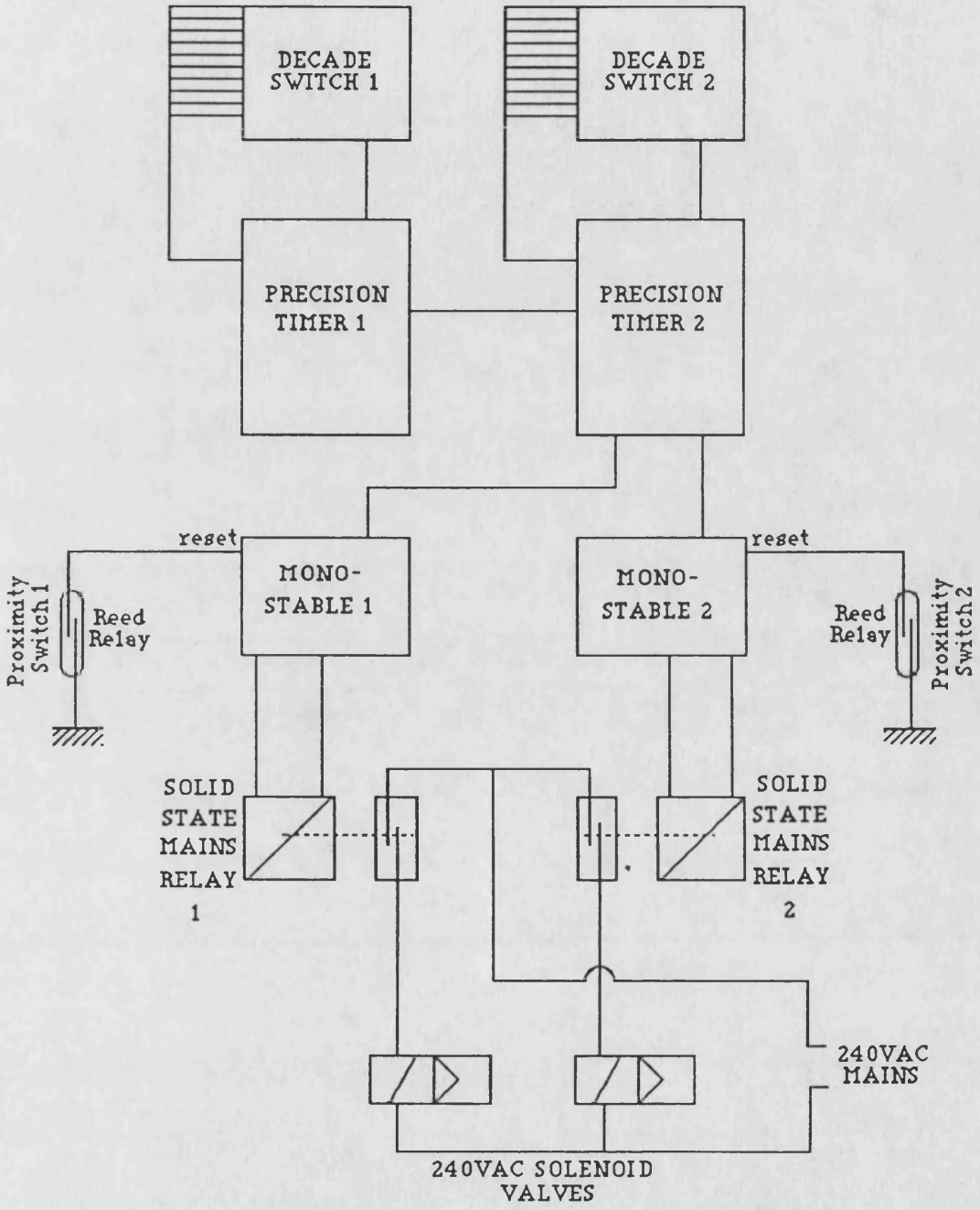

Figure 2.29

Timing Diagram for Pneumatic Cylinder Controller

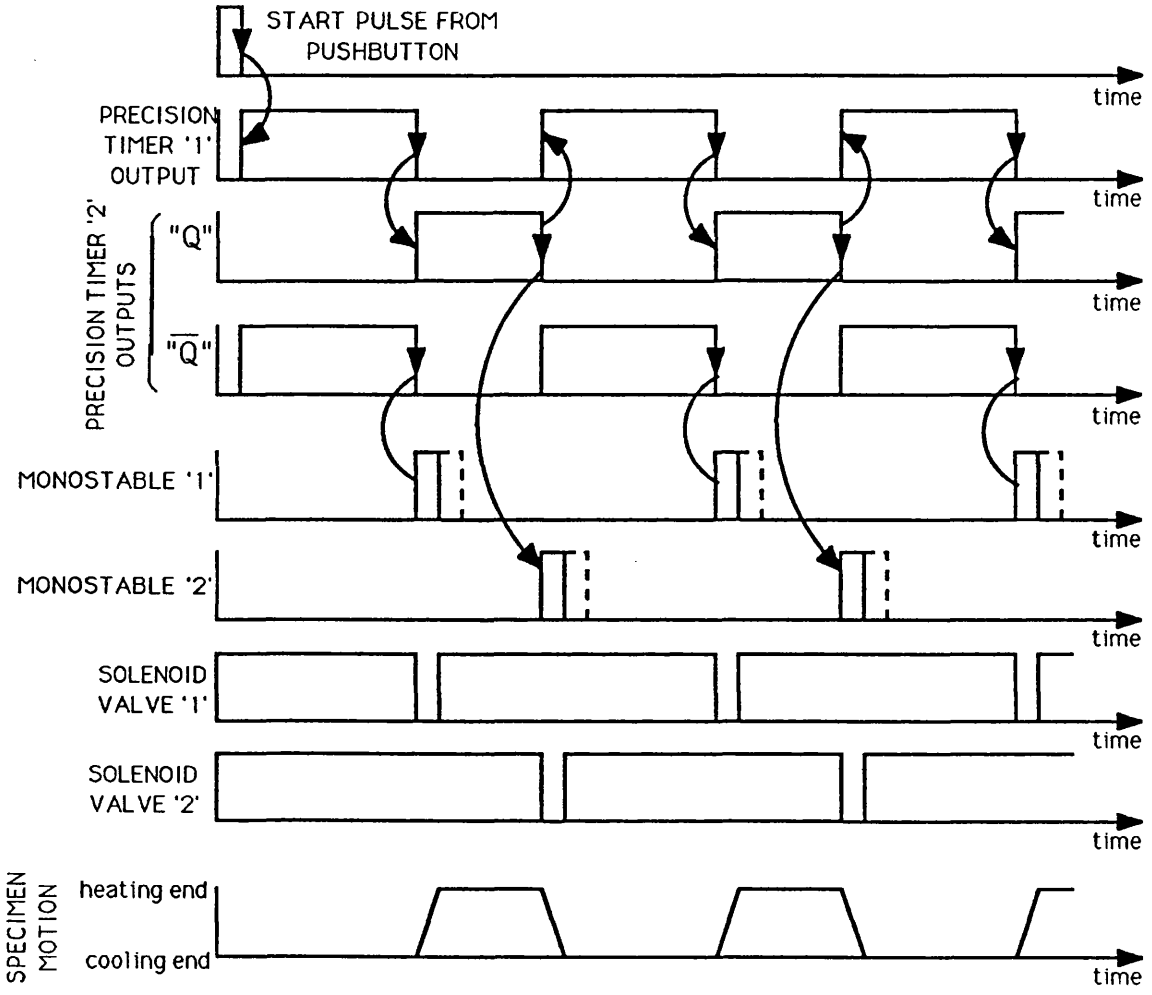

Figure 2.30

Precision Timer Circuit for use with Carriage Control

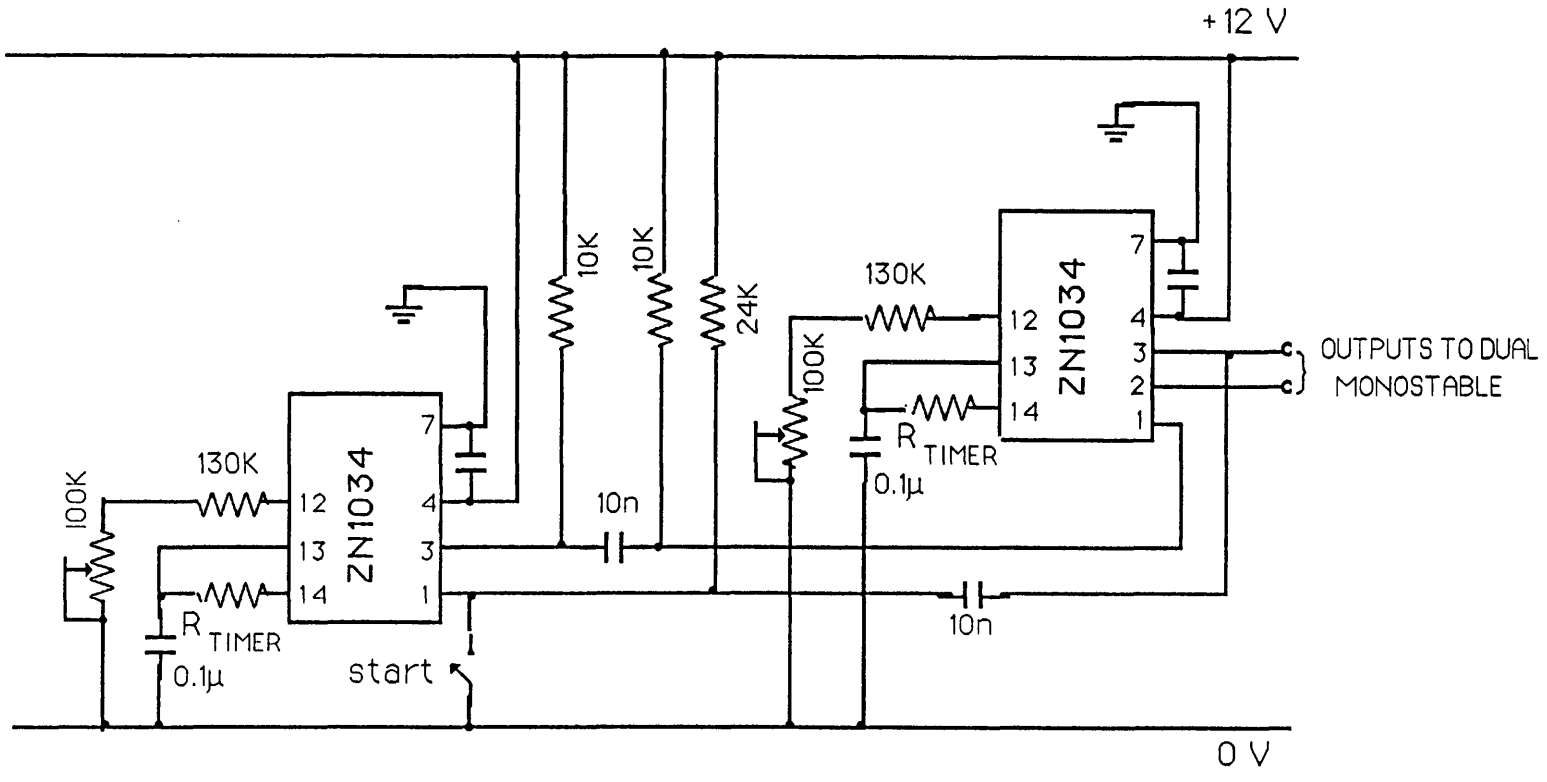

Figure 2.31

Dual Monostable Circuit for use with Carriage Control

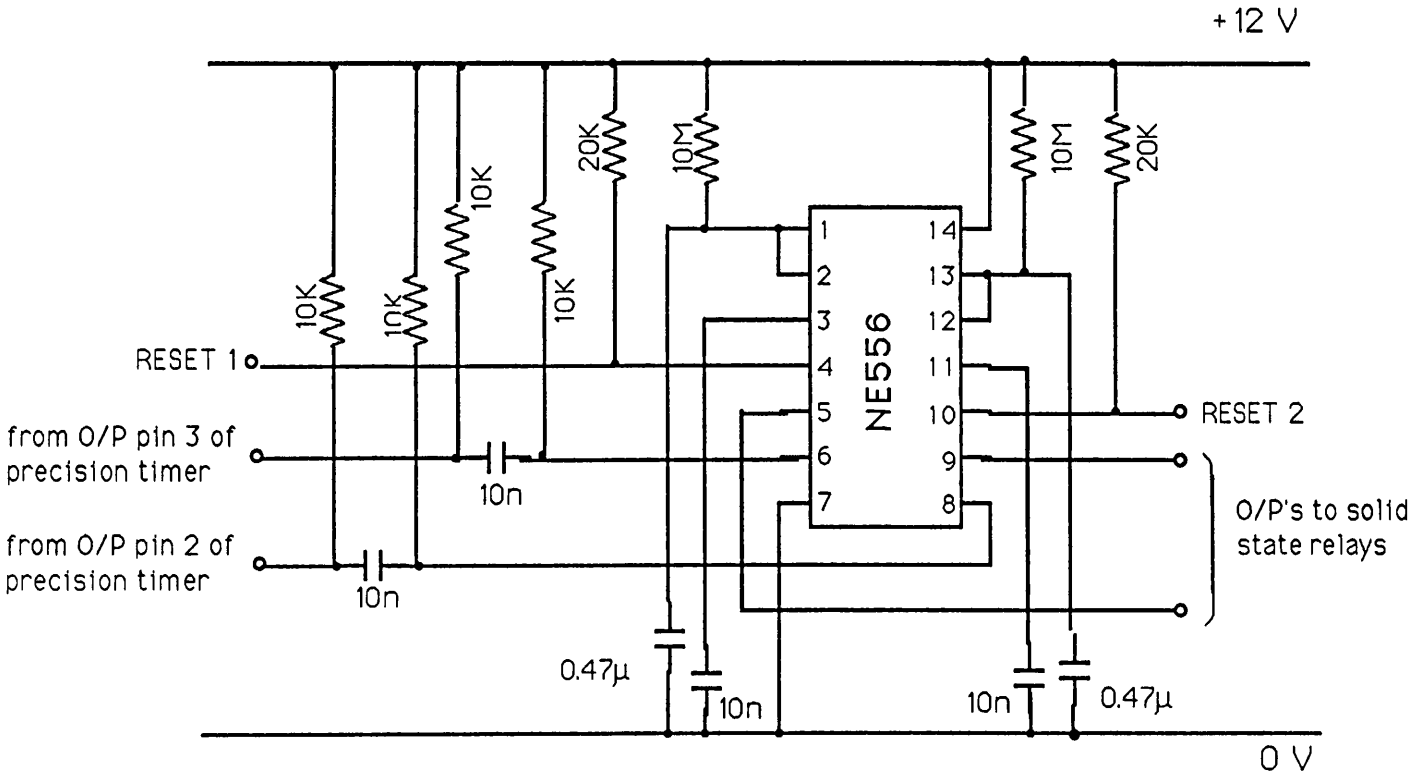

Figure 2.32

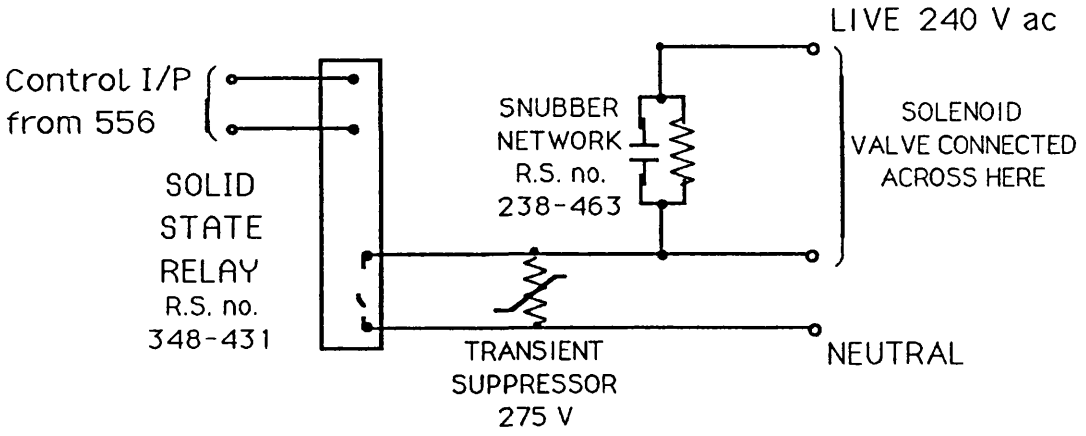

Figure 2.33 - **Solid State Relay Circuit for Pneumatic Cyliner Control**

WATER CIRCUIT FOR THERMAL SHOCK RIG

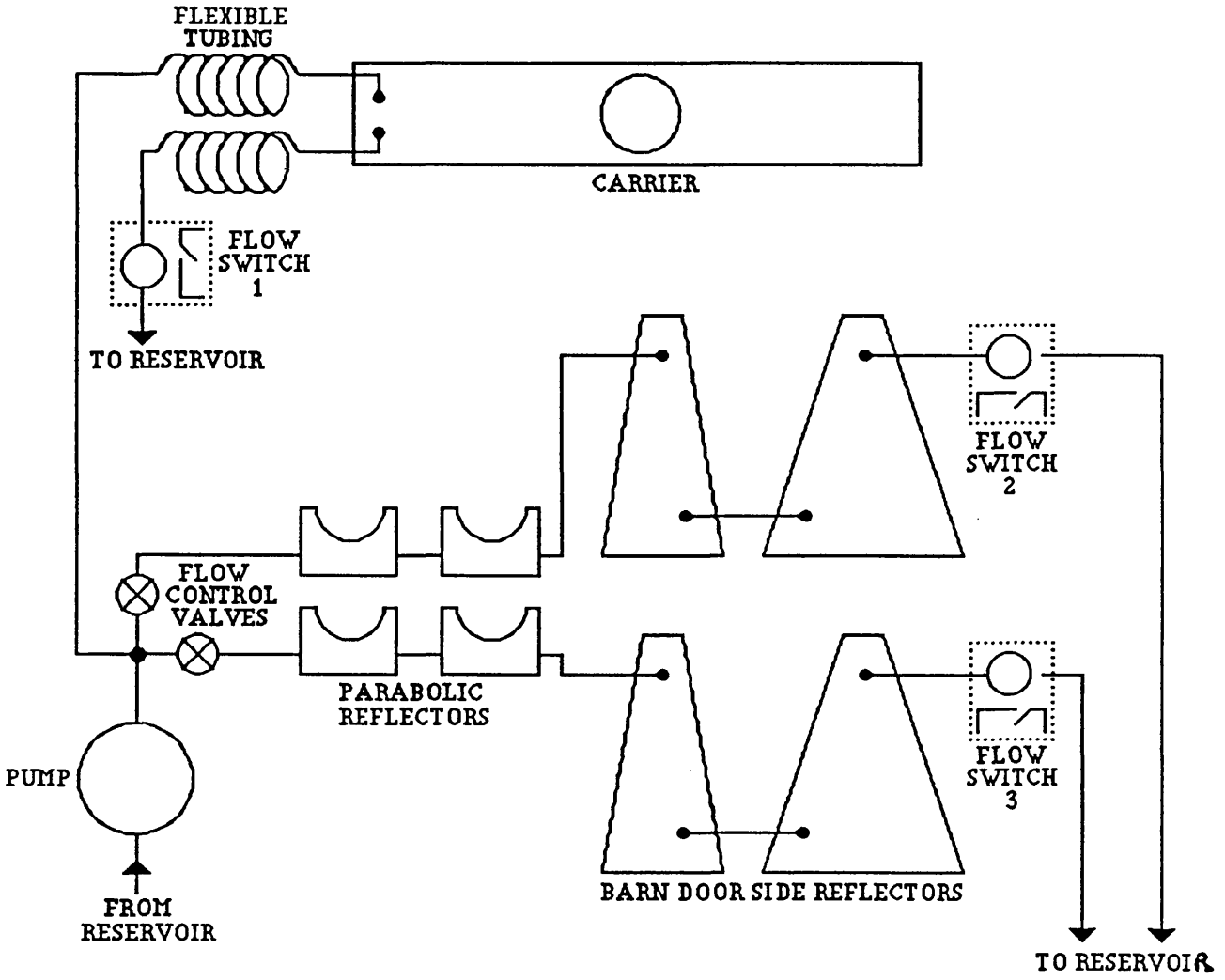

FLOW SWITCH 1 - DELAVAL GEMS FLOW SWITCH

FLOW SWITCH 2
&
FLOW SWITCH 3
- FLUVATEST FLOW SWITCHES

Figure 2.34

Cooling Passages of New Reflector

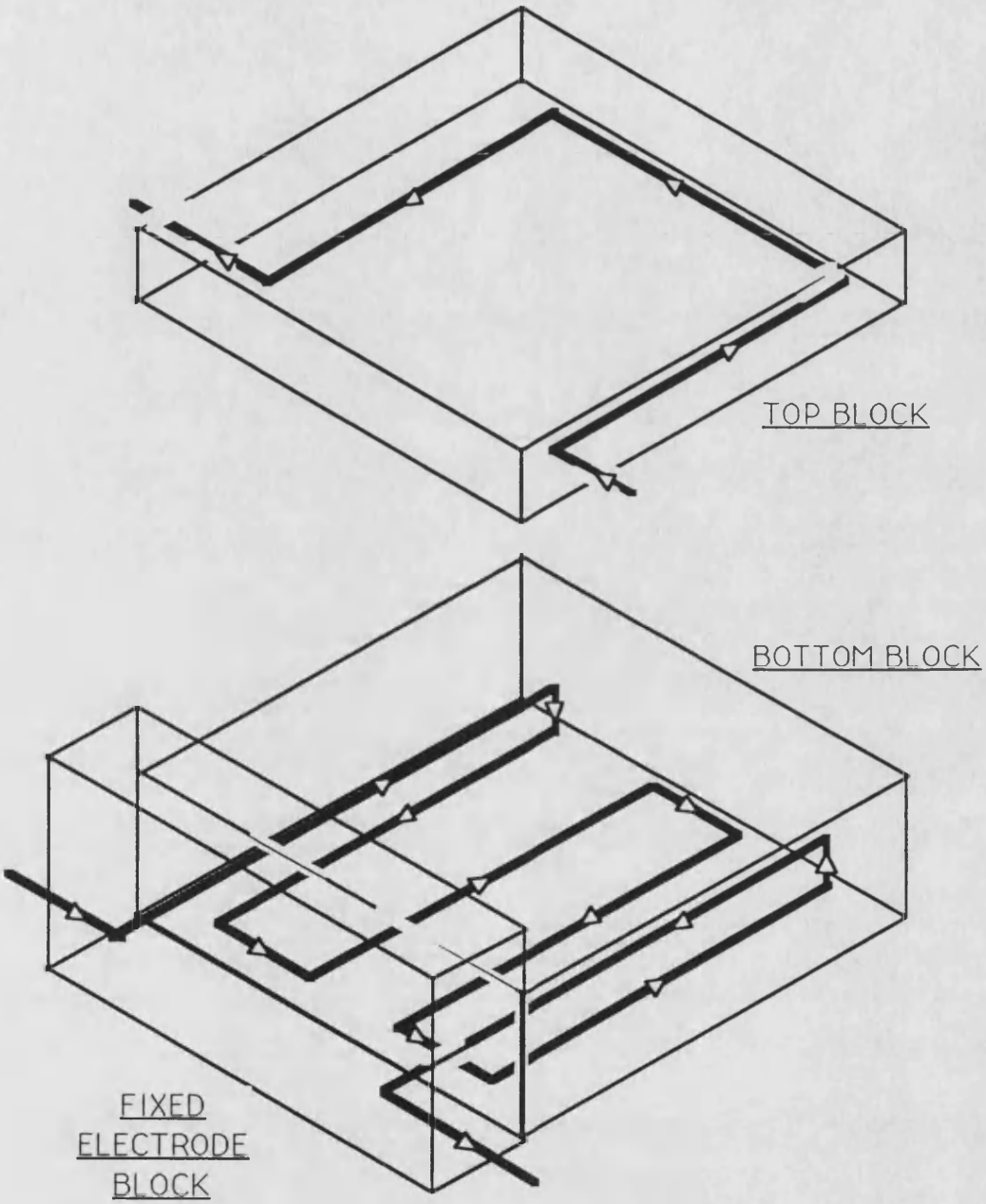

Figure 2.35

Thermal Conductivity Calorimeter Cooling Circuit

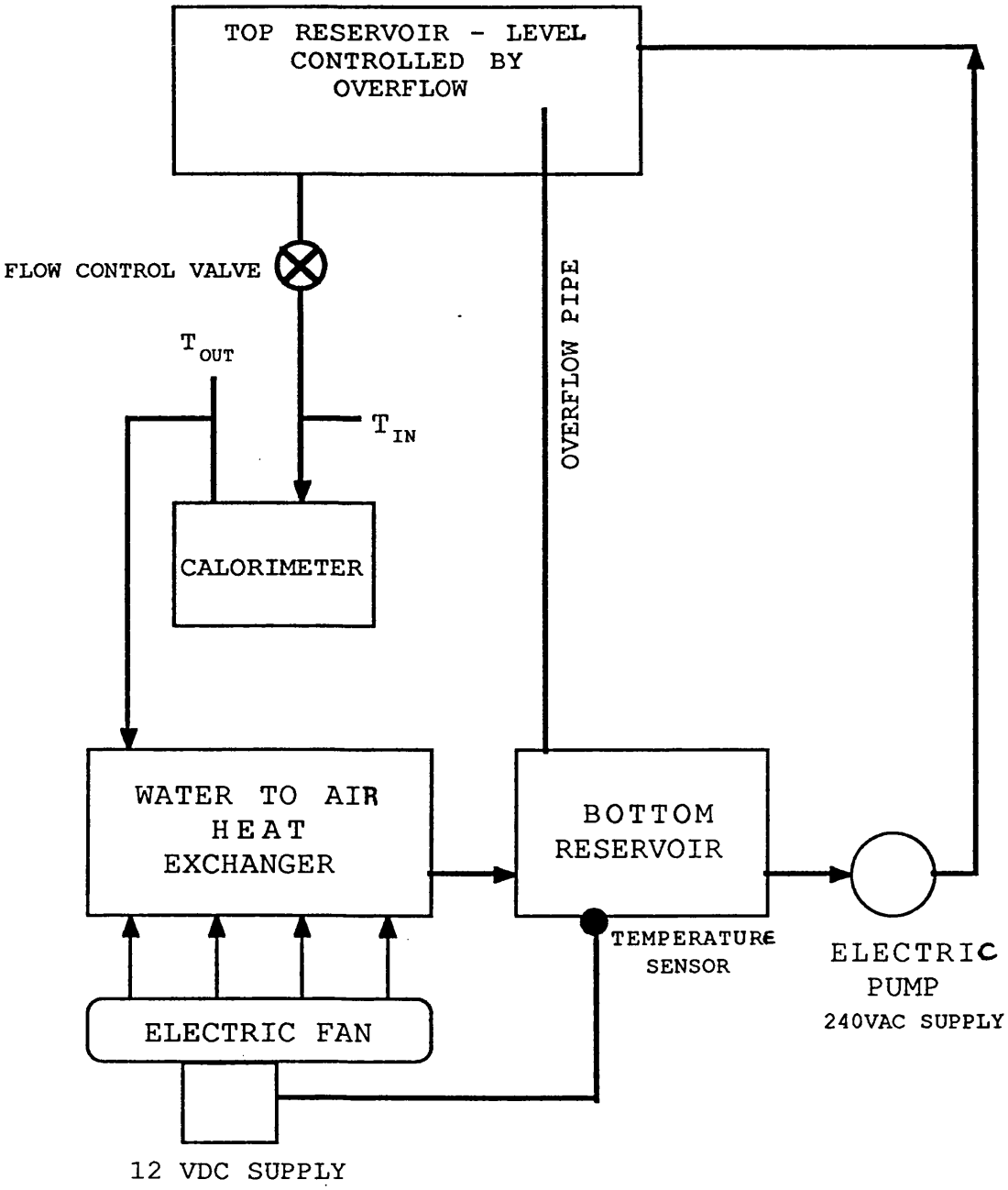

Figure 2.36

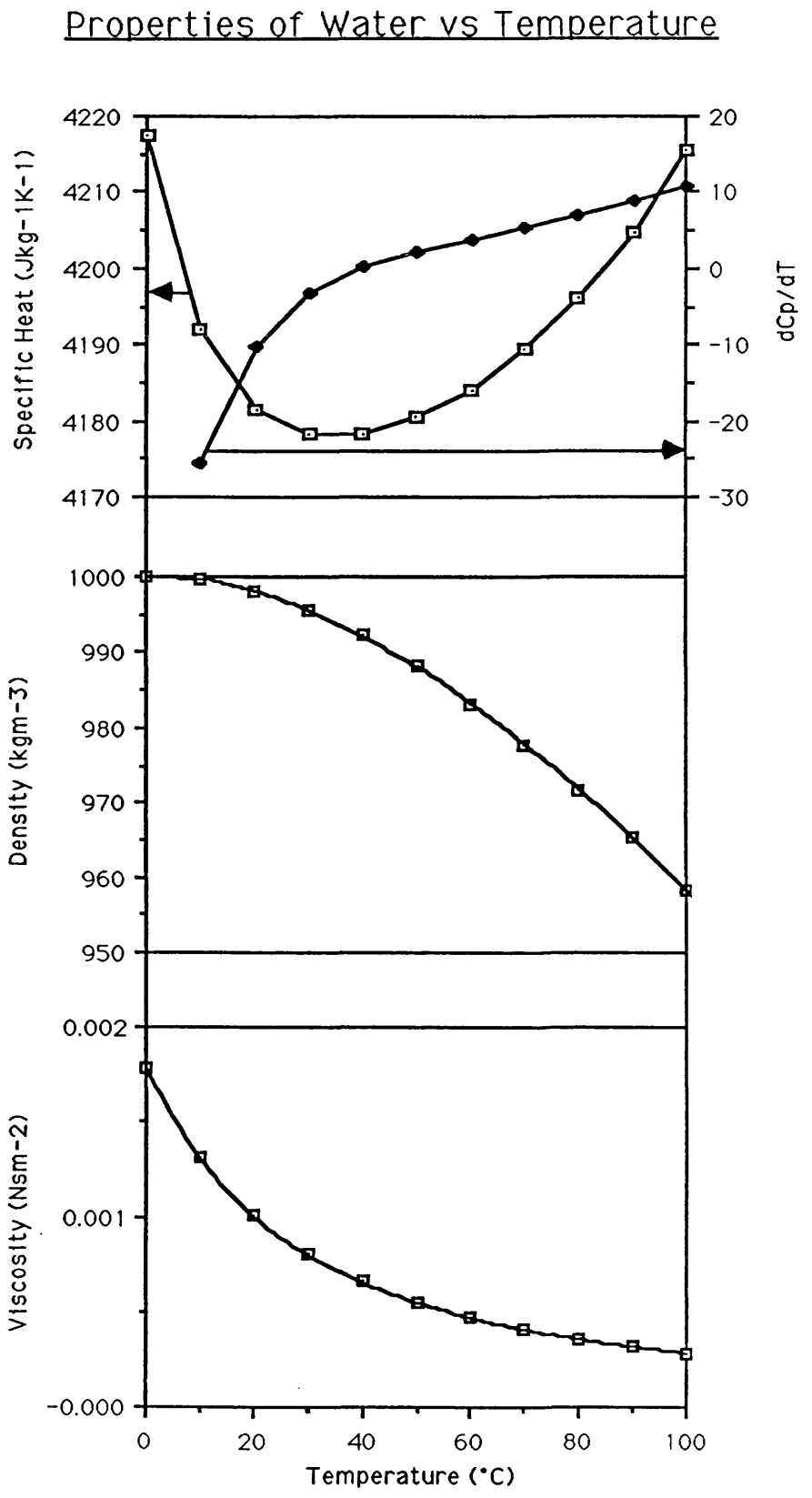
Properties of Water vs Temperature
Specific Heat (Jkg-1K-1)
4220
4210
4200
4190
4180
4170
20
10
0
-10
-20
-30
dCp/dT
Density (kgm-3)
1000
990
980
970
960
950
Viscosity (Nsm-2)
0.002
0.001
-0.000
0
20
40
60
80
100
Temperature (°C)

Figure 2.37

Figure 2.38

Logic Diagram of the Carriage Travel Failure Detection Circuit

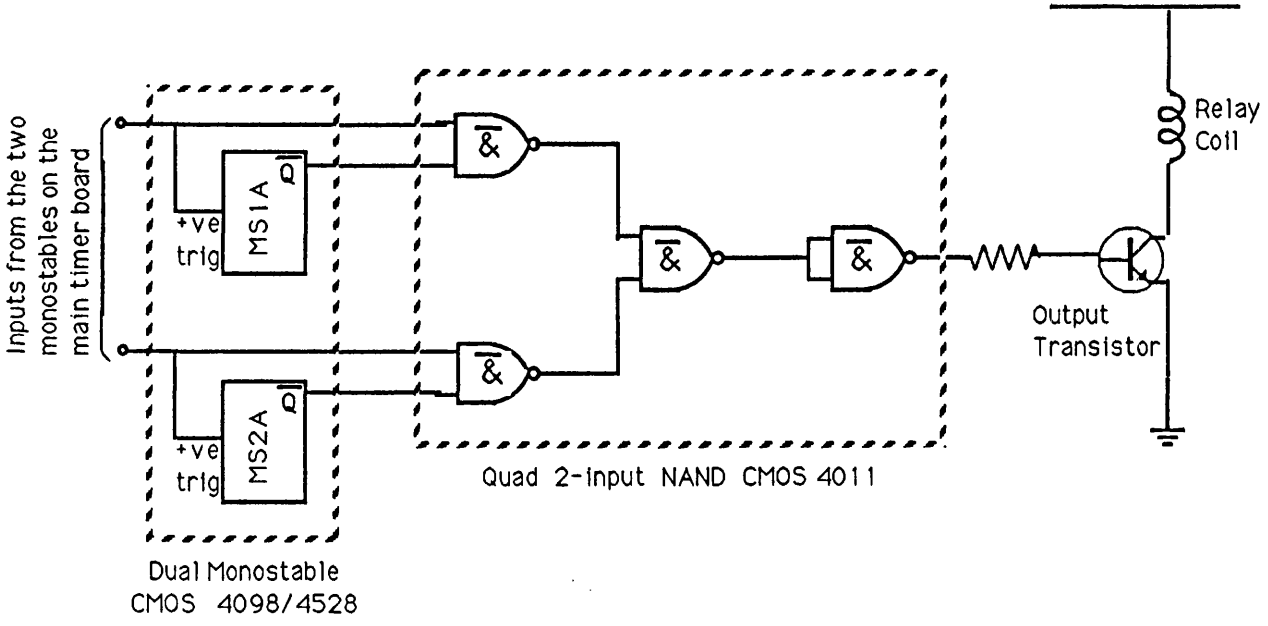

The period of the two monostables is set to the maximum acceptable travel time in each direction for the carriage. In the event of carriage travel failure, such as might be caused by :- excessive travel time (caused by high bearing friction) or jamming of the carriage during its travel, or by the carriage sticking at one end of the travel , a low output to the transistor will result, which will cause the relay to open and thus give the automatic shutdown system a failure signal.

Circuit Schematic for Actuator Failure Detect

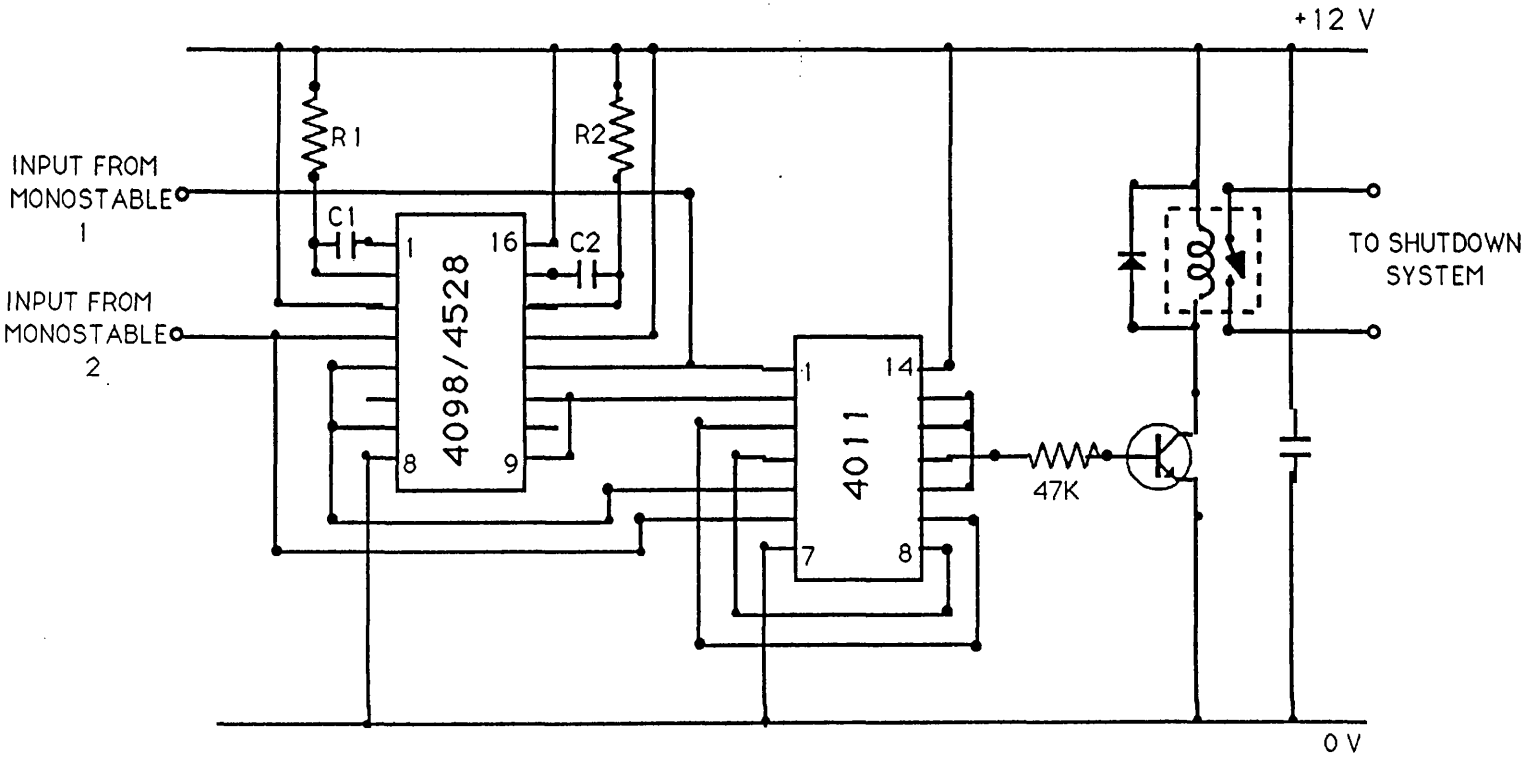

Figure 2.39

Timing diagram for the Carriage Travel Failure Detection Circuit

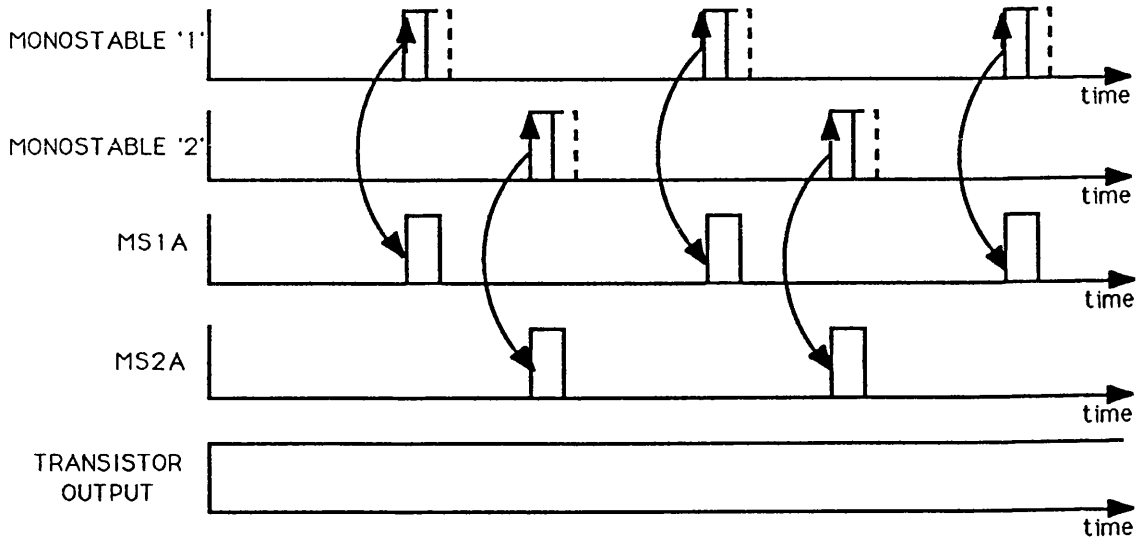

Correct operation of the carriage produces a fixed (high) output from the transistor, the auto-shutdown system will not trip out.

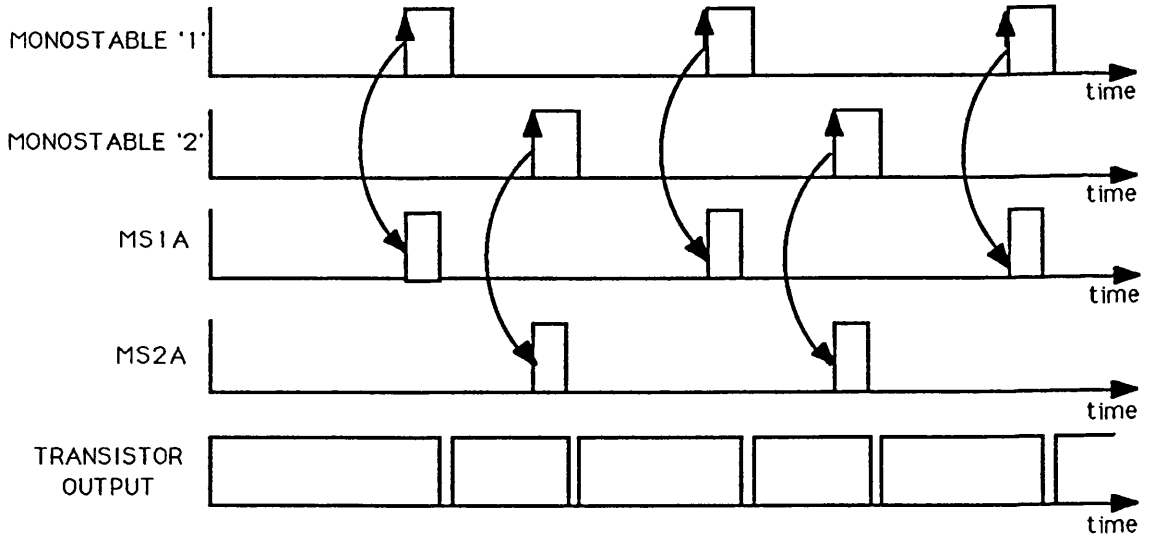

Excessive travel period of the carriage produces a pulsed transistor output which is sensed by the auto-shutdown system.

Figure 2.40

Circuit Schematic for Auto-Shutdown System

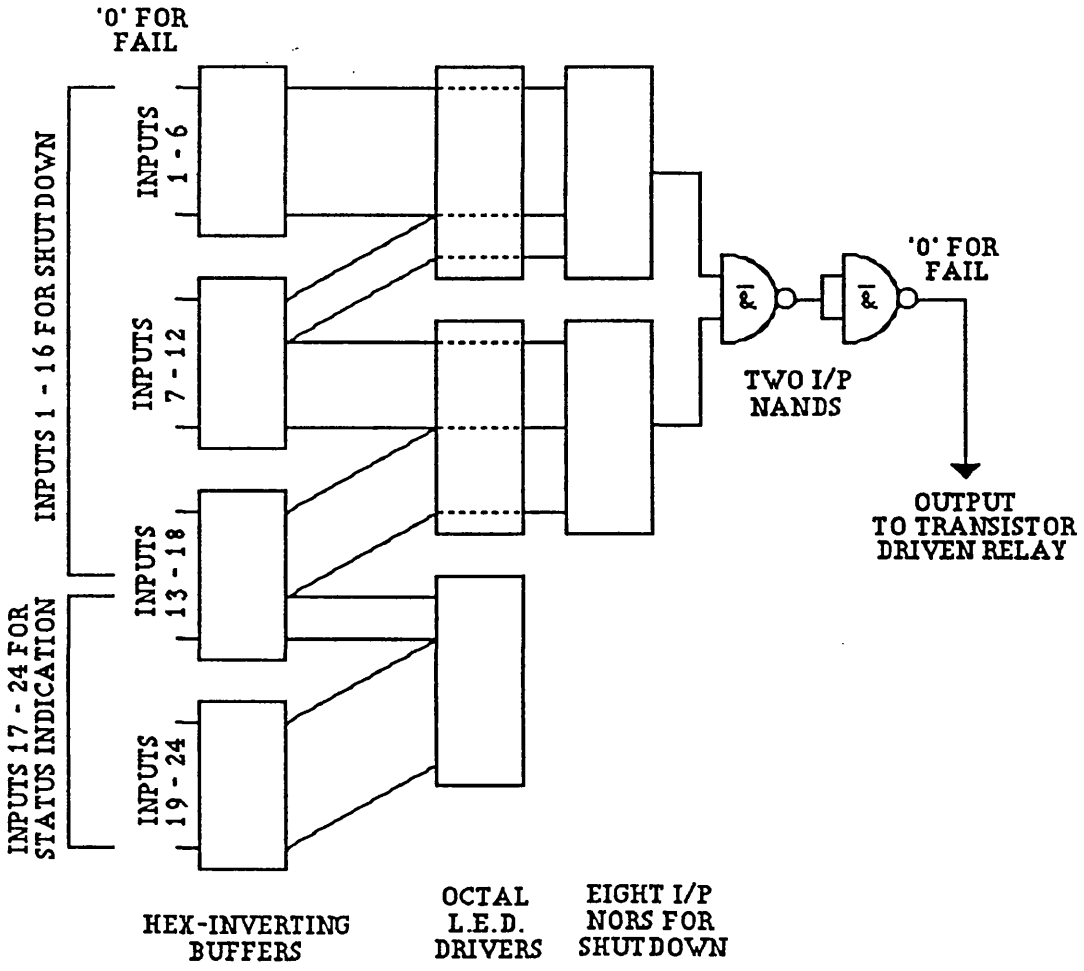

Figure 2.41

CHAPTER 3 - DESIGN OF SURFACE TEMPERATURE PROBES

3.1 Thin Film Surface Temperature Sensors

3.1.a Introduction

Heat transfer within the combustion chambers of reciprocating engines is an important aspect of engine operation. The design of combustion chamber components requires a knowledge of the thermal boundary conditions present within the combustion chamber. This is also the case for cycle simulation programs which are used to predict the performance of such engines. Transient surface temperature data is also required for the control and monitoring of the test specimens which are used in the thermal shock and thermal conductivity test rigs. The acquisition of equilibrium temperature field data from both the piston and the liner, has been treated elsewhere in this thesis, and this section will concentrate only on the acquisition of transient thermal data.

Attempts have been made to validate a number of the heat transfer correlations which are currently used within cycle simulation programs, utilising thin film surface temperature probes. A number of these experiments have been conducted using the traditional, Bendersky, type of probe **(Refs. 18, 19, 20)**. The form of this probe is coaxial, and is essentially comprised of an electrically insulated wire surrounded by a plug of metal. The central wire, of one thermocouple metal, is connected to the outer, coaxial, metal plug, with a thin metal film, evapourated across the exposed surface. This produces a thin thermocouple junction across the end of the central wire, as shown in **Fig. 3.1** . The advantage of this type of sensor is that it is relatively simple to produce and may be used when the transient surface temperature of a metal body is required to be measured. It has the further advantage that should the thin film be ruptured by accident, or by use in rigorous conditions, that the surface may be prepared and the thin film redeposited.

Finite element, and finite difference analyses of this form of surface thermocouple were carried out by Enomoto and

Furuhama (**Ref. 21**). The equilibrium analysis shows that the thin, central wire, has little effect on the equilibrium temperature field in the surrounding plug. However, this analysis is followed by transient modelling which shows the effect of two dimensional heat transfer on the response of the thin film thermocouple. Another series of transient finite element analyses were carried out by Jackson et al (**Ref. 22**), and these also show the effect of transient thermal boundary conditions, on the response of the probe. However, although this paper is generally of a high standard, one of the assumptions which is made, regarding the output from the probe, overestimates the heat flux by approximately 20% . This error arises from nature of the probe on which the analyses were carried out. The probe front face is comprised of two thermocouples junctions by virtue of the metal which is deposited over the wire leadthroughs. However, with the correct choice of deposited, front face thin film, material, errors can be reduced to negligible levels. This point is examined in further detail in Rassihan's thesis (**Ref. 23**).

It was recognised that the coaxial form of probe might be prone to inaccuracy, as a result of the two dimensional heat transfer from the thermocouple junction area which occurs under transient thermal conditions. Alternative forms of probe design were therefore examined.

Little work has so far been carried out on detailed two dimensional finite element or finite difference modelling of prospective probe designs due to time limitations. However, one or two points which have already arisen are worthy of note. The first of these is concerned with the aspect ratio of the elements which are used for the mesh. The mesh which is used for the transient finite element analysis of such probes must model the extremely thin surface layer of metal which is deposited to form the thermocouple junction on the front face of the probe. Wires which are brought to the surface of the probe are generally much larger than this thin layer, leading to elements on the surface which have poor aspect ratios. Care must therefore be taken in the choice of element type as this will influence the accuracy which may be expected and the

limits of aspect ratio which are considered acceptable. A further point is the thermal starting condition which is chosen for the model. This arises from the fact that there are two solutions for the differential equations. This is probably best explained with the aid of **Fig. 3.2** which shows the result, in graphical form, of the same probe subjected to the same thermal conditions on the front face, but with different starting conditions. It is for this reason that it is desirable to analyse the equilibrium temperature field before applying the cyclic thermal boundary conditions. The reason for this is that errors in the solution will be more readily recognised, and that the run time for steady state oscillatory behaviour will be much shorter.

The analysis of probe designs is, as stated, in its early stages, but offers the means by which simpler and more robust surface heat flux probes may be constructed. Considering the coaxial probe in the limit (of wire thickness), it should be possible to estimate the error in the performance of such probes, as the wire, or tape, thickness diminishes to the same level as for the thin film. However, two probe designs were drawn up, which avoid the problem of the leadthroughs interfering with the heat transfer around the thermocouple junction.

Although it has been assumed that thermocouples would be the preferred choice of temperature sensor, the requirements for a surface temperature sensor will now be examined, to justify the choice of thermocouples for this purpose.

3.2 Surface Temperature Sensor Requirements

A list of requirements for surface temperature sensors is given in **Fig. 3.3** . Briefly going over the points mentioned in this figure : -

a). the sensor must be physically small and ideally be capable of monitoring point temperatures, this essentially rules out resistive gauges.

b). the sensor must be capable of operating in oxidizing atmospheres up to around say, 800°C .

c). the sensor must be capable of being fitted to

the specimen surface without the application of heat or such that the specimen temperature during fixing does not rise above about 250°C. This requirement is largely for the production of surface temperature sensors which are to be used for thermal shock specimens, and does not apply to general engine temperature sensors, where it is assumed that no damage to the ceramic will occur during the manufacture of such probes.

d). the application of the sensor to the substrate should not involve the use of any intermediary material which will affect the thermal response characteristics of the sensor. This is a problem when using foil type thermocouple gauges which require some form of adhesive to bond the gauge to the surface of the specimen, or probe.

e). the response of the sensor to temperature should be linear to a reasonable degree, otherwise signal processing becomes complex and expensive both in terms of equipment and time. This is a further reason why resistive gauges are not preferred in this application, as the temperature swing may be large for the case of low thermal conductivity ceramic substrates.

f). the signal which the sensor produces should be of a magnitude where noise is unlikely to present an additional problem.

g). gauge materials should be readily available in the forms required for the production of the sensors and of the interconnections between sensor and conditioning.

h). the sensor should be capable of withstanding reasonable levels of surface damage, without the calibration of the device changing. This point is particularily important for the case of surface temperature sensors which are to be used with plasma sprayed coatings. A microcracked surface which is prone to further crack growth during service will cause problems with resistive type gauges.

After due consideration of the above requirements it was concluded that the sensor most likely to be capable of fulfilling them was a thermocouple sensor. Of the thermocouple materials readily available, type K was the preferred choice.

However, some explanation of the choice of sensor will now be given.

Points a)., c)., d)., and e). favoured the choice of thermocouples over resistive type gauges. Point d). implied that the sensor be directly bonded to the specimen surface. Numerous techniques were considered for the direct bonding of metallic layers to ceramic substrates, these included :-

i). vacuum deposition methods, which include
   evaporation
   sputtering
   molecular/ion beam
   plasma assisted chemical vapour
ii). electroless deposition methods
iii). plasma spray
iv). conductive pastes and enamels

It has already been stated that thermocouples were the favoured type of sensor, further, if the response of the thermocouple was to be linear (point e).) and of reasonable magnitude (point f).) then type K was the obvious choice among the readily available (point g).) thermocouple alloys. Type K is comprised of two, complex alloys each of which must adhere to tight specifications on composition, this therefore reduced the options as far as the deposition method was concerned. The only vacuum deposition techniques which were available "at hand" were evaporation and sputtering. In order to deposit alloys, either electron beam evaporation or flash evaporation are required, and neither of these techniques were available. The conclusion was that sputtering be used to apply the thin films.

3.3 Notes on Thermocouple Materials

A number of attempts were made to deposit chromel and alumel thermocouple alloys, on different ceramic substrates, with rather limited success. X-ray diffraction analysis showed that the composition of the thin films which were deposited, was considerably different from the starting material. This, together with problems of oxidation of the

sputtered material, indicated that alternative thermocouple metals be used.

Successful sputtering of pure nickel had already been achieved, and it was known that gold was sputtered on a regular basis by the electron microscopy team. A thin film thermocouple of gold - nickel was therefore produced. This combination of metals gave good adherence to the ceramic substrates, but proved to be unstable above about 400°C. This instability was traced to crazing of the nickel thin film. The next combination of metals to be tried was gold - platinum. The low chemical activity of these metals overcame any problems likely to be related to oxidation, and indeed the thermocouples produced, were both adherant, and stable under the thermal cycling to which they were subjected, in the thermal shock test rig. However, when the gold - platinum thermocouples were deposited on plasma sprayed zirconia and on pyrophyllite substrates, a long term stability problem arose. During calibration of such thermocouples, on these substrates, it was noted that after only relatively short periods of time at 800°C, that the gold started to diffuse into the substrate material. The diffusion rate was sufficient to completely rupture the 1 to 3 μm thin films in around one hour. This point did not come to light until after some considerable amount of testing had been accomplished on zirconia sprayed test specimens in the thermal shock test rig. Some samples had executed over 1000 thermal cycles without changes in the calibration being noted. The usual peak surface temperatures were around 700 to 750°C, with minimum surface temperatures of around 200°C. However, inspection of the front face temperature versus time shows that the residence time at the higher temperatures was only a small portion of the total cycle period.

The final choice of thermocouple materials was platinum against rhodium. Long term testing of this combination has yet to be carried out, but the "noble" nature of both thermocouple metals coupled with their high melting points should ensure adequate long term stability. However, the cyclic strains imposed on the rhodium might yet prove to be problematical, as

this material is relatively brittle compared with gold and platinum and may not be able to accomodate high strains, plastically.

3.4 Thin Film to Wire Connections

The connection of the thin films to wire leadthroughs is essential if the output of the thin film thermocouples are to be taken to instrumentation external to the test rig. This connection was accomplished in the thermal shock and thermal conducitivity test rigs, by utilising a mechanical clamping system. Fingers of thermocouple material were brought to bear upon the thin films to provide simple mechanical contact. The connection of wires to the thin films in the heat flux probes had to be more secure, and allow for the assembled device to withstand the high pressures which would be present in the combustion chamber of the firing engine. This proved to be a more difficult task than had originally been envisaged. A mechanical clamping scheme was attempted with the disc specimen for the simulation test rig. The main problem associated with this method of attachment, was that of assembly. Indeed, all attempts at assembly failed, and this type of connection was abandoned. Another form of connection which was tried is shown in **Fig. 3.4** where solid wires of thermocouple material were brought through the ceramic specimen and fixed in place with a pool of glass. The intention was to grind the glass flat after the assembly had been removed from the furnace and apply the thin films as shown. However, this method was used when chromel - alumel wire pairs were still being considered and the reaction between the glass and the oxides on the thermocouple wires proved to be excessive. Apart from the inability to produce a clean bond between the wires and the glass, it was obvious that the glass had a markedly different thermal expansion coefficient from that of the ceramic substrate, this led to separation of the glass, on cooling, from the surrounding substrate material. Glass to metal, and glass to ceramic seals such as were attempted above, are feasible, but the expertise, and materials, for such assemblies were not available within

the university at the time when these early tests were carried out. A good source of information on glass to metal sealing, in general, proved to be **Ref. 24** . This reference describes another form of wire leadthrough which is found in lamp manufacture. Thin wires or foils are sandwiched between glass, at the end of the device envelope. However, the solution to the problem of bonding the thin films to wire leadthroughs, which was finally chosen, involved the use of specialised ceramic adhesives and metallising of the ceramic substrate. The details of the two final designs are now given. The first of these is currently being produced, and the materials required for the second type is on order.

3.5 First Probe Design Details

The probe may be divided into three major sections as follows, with reference to **Figs. 3.5.a** and **3.5.b** .

The outer casing of the probe has been designed to contain all of the required elements within a body identical in size to a standard Kistler pressure transducer. This should allow ease of access to engine pressure transducer drillings already in existence, although it is recognised that spatial variations in heat transfer conditions will not be addressed by this approach. The outer case is manufactured from 303 stainless steel for three reasons : -

i). high temperature strength

ii). machinability

iii). medium range thermal conductivity, similar to alumina.

This latter point is an attempt to preserve one dimensional heat transfer within the probe, although the ceramic probe itself is isolated from the outer case.

The cooling body is deliberately simple in form, as the size of this section precludes any complex machining. The cooling body is manufactured in sterling silver, which although appearing rather extravagant, is done for good reasons. The silver alloy should be more readily machined than, say, pure copper, while retaining very high thermal conductivity. The requirement for high thermal conductivity

results from the simple water cooling passage form chosen. It was considered desirable to have only minimal axial temperature gradients to ensure good transfer of heat from the front face of this section. Silver tube, available from Johnson Matthey p.l.c, is actually considerable cheaper than precision copper tube from say, Goodfellow Metals Ltd.. This presumably arises from the fact that fine tube for jewellery work is mass produced whereas fine copper tube is not. A similar argument arises when considering the availability of brazes for joining parts of the cooling section. The design of the cooling body dictates that multiple braze stages be used, which in turn implies that more than one grade of brazing alloy be used. Here again, a range of brazing alloys were readily availble for the joining of silver alloys.

The ceramic probe itself is manufactured in Deranox 975 , which is a high strength alumina. This material has a thermal conductivity of around 25 $Wm^{-1}K^{-1}$, and thus is reasonably close to stainless steel 303 in this respect ("k" = 16 $Wm^{-1}K^{-1}$). The length of this section has been designed such that under typical maximum engine loadings, the mean temperature at the front face of the probe should not exceed around 450°C. This has been done for two reasons. The first of these is that it is intended that the probe should not present markedly different mean front face temperatures to the gas in the combustion chamber, over those that a metal surface would have. Thus the presence of the probe should produce minimal effects on combustion. The second reason is that the isolating sleeve which surrounds the ceramic, is produced from a polyimide resin, which is an excellent insulator ("k" = 0.125 $Wm^{-1}K^{-1}$), but has an upper operating temperature of around 450°C .

The thin films which make up the front face surface thermocouple are sputter deposited from targets of platinum and rhodium. To minimise problems associated with the sealing of the cermic probe to the outer casing, and also to ease the attachment of wire leadthroughs, the ceramic body is initially of split contruction. One half of the split ceramic is sputter coated, not only on its front face, but also along its length.

This allows the attachment of wires to the thin films to take place in a relatively cool region of the probe. The intention is to metallise small pockets at the cool end of the ceramic body and to bond the wires by soldering to this metallised region. In the event that this form of connecting the wire leadthroughs to the thin films should prove unsuccessful, then a lower temperature silver loaded epoxy bonding method will be attempted. The two halves of the ceramic body are bonded together using a high strength fine ceramic adhesive. The completed ceramic body is then finish machined to the size and shape required. **Fig. 3.6** shows the production route for the ceramic body, with **Fig. 3.5.a** showing the full assembly of the probe in two cross sectional views. **Fig. 3.7** is a photgraph showing the basic ceramic body, split and drilled, but before sputtering and final machining. The figure also shows the sputtering jig and mask, together with the other parts of the assembly.

3.6 Second Probe Design Details

The second probe design, is simpler than the first, but there are still doubts concerning the detail of the design, which may have to be modified.

This design utilises a low thermal conductivity ceramic material, namely fully dense cordierite. This has a low thermal expansion coefficient and medium strength and thus is tolerant of the thermal shock which it may be subjected to in the combustion chamber (the material is the same as that used for the piston crowns). An assumption which was made in the design of the first probe, was that the temperature differential between the front and rear of the pockets, retaining the wire to thin film junction was small. This assumption is not unreasonable when the thermal conductivity of the ceramic is high, and the axial dimension of the ceramic is large in comparison to the pocket depth. This assumption would not be valid with the low thermal conductivity material, simply because the ceramic axial dimension is so much shorter. An alternative method of bonding the wires to the thin films had to be found if secondary junction errors were to be

avoided. In this design the solution was to bring the thin connecting wires to the front face of the ceramic material and to bond them in place with ceramic adhesive. Thin sleeving is used to electrically isolate the leadthroughs from the cooling portion of the probe. The thermocouple is formed by sputter coating material over the ends of the wire, but forming the junction over ceramic, as shown in **Fig. 3.8** . The back face temperature of the ceramic body is monitored using a thin (0.5mm diameter) sheathed thermocouple, as for the first probe design.

The second probe does not rely on water cooling, but on attachment to a cooler portion of the engine head, removed from the flame face. It is essential that the screwed portion of the probe which mates with the head be in good thermal contact, to avoid overheating of the probe. This is ensured by using a precision thread 1/4" 36 UNS, and coating the threaded portion of the probe with heat transfer paste. **Fig. 3.9** shows the proposed probe in postion, with the heat flux path highlighted. The ceramic is isolated from the surounding metal of the head using polyimide foil, as for the first probe design. In both designs, the polyimide foil is present to reduce side losses to the surrounding metal, and to prevent heat transfer from the gas to the side walls of the ceramic body. In other probe designs (**Ref. 22**), this has been achieved by the incorporation of an airgap. The use of an airgap automatically implies that some form of front face sealing be provided. This is necessary to exclude combustion chamber gases from the airgap. Unfortunately the front face seal can produce undesirable radial heat loss from the probe. The durability of the polymer thermal isolator, used in the two heat flux probes designed by the writer, has yet to be tested.

CUTAWAY SCHEMATIC OF CONCENTRIC TYPE SURFACE THERMOCOUPLE SHOWING MAIN FEATURES

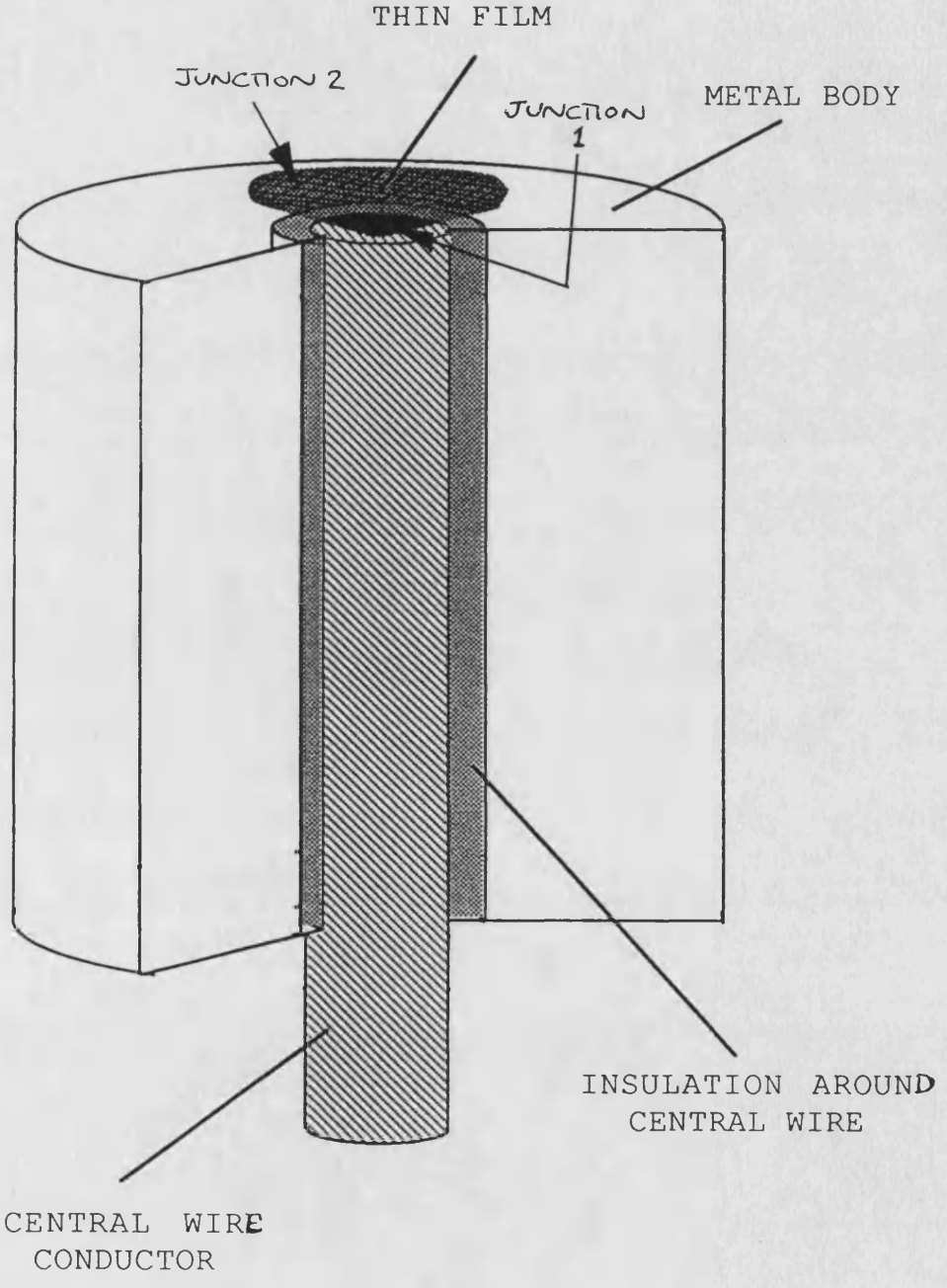

Figure 3.1

Figure 3.2

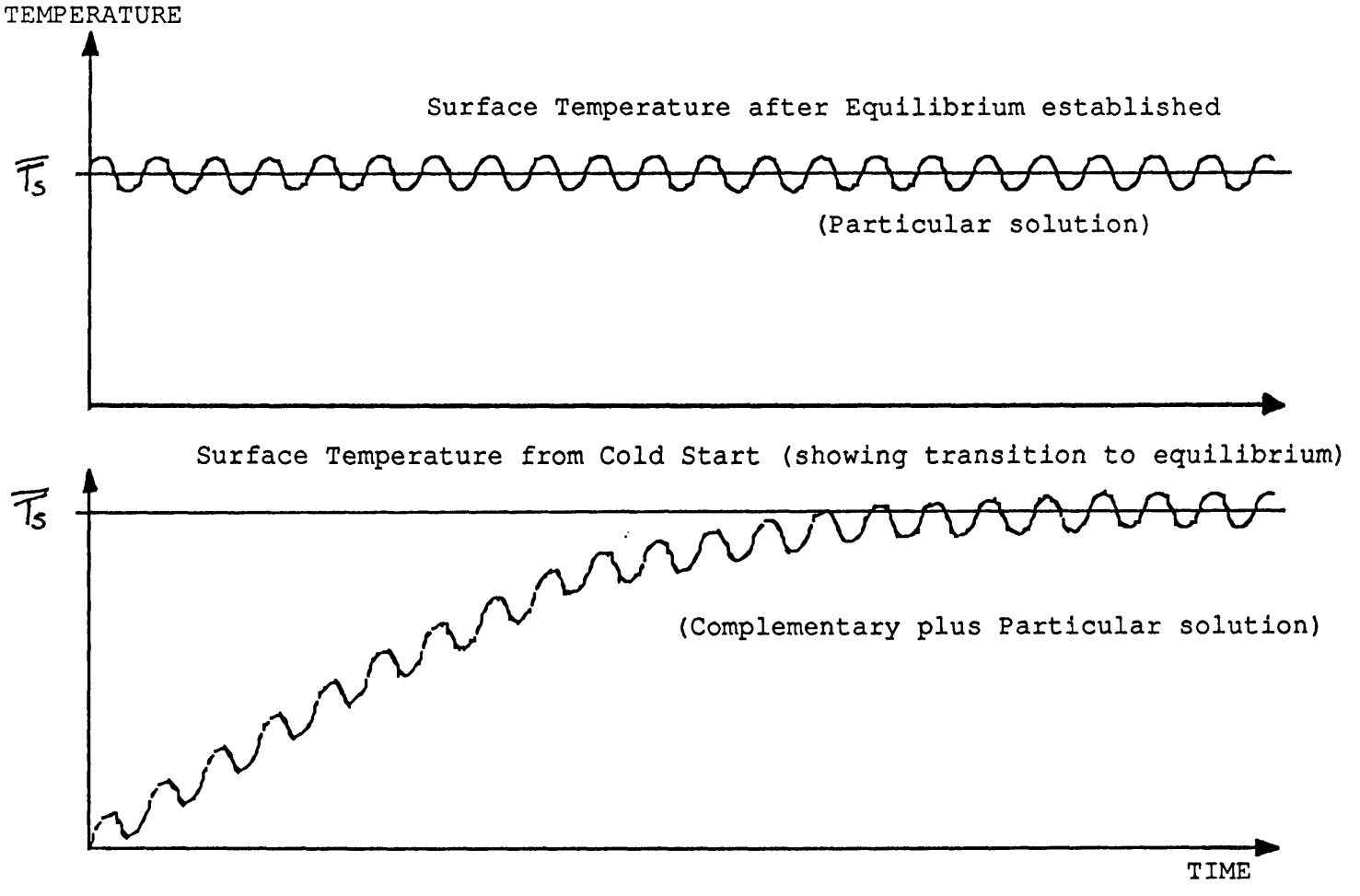

Effect of Starting Condition on the Solution to the Surface Temperature

SURFACE TEMPERATURE SENSOR REQUIREMENTS

A — SMALL PHYSICAL SIZE

B — ABILITY TO WITHSTAND OPERATING CONDITIONS

C — FITTING OF DEVICE TO SURFACE SHOULD BE WITHOUT HEATING

D — FITTING OF DEVICE TO SURFACE SHOULD BE WITHOUT THE USE OF AN INTERMEDIATE LAYER

E — LINEARITY OF THE SENSORS OUTPUT IS DESIRABLE BUT NOT ESSENTIAL

F — SENSOR SIGNAL SHOULD BE AS LARGE AS POSSIBLE TO AVOID NOISE PROBLEMS

G — MATERIALS FOR PRODUCTION OF THE SENSORS SHOULD BE READILY AVAILABLE

H — ABILITY OF SENSOR TO WITHSTAND REASONABLE LEVELS OF SURFACE CRACK DAMAGE, WITHOUT CHANGING CALIBRATION

Figure 3.3

Wire Leadout based Thin Film Surface Thermocouple

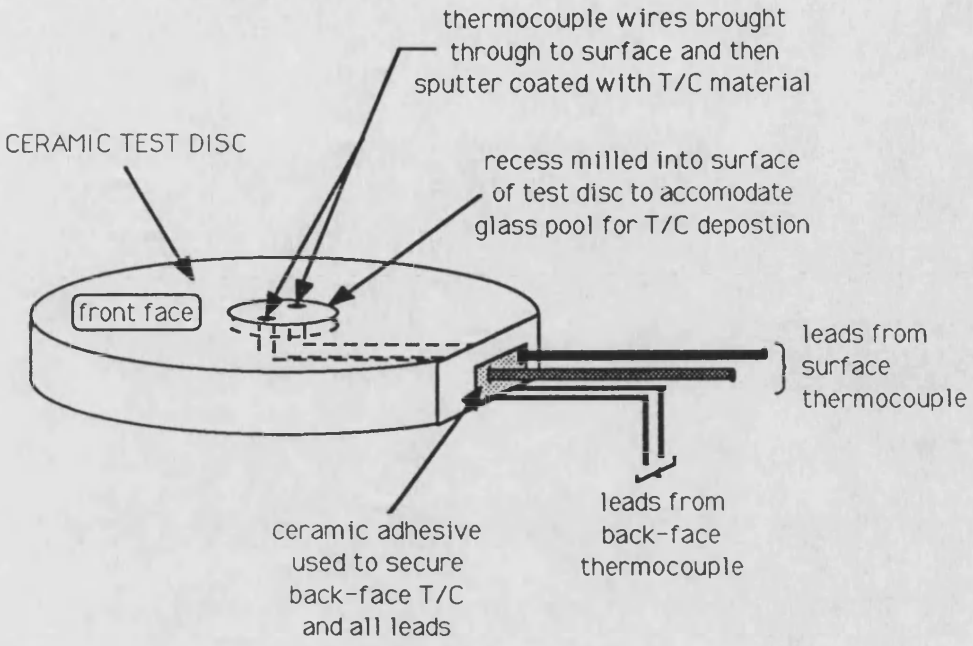

ENLARGED PLAN VIEW OF GLASS WELL

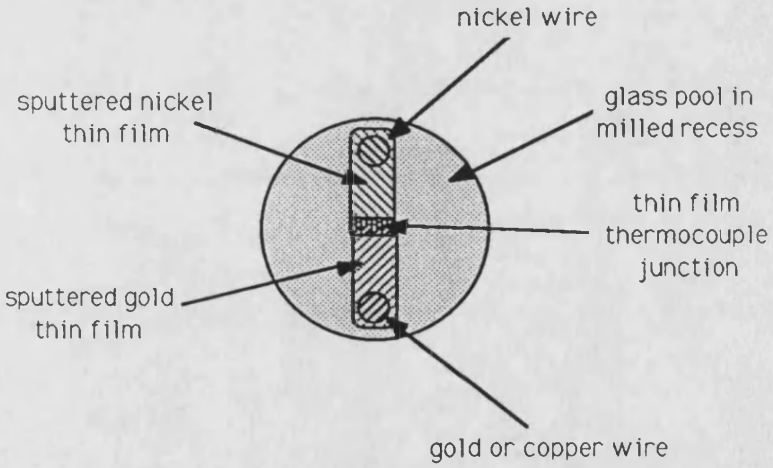

Figure 3.4

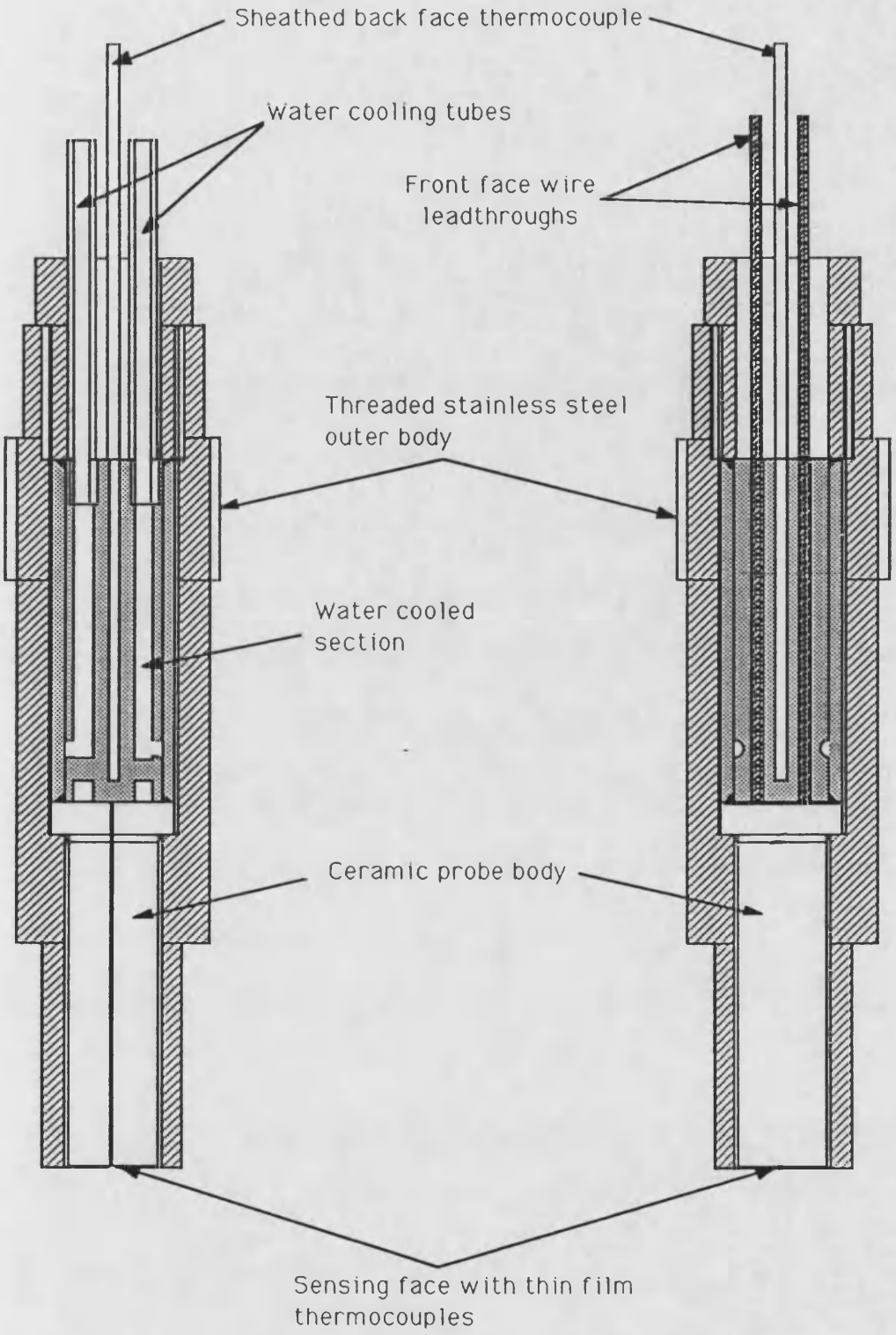

Figure 3.5.a WATER COOLED HEAT FLUX PROBE

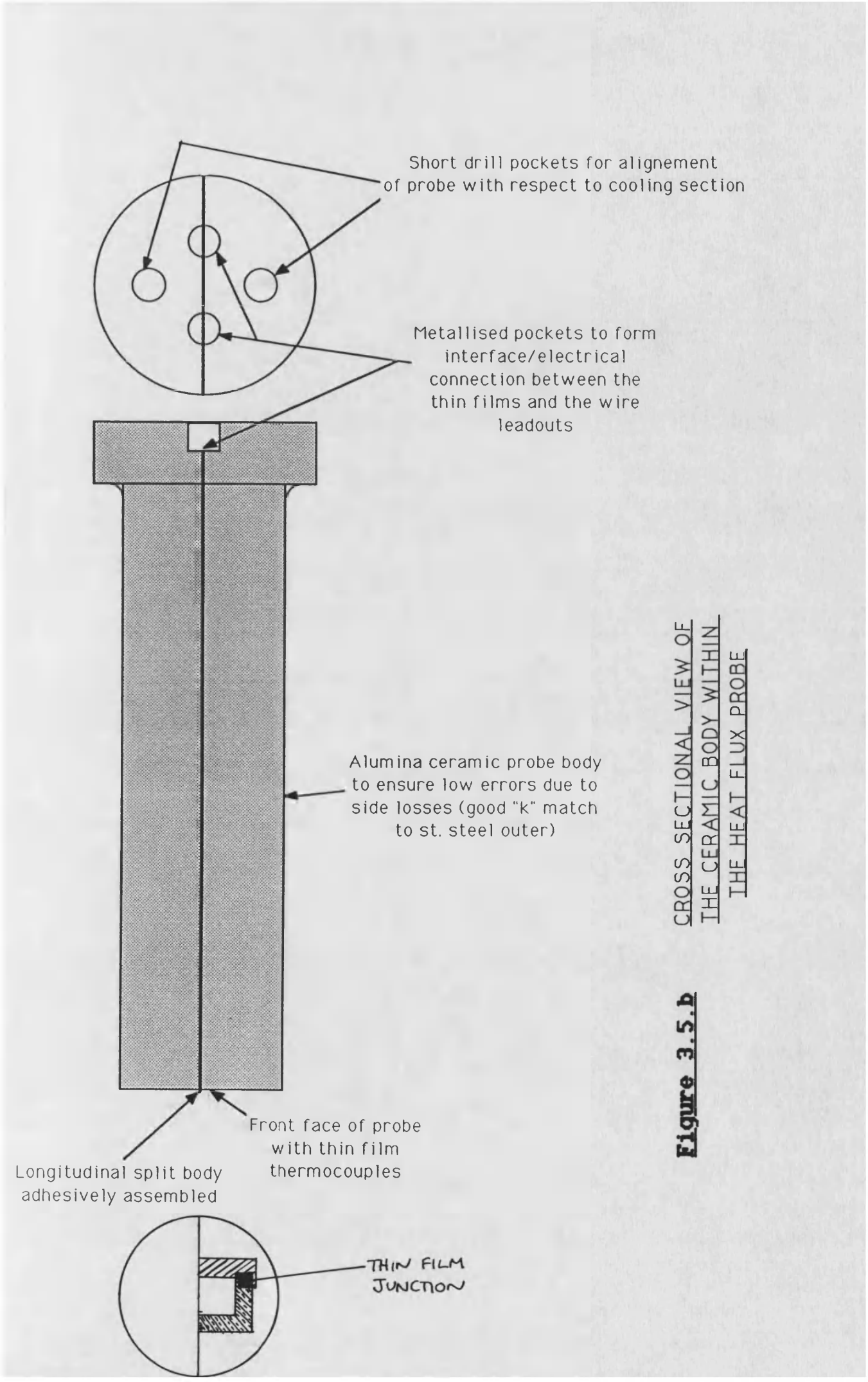

CROSS SECTIONAL VIEW OF THE CERAMIC BODY WITHIN THE HEAT FLUX PROBE

Figure 3.5.b

Production Route for Ceramic Probe Body as used in the Heat Flux Probe (Type 1)

1. Machine ceramic body oversize on diameter but to finish length. Split body longitudinally, and fine finish the two flats created. Rebond two halves and turn back to cylindrical form.

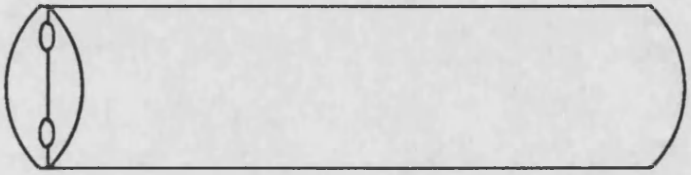

2. Drill shallow pockets, on split line.

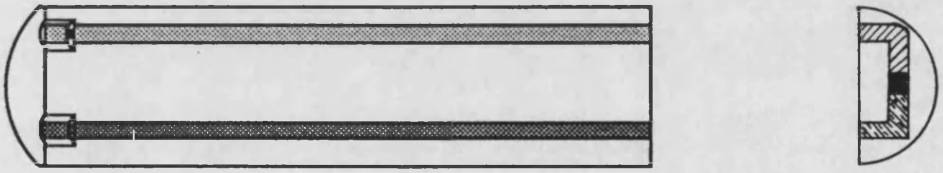

3. Sputter on both legs of the thin film thermocouple along full length of the ceramic body, in the pockets and across the front face of the body. Metallise the pockets.

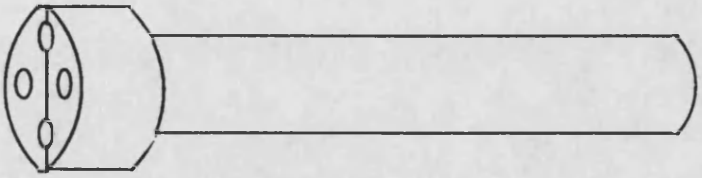

4. Rebond the two halves of the ceramic body using high strength ceramic adhesive and finish machine. Final operations include taking both diameters of the body to finish dimensions, and drilling of two further shallow pockets for alignement purposes.

Figure 3.6

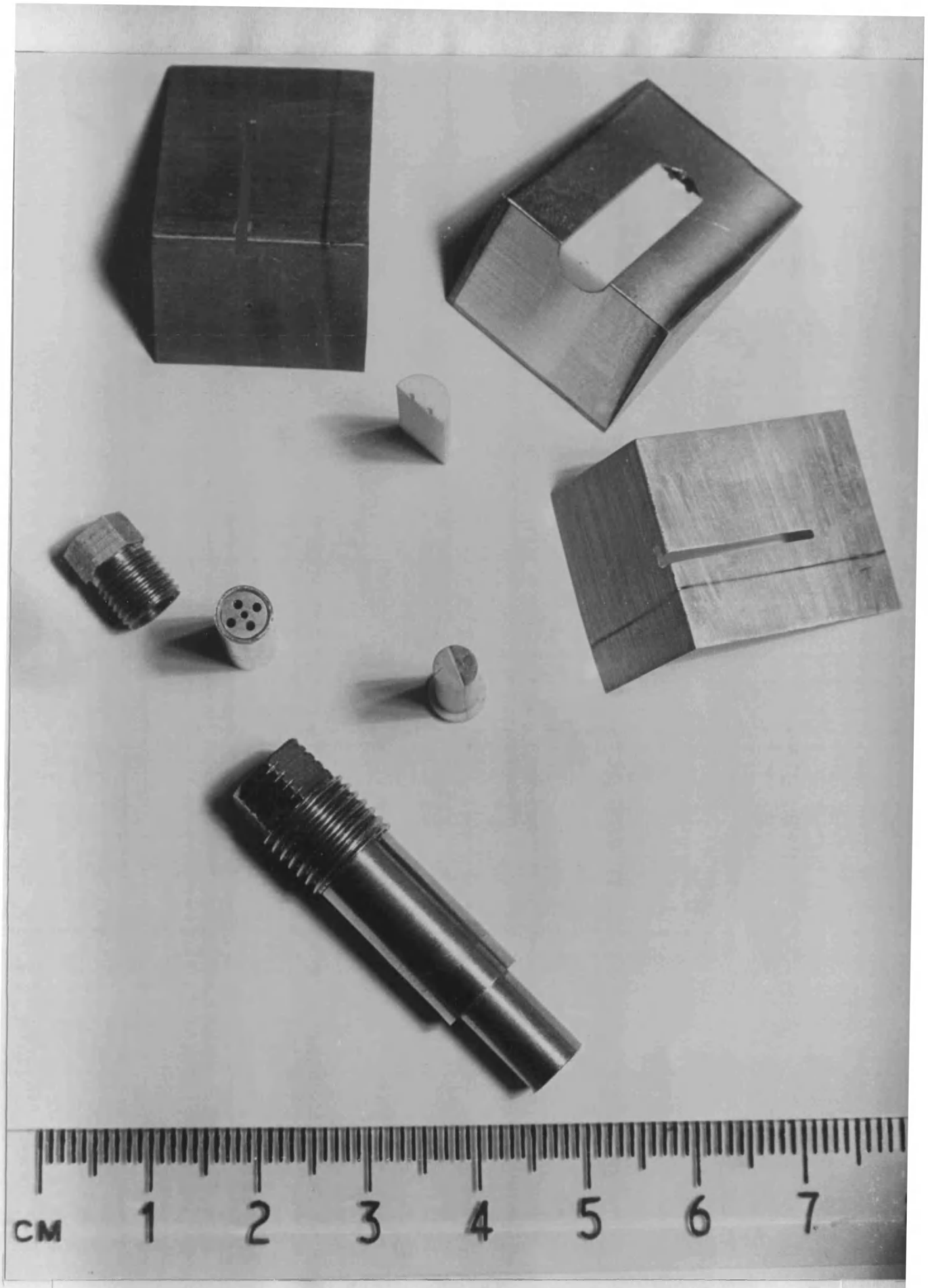

Figure 3.7 - Surface Temperature Probe Split Bodies, Sputtering Jigs, and Main Probe Body

TYPE 2 HEAT FLUX PROBE DESIGN

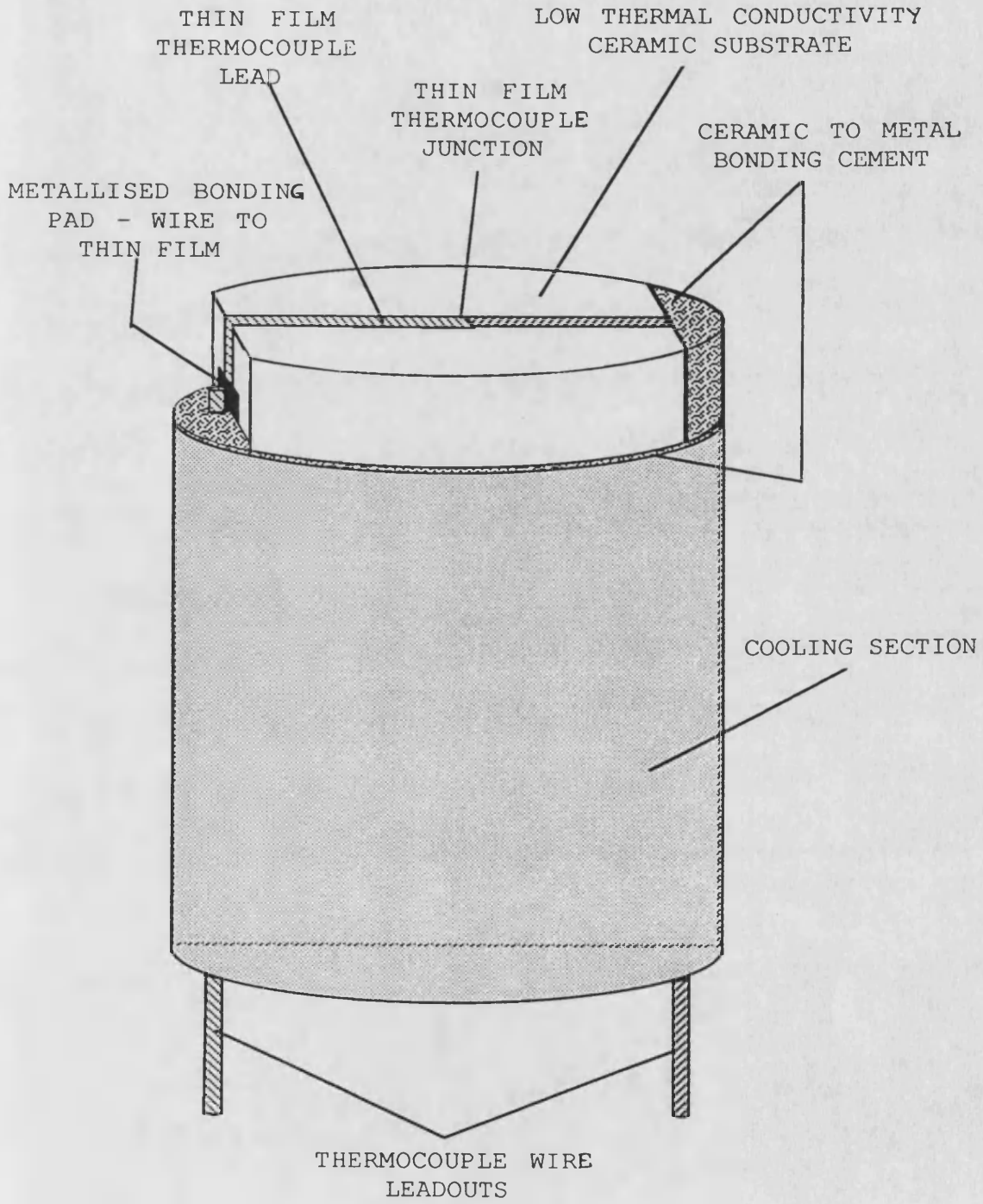

Figure 3.8

Second Heat Flux Probe Desig showing Heat Flux Lines

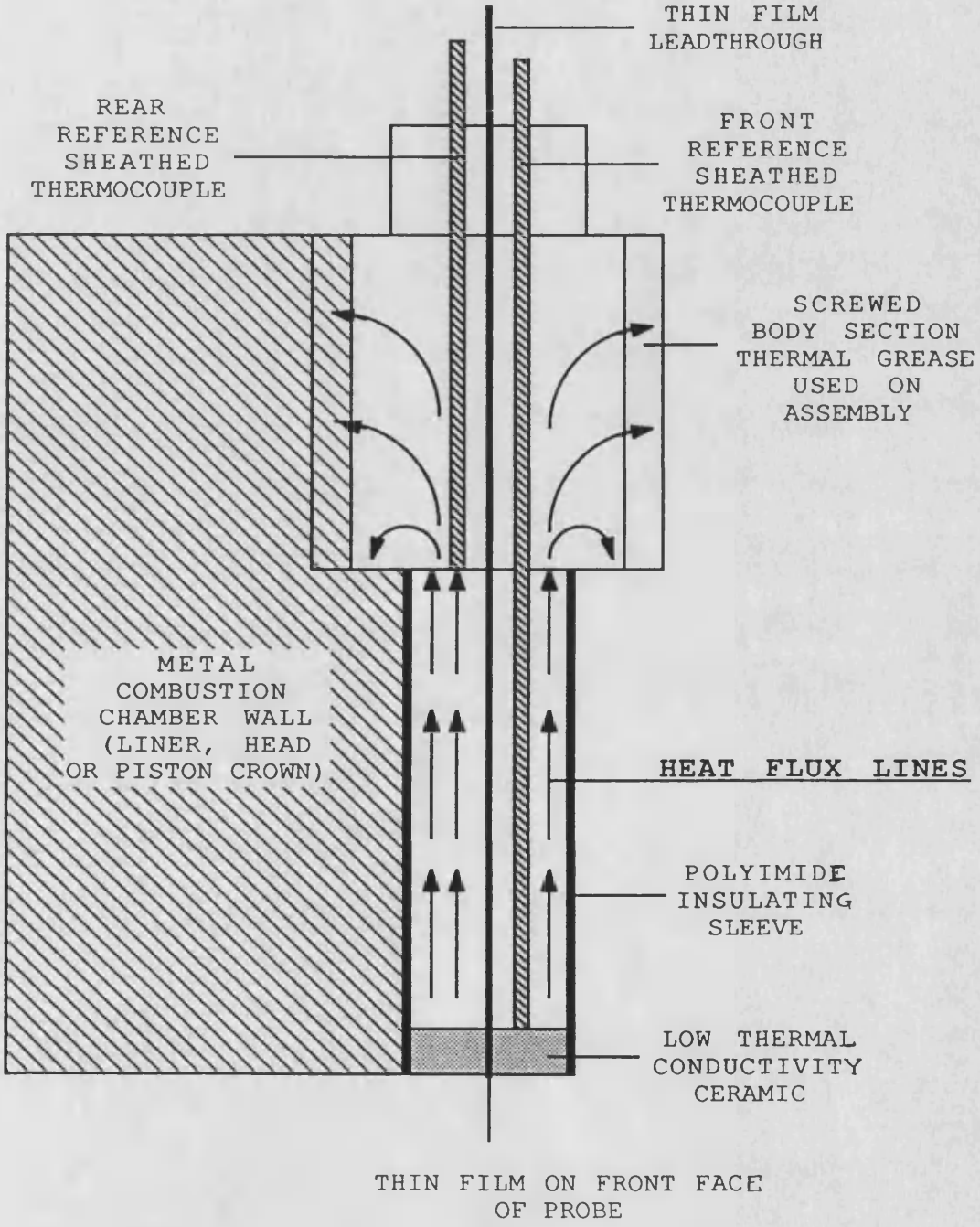

Figure 3.9

CHAPTER 4 - ENGINE TEST RIGS

4.1 Introduction

The firing engine test rig was the first of the test rigs to be built, and was designed to allow the four major areas of interest to be covered. These were :-

i). the engine performance

ii). the heat balance of the engine

iii). combustion.

and iv).the component temperature fields

A proof testing facility for the ceramic components was also considered to be of some importance and thus a second engine test rig was built to provide motored running. This second test rig was designed to simulate inertial and pressure loading of piston components, prior to their introduction to the engine, but with only moderate thermal loadings. A description of the original build of the simulation test rig facility is given by Manton in his thesis (**Ref. 4**). This facility has been modified to cater for the proof testing of I.D.I. piston/piston crown assemblies. A brief description of this conversion is given at the end of this chapter in section 4.7. The remainder of this chapter deals with the firing engine test bed instrumentation, for which the writer was largely responsible.

4.2 Test Rig Conversion from D.I. to I.D.I. Operation

For the purpose of the "CERAMICS IN ENGINES" project the engine was converted from D.I. to I.D.I. operation. While the direct injection diesel offered the best potential with regard to fuel economy, the indirect injection diesel offered a simpler design of piston. This point was considered to be of great importance in the early stages of development, particularily when dealing with a new material. The simple flat topped piston design which featured in the I.D.I. build of the engine meant that production of the piston in ceramic was simplified over that which would have been necessary had the D.I. form been retained. The attachment

systems for this form of piston were less constrained by space considerations than for the D.I. form. These factors, coupled with interest from Ford (U.K.) in pursuing an insulated form of I.D.I. engine, led to the conversion of the PH1W to an AVB.

The conversion of the D.I. to the I.D.I. was essentially comprised of changing the top half of the engine, the crankcase and fuel injection equipment being common to both models. The engine cylinder bore was reduced from 88 mm to 80 mm with subsequent reduction in the capacity of the engine from around 650 cm^3 to around 550 cm^3 .

4.3 Instrumentation for Engine Performance

The basic requirements for the study of this topic are the engine itself, together with some form of loading, a means of monitoring shaft output torque, engine speed and fuel flow rate. Apart from these it is essential that several other engine parameters are monitored and/or controlled, in order that a datum or 'control' condition be established. Among these are :- coolant inlet and outlet temperatures, fuel temperature, inlet air and exhaust temperatures and pressures, and oil temperature. **Fig. 4.1** schematically shows the basic firing engine test rig, and **Fig. 4.2** is a photograph of the test rig.

4.3.a Engine Loading

The loading system for the engine comprises a D.C. excited dynamometer, with variable field excitation for fine control of loading and a bank of water cooled resistance elements for coarse adjustment. The engine output shaft is coupled to the cradle mounted dynamometer by a rubber 'doughnut' type coupling. This type of coupling allows some degree of misalignement between the two shafts and also reduces the level of the torque peaks which can be an important factor when considering the fatigue life of load cells attached to the dynamometer for torque measurement. The 'wind up' which is a feature of doughnut couplings such as these, may be undesirable for transient engine testing, however only steady state testing was envisaged for this

particular rig.

4.3.b Engine Torque

Torque was monitored using a load cell connected between a rigid bed member and a stiffened beam attached to and running under the swinging dynamometer. Any static offsets could either be nulled out mechanically, by balance weights on the arm or electrically in the signal conditioning. In order to afford a large measure of protection for the load cell while not interfering with the readings obtained a spring/damper system was inserted in series with the load cell. The output from the load cell was found to contain large amplitude pulsations, at firing frequency. The electrical signal was therefore damped with a resistor/capacitor filter to obtain a steady reading on the panel meter. This is justified on the basis that it was only the torque signal which is unsteady, and thus averaging this will produce correct figures for the engine power output. Calibration of the torque cell was carried out statically, using weights placed on the dynamometer arm at a known horizontal distance from its swinging axis.

4.3.c Engine Speed

Engine speed was monitored using a variable reluctance type pickoff mounted above the flywheel teeth, the output of which was fed to a variable gate time digital tachometer. This allowed the speed of the engine to be displayed either in revolutions per minute or in radians per second.

4.3.d Engine Fuel Flow

Fuel flow is monitored using a graduated burette with appropriate valving, to switch from a diesel day tank supply to burette supply, together with a stop watch. Although this system has the advantage of being relatively low cost, it cannot compete on an accuracy basis with the more sophisticated fuel weighing methods with electronic timing. It is also necessary with this system to make corrections for fuel density with temperature.

A further problem which arose with this form of fuel flow monitoring was that of pressure pulsations produced by the injection pump. During fuel flow monitoring periods, the level of fuel in the burette would oscillate wildly making readings very difficult. To cure this, a gas damper was inserted in the fuel line between the burette and the fuel pump. This received little attention at the time, largely because it cured the problem and results appeared consistent with manufacturers data. Closer examination at a later date revealed the addition of the damper to be a source of error, unless tight control of the gas volume was observed. However, the error is accountable for and corrections to fuel flow can be made. See **Appendix 4.**

4.3.e Engine Condition

As stated earlier in this section, apart from the basic requirements of fuel flow , output shaft torque and engine speed monitoring, it is essential that several other engine operating parameters are maintained at a constant level, these are :- inlet manifold air pressure and temperature (in the boosted test cases), engine coolant inlet temperature, sump oil temperature and the exhaust back pressure (in the boosted test cases). Each of these will now be dealt with in more detail, with particular reference to **Fig. 4.1** .

Inlet air temperature is not strictly speaking controlled by the engine operatives during naturally aspirated engine runs, when the engine 'breathes' from the test cell. However, the laboratory is supplied with warm air heating ducts, which are thermostatically controlled and maintain the test cell to within ± 5°C of 20°C(unless the exterior doors are opened). Operating under 'boosted' conditions the engine takes its air supply from the large Bellis & Morcom compressed air supply. In order to simulate aftercooled 'boosted' conditions, and to ensure that inlet air temperature was held constant, an electrical heating section was installed in the line from the compressor reservoir to the engine. The power to the heater was controlled using a commercial 3-term controller, and

thyristor control unit. Temperature sensing of the inlet air was facilitated by a thermocouple sensor in the air inlet manifold. It was found that after careful setting up of the proportional, integral and derivative terms on the controller had been made, a stability of better than ± 1°C could be maintained, together with minimal settling times between engine operating points.

The air preheater itself, comprised two 1.5 KW elements, together with stainless steel gauze. This assembly was enclosed in a leak tight stainless steel cylinder of welded construction. An estimate of performance predicted a temperature rise across the preheater of 97°C at 2 Bar(abs.) boost and full engine speed (2000 r.p.m.),thus enabling inlet manifold temperatures of around 117°C to be attained.

To minimise resonance effects in the inlet air piping, which could affect engine operation as well as the operation of the pressure control valve on the inlet air system, and to enable pressure and flow to be easily monitored, a large damping tank was installed in the inlet air system, as close as possible to the inlet air manifold. This tank was sized using methods suggested by Kastner (**Ref. 25**)

The inlet air pressure was regulated by a dome valve regulator, type RL5M, manufactured by Hale Hamilton Valves Ltd. This provided a very stable air inlet pressure over the entire engine operating speed range.

Control of exhaust back pressure was necessary to simulate the presence of turbomachinery in the exhaust. Control of this aspect presented a number of problems. The first of these was to find a valve which would survive under the conditions expected to prevail in the exhaust duct. No such valve could be found at reasonable cost, and therefore a simple, manually operated valve was designed and fabricated to fulfil the requirements. A stainless steel disc with an offset centre pin was contained within a recessed stainless steel block and cover plate, see **Fig. 4.3** . To avoid seizure of the device, generous clearances in manufacture were included, together with the addition of an anti-seize compound (R.S. no.

557-089).

In order to minimise reflection of the pressure waves created by the highly pulsating nature of the exhaust stream, the back pressure control valve was placed well downstream of the exhaust manifold, and separated from it by a large damping volume. The in line exhaust chamber also allowed simple monitoring of the back pressure using manometers. Design of this chamber was more influenced by safety considerations than by damping capacity. The chamber was designed for a minimum life of 1000 hours at 650°C using mild steel with a safety factor on stress of five times, using data on lifetime to rupture from Woolman and Mottram **(Ref. 26)**. Thinning of the walls, due to corrosion, and the subsequent reduction in the safety factor require that this vessel be replaced periodically, or, preferably, by a vessel constructed of corrosion resistant material such as a suitable grade of stainless steel.

A further point regarding safety is the inclusion of an overpressure relief valve, which was installed in parallel with the back pressure control valve. Again, a low cost device could not be found to perform adequately under the conditions prevailing in the exhaust system and thus a simple sprung ball blow-off valve was designed, fabricated and subsequently tested. In the event that the back pressure valve is inadvertantly closed completely or that it should fail 'closed' for some reason, then the relief valve will operate. Set opening pressure for this device is presently 2.5 Bar absolute.

As stated earlier the actual values of pressure in both the inlet and exhaust manifolds were monitored using either simple water in glass (naturally aspirated), or mercury in glass manometers (boosted cases) to **B.S. 1042 (Ref. 27)**.

Sump oil temperature was controlled by varying the flow rate of mains water through a heat exchanger external to the engine. Petters Ltd. supplied the necessary data concerning the connection of an external oil cooler to the existing engine oil gallery system. An appropriate oil cooler was

purchased (Bowman type no. EC80 - 1425 -1) and piped into the engine. Thermocouples were inserted in the water inlet and outlet piping together with a flowmeter (R.S. no. 339-730). Actual sump oil temperature was monitored by a thermocouple placed therein.

The main engine coolant system is shown in **Fig. 4.4.** The figure shows both the primary, closed loop coolant path as well as the external mains supply to the heat exchanger (Bowman FC100 - 1426 - 2). It is in the external flow path that the control element is inserted. The control element itself is a low cost three port valve (Danfoss RAV1). Mains water supply is first fed to a header tank, via a simple ball-cock mechanism to reduce the pressure above the valve, and to maintain this constant, regardless of mains pressure fluctuations. Although reliability of this system has proved to be good, the actual control afforded by this unit is inadequate to cover the full operating range of the engine and adjustments have to be periodically made. This is simply due to the range of flow rate control required for this application, together with the fact that the valve is only a proportional device.

4.4 Instrumentation for Engine Heat Balance

4.4.a General

Engine heat balance is a particularily important consideration when modifying components for low heat loss. The major heat flow paths to and from the combustion chamber are as follows :-

i). directly through the liner to the engine coolant

ii). through the piston crown to the liner and thence to the coolant together with flow from the piston underside to the engine oil

iii). through the head deck and valves to the engine coolant.

Fig. 4.4 outlines, schematically, the essential details of the instrumentation for heat balance measurement.

On simple energy conservation grounds it should be

possible to equate energy flowing into the engine with energy flowing out. In reality this proves to be difficult due to the number of heat flow paths and their relative magnitudes. It is usually considered adequate if the balance of inflowing to outflowing energy agrees to within about 5%, as the burden of work required to "nail down" the last 5% is not justifiable in terms of the amount of effort which is demanded. For this reason, the following were taken into account :- fuel flow rate ; heat rejection to coolant ; output shaft power ; heat rejected to oil ; inlet and exhaust enthalpies. Not included in the list are such things as :- convective and radiative transfer from the external surfaces of the engine, engine and rig noise and the possibility of chemical energy in the form of unburnt fuel being carried away in the exhaust, and blow by losses. Order of magnitude estimates of radiative and convective losses from the exterior of the engine were made and broadly agreed with the "unaccounted" portion in the heat balance.

Fuel flow rate measurement has already been covered in an earlier section, however an additional note is that there is a correlation between fuel specific gravity and its lower calorific value, this allows spot checks on the fuel energy content to be made without recourse to full combustion tests in calorimeters, see Taylor and Taylor (**Ref. 28**)

4.4.b Heat Lost to Coolant

To monitor heat rejection to coolant requires not only the coolant flow rate and temperature rise as it passes through the engine but also the absolute temperature of the coolant, as this has an influence on its specific heat, as well as on the calibration of the orifice plate used for flow measurement. For this reason a simple differential thermocouple system was not used. The actual monitoring of the coolant inlet and outlet temperatures was initially taken using two stainless steel sheathed thermocouples. It was found, however, that short term fluctuations in the inlet and outlet temperatures occurred. Considering this to be possibly due to flow instabilities around the exit and entry points of

the coolant into and out of the block, three sheathed thermocouples were used on both the inlet and outlet coolant ports. The three thermocouples on each port were then electrically parallelled to give mean exit and entry temperatures. The thermocouples were first calibrated using 'ice point' and 'boiling point' apparatus, together with appropriate isothermalising blocks in order to match thermocouples as closely as possible. This requirement is necessary as the specification for the thermocouples does not guarantee their output to be closer than ± 1.1°C in this operating range (ANSI C96.1 special - type K 0° to 277°C).

Coolant flow rate was monitored using standard orifice plates to **B.S. 1042 (Ref. 27)** with corner tappings mounted on one inch inside diameter cold drawn seamless tube. Upstream and downstream straight tube requirements were actually above those stated in the standard. Flow rate was controlled manually (using a gate valve outside the straight section) at each engine operating point to obtain the combination of flow and temperature rise whch resulted in the lowest combined error. The temperature rise was monitored using a cold junction compensated digital thermometer (Keithley type no. 870) which has a resolution of 0.1°C. This instrument also hac "on-board" linearisation.

4.4.c Heat Lost to Oil

As already mentioned an external oil cooler was fitted to the engine. This allowed the oil temperature to be held at reasonable levels even when operating the engine at high boost and load. It also allowed the measurement of heat flow to the oil by monitoring the temperature rise of external water flowing through this heat exchanger together with its flow rate. Flow rate of water through this section was monitored using a low cost vane type meter which produces a square wave voltage pulse output, the frequency of which is directly proportional to flow to within ±1% . Output from the device is fed straight into a digital frequency meter and the reading obtained, is converted to appropriate units in the data reduction program. The outputs of the thermocouples,

reading coolant inlet and outlet temperatures, were fed into a twelve-way selector switch, and then into a panel mounted digital thermometer with internal cold junction compensation (Jenway type no. 7500). This data was also manually fed into the data reduction program on the PET computer, and, together with the data on flow was used to calculate heat loss to oil.

4.4.d Inlet Air Enthalpy

Inlet air enthalpy presented little difficulty. Inlet air temperature was simply monitored using a sheathed thermocouple inserted as close as practicable to the inlet manifold, and connected to the panel mounted digital thermometer via the twelve-way switch. The immersion length of the thermocouple was maximised, and due to the small temperature difference, between the air and the wall, only small radiation errors were expected.

Inlet air pressure was assumed to be the same as that in the inlet air damping tank, from where a pressure tapping was taken to a manometer board. A water manometer was used for naturally aspirated tests and a mercury manometer for boosted tests. As a number of pressure measurements on the rig were read using water manometers for naturally aspirated tests and mercury manometers for boosted tests, a board was constructed with all the appropriate manometers on it. To simplify the changeover from naturally aspirated testing to boosted testing, the board also incorporated a number of changeover switches, together with a liquid trap above the manometers in the event of manometer 'blowout', see Cole **(Ref. 3)**.

For inlet air flow, standard orifice plates were used, again to **B.S. 1042 (Ref. 27)**. In this case however, two orifice plates were necessary to cover the total flow range experienced, while maintaining an acceptable level of accuracy. This was the price paid for the utilisation of a low cost instrument with poor turn down ratio, however, higher priced flowmeters were beyond the scope of the project budget. A further point is the reading of flowmeters, and the subsequent entry of this data into data reduction programs. It is now possible to purchase digital display units built around

microprocessors which linearise the input signal and are particularily suitable for use with non-linear transducers such as orifice plates with pressure pick-offs. However, although this type of meter is capable of linearisation and of providing a signal compatible with microcomputers it does not solve the problem of a transducer with a poor turn down ratio. Other problems which may arise with this type of instrument are : - their slow response, due to the long pipe runs which inevitably exist between the pressure tappings and the manometer ; air bubbles in the pipe runs, which can lead to erroneous water "head" differentials ; and the non linear response. It was essential that all pressure signals obtained using manometry, were static and did not come from pulsating sources. The effect of pulsating signals on flow measurement using such non-linear devices, is treated in **BS 1042 (Ref. 27)** .

4.4.e Exhaust Enthalpy

Exhaust enthalpy determination presented several problems. Exhaust mass flow was computed from the sum of the inlet air mass flow together with the fuel mass flow. Blow - by losses were assumed to be negligible. The problems associated with the measurement of exhaust enthalpy are :-

i). accurate monitoring of exhaust gas temperature and

ii). finding an appropriate correlation between this temperature and the enthalpy calculated from it, and the actual enthalpy.

4.4.e(i) Exhaust Gas Temperature Measurement

Firstly, consider the exhaust gas temperature. The nature of the exhaust gas stream suggested that a sheathed thermocouple would be the most suitable monitoring device. Type K thermocouples have an operating temperature range from below 0°C up to at least 1100°C. Although this type of thermocouple material has good chemical resistance, the stainless steel sheath affords added protection and the prospect of the device giving longer reliable operation. The equilibrium temperature which the thermocouple attains for a given set of engine operating

conditions, will depend upon a number of factors. The main aim is to make the reading of the gas temperature independent of factors other than gas temperature, such as the exhaust duct wall temperature, and exhaust gas velocity. The thermocouple itself is exposed to all three major types of heat transfer, namely :- convective transfer from the gas to the thermocouple body ; radiation to or from the wall of the exhaust duct in which the thermocouple is sited and conductive heat transfer from the measuring junction of the thermocouple along its length to the wall or the outside of the exhaust duct. Obviously the transfer of heat from the gas to the thermocouple is essential for its operation but the latter two transfer mechanisms result in errors. This subject is treated more fully in **Ref. 29** . Suffice to say at this point, that to enable accurate measurement of exhaust gas temperature it is necessary to ensure an adequate immersion length of the thermocouple body in the gas stream, together with a high degree of radiation shielding of the thermocouple tip. Qualitatively, the substantial immersion length is to ensure good transfer of heat to the thermocouple from the gas stream and to provide a long path length for conduction from the tip. The radiation shielding becomes increasingly important as the gas and thermocouple temperatures go up, with subsequent increases in radiative transfer to the walls of the exhaust ducting from the thermocouple.

4.4.e(ii) Mass and Time Averaged Gas Temperaures

Secondly, in the monitoring of exhaust gas enthalpy, the difference between mass averaged and time averaged temperatures must be considered if the true exhaust gas enthalpy is to be calculated.

Two choices existed for the monitoring of exhaust gas enthalpy. One of these was mechanically simpler while the other was mathematically simpler. The mathematically simpler system assumes zero, or at least negligible losses, from the exhaust gas before its pressure fluctuations, and hence the temporal variations in mass flow are damped in a large exhaust receiver. This receiver must also be of low loss design; if

both of these conditions are fulfilled then measurement of the exhaust gas temperature and pressure in the damping volume will give the true exhaust gas enthalpy. In actual fact these conditions are very difficult to obtain even with good insulation surrounding the exhaust duct and the exhaust receiver. An example of this type of system is analysed in **Appendix 5** . An alternative design uses the exhaust duct itself as part of a water fed calorimeter. This design would immediately remove the stringent requirements on insulation of the exhaust duct as well as alleviating the high temperature stress situation which the inner wall of the duct would 'see' in the previous method. Further calorimeter tubes would be required in the receiver, however, leading to a mechanically rather complicated design. The temperature rise and flow rate of the coolant water through the calorimeter as a whole are readily combined to give part of the exhaust gas enthalpy, and together with the uniform pressure and temperature of the exhaust gas leaving the receiver may be used to directly calculate an accurate value of true exhaust gas enthalpy.

The mechanically simpler method of determining exhaust gas enthalpy involves the use of shielded thermocouples placed near to the exhaust port on the engine, together with pressure and temperature monitoring in a receiver downstream. The problem arising from this system is due to the highly pulsing nature of the exhaust stream just outside the engine port and the fact that a). the temperature which the thermocouple indicates is not an instantaneous value of gas temperature, and b). the mass flow of the exhaust stream may not be in phase with the temperature variations of that flow. The effect that this has on the calculated value of enthalpy has been studied by a number of researchers, for example Caton (**Ref. 30**), and Caton and Heywood (**Ref. 31**). These studies revealed correlations between calculated and true values, assuming certain conditions are maintained. These correlations only hold for one engine type and over limited operating ranges, if high accuracy is to be obtained. Further details of this method are given in the above references.

Although the calorimetric method is the more fundamental and accurate method, the time constraints imposed on the project necessitated the use of the mechanically simpler system.

As mentioned at the start of this section on engine heat balance there are a few energy flow paths which are not monitored. The magnitude of these remaining paths is unlikely to exceed about 5% of the total heat balance at the higher engine loadings but might reach 10% under light engine loadings. These paths are very difficult to monitor, but should not be ignored.

4.5 Instrumentation for Combustion Monitoring (with reference to **Fig. 4.5**)

4.5.a General Considerations

The study of combustion processes within a working engine cylinder is a particularily difficult task. In spite of this fact and because of the importance of the topic, a number of different techniques have been developed. The various techniques may be broadly divided into two categories, namely intrusive and non-intrusive. A useful summary of the techniques in both categories is by Amman (**Ref. 32**).

Of the non-intrusive techniques, the most frequently used is probably that of in cylinder pressure measurement. The reason for this technique's popularity lies in the relative ease with which a pressure tapping into the combustion space may be made. Certainly the physical difficulties of obtaining access in order to use some of the other techniques virtually preclude their use on standard, small engine combustion chambers. The only other truly non-intrusive technique currently available, for qualitative assessments only, is the endoscope which in conjunction with high speed photography, is capable of viewing combustion as it occurs.

4.5.b Pressure/Crank Angle Measurement

The technique chosen for this project was in cylinder pressure measurement. From this pressure versus crank

angle data, the apparent rate of heat release may be computed. This is an important parameter, which is currently used within cycle simulation programs in the form of experimentally derived correlations, to predict engine performance. Of particular interest in this research programme, was the effect of hot combustion chamber walls on the heat release. Also of interest was the heat transfer between the working fluid in the combustion chamber and the combustion chamber walls.

Although the acquisition of pressure versus crank angle data is the simplest method to apply, it is not without a number of difficulties if an accurate picture of the processes involved, is to be obtained. The time interval from start of injection to end of combustion for this engine is only a few milliseconds. Automatically therefore there is a requirement for an high speed data acquisition system.

4.5.c Pressure Measurement

To monitor the rapidly occurring events, within the combustion chamber, the pressure transducer must have a high frequency response. A further condition is that it must also be capable of surviving the rigours of in-cylinder conditions, this places stringent demands on the transducer, mechanically, thermally, and chemically.

4.5.c(i) Transducer Thermal Shock Effects

Initial monitoring of cylinder pressure was carried out using a water cooled piezoelectric device, the AVL 8QP 500ca. This device had more than adequate frequency response accurately to follow cylinder pressure and being water cooled was capable of being positioned in the wall of the combustion chamber. A reference to thermal shock effects relating to engine pressure transducers, **(Ref. 33)** led to a close examination of the results obtained from this transducer, leading to its replacement with a type which had been specifically designed to reduce the effects of thermal shock arising during the combustion phase of the engine cycle.

Thermal shock effects are evidenced by the presence of pressure signals which have no real origin, and are most noticeable during periods of small changes of pressure. These

effects result from the transient thermal stress behaviour of the transducer pressure sensing diaphragm. Under conditions where pressure fluctuations alone, are present at the front of the diaphragm, the integrated force developed across the diaphragm is transmitted to the sensing element and an output is produced which is proportional to the pressure applied. However under conditions where the pressure is static but there are thermally varying conditions then fluctuating temperatures produced on the front face of the diaphragm are carried through the diaphragm as a temperature wave, accompanied by an associated stress wave. It is therefore possible , unless precautions are taken to minimise the magnitude of this wave, that the sensing element will 'see' stress variations which do not have a pressure origin. The technique usually adopted to minimise this effect is to damp the temperature wave and thus the stress wave before it reaches the sensing element. The necessary damping is provided by a thermal barrier coating on the front face of the diaphragm. The thickness and composition of this coating has to be a compromise between reducing the thermal shock effects and of maintaining the frequency response of the transducer which needless to say is reduced when mass is added to the diaphragm.

4.5.c(ii) Transducer Communicating Passage

Apart from the thermal shock behaviour of the pressure transducer, concern was voiced regarding the communicating passage between the combustion space and the transducer. Evidence in the literature suggested that unless the transducer diaphragm was located as close as practicable to the combustion chamber wall, the response would be affected **(Ref. 34)**, and that communicating passages should be avoided altogether. This was at variance with information from the transducer supplier, which suggested that the passage, which was already present in the test engine, would not affect results. To be on the safe side, the former advice was observed and resulted in relocation of the transducer drilling to bring the front face of the diaphragm flush with the

combustion chamber wall. At the same time a new transducer incorporating the thermal shock barrier was purchased, namely the Kistler 6121 .

Neither of the transducer sitings was ideal but they were the best that could be attained within the constraints imposed by the engine head geometry. The first siting, as already outlined, positioned the transducer back from the wall of the combustion chamber. This led to a communicating passage of approximately 6mm in length with a diameter of about 3mm. Initial calculations using 1/4 wavelength and Helmholtz resonance formula seemed to suggest that this length of passageway would have negligible effect on pressure readings. The positioning of the transducer resulted from the double angled drilling which was considered necessary in order that the transducer to combustion space passageway remained unimpeded by the presence of the piston at any point in the cycle. The second siting of the transducer, while ensuring that the diaphragm was flush mounted with the wall, unavoidably resulted in an effective passageway being created when the piston was around top dead centre, albeit of short length.

4.5.c(iii) Problems Specific to Piezoelectric Transducers

A piezoelectric transducer was chosen for the task of monitoring cylinder pressure for a number of reasons some of which have already been mentioned. Of the currently available transducers, it is the only one which combines high frequency response with high operating temperature capability, high linearity over the full operating pressure range, good long term stability, and generally good accuracy even at a fraction of its fullscale operating conditions. There are, however, a number of problems associated with the use of this type of transducer. Essentially piezoelectric transducers are charge generating devices, and as such need specialised conditioning of their output signal. The most common type of conditioning device used in conjunction with transducers for this application is the charge amplifier. As the name implies, the amplifier converts the charge generated by the transducer

into a voltage output which is linearly related to it. Associated with the operation of this combined system of transducer and charge amplifier is an inherent time constant. The effect of this time constant is the steady decay, with time, of the signal produced by the system, after a pressure excursion is applied to the transducer. This point is addressed in further detail in **Appendix 6.**

In terms of the practical application of such transducer/amplifier combinations, the most important consideration is the condition of the connecting cables and their connectors between the transducer and the amplifier. Standard type coaxial cable is not suitable, due to charge generation in the cable brought about by friction between the screen and the insulator (microphony). This is avoided by the use of low noise cable. The cable itself must exhibit very high isolation between the centre conductor and the outer screen and values greater than $1.0 \times 10^{+13}$ ohms is a typical requirement. The connectors in the line between transducer and amplifier are a weak link and contamination here may result in poor performance. Standard practice concerning connectors is that they are periodically cleaned, preferably with a triflouro-trichloro ethylene solvent, and then baked for more than twelve hours in a hot air cabinet. This practice can lead to serious delays in testing but unfortunately is required if truly representative pressure signals are to be obtained.

Another problem which was experienced with this type of transducer, was that of carbon packing in the groove between the heat shield /diaphragm and the transducer body. This occurrence required the periodic cleaning of this space, again to ensure accuracy of pressure reading.

Going back to the inherent time constant associated with piezoelectric transducer/charge amplifier combinations, it must be recognised that because of this, absolute pressure readings are not possible. To overcome this difficulty, either some point in the engine cycle pressure diagram must be known to be at some fixed reference pressure, or another absolute pressure transducer must be fitted, the output of which may be

related to the pressure diagram from the piezoelectric transducer. Yet another method is to use a piezoelectric pressure transducer fitted with a fast acting valve. At some non-critical point in the engine cycle the valve is actuated to present the diaphragm of the transducer with a known reference pressure. The obvious disadvantages with this system are i). the special transducer/valve combination is physically large and therefore difficult to fit to a small engine head ii). part of the engine pressure cycle is lost due to the referencing action of the valve.

The simplest of the three methods was chosen, to be used in conjunction with careful analysis of the outputs from the heat release and cycle simulation programs. That is, it was assumed that at bottom dead centre, intake, that the cylinder was at manifold pressure. Resorting to the analysis of P - V diagrams, to ensure correct operation of the pressure transducer, did bring about dealys in identifying faults within the system. This situation could, as stated above, be remedied by the inclusion of a second transducer which would give an absolute reading of pressure around bottom dead centre of piston travel. A system similar to this was proposed by Way **(Ref. 35)**.

4.5.d Start of Injection Monitoring

As a result of combustion modelling still being at an early stage of development, most cycle simulation packages rely on empirically fitted combustion correllation type sub-models. The particular correllation used in conjunction with this work is based on research by Wiebe **(Ref. 36)**, and by Marzouk **(Ref. 37)**. In simulation programs using this type of combustion model, only the start of injection and a few engine operating parameters are required to give a correlated heat release profile which the cycle simulation program then uses to predict the behaviour of the engine, at that operating point. To match the experimental results to those predicted and to see how changes in the engine build affect the correlations, it is thus necessary to know the start of fuel injection.

A number of means have been used to detect the flow of fuel into the combustion chamber. Some methods rely on monitoring of the fuel line pressure. One system relies on stresses developed in the wall of the fuel line, which has the advantage over other systems in that the strain sensitive device (piezoelectric) may be simply clamped to the outside of the fuel line between the fuel pump and the injector. While this method is useful for rough setting of injection timing it is prone to errors due to reflected pressure waves in the fuel line, and furthermore does not actually detect the exact point of fuel delivery. The most reliable and accurate systems are based on displacement transducers which monitor the lift of the injector needle. Even with these systems there is a small but finite time interval between the needle lifting and the fuel entering the combustion chamber, however this interval is usually very small in comparison with the errors which can result in the other systems. The particular transducer chosen for this research was a Lucas C.A.V. variable inductance type. Basically, the device comprises a ferromagnetic core which moves within a stationary coil. The core section is attached to the needle by a light, thin rod. The stationary coil is mounted in a cap which fits on top of the injector. The fitting and alignement of these components depends on the individual injector type being instrumented, and was carried out by Lucas C.A.V.. The operation of the device relies upon the fact that as the magnetic core moves in and out of the coil the inductance of the coil varies. The coil forms part of an high frequency oscillator, and as the inductance of the coil varies, so does the frequency of the oscillator. This type of system places an immediate constraint on the distance the oscillator may be placed relative to the variable inductance coil. This is due to limitations on connecting cable capacitance and noise generated within the cable. However, little trouble was found in siting the oscillator box close to the injector, while at the same time ensuring that the box was not subjected to high levels of vibration and temperature which might affect its operation. The output from

the oscillator/coil/core combination is a frequency modulated signal, the degree of frequency modulation being related to the position of the core in the coil. This signal is fed to a frequency demodulator/signal conditioner mounted in the main instrument rack, here the frequency modulated signal is converted to a voltage which is directly proportional to the needle lift. The frequency demodulator/signal conditioner was also supplied by Lucas C.A.V. One problem experienced with the system was that of temperature drift of the output signal, a considerable time having to be allowed, after powering up the instrumentation, before stable readings could be taken.

4.5.e Fuel Line Pressure

A further channel of the high speed data acqusition system was used to monitor fuel line pressure. Although this channel of data was not used for heat release analysis, it proved to be useful when used in conjunction with the needle lift trace to detect faults in the injection system, and indeed in the testing of the special nozzle which was supplied for use on the 'boosted' test runs. The type of transducer used to monitor fuel line pressure was a specialised half bridge strain gauged cell with good high frequency response, manufactured by Leefield Electronics for Lucas C.A.V. A characteristic of this type of transducer, of particular importance, is that of being capable of monitoring absolute pressures. The pressure remaining in the fuel line between injections of fuel can give an indication of either faulty fuel delivery valve operation or incorrect injector needle seating. These faults will result in fuel leaking out of the fuel line between the fuel pump and the injector, and thus cause a fall in pressure.

The facility to monitor fuel line pressure together with needle lift may be used at a later date to monitor actual fuel delivery rates to the combustion chamber, assuming that a theoretical model is developed to analyse the data obtained. However the present research assumes that injection rates are largely unaffected by changes to the heat flow through the combustion chamber walls, and comparisons between engine

builds are based on this assumption. Future work may involve optimisation of the injection rates, but this was beyond the scope of the present project.

4.5.f Crank Angle Signals

All of the high speed signals obtained have to be related to crank angle. For the purpose of timing this data, two shaft encoders are employed. One encoder on the crankshaft itself provides two outputs in quadrature at 1° crank angle intervals. This automatically allows for pulses to be generated at 1/2° crank angle intervals by combination of the two signals, and 1/4° intervals may be generated for data acquisition, if required. The second encoder is attached to the camshaft extension, which, as it is a four stroke engine, rotates at half engine speed. This encoder is used to supply the 720° marker pulse, that is, one pulse per engine cycle. I the region of most interest lies around top dead centre, firing, the marker pulse is positioned at top dead centre exhaust, allowing the most important data to be in the middle of the data stream.

4.5.g High Speed Data Acquisition System

All of the high speed signals discussed above, may be captured and stored for further analysis by the high speed data acquisition system. This system is dealt with more fully elsewhere, in **Ref. 38**, but basically it comprises a set of individual data acquisition channels, each channel being independent of the others and consisting of:-

conditioning amplifier

high speed analogue to digital converter

independent microprocessor

independent memory

independent input/output communications to the host computer and independent digital to analogue converter

This particular system allows the signals from independent channels, to be in perfect synchronism rather than the skewed data which can result from a multiplexed system. The development of this system was carried out by the Instrumentation group within the School of Engineering

(Ref. 38).

The high speed data acquisition system has at present five independent channels, although only three high speed inputs have so far been mentioned. This leaves two other channels available for further high speed data acquisition, such as monitoring of valve lift, to be used, when needed, at a later date. The system is capable of storing forty cycles of data taken at one degree crank angle intervals, or twenty cycles at half degree intervals, up to the full engine speed of 2000 r.p.m. The data collected may be viewed on a standard oscilloscope mounted in the instrument rack. All five channels of data may be simultaneously displayed on the oscilloscope by virtue of the incorporation of a multiplexing unit. This facility was provided in order that the data stream collected could be examined for such things as data corruption or 'rogue' cycle occurrence, before the data was reduced to a single cycle, averaged form. To control the processes of data acquisition, output of the data to the oscilloscope, and averaging, a Commodore PET computer was used. This machine effectively acts as the master controller, which supervises the flow of data to and from the individual channels, and instructs the microprocessors on each channel to carry out the averaging process on the data which is held in the memory of each channel. The instructions required for the averaging process, are stored in ROM (read only memory), in each channel. After the averaging process is completed, the averaged data from each channel may be downloaded from the channel memory onto floppy disc. From the disc the data may be transferred to the mainframe computer for analysis. This transfer is necessary simply because the PET computer has insufficient memory to store the analysis programs.

4.6 Engine Component Temperature Fields

4.6.a General

The engine components of interest when considering heat flow from the combustion chamber of a direct injection Diesel engine are :- the piston ; the liner ; the head deck ;

the valves. This research programme to date, has concentrated on the piston and the liner. The choice of the piston and the liner was based on two important considerations, i). the estimated relative importance to heat flow of the major components concerned and ii). the ability to compare predicted temperature fields and component heat flows with experimental data, which was dependent on available finite element program capabilities. The piston was identified as a major contributor to heat flow from the combustion chamber, while at the same time exhibiting axial symmetry in the region of most interest, thus allowing simple F.E. analysis. This component was therefore chosen as the first subject for analysis and experimental work. Details of the temperature sensors used in both the the standard and air gap insulated piston forms, are given in **Ref. 3** . A general outline of the temperature field instrumentation for the whole engine test rig is given in **Fig. 4.6** . However, only liner instrumentation will be described in detail.

4.6.b Liner Temperature Fields

The liner temperature field was monitored by thermocouples, the main reason for this was the physical size of the sensor. However, for the case of the insulated liner, temperatures above the capabilities of thermistors were predicted, especially around the top of the liner, and thus thermocouples were essential. Although the axial dimensions of the liner are of the same order as those of the piston, the wall thickness of the liner is much less. Another consideration was that of minimising the disturbance of the leadouts from the sensors. A study of the effects of the thermocouple wire insulation, and the effect of haet transfer from the thermocouples into the gallery water, on the temperature fields was carried out, the results of which are to be found in **Chapter 6 section 6.1.b** .

The positions of the thermocouples in the liner were set to coincide with node positions in the finite element mesh of the liner thermal analysis model. A total of forty four thermocouples were fixed in the wall of the liner. Twenty two

axial positions were used with two thermocouples disposed at each of these positions. The two radial positions were fixed at 1mm and 6mm back from the inside diameter of the liner, at all of the positions. The thermocouples on the engine test rig had already been standardised as type K, this being the most suitable type to cover the range of temperatures and environments found. The thermocouples used for the liner instrumentation were of type K and insulated by a polyimide heat resistant polymer (Du Pont's Kapton film), produced by Thermoelectric Ltd. More detail of the thermocouple installation is shown in **Fig. 4.7** . The same basic installation was used for both standard and insulated forms of the liner.

The thermocouples were taken to three 24-way automatic switching units using thermocouple wire, care being taken to ensure that any junctions were isothermal and boxed to exclude draughts. Initially the three outputs from these switching units were led to a three way manual switching unit and thence to the Ferranti digital voltmeter. Indeed while the necessary electronic interface unit and additional hardware for the automatic switching units were being built, all switching was carried out manually. This was eventually replaced by a fully automated switching system under computer control, the "slow speed data acquisition system". Diagrams showing both of these systems are in **Fig. 4.8**, with full details of the hardware and software used, in **Ref. 39** .

As one of the intended uses of the liner thermocouples was to provide precision monitoring of the liner temperature field for piston/liner heat transfer studies, it was essential that all of the thermocouples used for the liner had the same calibration. This feature was ensured by making all of the thermocouples from the same batch of thermocouple wire and then by comparing the outputs of the thermocouples at the ice point and boiling of water. A copper isothermalising block was fabricated, and fitted with two thermocouples at a time, the output from these was then monitored at the two temperature points, using a precision digital thermometer. All

thermocouples fabricated for the liner were found to agree to better than ± 0.1°C, at both temperature testing points.

4.7 Engine Simulation Test Rig

The purpose of this test rig was to simulate the temperature and pressure conditions found within the combustion chamber of a typical diesel engine, for the purpose of testing candidate ceramic materials. The intention was to produce such conditions without combustion occurring, and thus avoid any ambiguity regarding the source of component failures which might result if chemically active species were present. The basic test rig layout is given in **Fig. 4.9** .

In order that high peak temperatures and pressures were produced it was necessary to consider a high compression ratio build of motored engine. The original design of test rig attempted to hold the test specimens in the head of the engine in order to simplify instrumentation. This configuration led to considerable problems both in the design and in the subsequent running of the rig.

The conversion of the firing engine test rig to indirect injection operation involved the use of flat topped pistons. This change allowed the use of ceramic capped pistons to be directly installed in the simulation test rig for testing, while still achieving a high compression ratio, and thus high peak temperatures and pressures. The engine head design was no longer a problem, as a standard head could relatively simply be modified. The prechamber present in the indirect injection engine head was machined out and a metal plug inserted. The purpose of the plug was twofold; the main purpose was to raise the compression ratio, the second purpose was to provide a convenient site for either a pressure transducer or a surface temperature probe. **Fig. 4.10** shows the plug together with drillings for transducers and water cooling. Results from this test rig are limited to the successful running of two of the ceramic crowned pistons for periods of over 30 hours each.

The surface temperature probe mentioned above has already been described in Chapter 3, and it is hoped that installation

of the finished probe will shortly take place in this test rig.

ENGINE INSTRUMENTATION
(PERFORMANCE)

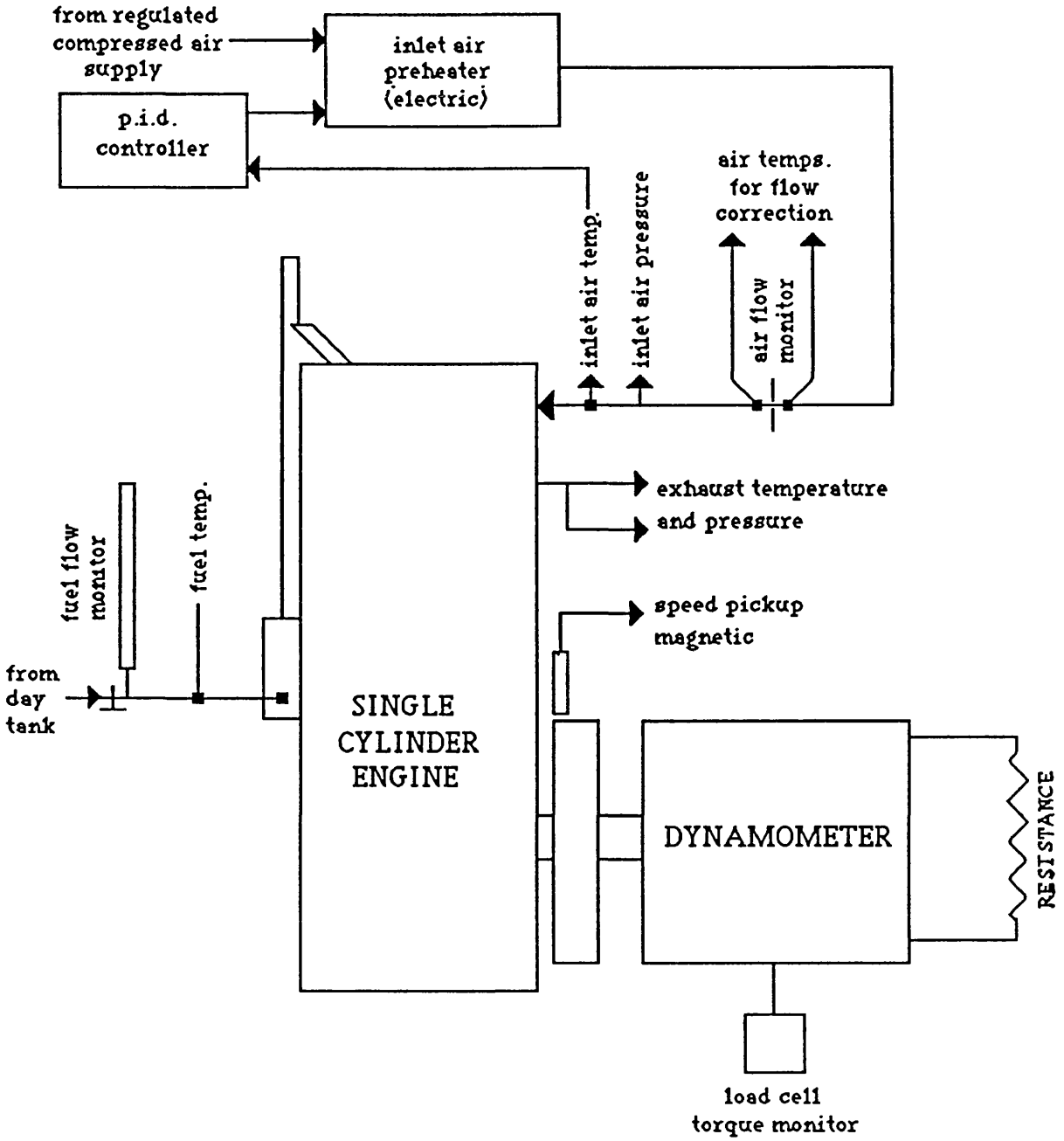

Figure 4.1

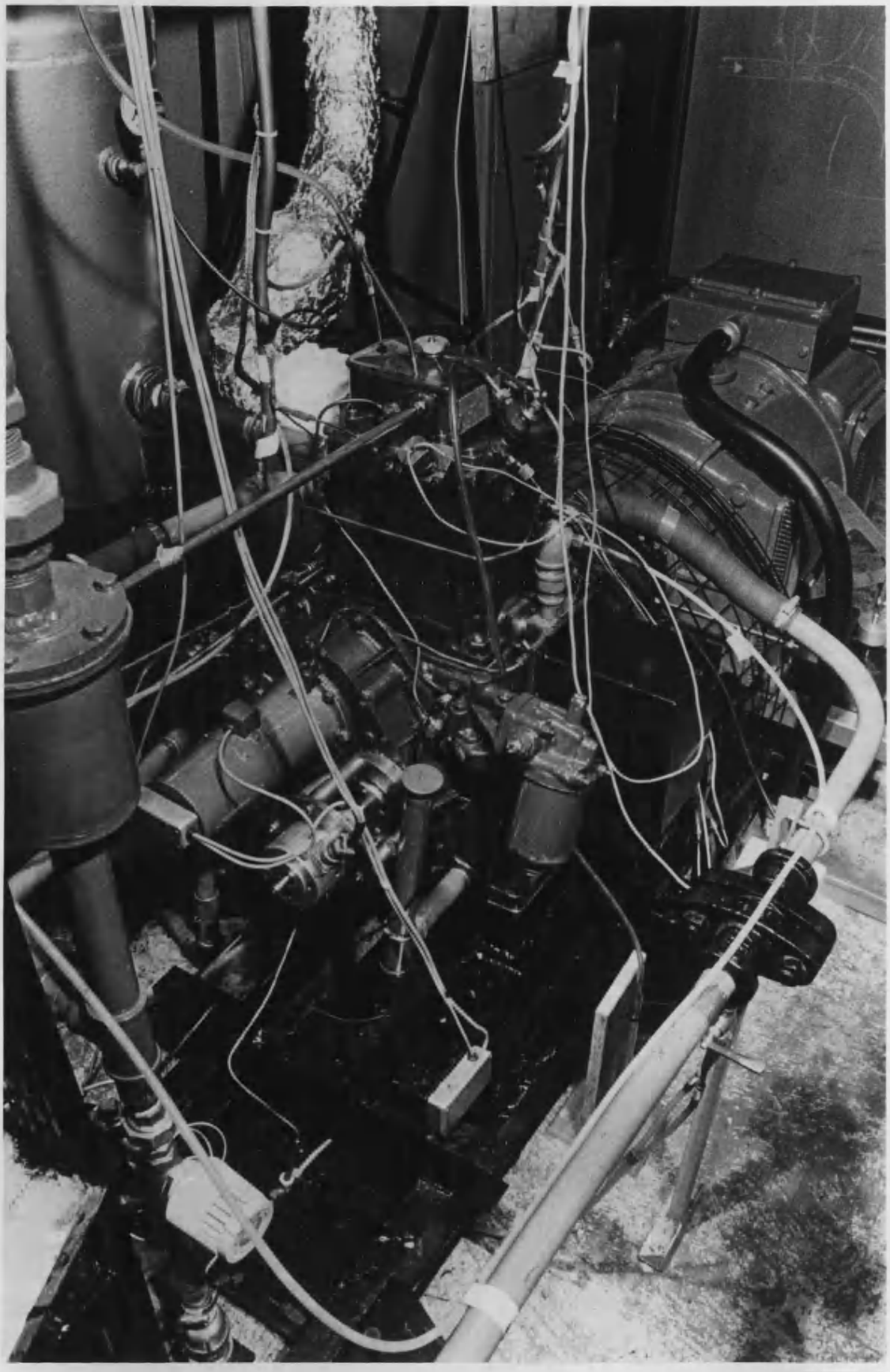

Figure 4.2 - The Firing Engine Test Rig

Exhaust Back Pressure Control Valve

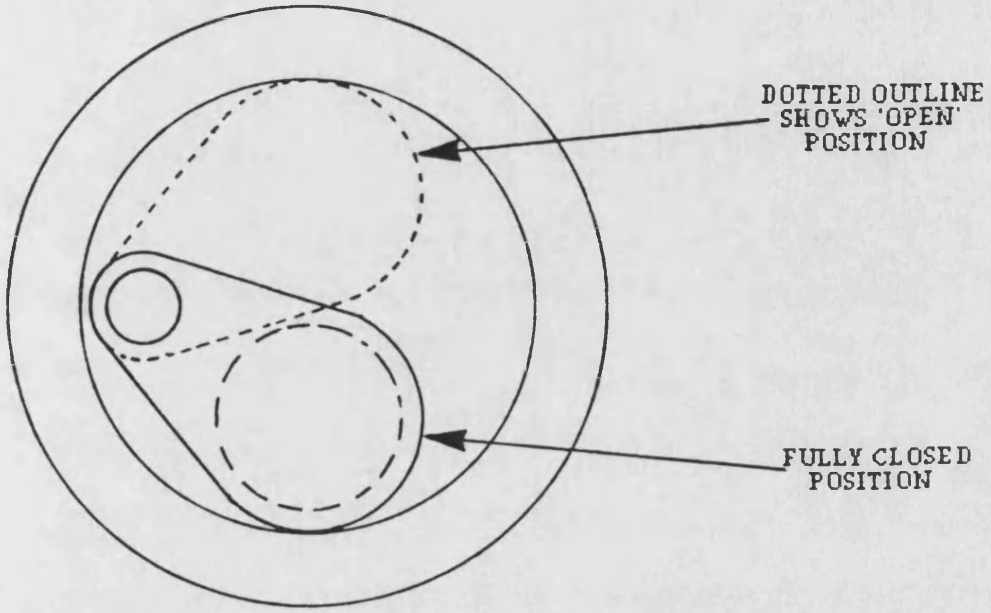

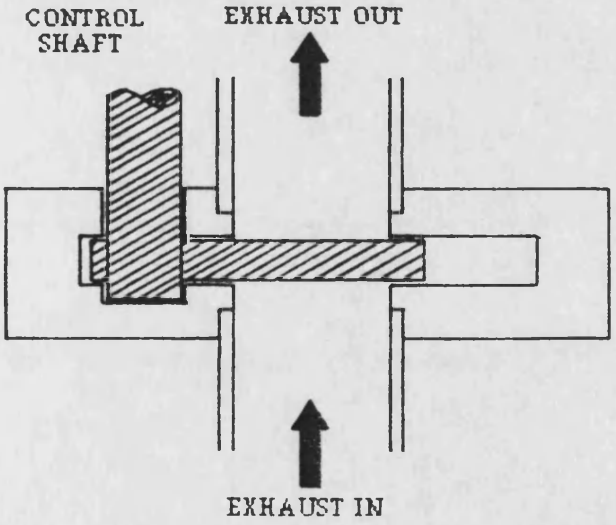

Figure 4.3

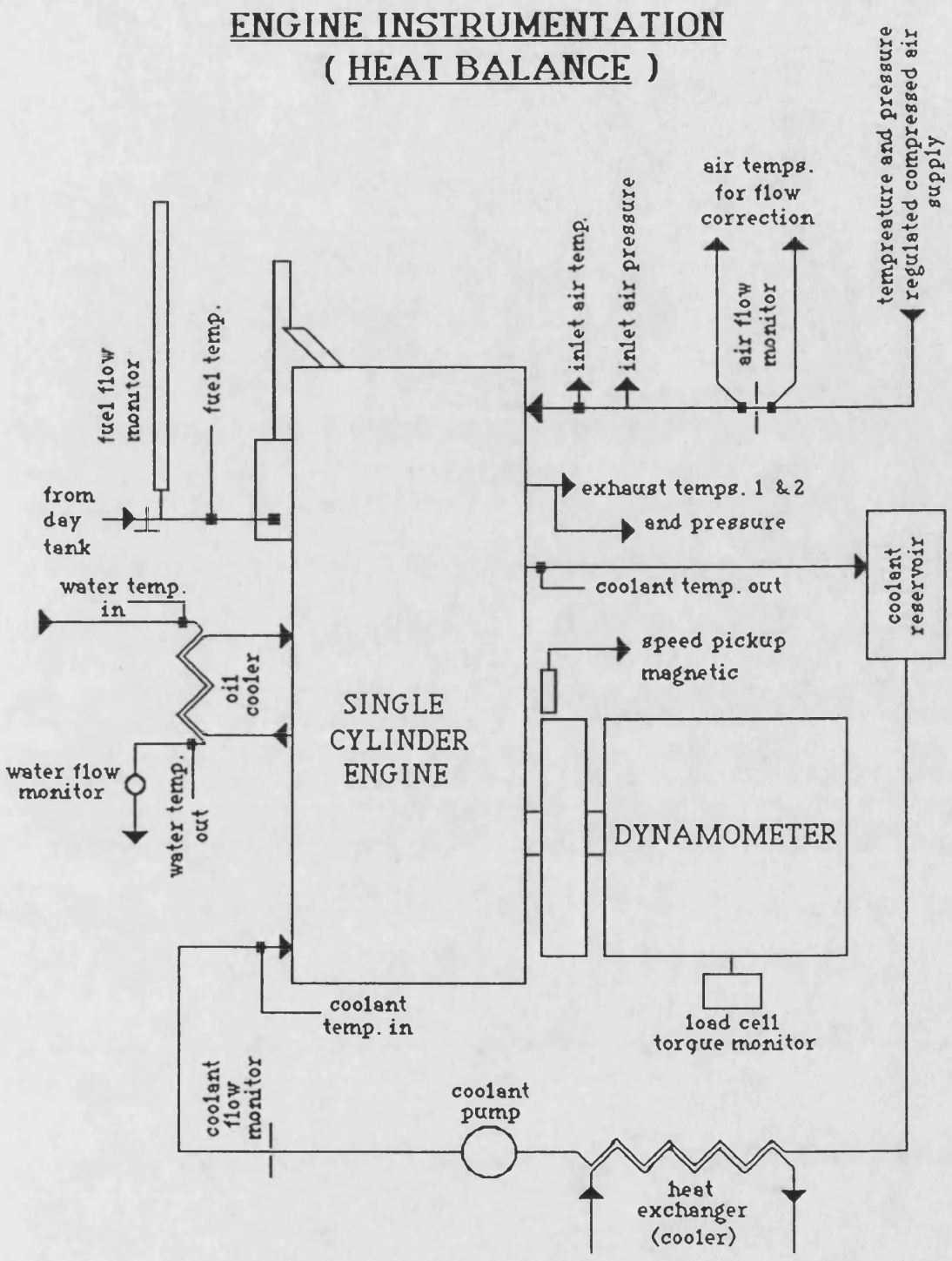
ENGINE INSTRUMENTATION
(HEAT BALANCE)
fuel flow monitor
fuel temp.
from day tank
water temp. in
oil cooler
water flow monitor
water temp. out
SINGLE CYLINDER ENGINE
inlet air temp.
inlet air pressure
air temps. for flow correction
air flow monitor
tempreature and pressure regulated compressed air supply
exhaust temps. 1 &2
and pressure
coolant temp. out
coolant reservoir
speed pickup magnetic
DYNAMOMETER
load cell torque monitor
coolant temp. in
coolant flow monitor
coolant pump
heat exchanger (cooler)

Figure 4.4

ENGINE INSTRUMENTATION
(COMBUSTION)

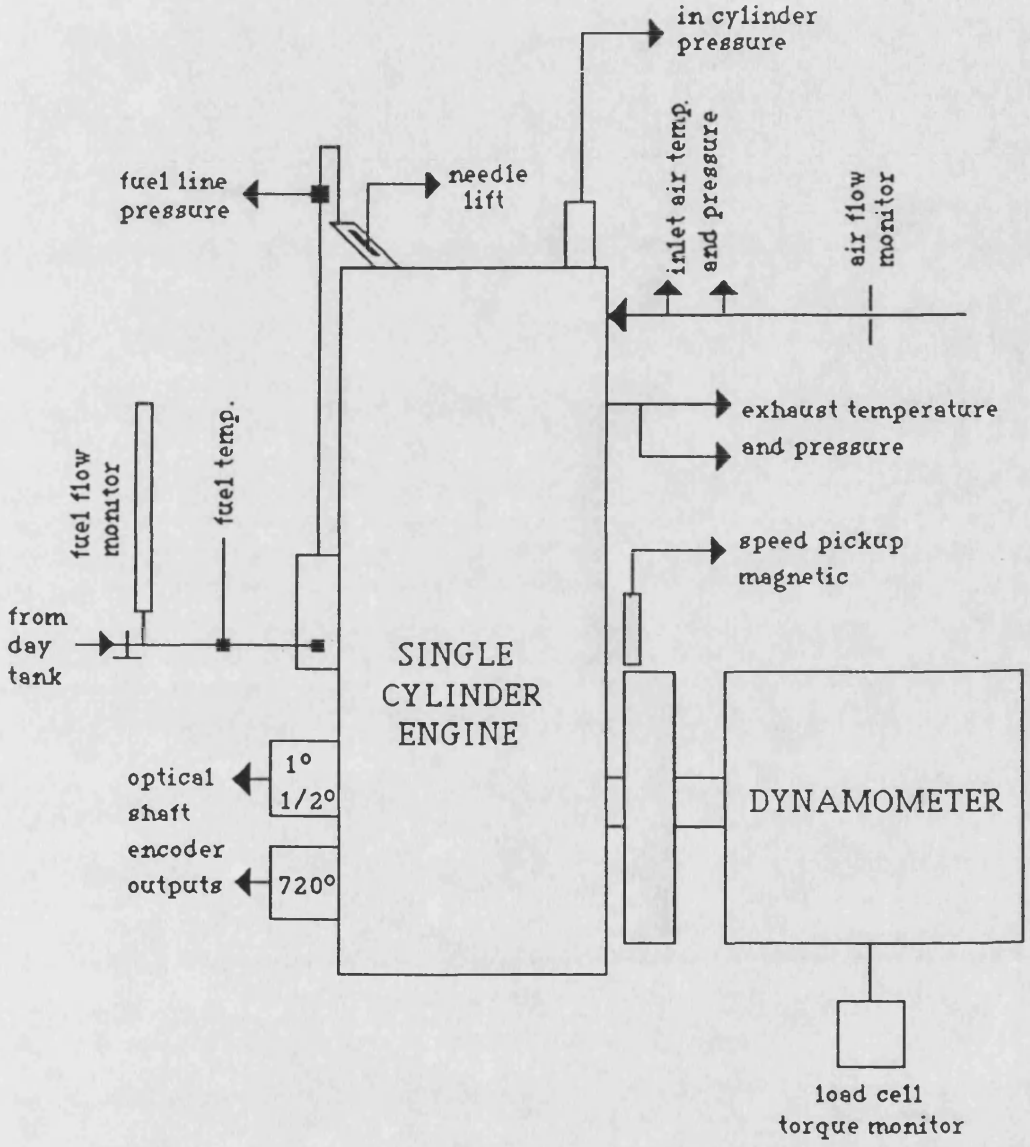

Figure 4.5

ENGINE INSTRUMENTATION
(COMPONENT TEMPERATURE FIELDS)

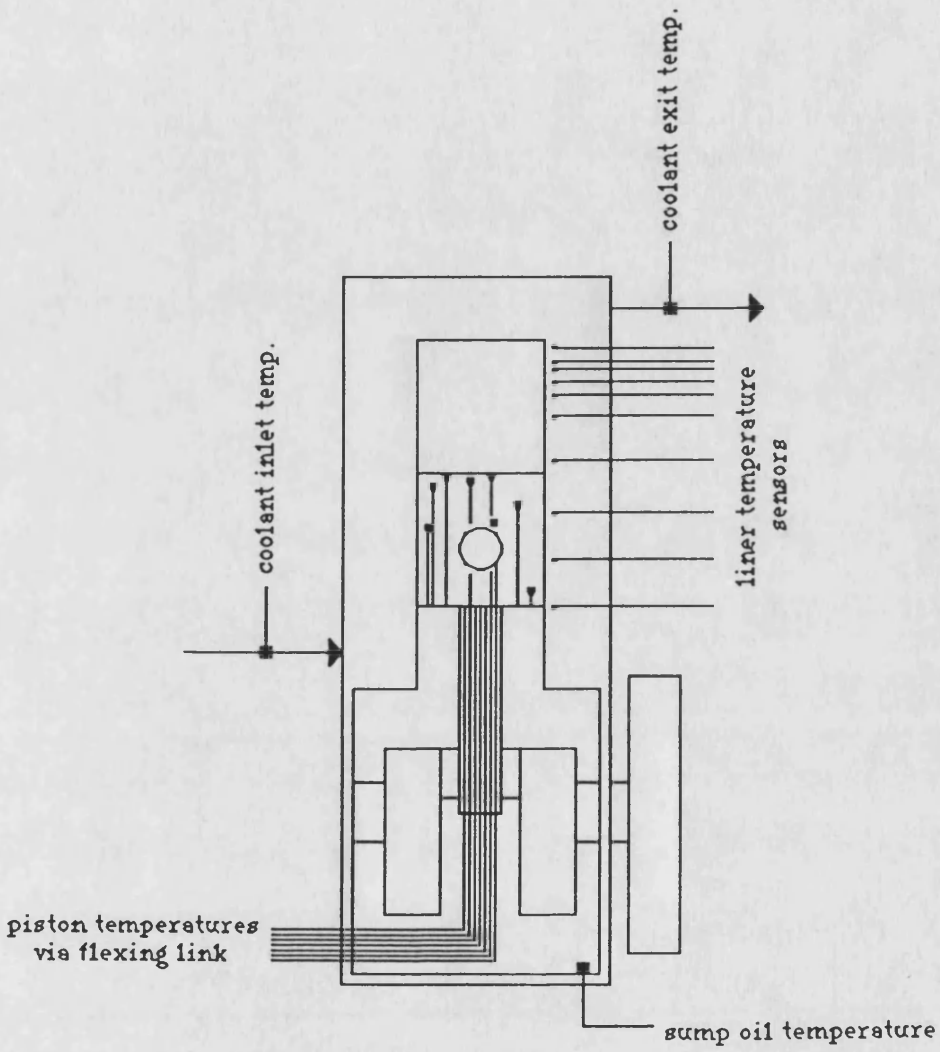

Figure 4.6

Liner Thermocouple Installation

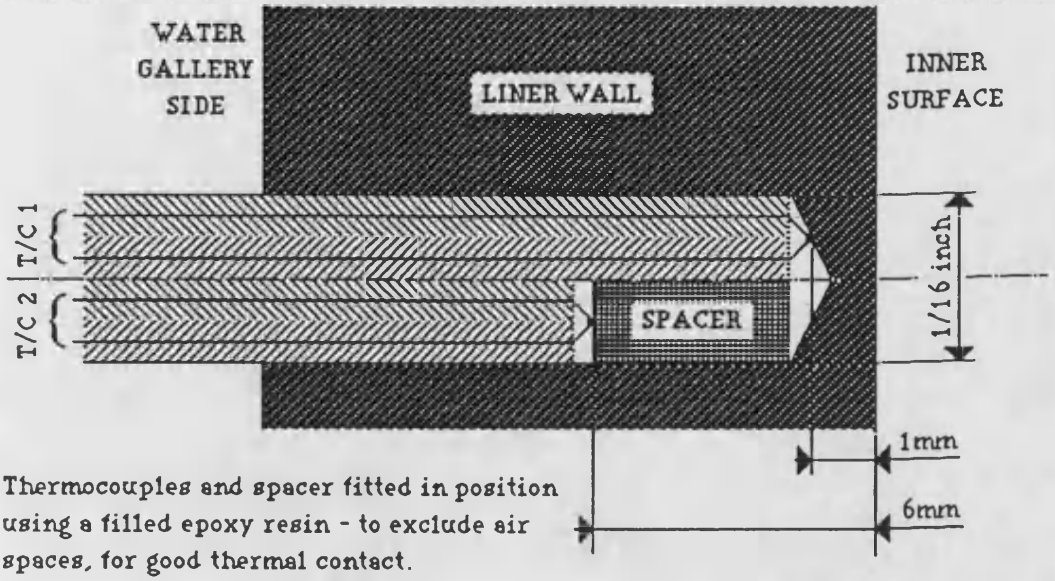

Thermocouples and spacer fitted in position using a filled epoxy resin - to exclude air spaces, for good thermal contact.

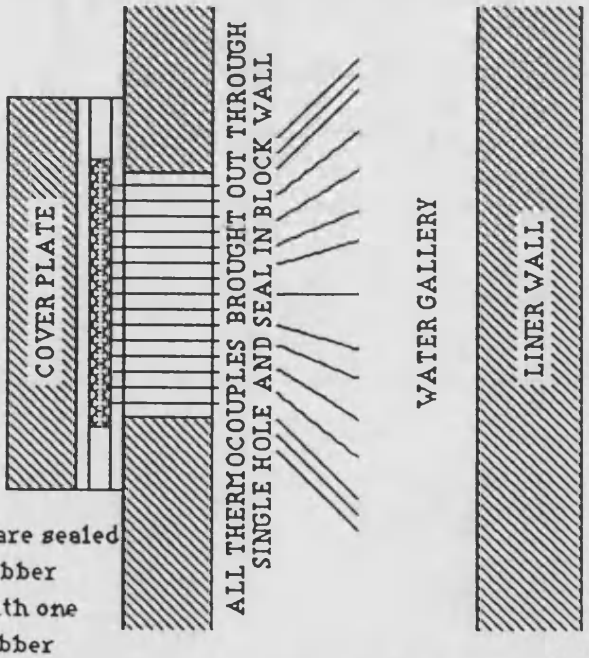

Thermocouples are sealed in place with rubber gasket coated with one part silicone rubber

Figure 4.7

Slow Speed Data Acquisition Systems

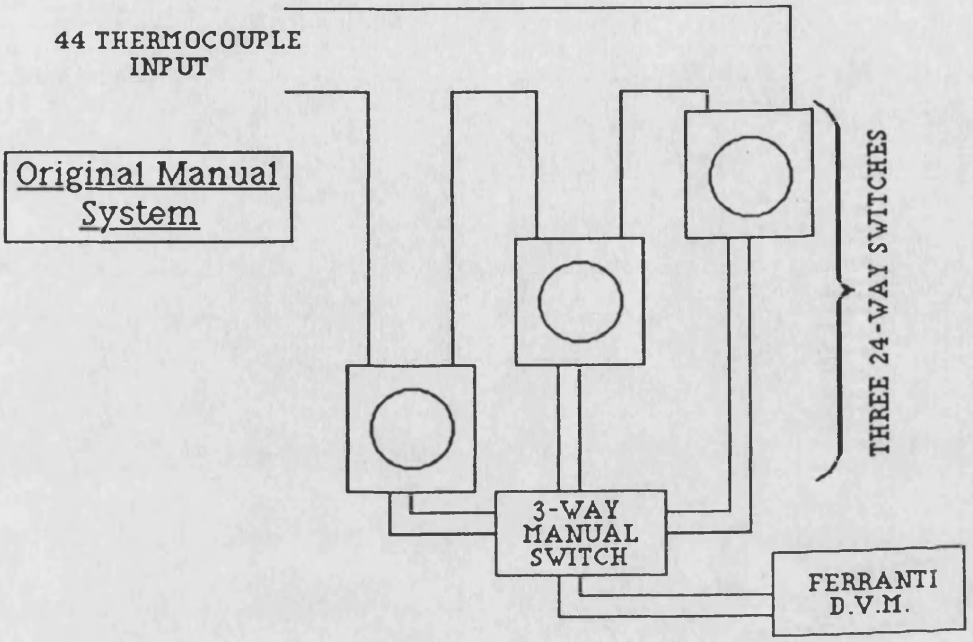

Final Automated System under Computer Control

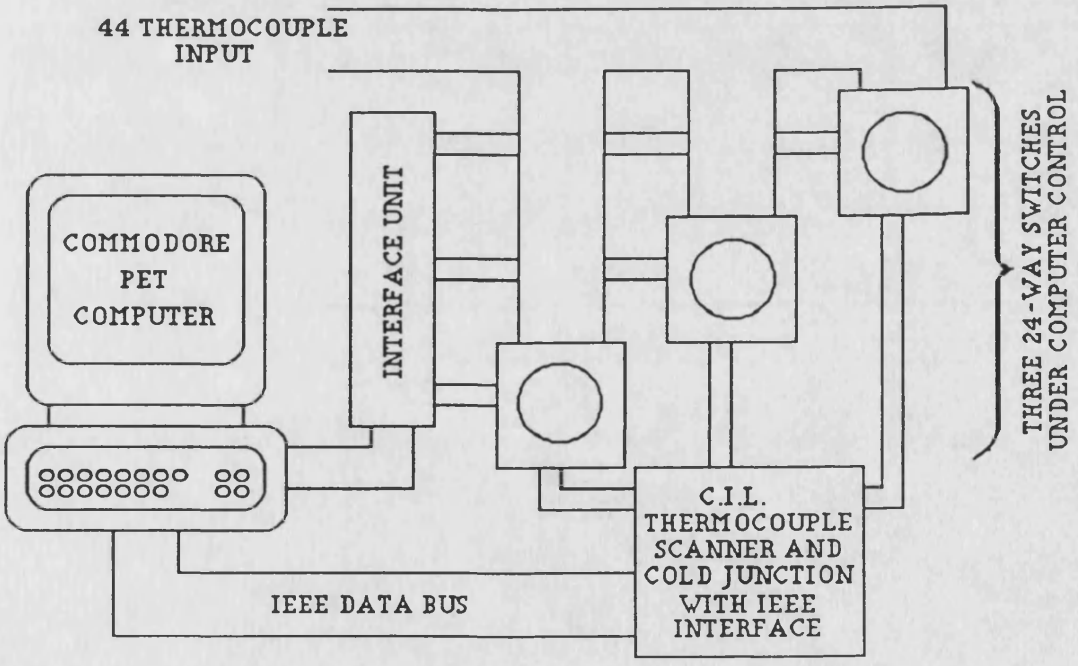

Figure 4.8

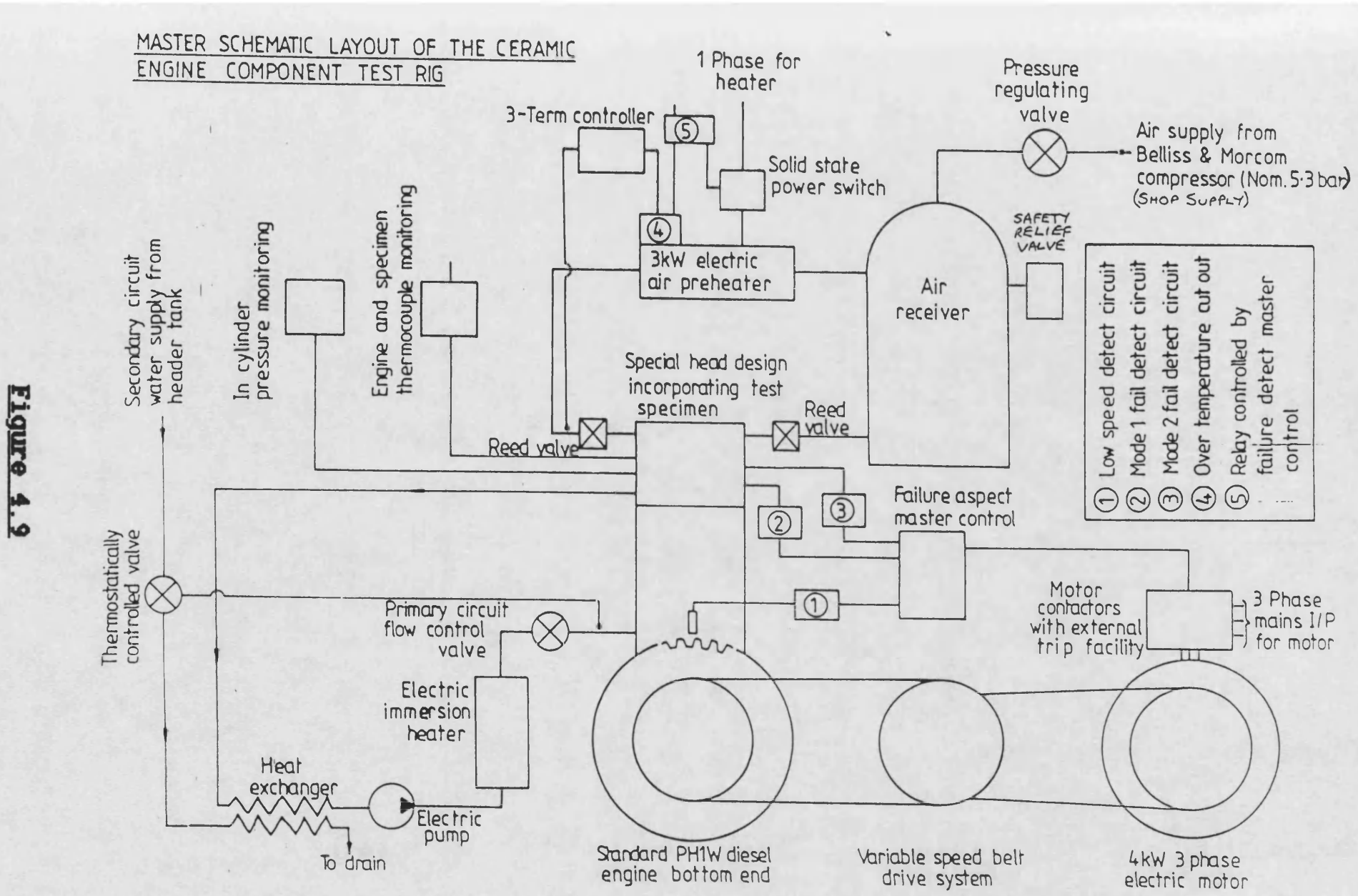
MASTER SCHEMATIC LAYOUT OF THE CERAMIC ENGINE COMPONENT TEST RIG
1 Phase for heater
3-Term controller
Solid state power switch
Pressure regulating valve
Air supply from Belliss & Morcom compressor (Nom. 5·3 bar) (SHOP SUPPLY)
SAFETY RELIEF VALVE
3kW electric air preheater
Air receiver
Secondary circuit water supply from header tank
In cylinder pressure monitoring
Engine and specimen thermocouple monitoring
Special head design incorporating test specimen
Reed valve
Reed valve
① Low speed detect circuit
② Mode 1 fail detect circuit
③ Mode 2 fail detect circuit
④ Over temperature cut out
⑤ Relay controlled by failure detect master control
Failure aspect master control
Thermostatically controlled valve
Primary circuit flow control valve
Motor contactors with external trip facility
3 Phase mains I/P for motor
Electric immersion heater
Heat exchanger
Electric pump
To drain
Standard PH1W diesel engine bottom end
Variable speed belt drive system
4kW 3 phase electric motor

Figure 4.9

Two Orthogonal Cross Sectional Views of the Instrumented Plug for use in the I.D.I. Version of the Engine Simulation Test Rig

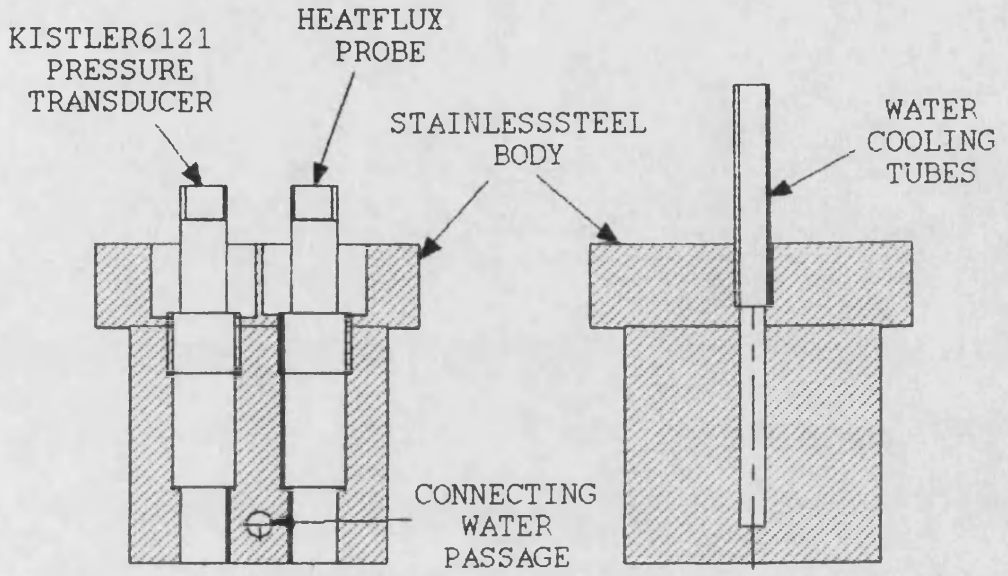

WATER COOLED INSTRUMENTED PLUG FOR USE IN THE FIRING ENGINE TEST RIG

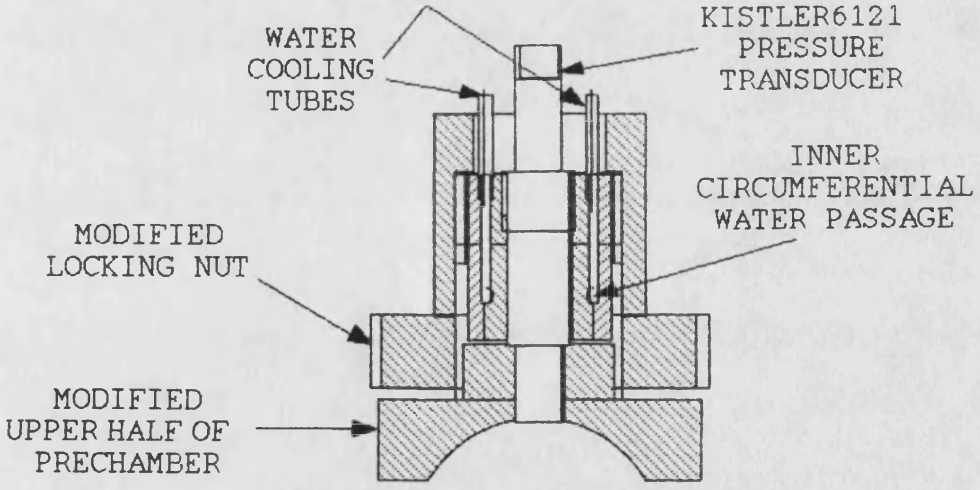

Figure 4.10 - Instrumentation Plugs for use in the Simulation Test Rig and the Firing Engine Test Rig

CHAPTER 5 - CERAMIC PISTON CROWN DESIGN

5.1 Introduction

The initial work on low heat loss diesel engines carried out at Bath University concentrated on piston crowns insulated by air gaps and superalloy shields. The design of the air gap piston used in this early research was a joint effort between the University of Bath (Alexander, Kao, and Wallace) and Wellworthy Ltd. (see **Ref. 40**). Analysis of the air gap piston design is given in **Ref. 2** , with engine performance and heat release results given in **Ref. 3** .

Success with the air gap design together with improvements in ceramic materials prompted further work. This work was to concentrate on insulation of the combustion chamber utilising ceramics. Again the piston crown was the obvious choice for the first component to be examined. Firstly, the axial symmetry of the piston crown above the gudgeon pin allows axisymmetric modelling of the component, as well as simplifying manufacture. Secondly, the piston crown is an important region with respect to heat loss from the combustion chamber.

5.2 Ceramic Piston Crown Insulation

Two major routes to insulation may be identified for engine components. One of these is by the deposition of insulating coatings, the most promising of which is by the plasma spray technique. The other route is by the incorporation of a ceramic monolith within the body of the component, either with, or without an air gap. This section will be devoted to schemes utilising the monolithic method of insulation, as this was chosen as the preferred design for testing.

Monolithic insulation of the piston crown was chosen as the preferred method for a number of reasons, partly related to cost. At this point in time the total costing for a production piston is unavailable. This is due to widely varying estimates both for the cost of the raw ceramic

material as well as for the production and assembly. A great deal of time and effort has presently to be expended to produce a powder of the correct size distribution and surface morphology, and thus the powder required for plasma spraying is costly. The starting material for the production of sintered, or reaction bonded ceramic monoliths is likewise expensive as, again, the starting powder characteristics are important. The production of glass ceramics, on the other hand, relies on a processing route which includes a completely liquid phase. This fact means that the starting material form is less critical, although adequate and even dispersion of the nucleating phase is important.There should therefore be a cost advantage in using a glass ceramic route over the other possible routes for the production of monoliths, and indeed insulating components in general. Pilkington Bros. p.l.c. showed interest in the potential of glass ceramics for the production of engine components, and this resulted in close collaboration with the University. The following sections will describe the design of monolithic ceramic piston crown inserts which has been carried out by the writer.

5.3 Detailed Design of Monolithic Piston Crown Inserts for Insulation

At the outset the problem of attaching ceramic materials to metallic piston bodies was identified as the major design challenge. It was obvious that one solution to the attachment problem would be some form of compliant material introduced between the ceramic monolith and the metal section. In the case of the direct injection piston, for the Petter PH1W engine, the requirement for both axial and radial compliance was met by the use of a stainless steel spring ring as described in U.K. Patent GB 2172084 B (**Ref. 41**) This patent was basically the starting point for the design of attachment schemes later to be used in both the Petter and the Ford Diesel test engines at Bath University.

5.3.a Attachment Schemes

The mechanical system of clamping which is described in the patent specification noted above, is only one

of a number of different schemes which were considered. The main types of piston crown attachment system will now be examined before studying the mechanical system in more detail. These systems may be broadly divided into the following classes : -

i). mechanical/spring systems
ii). direct casting around the ceramic
iii). shrink fitting systems
iv). polymeric resin/adhesive bonding systems

Figs. 5.1 through to **5.7** inclusive are schematics showing the major attachment systems considered, accompanied by some initial design considerations.

i). The mechanical systems (**Figs. 5.1, 5.2** without boss and **Fig. 5.3** with underside boss) have the advantage that the ceramic and metallic portions of the piston may be manufactured entirely separately and then assembled. This allows separate development of the technologies related to the production of each of the parts. It should not be necessary to modify greatly the standard practices at either the metal forming or the ceramic production sites to ensure that the assembled end product meets the design requirements. Having said this, the design has to be very carefully thought out to ensure that assembly is straightforward and without error. The design must also ensure that assembly stresses are not beyond material limits, or where plastic deformation of the metallic components is involved, that this is both reproducible, and results in the assembled product fulfilling the design requirements.

ii). The direct casting (**Fig. 5.4**) of the piston body metal around the ceramic would appear to offer the simplest solution, in that no additional components are required other than the ceramic component and the metal to be cast. However, this is not the case for all ceramic materials simply on the basis of the ceramic materials strength together with the very large strains (and thus stresses) which are generated during solidification of the molten alloy around the ceramic material. One solution to this problem is to ensure that there is a compliant layer surrounding the ceramic, where the metal

is to be cast. This automatically increases the component count. However, tolerances looser than for some of the other attachment schemes may be allowed, with subsequent cost savings. Further points to be borne in mind, related to direct casting schemes are that although it might appear as though only compressive stresses are generated in the ceramic material, if the metal is cast around the ceramic, this is not always the case. It is generally the case that large compressive strains imposed on a body induce both compressive and tensile stresses at the edges of the deformation, as shown in **Fig. 5.5** . This point is considered in the finite element analyses of **Chapter 6** .

iii). An important class of attachment system to be considered is that of shrink fitting (see **Fig. 5.6**). This method of attachment requires very high precision machining of fitted diameters to be successful, and although the geometry would appear to be simple it carries the point noted above, that of compressive strains bringing about tensile stresses in the ceramic body. The requirement for very tight tolerances on the interfering diameters is essential for the case of the crown/piston body attachment simply because of the wide temperature range which the assembly may "see". A minimum storage temperature of -40°C is required , together with a maximum operating temperature of around 150°C (depending on the geometry of the design). The alloy used for most piston bodies has rapidly decreasing maximum tolerable stress values, above about 250°C. This implies that interference fits accomplished above this temperature may promote a degree of plastic deformation or creep in the metal body. This then leaves a relatively small temperature band to accomplish the desired fit, which in turn implies tight tolerances to achieve reproducible results. The problem of tight tolerancing may be overcome by using compliant interlayers but this brings back the need for additional components in the design. This then produces a solution similar in form to the sprung design.

iv). The use of polymeric resins or adhesives (see **Fig. 5.7**) is another possible attachment method which has been proposed. An initial appraisal of such systems

concluded that existing polymeric resins or adhesives had insufficient strength and creep resistance at the operating temperatures expected to exist within low heat loss piston bodies. These facts were particularily important when the adhesive line interrupted heat flow paths from the piston crown to the liner and piston underside. The low thermal conductivity of all polymers would act as a thermal barrier and thus impose a large temperature gradient across themselves, by virtue of their presence. However, it was later considered that a potential solution to this problem would be to simply ensure that the adhesive bond line was orthogonal to piston isotherms and thus would have no effect on heat flow. This task is not a trivial one to incorporate in a piston design, but the adhesively bonded systems have the advantages of simplicity, intrinsic sealing of the assembly, and again, wider relative joint tolerances are possible.

5.3.b Summary of Attachment Methods

Summarising the points, it may be seen that the general problem is that of mating together materials of widely differing expansion coefficients. The ceramic piston crown must be held strongly enough to overcome the forces due to its own accelleration. The clamping device, or system, must be simple in terms of the manufacturing process and assembly. There is the requirement that the attachment system must be reliable and of low cost. Minimum component count helps on both of these points. Differential thermal expansion of the ceramic and metallic bodies, both radially and axially, must be allowed for in the design, as well as effective sealing of the high pressure gases generated during compression and combustion. Further, the design must minimise heat loss through the piston, although some compromise may have to be accepted here on the grounds of potentially deleterious effects upon combustion, volumetric efficiency, and the maximum operating temperature capability of the ceramic. A final point to be noted here is that for the purposes of this research project it was almost essential that the design be capable of incorporation within a standard piston, or with minimal modifications to the piston design. This design

constraint being necessary on the grounds of project time period and budget. The full list of design aims is shown in **Fig. 5.8** .

5.4 Mechanical Clamping Schemes

5.4.a General Considerations

It was evident that the manufacturing capabilities available at the university would favour the mechanical clamping schemes, in terms of the ease with which the components could be produced. This fact together with consideration of the design aims lead to the choice of mechanical schemes for attachment of the ceramic piston crown to the piston body. However, although the mechanical route was the first choice, the other routes were not precluded from further examination.

Prior to providing the ceramic producer (Pilkington Bros. p.l.c.) with a suggested crown design, a number of potential clamping schemes were considered. **Figs. 5.1** through to **5.7** inclusive show these in schematic form with appropriate comments.

The first notional design for a ceramic crown for use in the I.D.I. build of the Petter test engine is shown in **Fig. 5.9** . This differs from the original patent specification drawings (**Ref. 41**) in two respects. The piston in the patent specification was intended for direct injection operation whereas the intention was to perform testing using an engine in indirect injection form. This led to an essentially flat topped piston rather than the deep bowl piston crown originally considered. A further change was the reduction of the complexity of the crown underside boss. This change was made to simplify both the production, and to simplify the mesh necessary for the analysis, of this section of the piston, and indeed the analysis of the sprung section.

The first, notional design, of ceramic piston crown was subsequently changed when further considerations of the sprung section had been made. These changes were made to reduce the potential "rocking" of the sprung section within the curved

section of the piston crown boss section, which might occur during engine operation, under inertial loading. The boss section on the underside of the crown was modified to allow a more positive spring clamping to be achieved, as shown in **Fig. 5.10.** Finite element thermal and stress analyses of this crown form were made, details of which are given in **Chapter 6** . Some analysis of the spring to be used with this design was also undertaken. The crown design was despatched to Pilkingtons for inspection and comments. While awaiting feedback on the design from Pilkingtons, further more detailed examination of the sprung section showed that problems with this component were likely to arise during assembly. Numerous design forms for the sprung section were then considered and examined in detail. A recurring difficulty with the design of the sprung section was that of providing the required holding force, together with ease of manufacture and assembly, while working within the space limitations which the standard piston body imposed. At the same time it was desirable to ensure that the sprung section remained within elastic limits such that reliable finite element analyses could be carried out. A number of potential designs were indeed rejected simply on the grounds that elastic to plastic deformation could not be allowed for in the analysis.

After examination of the proposed ceramic piston crown, Pilkingtons suggested a number of modifications of the design. Concern was expressed regarding the rather tight radius at the spring mating section at the base of the boss. A further point was that for the purposes of ensuring uniform ceramming (the process by which the glass form is converted to a crystalline body) roughly equal section thicknesses were desirable. On the basis of these comments, further modifications to the design were made, namely an increase in the mating radius on the boss section, together with an undercrown recess, or dimple, which produced the required overall equal section thickness. The final, approved design for the ceramic crown for the Petter engine is shown in **Fig. 5.11** .

5.4.b Sprung Section Design

Although initially it was considered that a purely

mechanical system of attaching the ceramic crown to the piston provided the best solution, the difficulties of finding an appropriate sprung system proved beyond the time constraints of the project, particularily as a number of the potential schemes involved the plastic deformation of elements of the sprung section. Alternative fixing schemes were thus investigated with a view to ensuring a more rapid solution. A large number of alternative design schemes were examined. However, only those which were actually produced will now be described.

5.4.c Outspringing Internal Ring Method

This scheme relied on two components in addition to the ceramic crown section to afford the necessary clamping of the ceramic crown to the metal piston body. One component provided the necessary stress concentration reduction and mating surface for the boss setion of the ceramic, while the second component provided the actual locking of the crown in position on the piston body. Detailed section drawings of the assembly are shown in **Fig. 5.12** . A close up photograph of the ring, in place on the piston crown boss, is shown in **Fig. 5.13** . This scheme was eventually abandoned because of problems associated with tolerance build up and the need to force the crown and stress reducer/clamp, together with the outspringing ring, below a locating groove in the piston body. Although this problem could have been overcome by the introduction of a compliant layer between the ceramic crown and the piston body (as shown in the section drawing), there were doubts as to the long term integrity of the compliant layer. The compliant layer in this case has not only to seal the high pressure gases, but is also subjected to the gas pressure forces, which have to be carried through to the main piston body. The oscillating forces which this compliant layer would have to withstand were considered likely to bring about fatigue of the layer and thus eventually lead to failure of the assembly.

5.5 Cast-In Spring Section Method

This was the first successful method adopted and

relies on an annular, stainless steel, spring of simple cross section which is diametrially split and then assembled around the boss of the ceramic crown. Aluminium alloy is melted around the ring and a premachined piston body brought into contact with the molten pool with the aid of a jig. **Fig. 5.14** shows a cross sectional view of the design. A critical point here is the amount of metal which is needed to provide attachment of the ceramic crown to the piston body, while leaving suficient room for a compliant region of the ring to exist. **Fig. 5.15** is a photograph of the casting jig and the component parts. **Fig. 5.16** is a cross sectional view of the piston in place in the casting jig. Although this design has been successful in the simulation test rig, it suffers from two failings. One is that the quantity of molten metal has to be carefully measured, such that precise filling of the gap around the boss and the stainless steel ring is ensured. The other is that a subsequent post-casting sealing treatment has to be carried out to ensure that the crown to piston seal is tight. This operation has so far been successfully carried out utilising a high temperature epoxy resin system. However, it may well be that refinement of the stainless steel clamping ring would obviate the necessity to include the post casting treatment.

On transferring the piston to operation in the firing engine test rig, which places the crown under both inertial and thermal loading, failure of the piston crown was experienced. This point will be discussed later in the results section. However, it should be mentioned at this point that all of the analyses carried out were based on the assumption of axial symmetry, which for the case of the Ford I.D.I. engine is obviously incorrect when the offset position of the prechamber throat is considered.

A variant of the cast in spring system was also attempted with the later, FORD, design of piston crown. This scheme comprised an exfoliated graphite ring in contact with the underside boss section of the piston crown. The graphite ring was held in place by a press formed split copper ring. The assembly thus formed was then placed in a casting jig into

which molten aluminium alloy was cast. The purpose of the copper ring was to exclude the molten metal from the region immediately around the boss section during the casting process. The exfoliated graphite ring was incorporated to allow for the shrinkage which would occur during the solidification of the molten metal. The particular material chosen, offered the ability to accomodate large strains without appreciable stress build up in the ceramic. All of the salient features of this design are shown in **Fig. 5.17** . However the casting trial proved that this method was unsuitable, because of excessive clearance of the cast portion with the boss after cooling. Several reasons were put forward for the appearance of the excessive clearance ; oxidation of the graphite during the preheat of the ceramic/collar preheat period, larger compliance of the graphite at the solidification temperature than expected, distortion and plastic flow of the copper ring, and axial shrinkage of the cast collar. The failure of this method lead to the next system design.

5.6 Shrunk Fit or Adhesively Bonded Spring Section

Although it has been stated that a purely mechanical system proved beyond the scope of the project, the final design which has been tried is a combination of a sprung section and a shrink fitting process. The design attempts to overcome most of the major difficulties which the other designs have presented. This particular design was produced for use with the Ford type ceramic piston crown, shown in **Fig. 5.18**, which is a variant of the original Petter cap design. The ceramic crown for the Ford needed to be of thinner top section and of narrower boss diameter than for the Petter design. These modifications were necessary in order to comply with gudgeon pin to top of piston crown dimension, to meet the strict tolerance on piston mass, and to satisfy constraints on the maximum hole size which could be machined in the standard piston body to minimise piston body distortion.

The shrunk fit spring design, shown in **Fig. 5.19** , essentially comprises a split circular ring of catilever beam

cross section, probably better described as a coned disc type spring. The boss section of the ceramic cap has a section which is essentially conical in form the angle of the cone being 45° , the sprung section which is intended to surround this is therefore an extreme case of the coned disc type of spring. The annular ring which surrounds this sprung section acts against it on a smaller angle conical section. The purpose of this section is to roughly equalise the radial and axial expansions, which are in the opposite sense , and thus achieve a reasonably constant clamping force throughout the operating temperature range. A further consideration here was that some consideration of the tolerances of the components had to be taken into account. The annular ring is adhesively bonded back together after fitting to the coned spring section, and machined to provide a degree of interference, (at the lowest storage temperature expected), with the hole in the piston body. Fitting of the cap assembly is achieved by heating the piston body to a temperature of around 200°C, and then inserting the room temperature crown coned spring sub-assembly.

In the adhesively bonded scheme the components are identical to those in the shrink fit scheme, as shown in **Fig. 5.19** with the interference fit on the cylindrical surface "X - X" replaced by an adhesive bond. The adhesive used was a propriety product known as "Aremco-Bond 568" (manufactured by Aremco, U.S.A.) which performed well in the tensile tests which were conducted on the complete piston/crown assemblies.

Examples of Ceramic Crown Attachment Methods without Underside Boss

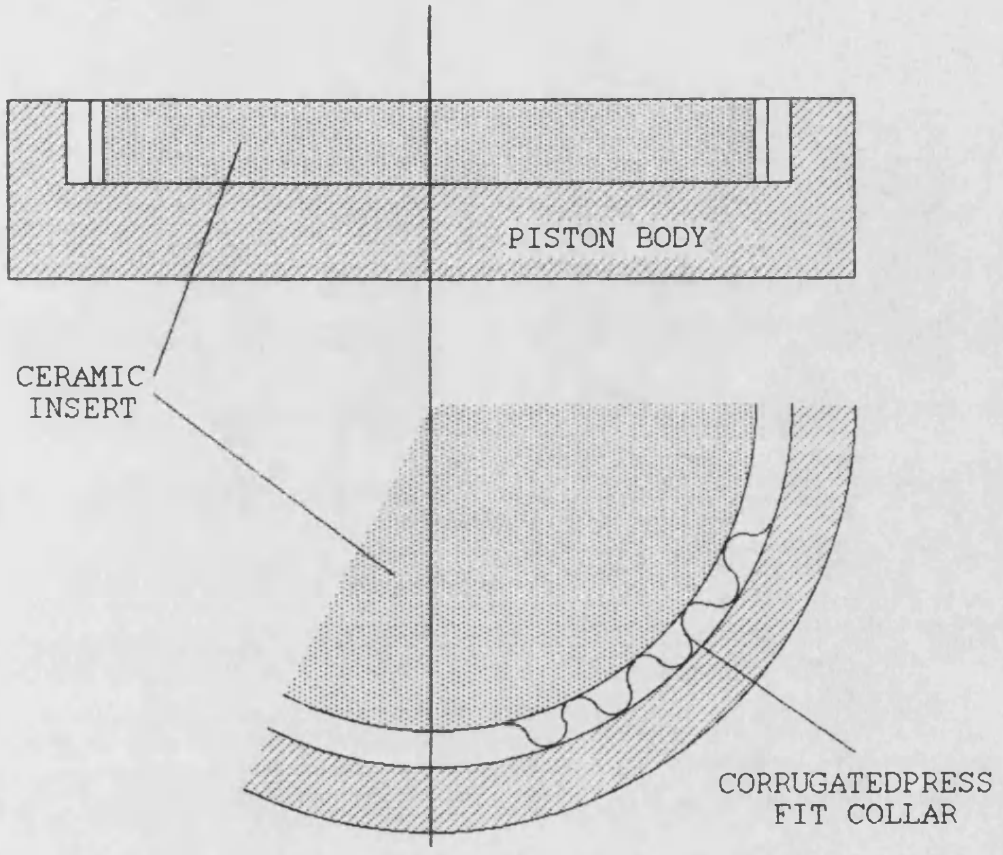

The above attachment method was rejected for general use on the grounds of increased compression dead space which results from the use of the surrounding corrugated clamping ring. The other major objection was that there was still potential for further reductions in heat loss by removing the outer, metal land in this design. The joint considerations of reducing heat loss to a minimum and exposing piston body to as low a temperature as posible led to the adoption of designs including an underside "boss" section.

Figure 5.1

Piston Crown/Piston Clamping Arrangements with External Clamping on Protruding Boss

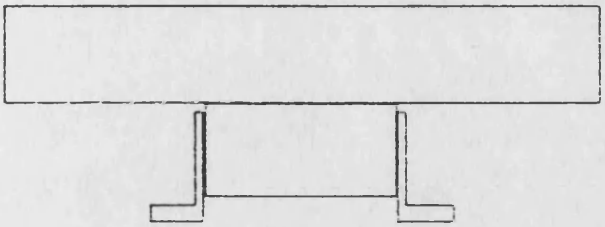

This method of attachment provides good surface area for contact. The ring may be held in place by shrink fit or braze bond, but in both cases care has to be exercised to allow for differential expansion.

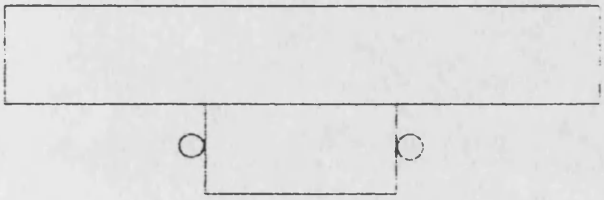

In this case the clamping arrangement is purely frictional brought about by the hoop stress in the hollow, elastic, circular cross section clamp member.

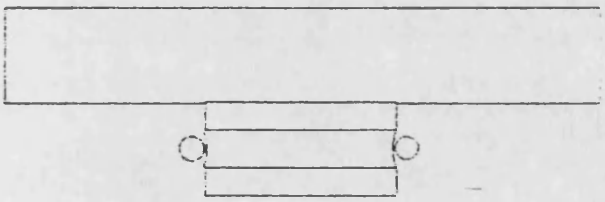

In both this case and the one below, some attempt has been made to facilitate a more positive clamping action through the use of a curved groove in the ceramic body. Although the disadvantage of pure frictional clamping has been overcome, the two, interfering curved surfaces will tend to allow small vertical displacements of the crown piece to occur under positive accelerations, which could lead to fretting wear of the two surfaces in contact. The deeper the groove is moved into the ceramic, the more difficult assembly becomes.

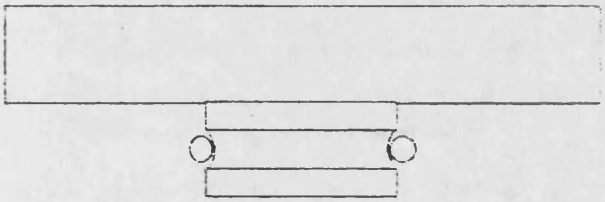

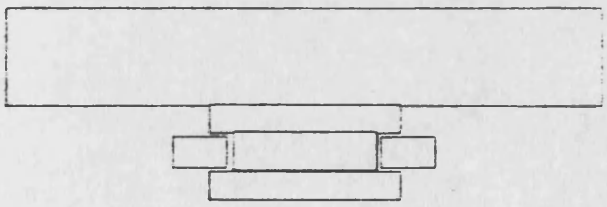

This is the last in the series of this type and represents the limit in the sense that no frictional clamping is intended, the clamp is very positive, but suffers from two problems. 1/. Assembly difficulties, which dictate that the ring must be of split construction and 2/. Tight radii in the groove will promote high stress concentrations, which are obviously to be avoided with ceramic materials.

Figure 5.2

Clamping Arrangements with Internal Ring

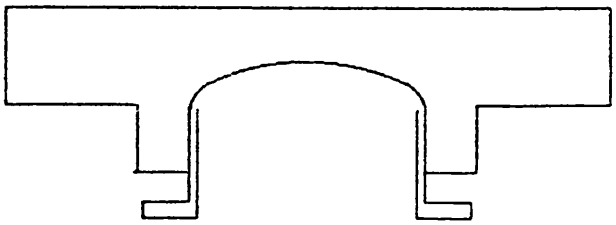

As for the external arrangement this method may be provided by either shrink fit or braze bond. The same limitation exists in that care must be taken to allow for differential expansion between the internal metal ring and the ceramic.

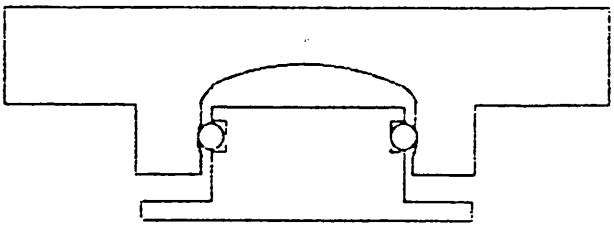

As for the external clamping arangements shown in the previous set of figures, clamping may be produced by a combination of frictional and positive means, this shows one such arrangement.

Generally, the external type of clamping is to be preferred for this application, rather than the internal arrangements shown above, reasons for this are as follows :-

A/. The top deck is reduced in thickness to facilitate incorporation of the internal clamping arrangement, this leads to an undesirable increase in the crown stresses due to the thinner section.

B/. Internal surfaces in the body of the ceramic are likely to be more difficult to form and inspect. This aspect is particularily important in this situation as tensile stresses are expected to be transferred through the inner surfaces of the ceramic.

C/. Secondary sealing arrangements are essential with this arrangement. due to the inboard position of the clamp. Basically, the internal clamp arrangement cannot act as both clamp and seal in this position.

D/. The clamp, being of metallic construction , will tend to promote the production of tensile stresses as the piston temperature increases (due to alphas for metals being higher than those for ceramics).

Figure 5.3

Aluminium Alloy Piston Body Cast around the Ceramic Cap

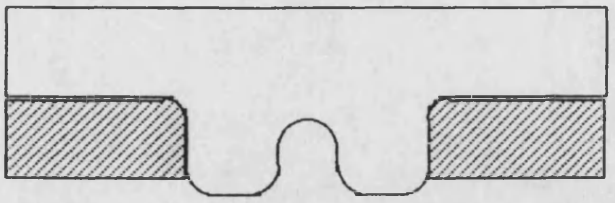

Assuming that the solidification temperature of the Al/Si alloy is about 540°C then if both the ceramic and the metal are at the same temperature, then the respective dimension changes will be :-

Al/Si dimensional change on return to room temp. = (540 - 20)* 20.0 e-6 L
Ceramic dimensional change = (540 - 20)* 3.0 e-6 L

This is a net change of 8.84 e-3 L where "L" is the dimension concerned. This is assuming that no stress relaxation occurs. However, this is rather a high value of strain to be accomodated, especially as a large portion of the strain is generated at temperatures well above those considered acceptable for high stresses in the Al/Si body. Normally the temperature limit for appreciable stresses to be acceptable for the metal body is around 300°C. Another route to a solution might involve the simplifying assumption that the maximum stress exists when the metal body is at room temperature and that this is the yield limit for the material in question. A typical limiting value of stress for an Al alloy is 550 MPa at R.T. Strictly speaking though this value must pertain at the lowest operating temperature for the engine, which will be around -20°C . The question now remains as to the value of stress which pertains at the maximum operating temperature of say 200°C. The strain in the metal at -20°C assuming a maximum stress of 550 MPa and a modulus of around 70 GPa will be 7.857 e-3 . A temperature rise of say, 220°C to the maximum operating temperature will give a residual strain of 4.117 e-3. This is still quite a high strain value. The above calculations assume that there is no take up of the strain within the ceramic body which is obviously not going to be the case. Therefore to model the situation more realistically, it will be necessary to know a great deal more about the behaviour of the metal alloy of which the body is manufactured, and to do a much more detailed stress analysis of the two bodies in contact.

It is evident, however, that a gap of around 0.2 mm will exist between the piston body and the cap, even if the dimension change is based on the differential expansion alone. A larger gap may well exist which will depend upon the casting shrinkage which occurs when the metal changes from liquid to solid. This implies that, unless some post casting treatment is given, the ceramic piston cap will be unsupported around its periphery, and that under engine firing conditions that there will be considerable forces acting on the joint between the ceramic boss and the Al/Si body.

Another point worthy of note is simply that the reduction in heat flow will be less than that for the sprung design because of the absence of an effective "air gap" around the boss.

Figure 5.4

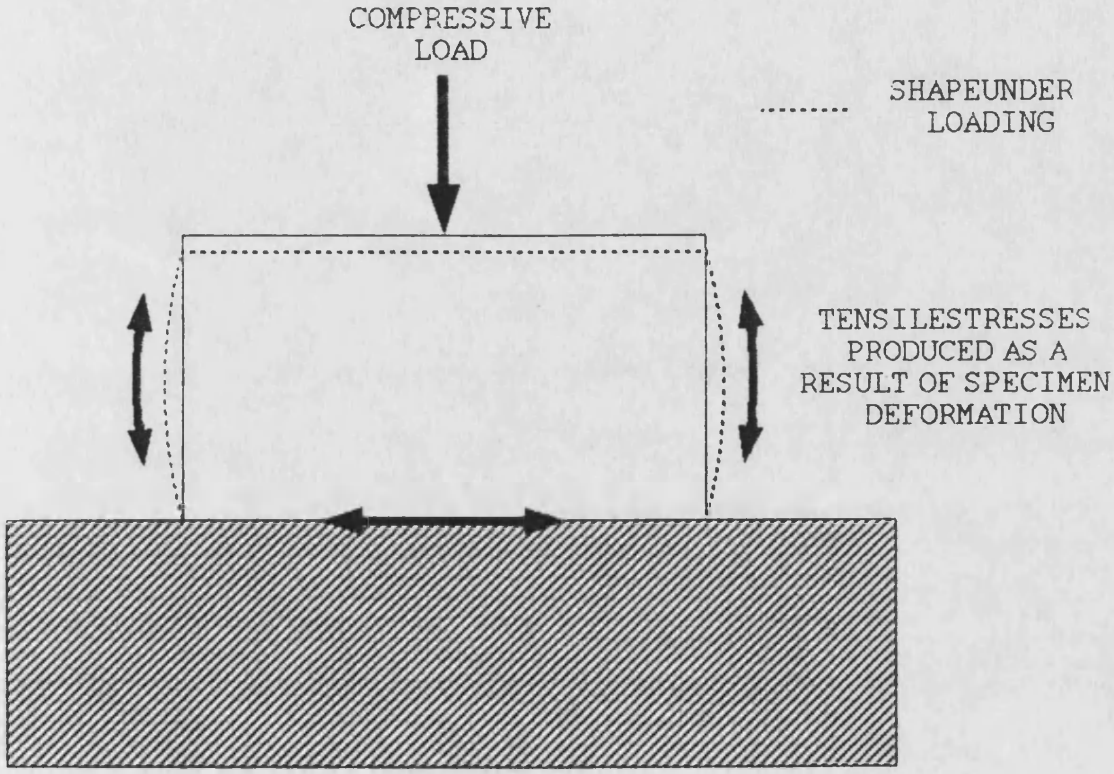

Figure 5.5 – Production of Tensile Stresses as a Result of Compressive Loading

Ceramic Cap Shrunk Fit into Aluminium Alloy Body

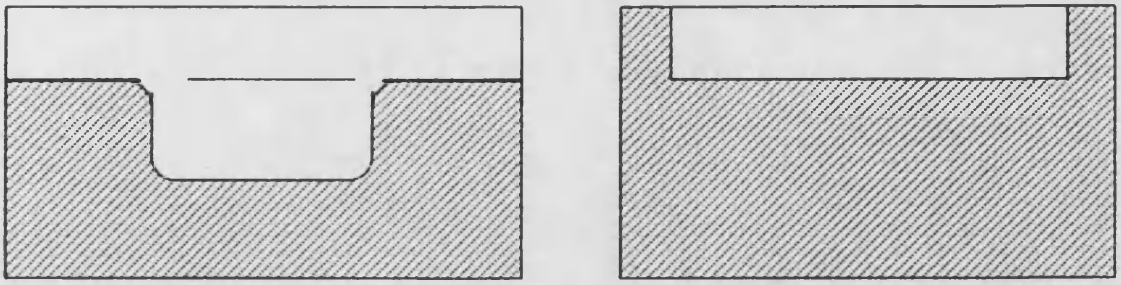

The two sketches shown above are examples of ceramic piston crowns shrunk fit into an aluminium alloy piston body. As with any piston design incorporating materials of widely differing thermal expansion coefficients, the design problem is one of attempting to cope with this mismatch.

Considering the two sketches above it is evident that the design on the right will not suppress heat loss as well as that on the left, due to the exposed region of metal body. This form might also give rise to problems due to the large radial temperature gradient which is likely to arise within the ceramic.

Any design which uses the shrink fit method of attachment will be applicable to only one ceramic. This results from the fact that the temperature distributions within the ceramic, and the metal, will have to be carefully controlled. The temperature field within the component parts determines their relative expansion and thus the fit, too large a difference may cause loosening of the cap at one extreme, or excessive stresses at the other extreme.

For the right hand case a typical metal temperature at the top section might be 250°C, with a mean temperature for the ceramic of say 600°C. The unconstrained difference in the strain values is therefore :-

Al alloy (200-20)*23 e-6 = 4.14 e-3

Ceramic (600-20)*10 e-6 = 5.8 e-3

or Ceramic (600-20)*3 e-6 = 1.74 e-3 dependent on which ceramic is used, this gives :-

strain diff. = +1.66 e-3 or -2.4 e-3

This rather crude calculation shows how the choice of ceramic might have a profound effect upon the initial fit used between the ceramic and the metal piston body, it also gives an order of magnitude "feel" for the strains likely to be encountered.

Figure 5.6

Ceramic Cap Bonded to Aluminium Alloy Piston Body with Polymeric Adhesive

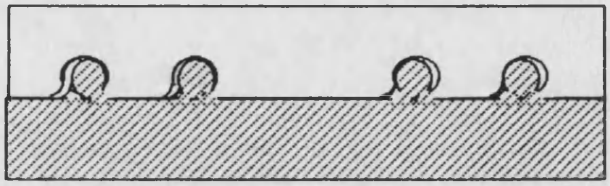

The design of an adhesively bonded ceramic cap/Al alloy piston body is likely to present a number of problems. The differential expansion between the ceramic the Al alloy body must be taken into account and appropriate allowances made. At the same time the distortion of the ceramic cap (due to the temperature gradient) must be examined and attempts made to minimise this through design of the contact between the cap and the main body. This is necessary if the adhesive layer is not to be overstressed. Although allowances must be made for differential expansion it is critical that firm heat flow paths are maintained, to ensure that the temperature at the adhesive is kept within its acceptable operating temperature range. The sketch shown above is obviously not a practical solution on a number of counts. The expansion of the hot, top surface relative to the lower, cooler face, will produce a "dished" profile in the ceramic, the top surface of which will assume a convex shape. This effect will promote a concave shape on the cooler face of the ceramic with potentially damaging high strains in the adhesive layer. The allowances made for radial expansion of the Al alloy body with respect to the cooler face of the ceramic cap, automatically insert air gaps into the structure, albeit at right angle to the direction of heat flow. However, axial expansion allowances also have to be made and this imposes air gaps in such a way as to interfere with heat flow, which is undesirable.

The low modulus and relatively high strain to rupture of the adhesive make it an attractive material in terms of a compliant layer. Low permissible operating temperatures, very low thermal conductivities, together with the relatively low strengths of the polymers which could be used for bonding, make design with polymeric adhesives difficult and in some instances impossible to achieve, due to conflicting requirements. The sketch shown above was possibly a poor example, but in order to fulfil the requirements of the design it is probable that some form of extension to the ceramic would be required. A last point which has not yet been mentioned is that polymeric adhesives all have thermal expansion coefficients much higher than those of metals or ceramics, typically in the region of 50 - 150 e-6K-1 as compared with 23 e-6K-1 for aluminium and around 5 e-6K-1 for typical ceramics.

Loaded polymer adhesives with higher thermal conductivities could allow the adhesives to be used in the same plane as the isotherms without appreciably changing the heat flow paths, but adhesives with high thermal conductivities tend to be weaker. If an adhesive of sufficient strength and conductivity could be found, then the design of composite bodies bonded together in such a fashion could be considered.

Figure 5.7

BASIC DESIGN AIMS

MINIMISE HEAT LOSS

MINIMISE THERMAL STRESSES WITHIN THE CAP

KEEP RING BELT TEMPERATURES LOW

ENSURE ALIGNEMENT OF CAP ON PISTON BODY

ENSURE RELIABLE AND POSITIVE
LOCATION OF CROWN ON PISTON BODY

KEEP STRESSES IN THE PISTON BODY
TO ACCEPTABLE LEVELS

MINIMISE COMPONENT COUNT

MINIMISE TOTAL PISTON MASS

KEEP TOLERANCES WIDE WHERE POSSIBLE

ALLOW FOR DIFFERENTIAL EXPANSION
BETWEEN PISTON BODY AND CERAMIC CAP

TAKE ADVANTAGE OF LOW ALPHA OF
CERAMIC TO MINIMISE DEAD VOLUME

Figure 5.8

First Notional Design for Ceramic Piston Crown

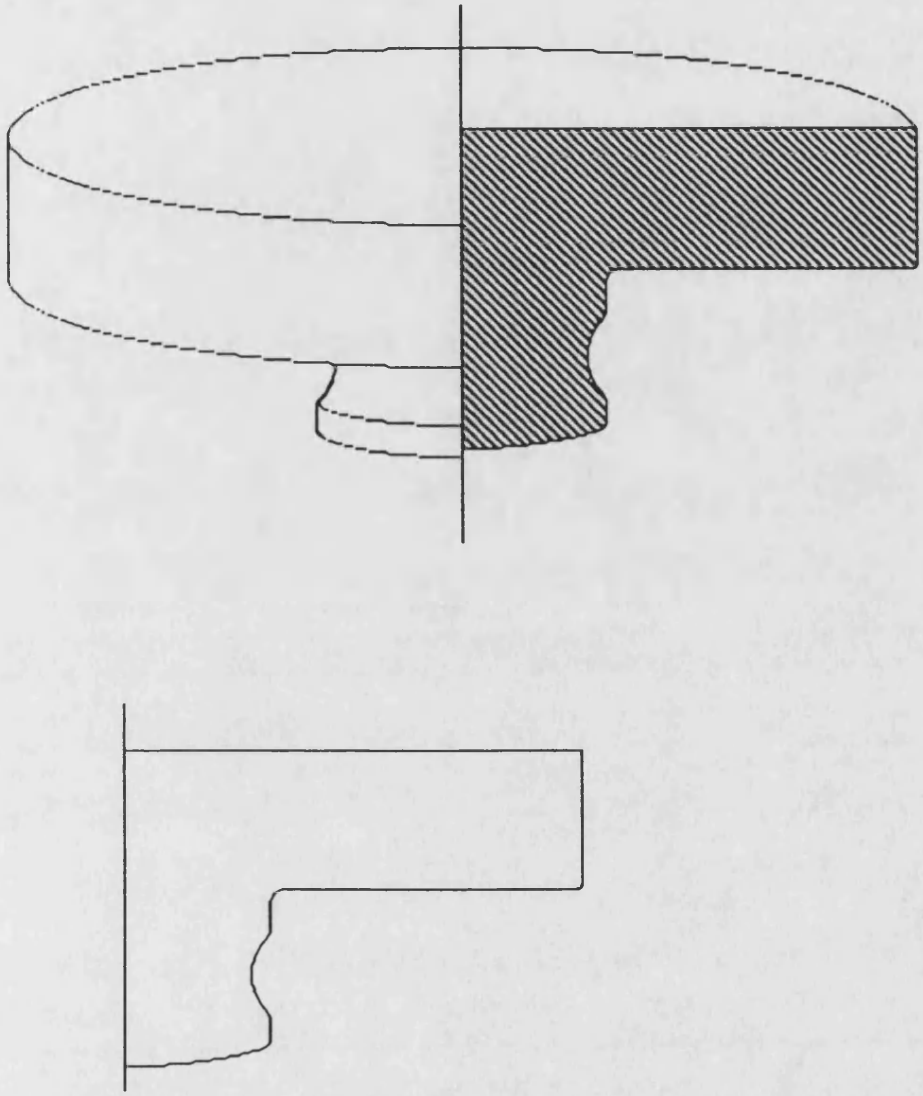

Figure 5.9

First modification to proposed Ceramic Piston Crown Design

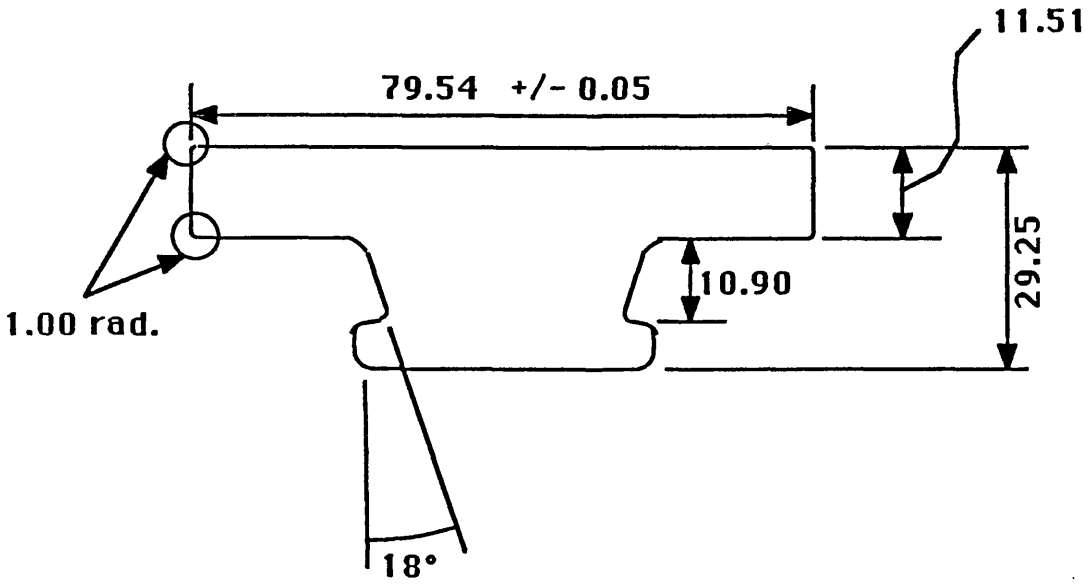

Figure 5.10

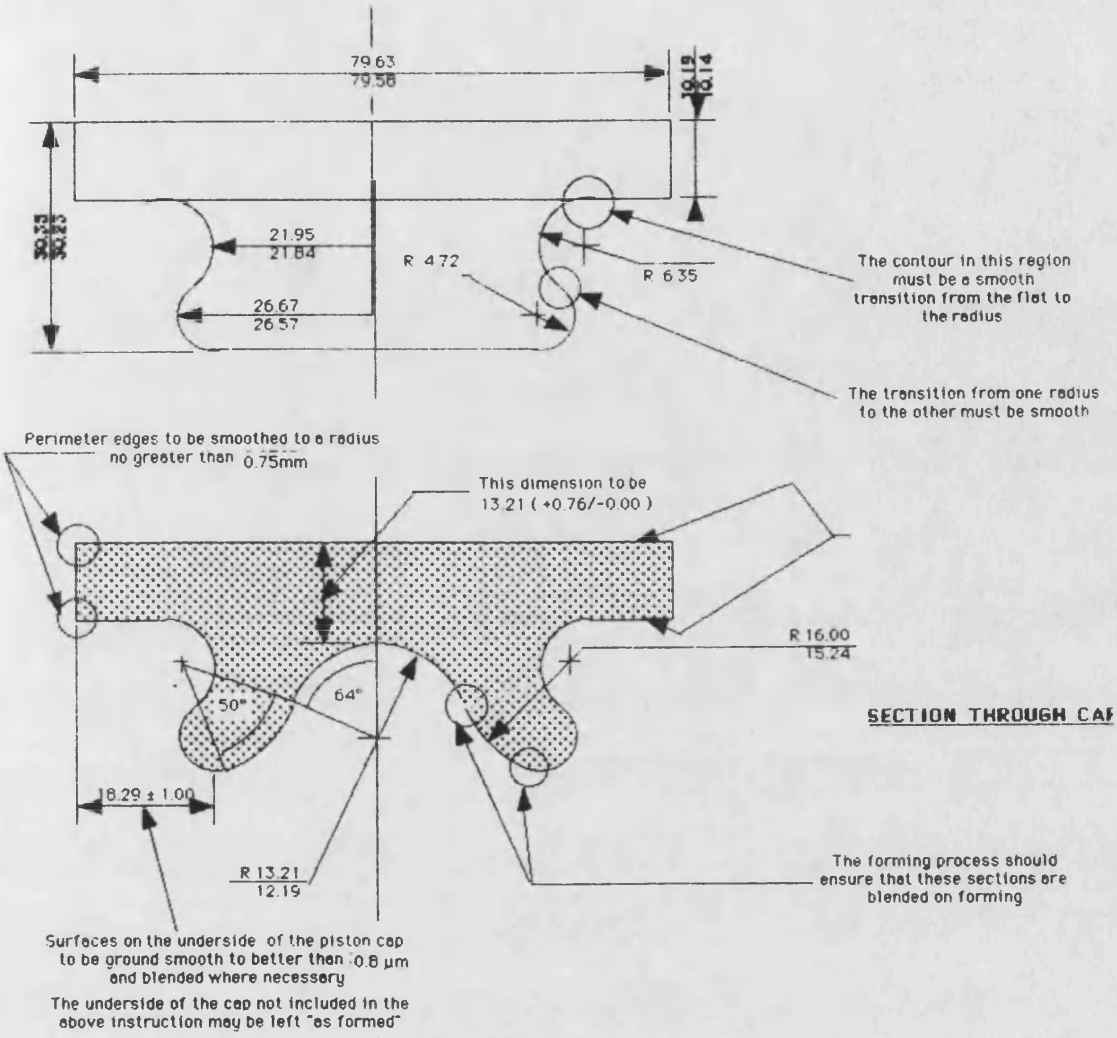

Figure 5.11 - First Crown Drawing Approved

Cross Sectional View of Outspringing Ring Attachment Design

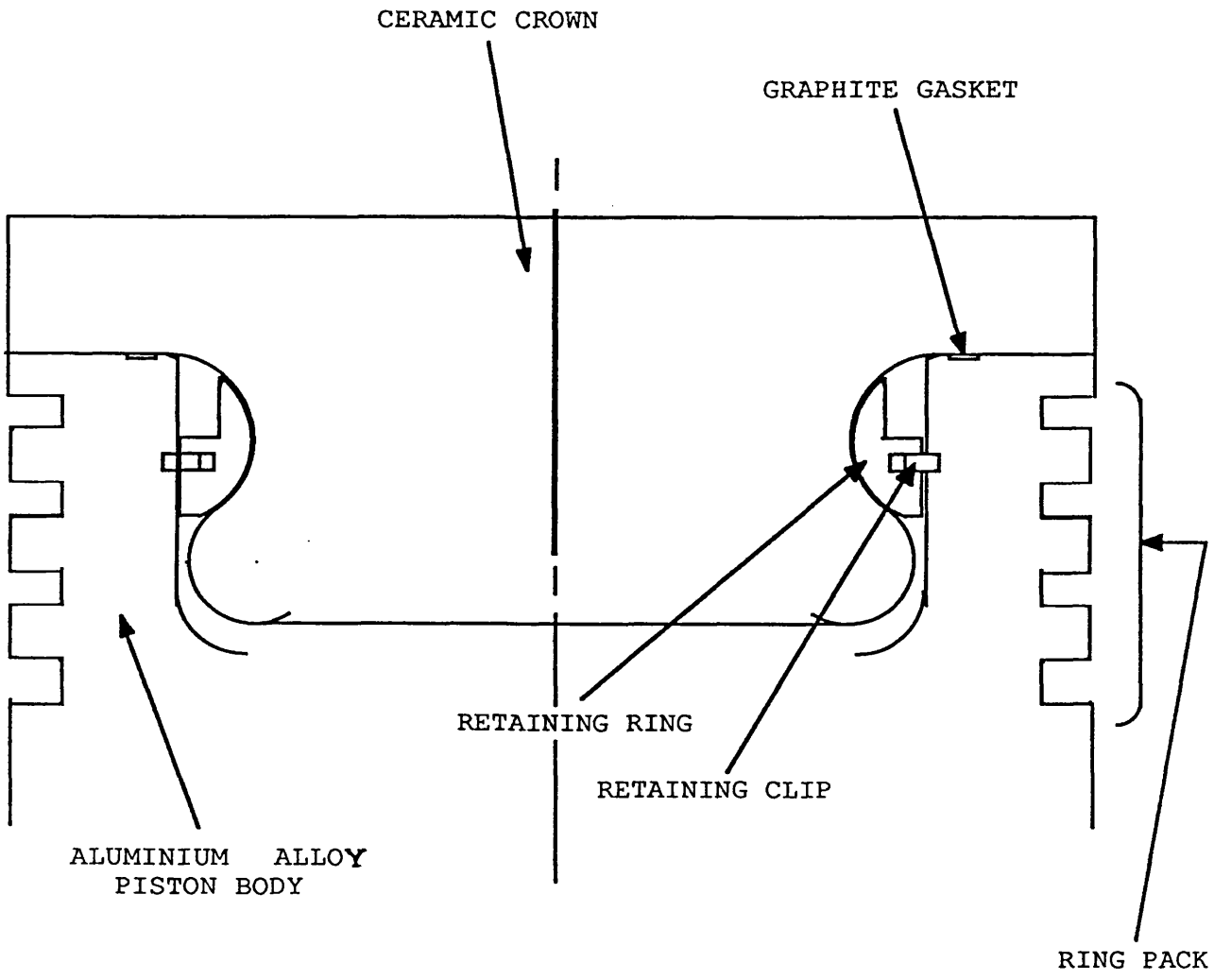

Figure 5.12

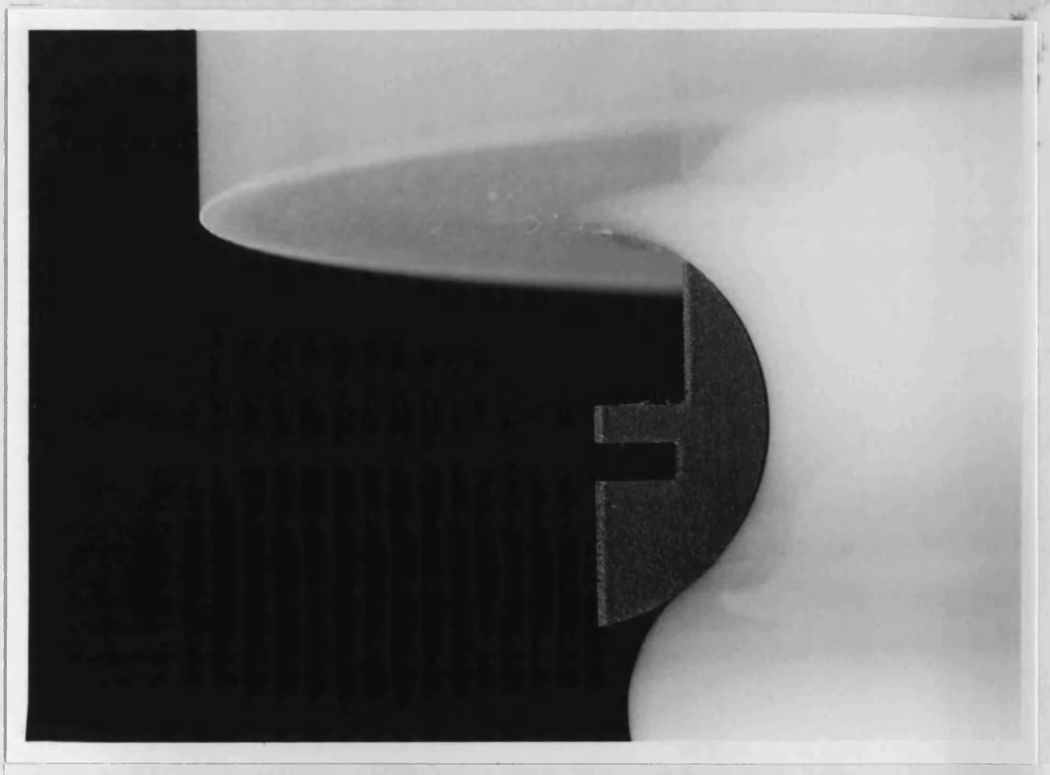

Figure 5.13 - Outspringing Ring Design

Cross Sectional View of Ceramic Capped Petter Piston
with
Stainless Steel Compliant Ring Cast into Position

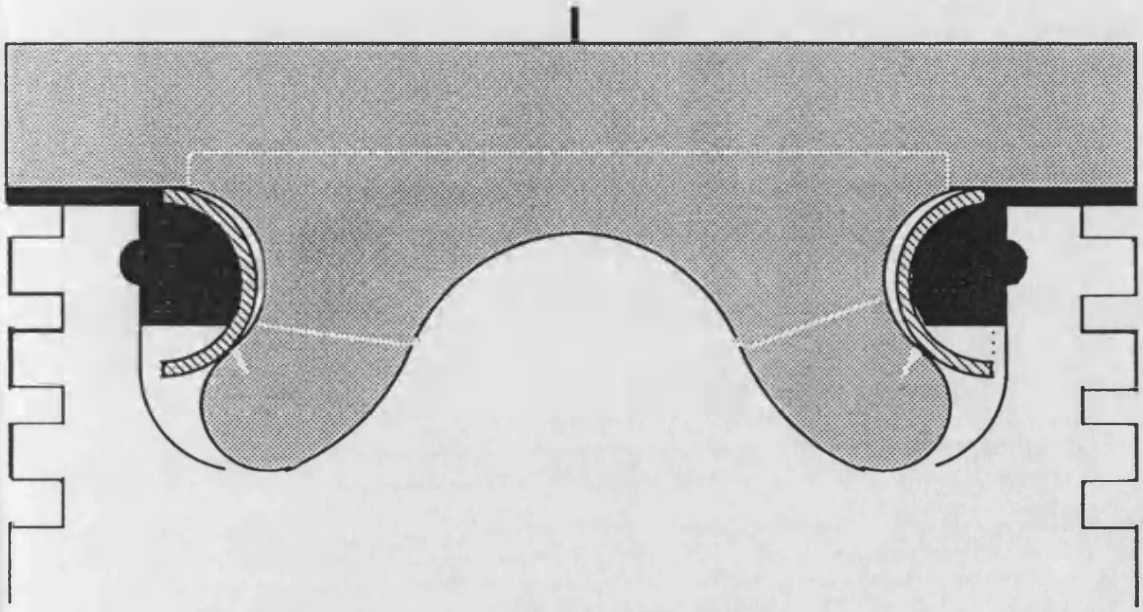

Figure 5.14

Figure 5.15 - Petter Piston Casting Jig

PreMachined Piston Body in Casting Jig

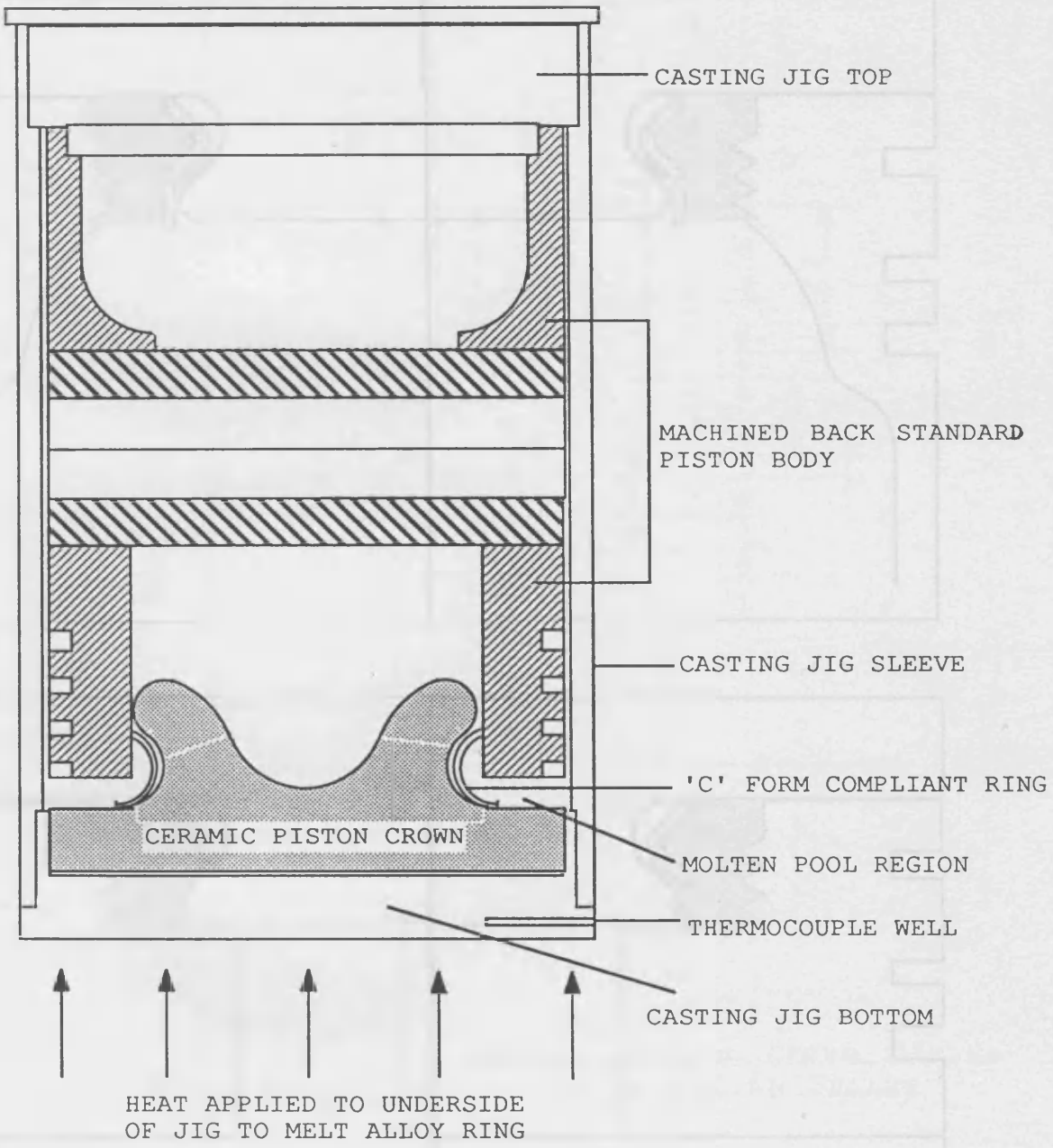

Figure 5.16

Orthogonal Cross Sectional Views of Fully Assembled Ford Piston with Ceramic Crown

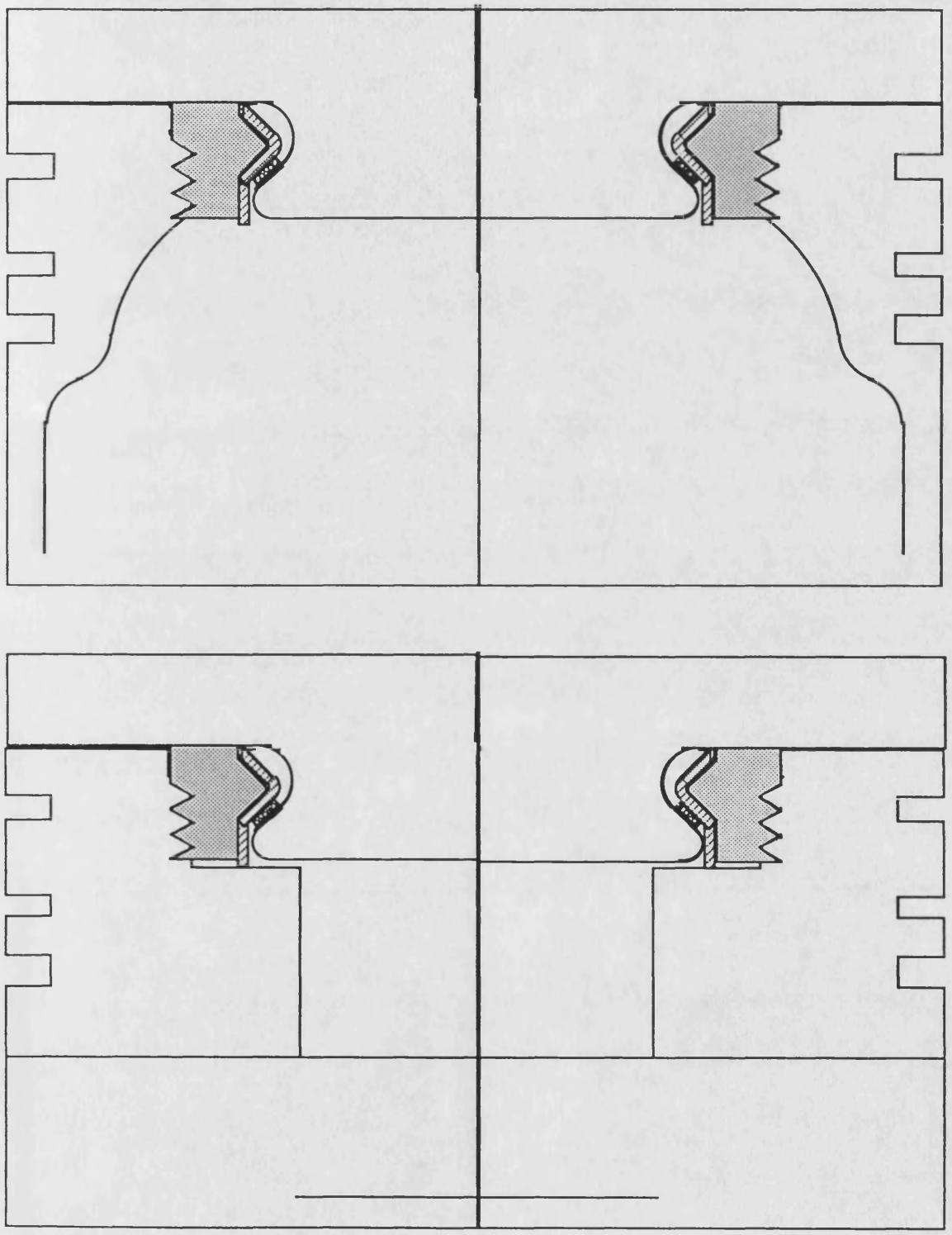

Figure 5.17

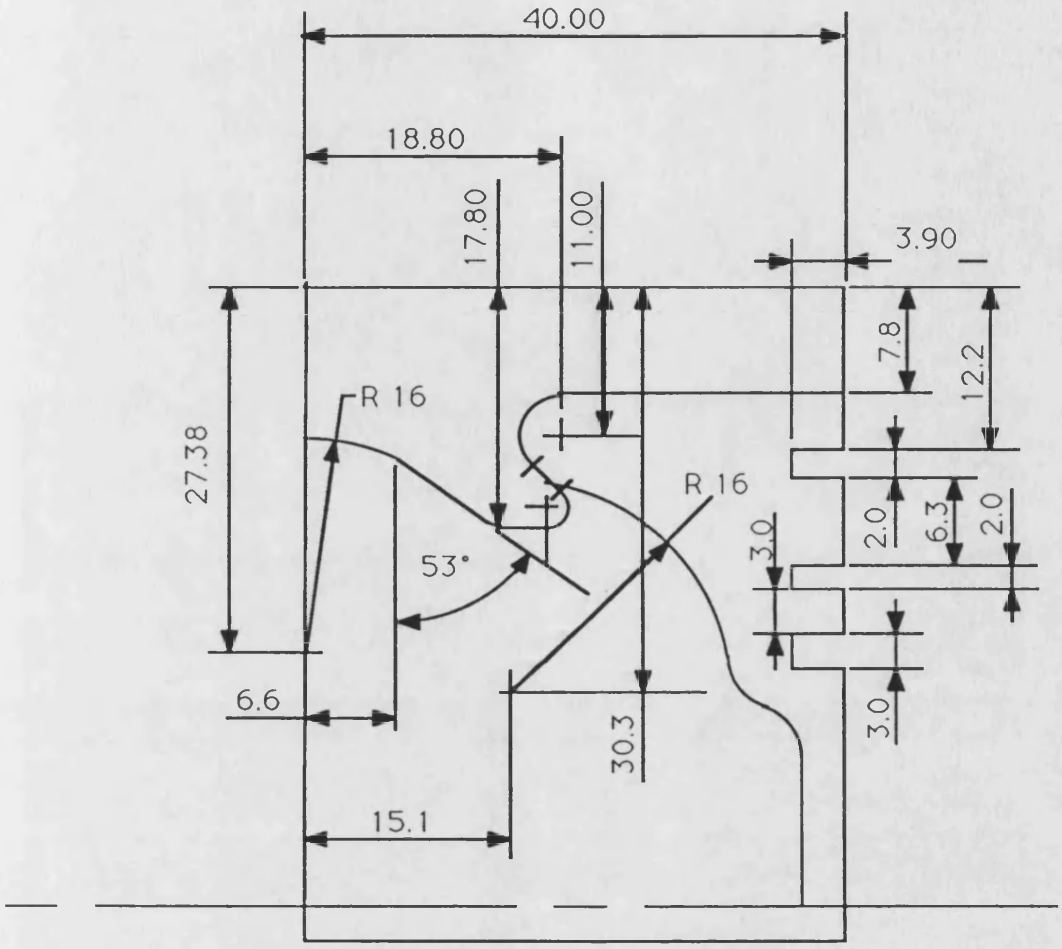

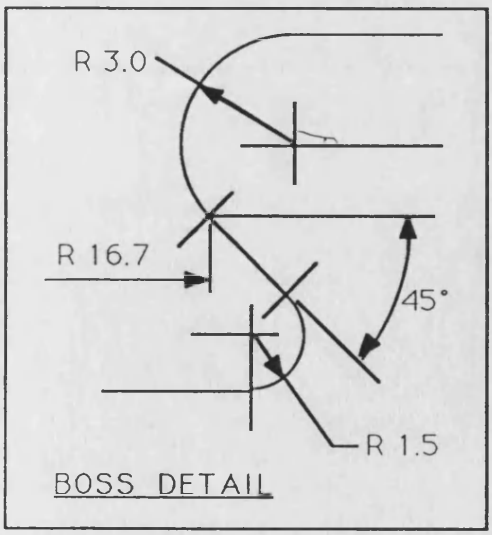

Ceramic Piston Crown Design
for Ford 1.6L Engine

Figure 5.18

Cross Sectional View of Ford Ceramic Piston Crown
with Stainless Steel Insert
and Shrink Fit/Adhesive Line Section

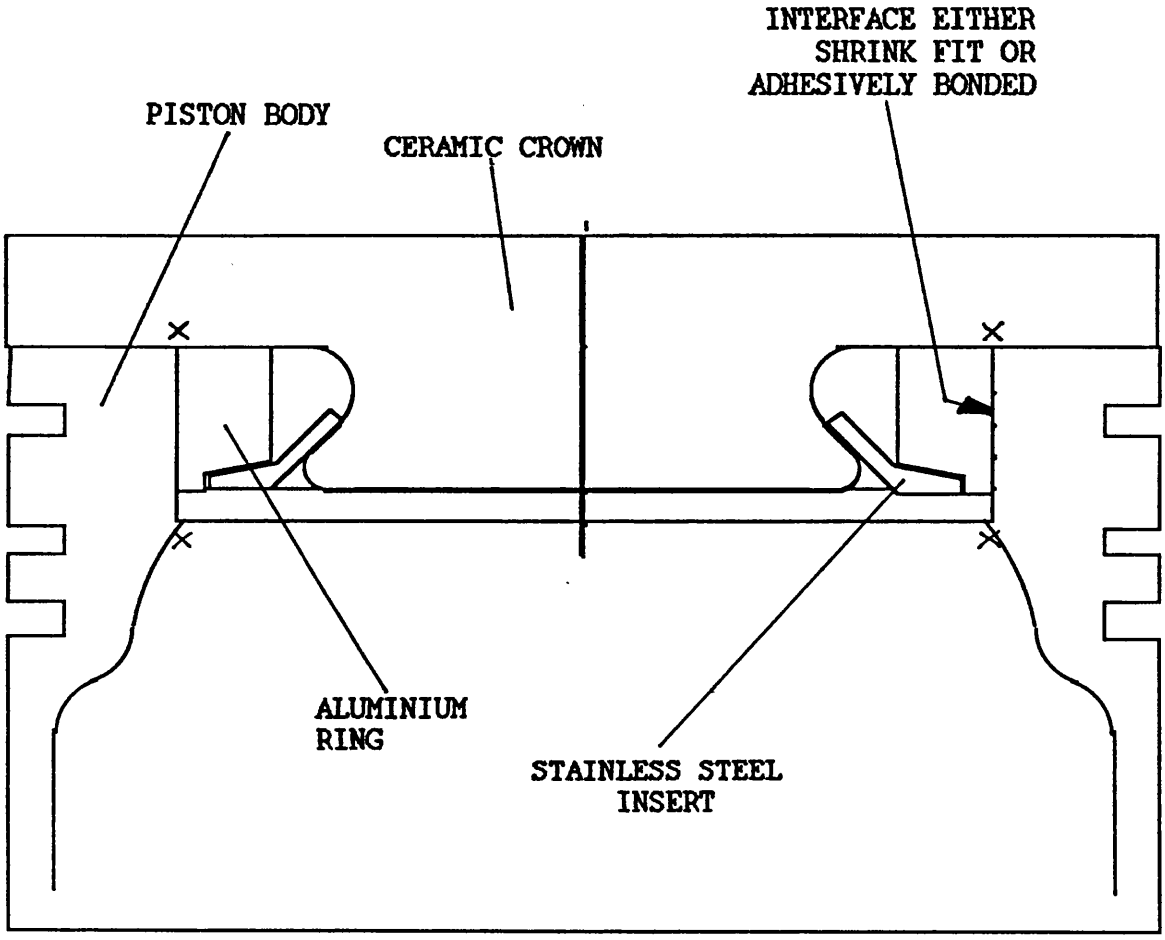

Figure 5.19

CHAPTER 6 - THERMAL ANALYSIS

6.1 Finite Element Modelling using Kao's suite of Programs

6.1.a Introduction

Generally speaking the finite element modelling was divided into two sections, namely ; those analyses carried out using Kao's F.E. analysis suite (**Ref. 1**), and those carried out using the ANSYS F.E. analysis suite. Only two examples of the use of Kao's finite element program suite are given in this thesis. Additional examples of the use of this program suite are the MSc theses of Pappas (**Ref. 10**) and Brouzakis (**Ref. 45**), which the writer supervised. The ANSYS suite of programs has been used mainly for axisymmetric, equilibrium thermal and stress analyses, although some preliminary work on three dimensional analyses and on two dimensional transient analyses has also been attempted. This thesis will confine itself to report the equilibrium, axisymmetric thermal and stress analyses carried out on the piston crown designs.

6.1.b Thermal Analysis of Cylinder Liner Thermocouples (Chapter 4, section 4.6.b)

It may be stated that the boundary conditions applied to any F.E. analysis are of great importance. However, it is seldom a simple task to assign appropriate boundary conditions. Input data for the piston analysis carried out by Kao are discussed in his PhD thesis (**Ref. 2**). It is evident that boundary condition data from several independent references differs widely, which in turn can lead to a considerable range of solutions. In order to improve the piston analyses it was decided to obtain further experimental data on the temperature field in the cylinder liner, which in turn influences the temperature field in the piston. In the case of the liner the most appropriate sensor type for monitoring the temperature field was considered to be the thermocouple. The type, construction and fitting of the thermocouples in the liner is described more fully in the **Chapter 4, section 4.6.b** . It is sufficient to state here that the thermocouples were twin wire with high temperature

polymer (Kapton polyimide) insulation. The influence on the temperature field of the presence of these thermocouples, and their insulation, was considered to be important, and therefore F.E. analyses were carried out to study these effects.

The local perturbations of the temperature field in the cylinder liner around the embedded thermocouples were considered to arise from three sources. One source was the insulation which surrounds the thermocouple wires. Another was the effect of the thermocouple wire extending from the back side of the liner into the water gallery. The third was the effect of an insulating medium on the water gallery side. A further source of error exists in the assembled form of the thermocouples in their liner pocket (see **Chapter 4, Fig. 4.7**). However, to avoid excessive model complexity, only the first three sources were taken into account. F.E. analysis runs were carried out for a variety of boundary conditions, this being necessary due to the lack of detailed information regarding the heat transfer coefficients in the water gallery. Further it was necessary to consider the effect on the temperature field when combustion chamber insulation was present. The major features included in the mesh are shown in **Fig. 6.1** . The four sets of boundary conditions applied, are shown in **Fig. 6.2** , and the four conductivity, or build, conditions shown in **Fig. 6.3** . The combination of conditions and builds led to a total of sixteen result files; for the sake of brevity, only four examples of the F.E. output plots are given. These plots are shown in **Figs. 6.4, 6.5, 6.6** and **6.7** . The plots themselves have been truncated to show only detail of the isotherms around the liner wall, although the mesh used for the analyses was taken right out to the block wall. The difference between the temperature in the absence of the thermocouple, and that which results when the thermocouple is present, is given for each case studied, in **Table 6.1** . This table also shows the discrepancy between the flux which is calculated from the temperatures registered by the thermocouples, and that which would arise if the thermocouples were not present. The percentage errors can be considerable,

and this highlights the need to consider carefully the effect which instrumentation can have, on the parameters to be monitored. Reductions in the perturbation of the temperature field which result from the presence of the thermocouples can be obtained by choosing thermocouple materials which more closely match the wall material in terms of thermal conductivity. It can also be seen that the insulation around the thermocouple has a marked effect on the temperature field. The thermal conductivity of polymers used for insulation is typically around 0.3 $Wm^{-1}K^{-1}$ which is a poor match for any of the metallic thermocouple materials. The only solution is to reduce the thickness of the electrically insulating polymer to a minimum, or to use a higher thermal conductivity, oxide insulator. This latter method has been successfully applied, but preparation of a reliable oxide film on the thermocouple wire is technically difficult.

6.1.c Thermal Analysis of Thermal Shock and Conductivity Test Specimens - Equilibrium only

The test specimens which are discussed in this section are described in more detail elsewhere in this thesis (see **Chapter 2**).

This study was initiated to examine the effects of departure from the ideal one dimensional heating and cooling of the thermal conductivity test specimen. It was found that the front face of the specimens were not subjected to an even distribution of heating flux. In the thermal shock configuration of the test rig it was also considered that the presence of the acoustic emission probe on the rear face of the specimen was likely to have an effect on the temperature field of the specimen. The two cases of thermal shock and thermal conductivity testing made the thermal analysis of the specimen under different condtions necessary.

Thermal conductivity case

Flux mapping at the specimen front face plane in the test rig showed that there was a variation in flux of around ±5%. It was therefore important for the determinati of thermal conductivity to know the magnitude of the error which such deviations from true one dimensionality would have.

At the time when this study was carried out it was not known to what extent the flux profile could be trimmed to approximate better to uniform heating of the front face. Several analysis runs were therefore executed to examine the effect of varying the profile and of varying the magnitude of the departure from uniform heating, while still maintaining the same overall value of mean front face flux. In order to simplify the calculations, three profiles were chosen for the front face heating flux, namely a cosine profile, a cosine squared profile and a cosine cubed profile. Although rather arbitrary, this choice of profiles was considered to give a reasonable spread. Three levels of flux variation for each of the profiles were examined, namely ± 2.5 % , ± 5.0 % , and ± 7.5 %. This being the variation in flux level from the centre of the specimen to the outside of the specimen. Axisymmetric analyses were carried out for all nine cases. The specimen material was chosen to have a thermal conductivity of 2 $Wm^{-1}K^{-1}$, which is similar to the glass ceramics, the actual mesh being shown in **Fig. 6.8** . **Fig. 6.9** shows the boundary conditions which were applied to the front face of the specimen. **Fig. 6.10** summarises the results from the nine F.E. analysis runs, for specimen front face temperature.

Thermal shock cases

A number of analysis runs were executed for these cases in an attempt to match the analyses to experimental equilibrium data. Once again the boundary conditions presented somewhat of a problem. The back face cooling was assumed to be uniform over the annular region of the specimen back face in contact with the aluminium cooling plate, and estimates only were available for the heat transfer coefficient and bulk fluid temperature in the central region where the acoustic emission probe was fitted. However, it was possible to obtain a reasonable match between the analyses and the experimental data, although this was somewhat limited. **Fig. 6.11** summarises the output from two of the analysis runs, for cases with different imposed mean front face fluxes, and different back face conditions. **Fig. 6.12** is an example of the F.E. output plots obtained. One outcome of the results was to show

the severity of the equilibrium temperature gradients and thus the thermal stresses, with an uncooled, centrally disposed acoustic emission probe. This fact pointed to the need to redesign the specimen holding scheme and the acoustic coupling system. A suggested alternative form of holder is shown in **Chapter 2 ,Fig. 2.25 .**

6.1.d Remarks

The finite element analyses covered in the foregoing subsections of this chapter have all been carried out using Kao's finite element analysis packages. Although the pre- and post-processing capabilities of this suite of programs are rather rudimentary by today's standards, the utilisation of them, forces the user to consider both the boundary conditions and the mesh, carefully before running.

The later finite element work on piston design was carried out almost exclusively using the ANSYS suite of programs. The pre- and post processing capabilities of this suite are generally much more sophisticated than for the Kao suite. However, the importance of correctly setting the mesh density and of applying appropriate boundary conditions still applies. Thermal and stress analyses using the ANSYS suite of programs will now be examined.

6.2 Piston Crown Finite Element Analyses using ANSYS

6.2.a Introduction

Details of the design route which led to the production of a number of ceramic crowns have already been given in **Chapter 5.** Those designs which were produced were first analysed for temperature distribution and thermal stress using the ANSYS suite of finite element programs. This suite of programs includes sophisticated pre- and post- processing of data files, as well as offerring a wide range of element types and analysis commands. The initial work was carried out by two students, supervised by the author. This work highlighted a number of points which provided useful data to be used in conjunction with further design stages. Among these points, which are more fully discussed in the students own literature (**Rentsch Ref. 42** and **Kassens Ref. 43**), are the

siting of the mechanical constraints, the use of gap elements, boundary condition data, and the use of T_{unif} and T_{ref} commands within ANSYS . The following section will be confined to brief discussions on :- the mechanical constraints used in the modelling particularily as applied to shrink fitting ; the use of gap elements ; and some typical thermal distribution and stress results.

6.2.b Mechanical Constraints

In all of the analyses carried out, radial pinning of the centreline of the component (i.e. the axis of symmetry) was necessary to ensure model integrity. A portion of the piston ring belt has been included in all cases for two main reasons. The first of these is to allow realistic thermal boundaries to be specified. The second reason is to allow the mechanical constraints for the model to be placed some distance from the critical parts of the crown to minimise the effects of such constraints should they be in error. It may be seen that care has to be taken, with reference to **Figs. 6.13** and **6.14** and **6.15** and **6.16** which show the effects of changing the mechanical constraints at the lower tip of the mesh below the ring belt, for the case of the shrink fit design. **Figs. 6.13** and **6.14** show the distortion and axial stress field for the case of single node pinning (the node at the lower right hand corner), which is contrained in the axial direction. **Figs. 6.15** and **6.16** show the effect of adding further pinning points (all of the nodes along the lower right hand corner of the mesh). A comparison of **Figs. 6.13** and **6.15** shows the difference this has on the distortion of the model, while **Figs. 6.14** and **6.16** show the difference in the axial stress values. The two shrink fit runs were conducted by assuming a stress free temperature, and then reducing the temperature of the whole "free fitting" assembly by 390°C. Although this situation does not model the usual shrink fitting procedure exactly, it simplifies considerably the analysis, and allows attention to be focussed on the geometry. The point made earlier in **Chapter 5 section 5.3.a** with reference to **Fig. 5.5** is well displayed by both of the shrink fit analyses here. The large compressive forces brought about

by shrinkage of the aluminium alloy piston body onto the ceramic body, promotes large compressive stresses in the ceramic, however, these are accompanied by high tensile stresses at the edges of the coupling zone.

The case of shrink fitting gives very large differences in stress values, dependent on the mechanical constraints chosen. It should be remarked that similar comparisons were made for the other forms of attachment analysed, and in all cases the differences were small. This is due to the relatively low radial stiffness which exists in the non-shrunk forms of piston attachment which have been designed.

6.2.c Gap Elements

It became evident at an early stage of the work carried out in collaboration with Rentsch (**Ref. 42**), that the use of gap elements was essential for the correct modelling of the multi-part piston assembly. The interpenetration of the crown with the main body of the piston, shown in **Fig. 6.17**, is obviously not realistic, and required some more detailed modelling of the interface region. The gap element facility available within ANSYS allowed such detailed modelling to be carried out. However, the use of these special elements was not without problems. Further work on the use of the gap elements was carried out in collaboration with Kassens. Although this work was an advance on that carried out previously there were still some doubts as to the validity of the input parameters to the gap elements. Later work was carried out by Dr. M. Wilson in collaboration with the author. One of the parameters which is required to be input is the gap element stiffness. The ANSYS manuals suggest that values of stiffness should be approximately one order of magnitude greater than the average modulus of the two regions either side of the gap. Dr. Wilson varied the stiffness over several orders of magnitude to see the effect that this had on the solution, the results of this are given in **Ref. 44** . A further point is that of the orientation of the gap with respect to the elements either side of the gap. This is a fairly simple situation where the displacements of the elements either side of the gap are coplanar. Problems arose

in one of the analyses when the displacements of the elements proceeded to run out of the plane in which they started. Again, this is discussed in more detail in the reference already cited.

6.2.d Typical Petter Piston Thermal Analyses

Examples of analyses which were run on two of the Petter piston designs, are given in **Figs. 6.18** through to **6.26** inclusively. **Figure 6.18** shows a typical set of boundary conditions which were used in the thermal analyses of the piston. **Figure 6.19** shows a resulting temperature distribution, with **Fig. 6.20** giving fine detail around the ring belt of the piston body. It can be seen that the top ring temperatures are well within acceptable limits, this is in spite of the fact that the top side boundary conditions represent a highly loaded case. **Figure 6.21** shows the thermal displacement for the model under the thermal loading described, the lower right hand portion of the mesh has been pinned axially to simulate the effect of the gudgeon pin. **Figures 6.22 , 6.23 ,** and **6.24** show the radial, axial and hoop stress distributions, respectively. The last two figures in this series of output plots, **Figs. 6.25** and **6.26 ,** show the effect of introducing an insulating layer between the piston body and the ceramic crown. While there is a noticeable decrease in the maximum axial tensile stress from 51 MPa to 37 MPa the largest change is in the maximum tensile hoop stress, which drops from 135 MPa to only 118 MPa. Indeed the purpose of introducing the insulating layer was to reduce the heat lost from the outer portions of the crown, to reduce the radial temperature gradient and thus the hoop stress levels in this region. A detailed account of each series of analyses is given in **Refs. 42, 43,** and **44.**

6.3 Summary of Progress of Finite Element Analyses

Finite element thermal and stress analyses on a number of ceramic crown/piston combinations have been carried out. The effect of changes in the thermal and mechanical boundary conditions and in the material properties have been examined, for several design schemes. The initial work on the first

design of piston crown for the Petter engine (see **Fig. 5.10**) was a useful precursor to the later F.E. work. This work is fully described in **Ref. 42** and provided a useful basis for further F.E. analysis. A quantitative idea of the temperature field which could be expected to arise under full load engine conditions was obtained as well as an insight into some of the difficulties associated with the treatment of interfaces. The second series of analyses (**Ref. 43**) examined changes in the thermal boundary conditions and material properties of the ceramic. These analyses were carried out on the first approved design of crown for the Petter piston(**Fig. 5.11**) and on the subsequent modification to this design which included the undercrown dimple. This dimple was included after difficulties were experienced in the production of the first design by Pilkingtons. The use of gap elements was further explored and indeed the first satisfactory use of these elements resulted. The analyses proved useful in progressing the design of the first Petter piston crown to be manufactured.

The first attempts to carry out modelling of a shrink fitted system of assembly were also carried out in this series of analyses. While these analyses did not take into account the almost inevitable plastic behaviour of the metal under such conditions, a good quantitative feel for the potential problem areas was obtained.

Generally, the use of F.E. thermal and stress analysis has progressed the design of the ceramic caps for diesel engine piston use. However, it should be stated that their use is not without problems and this point is discussed in **Chapter 8** .

6.4 Resistance Modelling

6.4.a General

This technique is commonly used for estimating the relative importance of sections within a component to be thermally analysed. Resistance modelling is a useful precursor to finite element thermal analysis, it is also useful for fault finding as shown in the following section, where it has been applied to solve an operational problem on the thermal

shock test rig, as reported in **Chapter 2, section 2.11.**

6.4.b Quartz-Halogen Lamp Thermal Resistance Model

Repeated, early failures were experienced with the operation of the high intensity quartz halogen lamps used in the thermal shock test rig. The failures all appeared to be the result of lamp overheating. A simple resistance model was therefore produced to examine the temperature field in a lamp, and to identify possible methods of overcoming the problems.

This model highlights problems which are likely to be encountered regardless of which analysis technique is used; it should also be mentioned that the model which is described was the result of several modelling attempts. The major resistances, sources, and sinks, for the final model, will now be identified, together with the problems encountered.

All of the initial lamp failures were due to overheating of the lamp electrode/end cap sections, and thus it was considered necessary to focus attention on this section of the lamp. The major source was considered to be the lamp filament, with the lamp envelope acting as a secondary source. The major sinks were identified as being the water cooled electrode block and the air around the end cap of the lamp, together with reradiation from the lamp pinch seal. Figure 6.26 shows the actual geometry of the lamp with the final resistance model shown in **Fig. 6.27** . As radiative terms were incorporated in the model it was necessary to use a small computer program to reduce solution times, a listing is given in **Table 6.2** . **Figure 6.27** shows the overall resistance network with **Figs. 6.28.a** and **6.28.b** showing resistance fine detail around the end cap and electrode.

The source temperatures assigned to the filament and the envelope are difficult to estimate. The envelope temperature was set to be around 750°C . This figure was arrived at through considerations of black body radiation from the filament being absorbed by the envelope, through some knowledge of the transmission characteristics of quartz, together with nominal values of convective transfer coefficients from the outside of the envelope. Earlier design work on the lamp reflectors gave some indication of the total

filament flux absorbed by the lamp. A further indication of the envelope temperature, though somewhat crude, was that there was some evidence of envelope softening, which from lamp literature suggested a temperature of around 800°C.

The temperature assigned to the end of the filament post in the model was 1500°C , which is a very crude estimate of temperature, lying somewhere between the actual filament temperature of around 3200 K and the envelope temperature at the pinch seal of around 500 to 600°C . Obviously this is a major potential source of error, although the relatively high resistance of the electrode post and the wire feadthrough to the pinch seal reduce the significance of this somewhat.

The resistance of the lamp envelope from the point at which the temperature of 750°C is assigned, to the pinch seal was calculated from measurements of the envelope thickness and mean conduction length. This procedure was also carried out for the resistances of :- the pinch seal section, the flat/circular electrical feadthrough sections, the alumina end cap, and the wire to the end cap.

Some account was taken of the radiation absorbed by the flat pinch seal, by estimating the radiation impinging on the copper reflector and being multiply reflected into the reflector end cavity.

Convective transfer estimates from the flat pinch seal were complicated by a lack of knowledge of the air temperature. At the start of the investigation, one end of the lamp was fitted into a sealed off section of the reflector and thus the air temperature was likely to be high. At the other end of the lamp (free eletrode end) there was an air passage, which presumably allowed air external to the reflector to pass into the reflector and over the lamp at this end. The temperature of the ambient air at this end was therefore likely to be much lower. Indeed the analysis assumed that both the ambient air temperature and heat transfer coefficient were markedly different at each end of lamp. An air temperature of 40°C with an H.T.C. of 15 $Wm^{-2}K^{-1}$ was assumed for the "free electrode" end of the lamp, and an air temperature of 200°C with an H.T.C. of only 2 $Wm^{-2}K^{-1}$ for the "fixed electrode" end

of the lamp.

The single resistance shown in **Fig. 6.25** from the end of the lamp through to the water cooled section at 40°C is actually a composite resistance which is calculated from the summation of a number of resistances in series. These resistances are as follows :-

contact resistance - lamp end cap to copper electrode

copper electrode resistance

copper electrode to electrical insulator air gap resistance

electrical insulator resistance

electrical insulator to copper block air gap resistance

copper block resistance

copper block to water resistance

These resistances are detailed in **Figs. 6.28a** and **6.28.b** Contact resistance between the lamp end cap and the tip of the copper electrode is rather difficult to estimate, however the significance of this resistance may be reduced by assuming a conductive grease is used between the two components. The geometry of the copper electrode may also lead to some errors in the estimate for its resistance. Any doubt in the resistance values had to be considered in the light of their significance and the other approximations used in the model.

The results obtained from the analyses are shown in **Fig. 6.29** , and broadly agree with the evidence from the lamp failures, however the results have not yet been validated experimentally. The three graphs in **Fig. 6.29** show how the end seal temperature varies with : -

assumed envelope temperature

assumed power absorbed in the lamp end seal

and assumed filament temperature at the input to the model

Four cases are examined in each of the aforementioned graphs, namely : -

for a fixed, ungreased, electrode

for a fixed, greased, electrode

for a free, ungreased, electrode

and for a free, greased, electrode

Thus it is possible with the aid of the graphs in **Fig. 6.29** to estimate the effects of changing the thermal boundary conditions around the lamp. The result of varying the assumed lamp envelope temperature from 600°C to 800°C is to bring about a variation of some 30°C in the end seal temperature. A variation of around 20°C in the end seal temperature results from variations in the assumed filament temperature from 1200°C up to 1700°C. However, the most dominant efffect would appear to be the amount of power which is assumed to be absorbed by the pinch seal, between the filament/envelope section and the end cap. Varying the assumed absorbed power from 7 Watts up to 18 Watts increases the end seal temperatures by around 75°C . The application of thermally conductive grease to either electrode decreases the end seal temperature by around 30°C . The essential difference between the "free" end seal and the "fixed" end seal was the convective boundary conditions applied to the model (as $R_{convective}$ and $T_{ambient\ air}$ in **Figure 6.27**) , and this gives rise to a mean temperature difference of around 40°C for these two conditions.

Temperature measurements of the end seals of the lamps were within about 20°C of those predicted, although it should be remarked that the presence of the temperature probe may have affected the readings. Although the introduction of thermally conductive grease did not cure the problem of premature lamp failure, it did serve to extend the life of the lamps from less than five hours to greater than ten hours. The subsequent addition of ventilation ports at the fixed end seal positions and forced air cooling provided by fans, cured the problem of end seal overheating, and generally lamp lives are now dominated by the survival of the central sections of the lamp envelope.

Details of Mesh used for Thermocouple in Liner Thermal Analyses

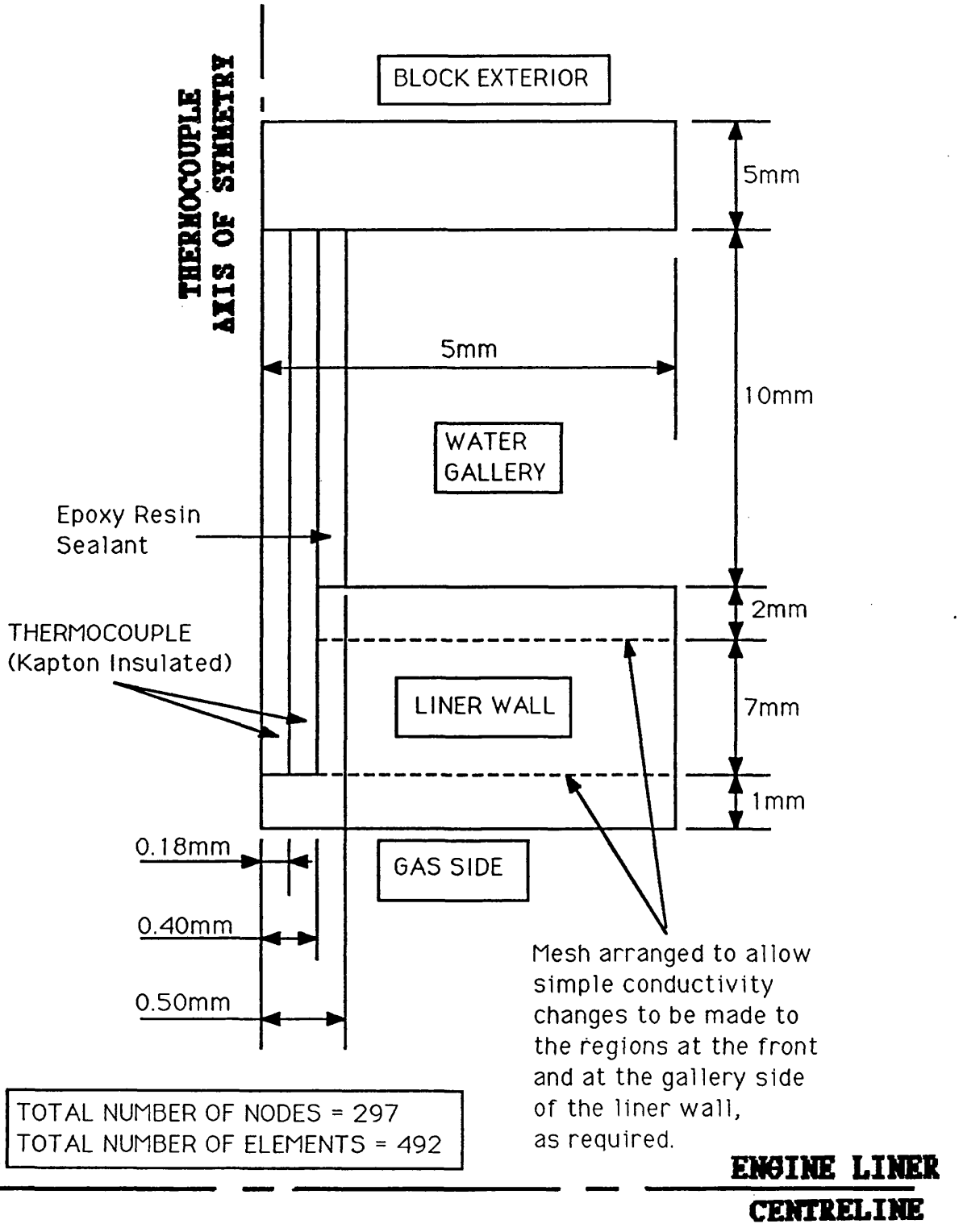

Figure 6.1

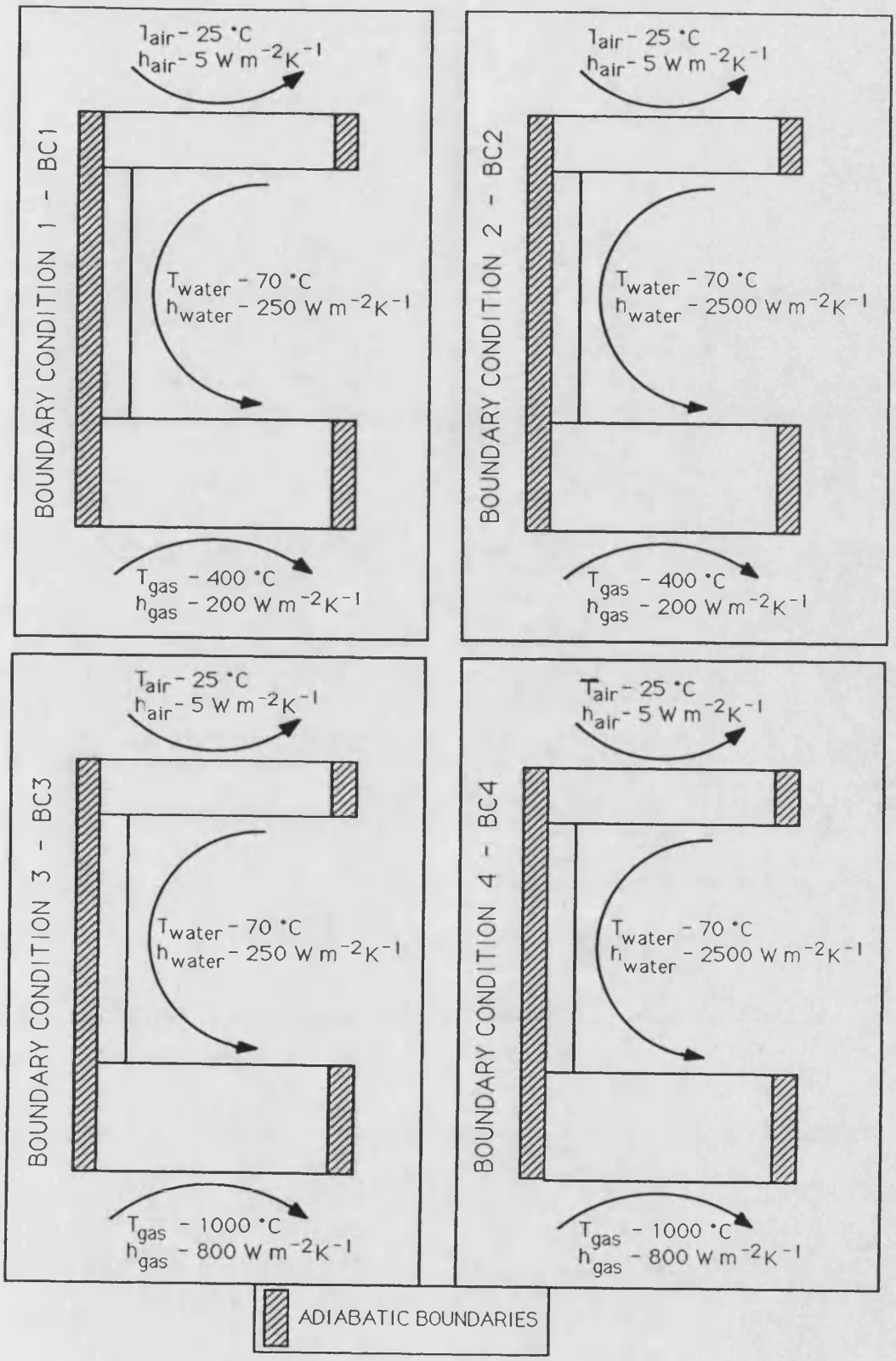

Figure 6.2 - Boundary Conditions used for Analysis of Thermocouple in Liner

Schematics of the Four Conductivity Cases of Liner Thermocouple Analysed

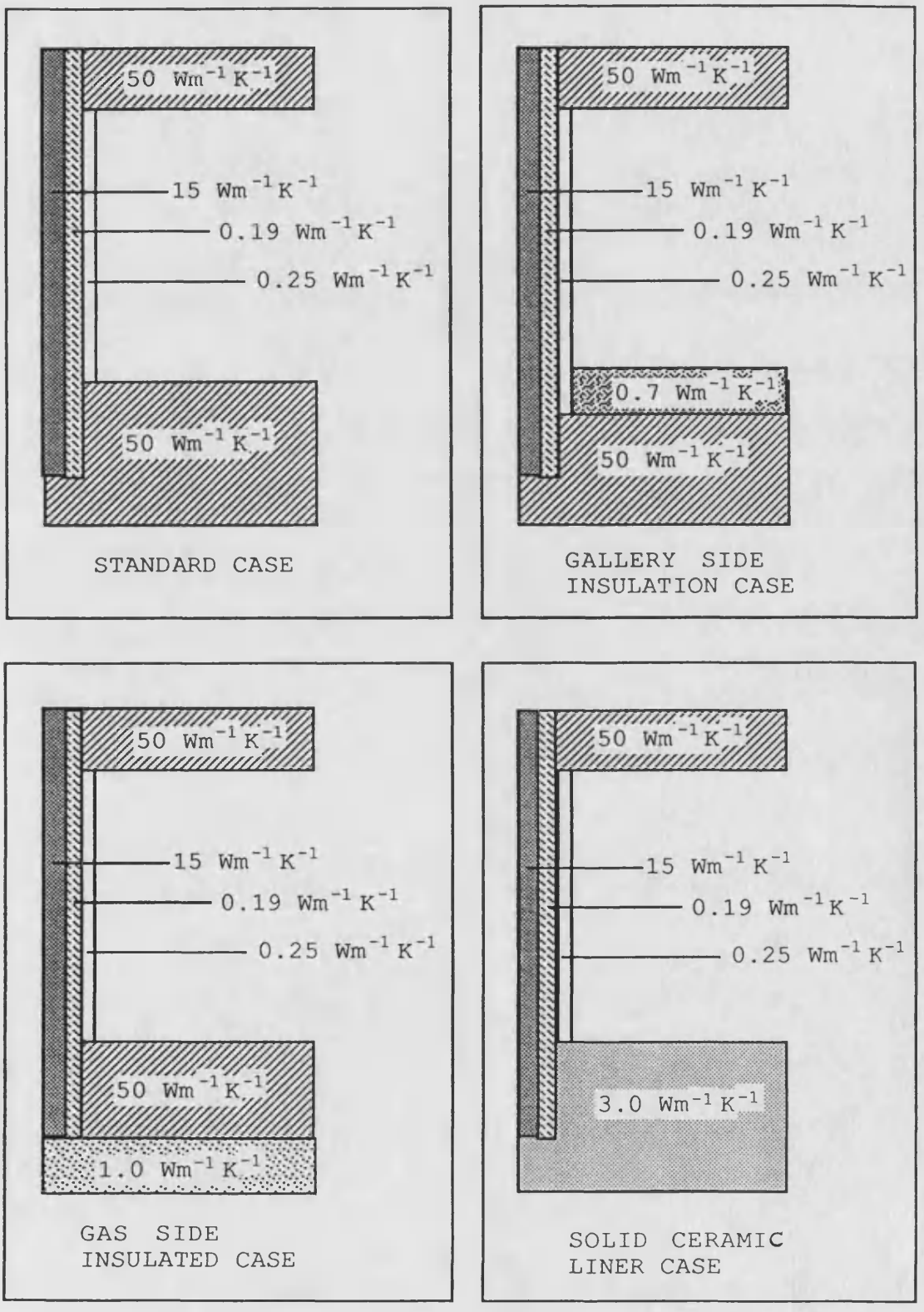

Figure 6.3

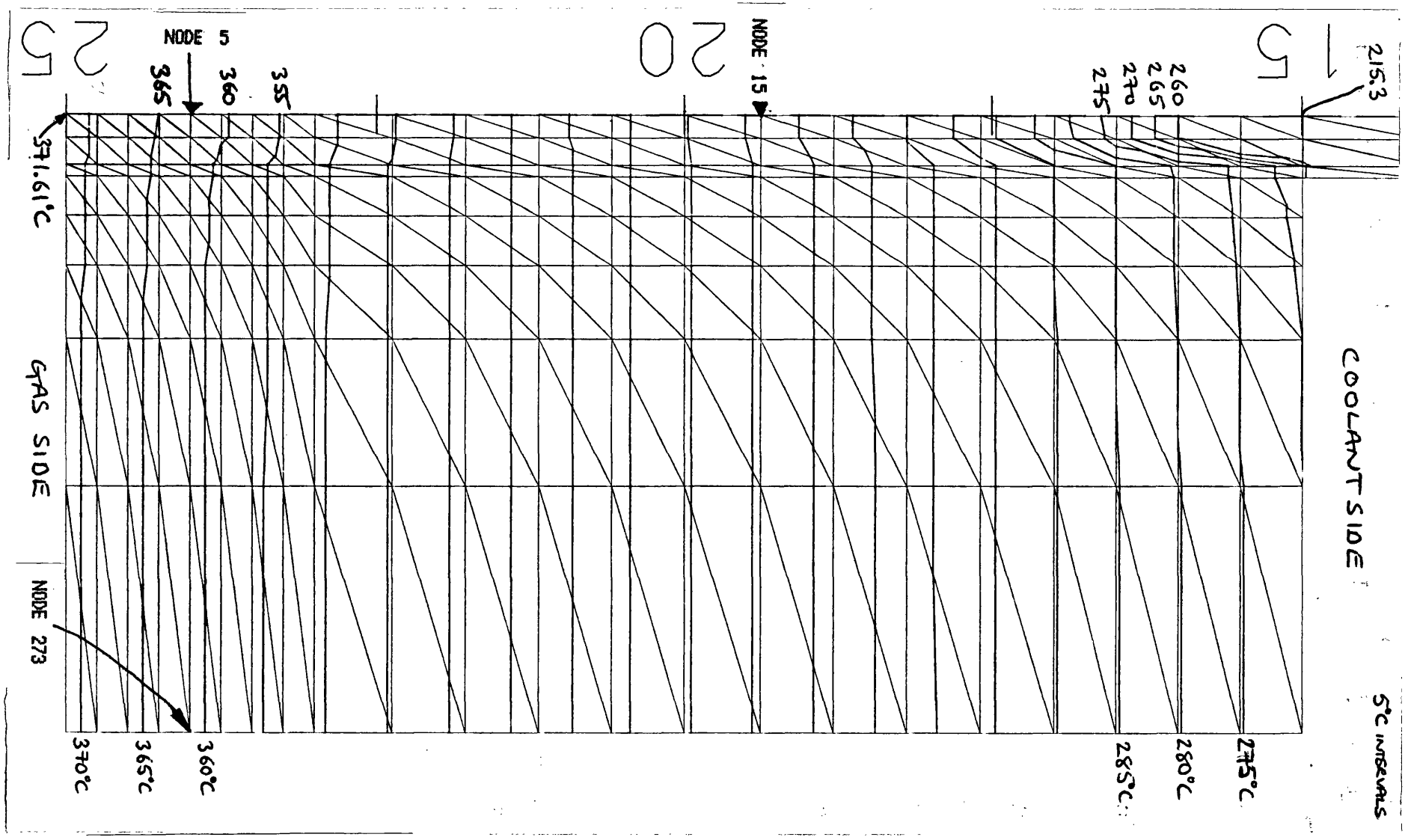

Figure 6.4 — STANDARD CASE UNINSULATED / BC4

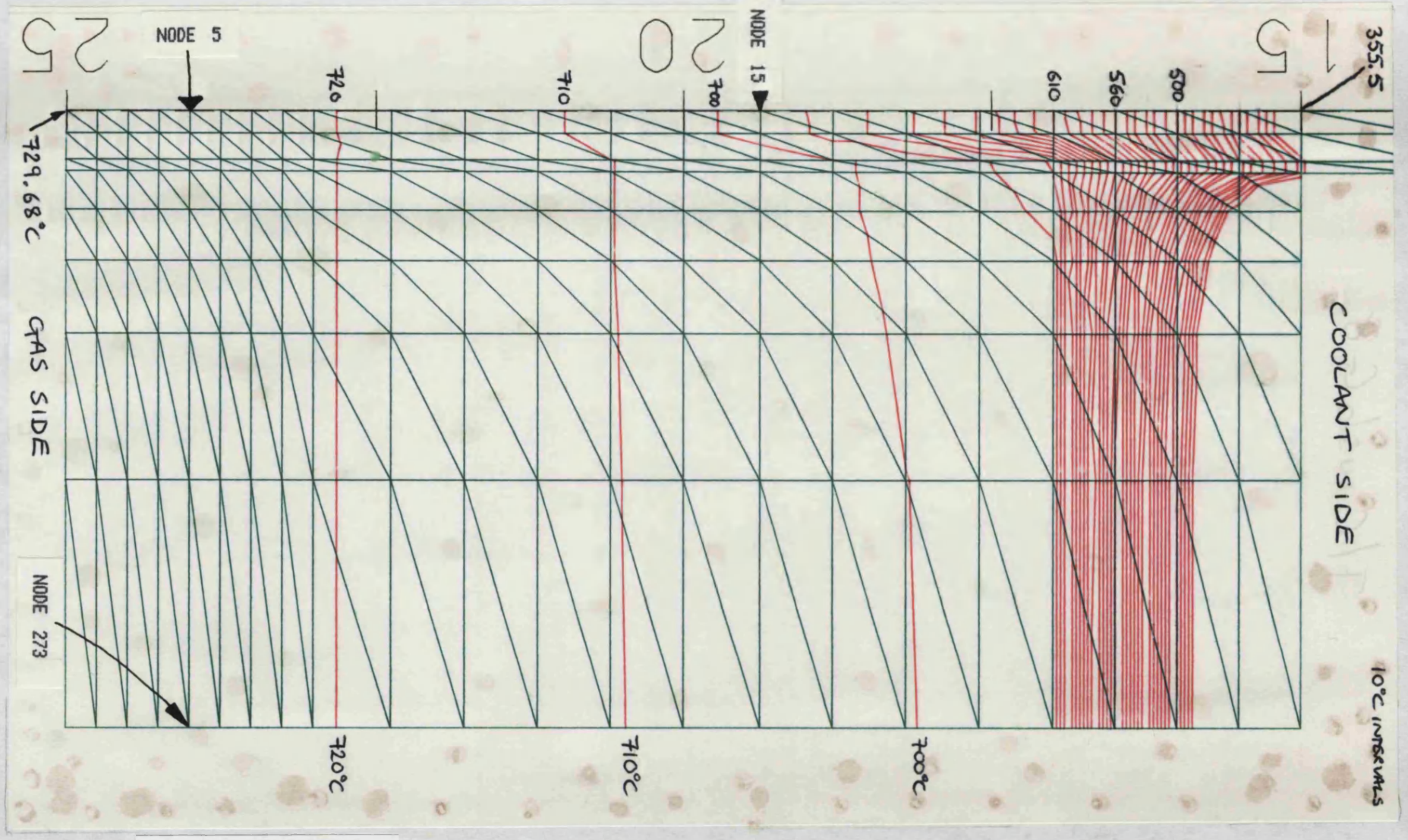

Figure 6.5 – COOLANT SIDE INSULATED / BC4

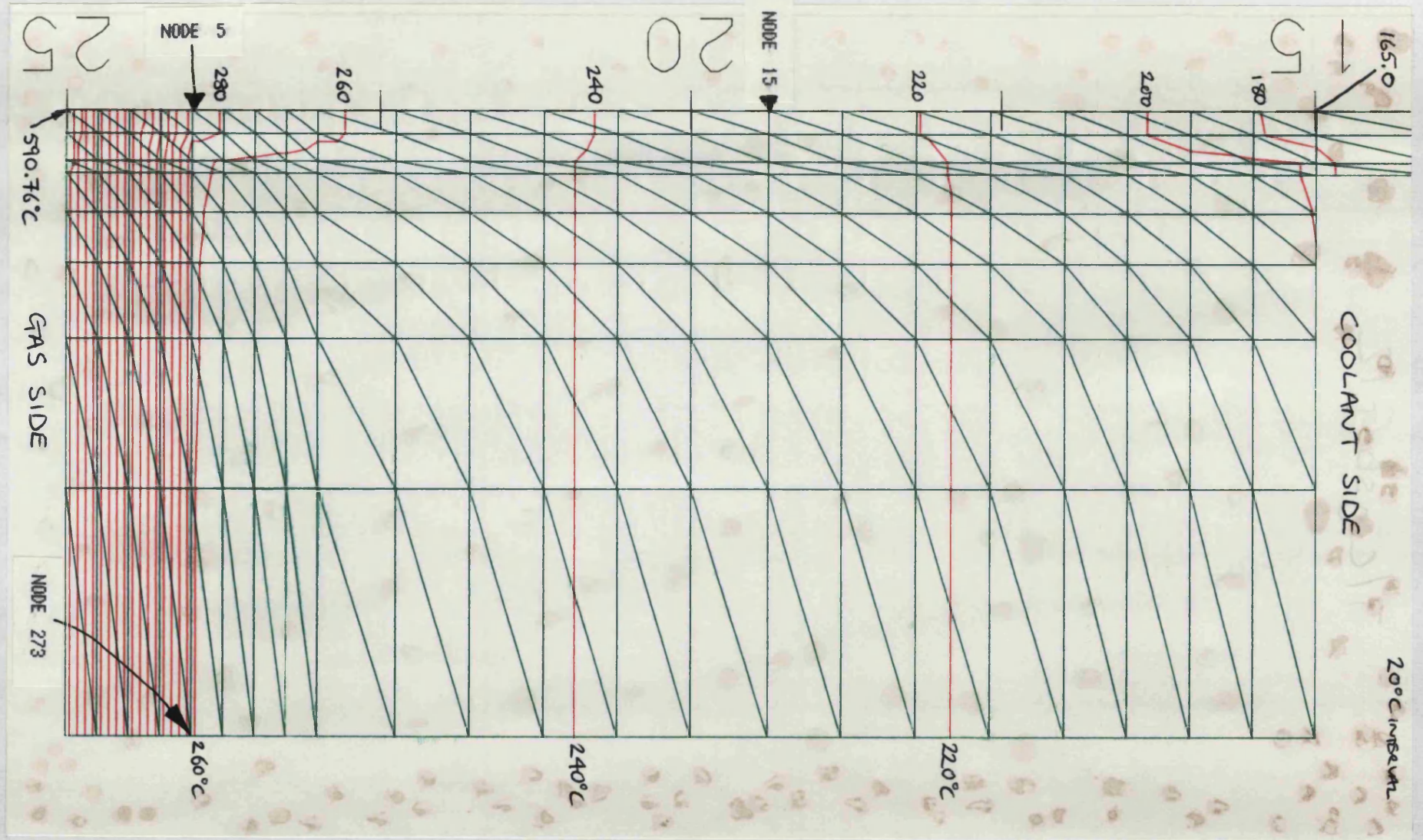

Figure 6.6 — GAS SIDE INSULATION / BC4

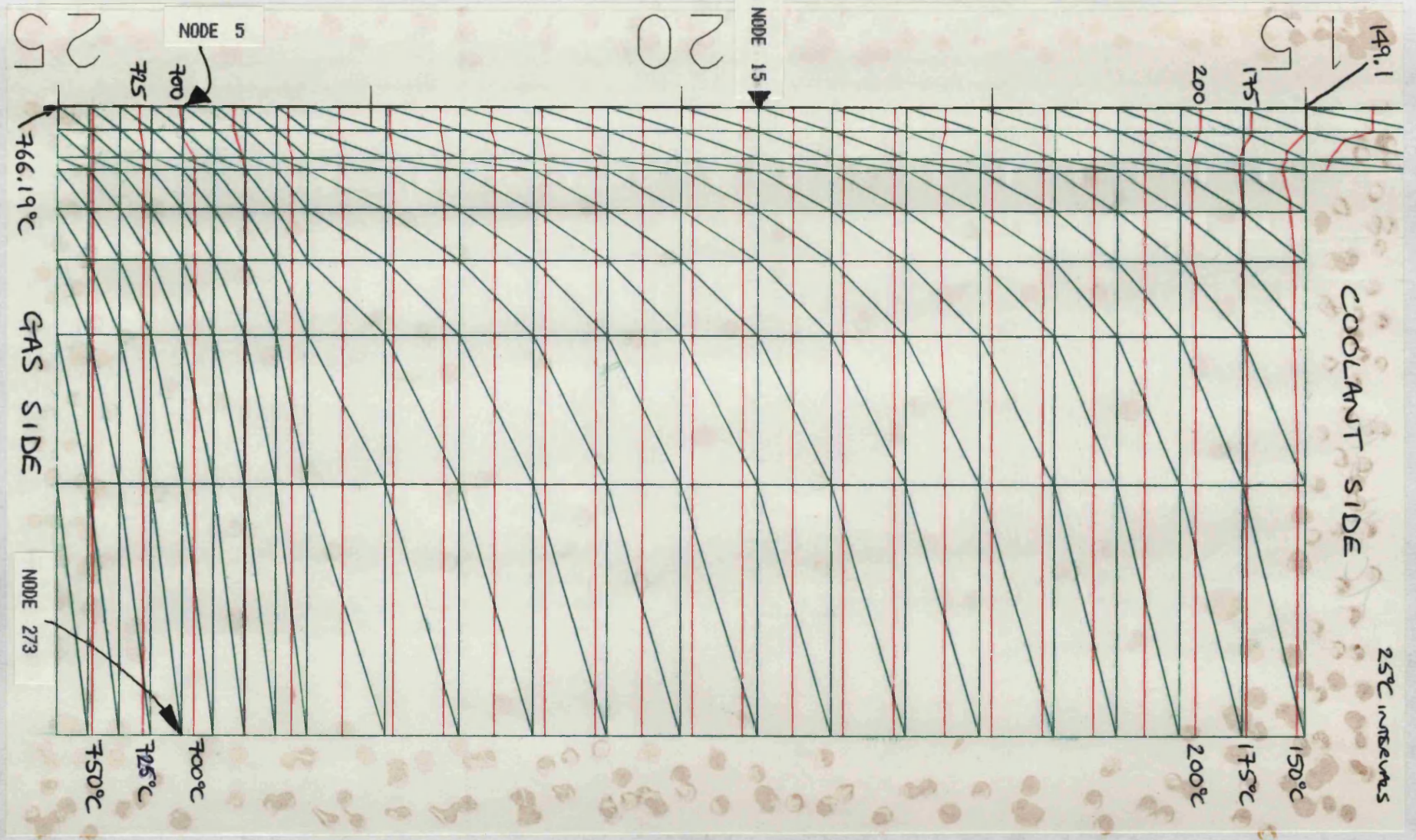

Figure 6.7 – SOLID CERAMIC WALL/BC4

Table 6.1 – Summary of Thermocouple in Liner Wall Analyses

	Boundary Condition Number	Finite Element Nodal Temperatures		Temp. Diff. $\Delta T_{5 \to 15}$ Node 5 to 15	Calculated Flux from Nodal Temperatures	Calculated Flux without T/C present in wall	Node 5 Temperature without T/C present	Node 273 Temperature with T/C present		Error in measurement of heat flux due to presence of T/C
		Node 5 Temp.	Node 15 Temp.							
Standard case uninsulated	BC1	217.37	213.41	3.96	43 045	35 870	219.93	217.18		+20%
	BC2	104.39	98.55	5.84	63 480	58 929	104.17	104.09		+7.7%
	BC3	778.50	759.50	19.00	206 530	170 642	783.29	777.61		+21%
	BC4	363.51	313.73	49.78	541 109	502 703	361.57	360.95		+7.6%
Coolant side insulated	BC1	256.22	252.17	4.05	44 024	27 454	262.18	258.08		+60.4%
	BC2	194.34	188.66	5.68	61 742	39 192	203.26	194.14		+57.5%
	BC3	848.38	831.43	16.95	184 247	112 455	857.18	847.79		+63.8%
	BC4	726.19	696.23	29.96	325 665	199 144	747.09	725.13		+63.5%
Plasma spray insulation on gas (hot) side	BC1	205.34	199.44	5.90	64 133	32 417	205.49	202.82		+97.8%
	BC2	102.86	94.34	8.52	92 612	50 152	99.09	99.00		+84.7%
	BC3	678.72	652.22	26.50	288 055	144 635	674.57	667.39		+99.2%
	BC4	285.34	229.53	55.81	606 655	328 622	260.60	260.10		+84.6%
Solid ceramic insulation	BC1	254.41	213.67	40.74	26 571	26 764	257.26	255.63		−0.72%
	BC2	196.70	140.42	56.28	36 706	37 801	198.40	198.39		−2.9%
	BC3	820.60	654.68	165.92	108 213	108 392	828.38	825.57		−0.17%
	BC4	695.97	417.90	278.07	181 357	186 747	704.32	704.32		−2.9%

Mesh and Boundary Condition Details for Analysis of Thermal Shock Specimen

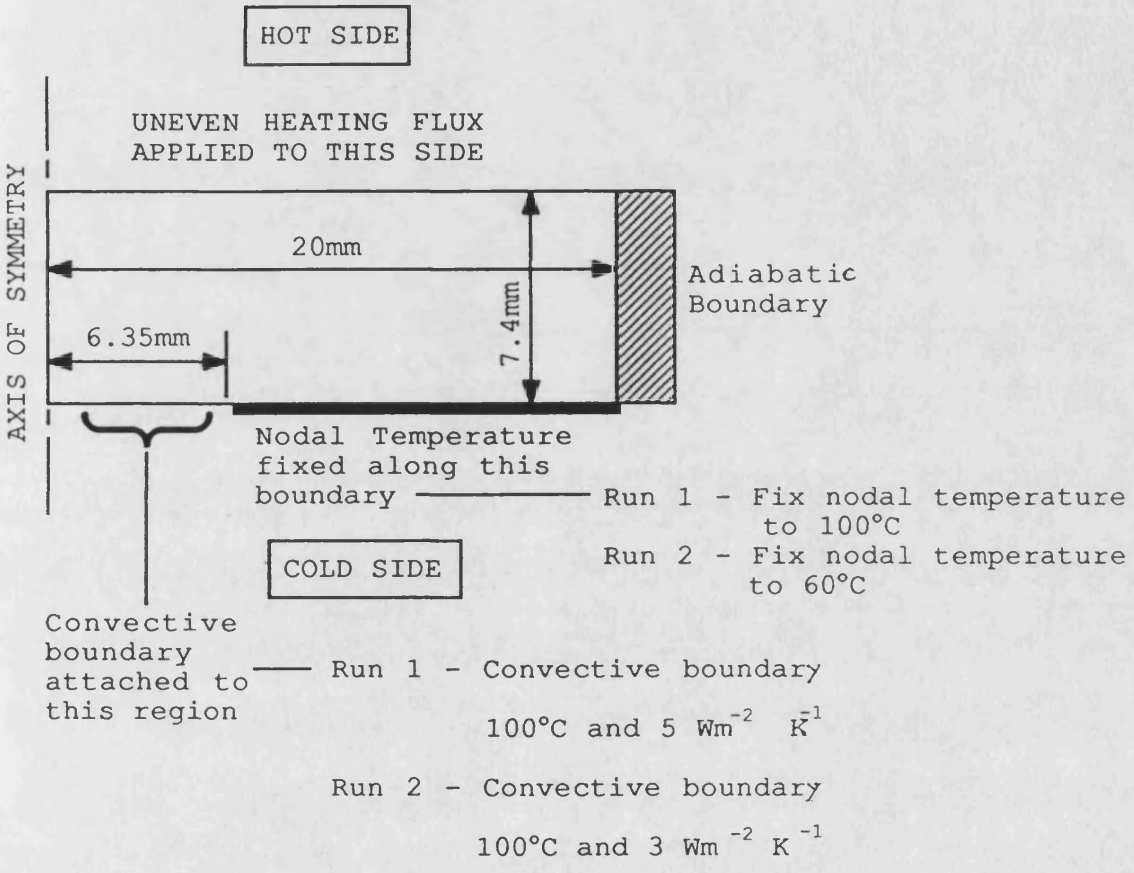

Figure 6.8

Imposed Flux at Specimen Plane vs. Radial Position used for F.E. Analyses

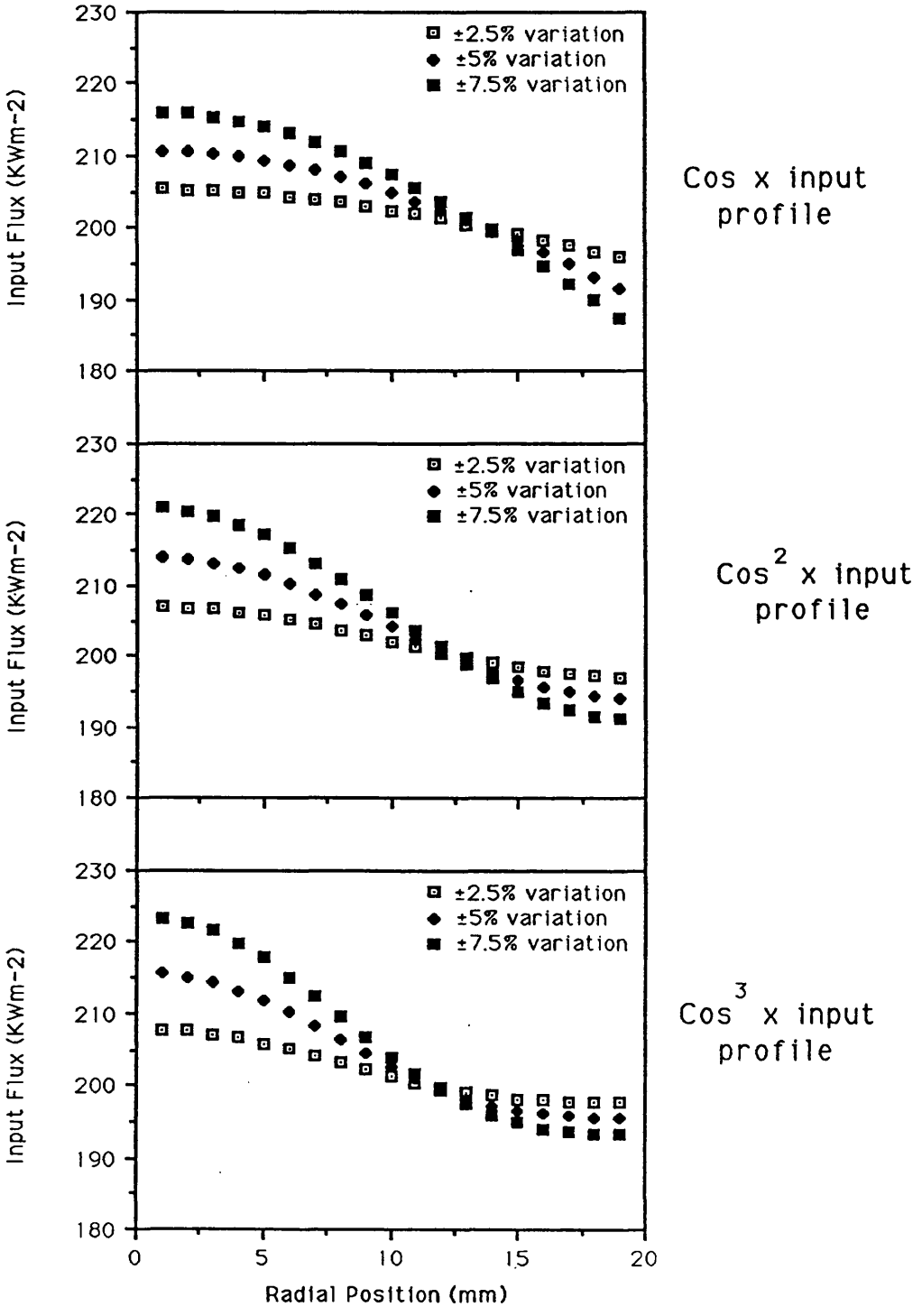

Figure 6.9

Specimen Surface Temperature Plots Calculated Using F.E. Analysis with Three Different Flux Input Profiles, and showing the Effect of Three Levels of Flux Variation across the Specimen Front Face

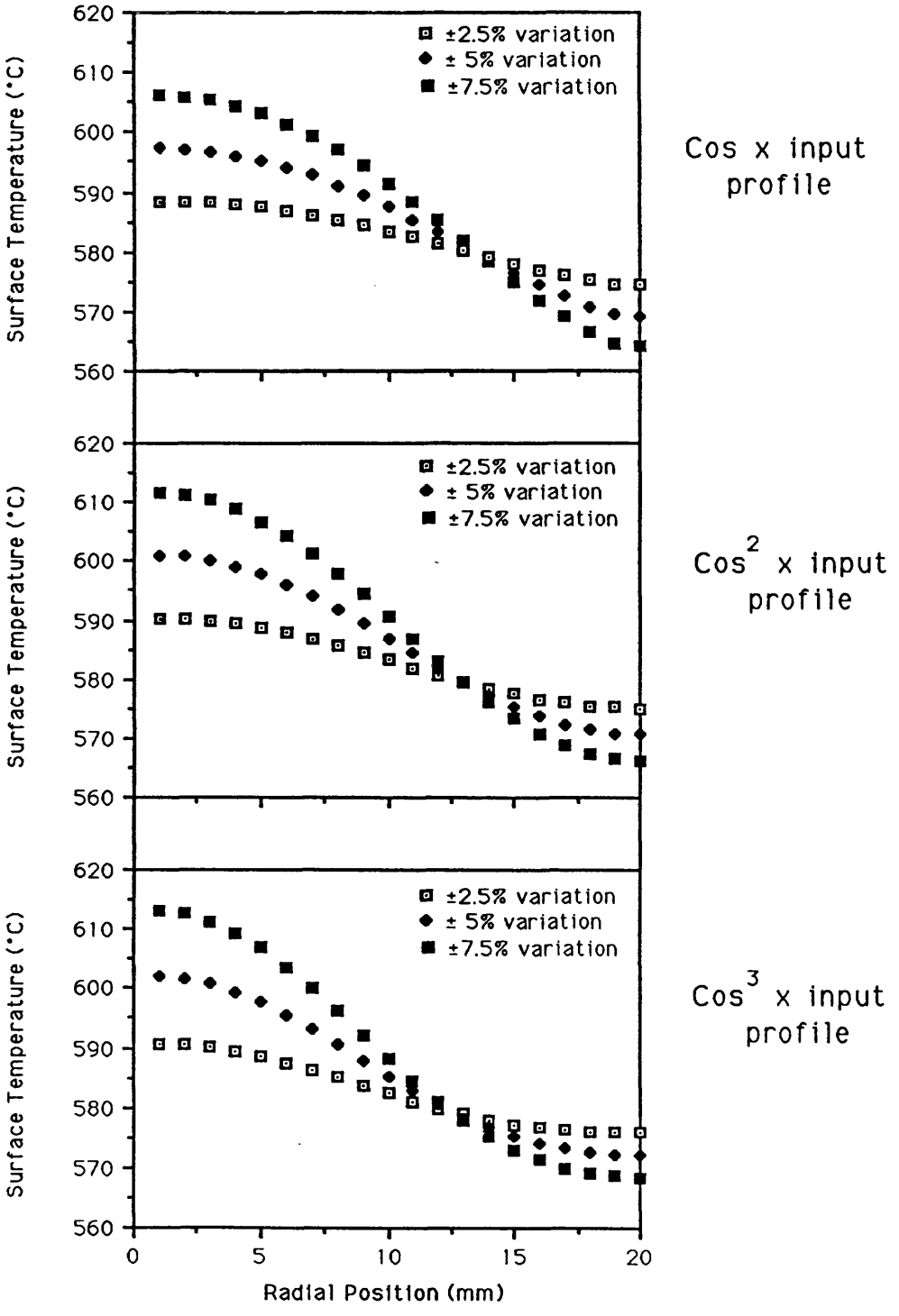

Figure 6.10

Results from F.E. Analyses of Ceramic Thermal Shock Test Specimen with Different Mean Flux Levels Imposed

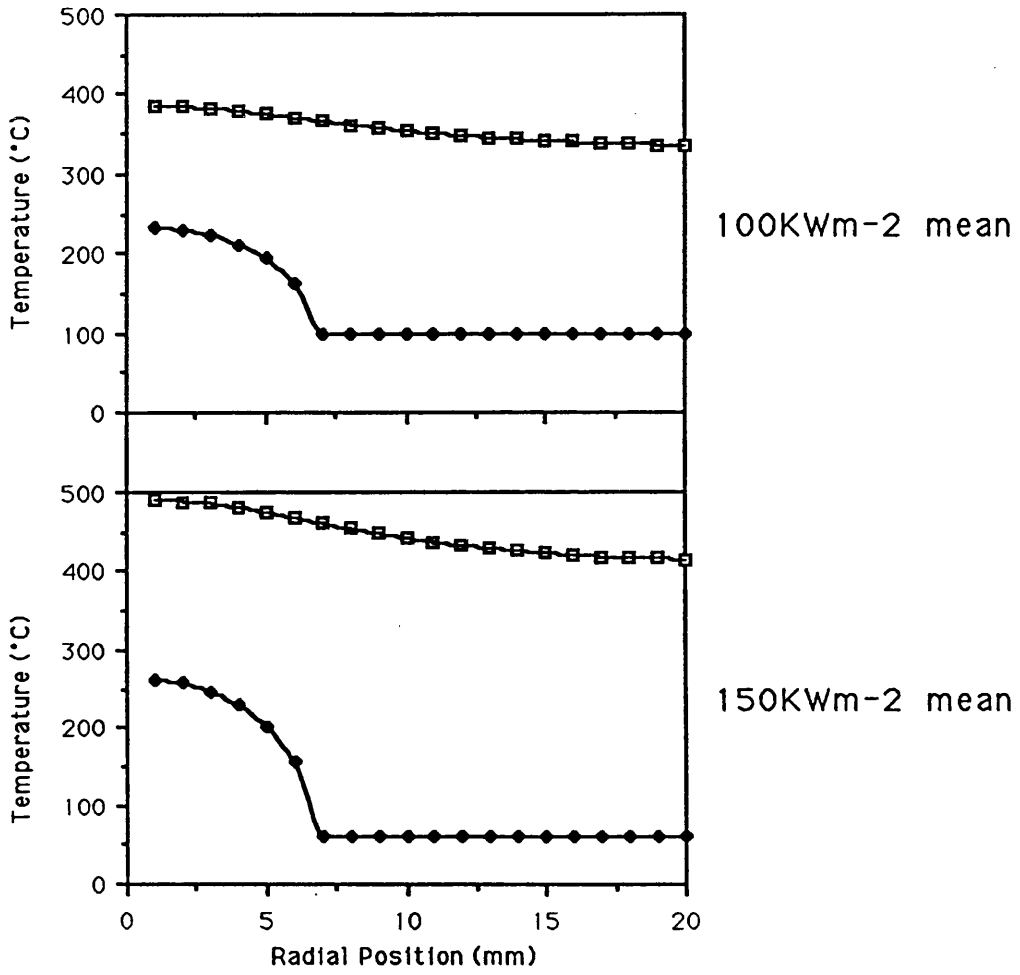

The above plots show the outputs from F.E. analyses of the thermal shock rig test specimen under different front and rear boundary conditions. For the case of both the upper and lower graphs the front face flux follows a cosine profile. The back face boundary condition for the top case is an isothermal surface at 100°C and with a central region of convective transfer T = 100°C and h = 5Wm-2K-1. The back face condition for the lower case is an isothermal surface at 60°C and a central region with T = 100°C and h = 3Wm-2K-1 . The specimen dimensions are :-

diameter = 40.0mm
thickness = 7.40mm
conductivity = 3Wm-1K-1

Figure 6.11

F.E. Thermal Analysis of Thermal Shock Specimen

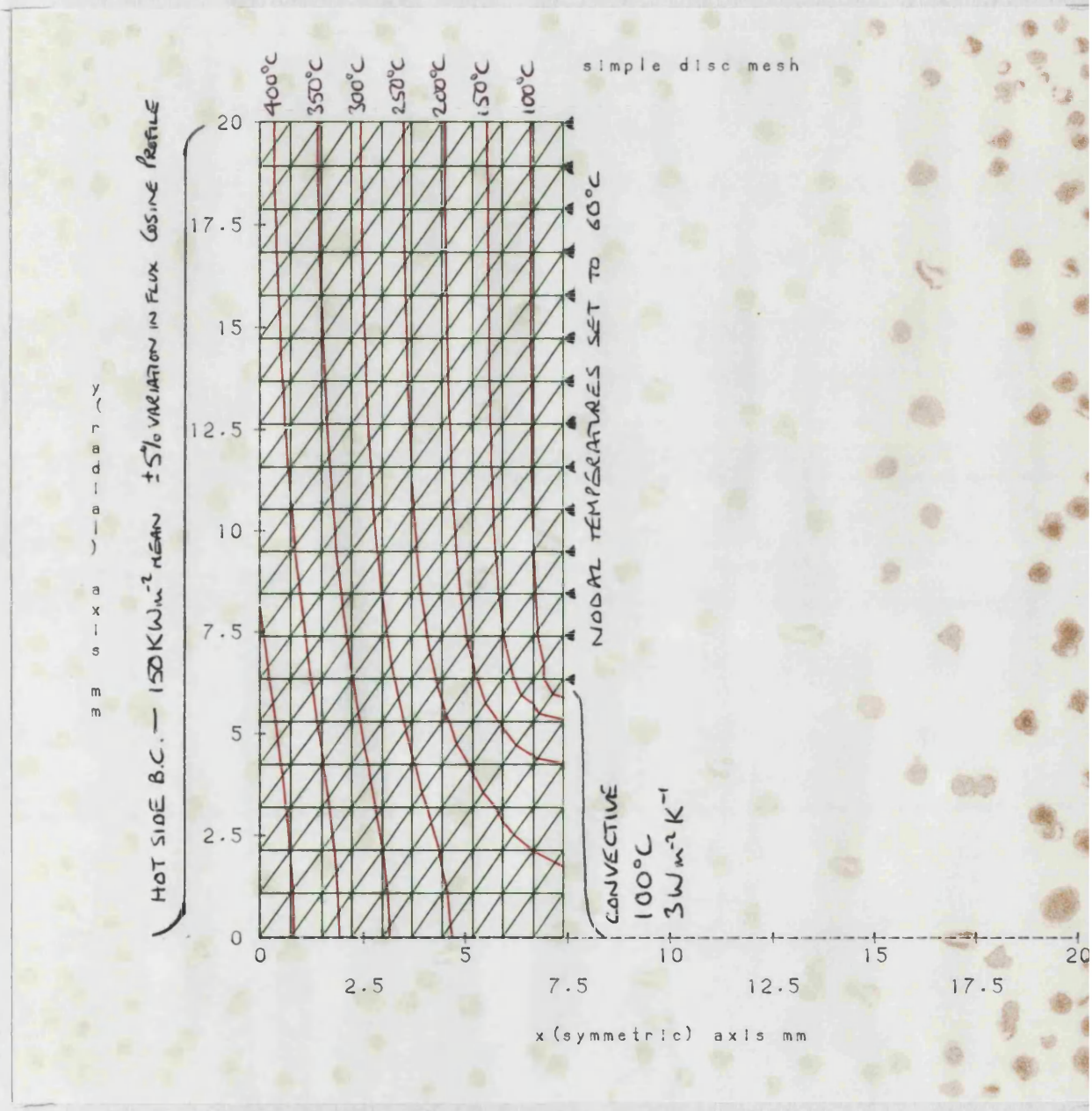

Figure 6.12

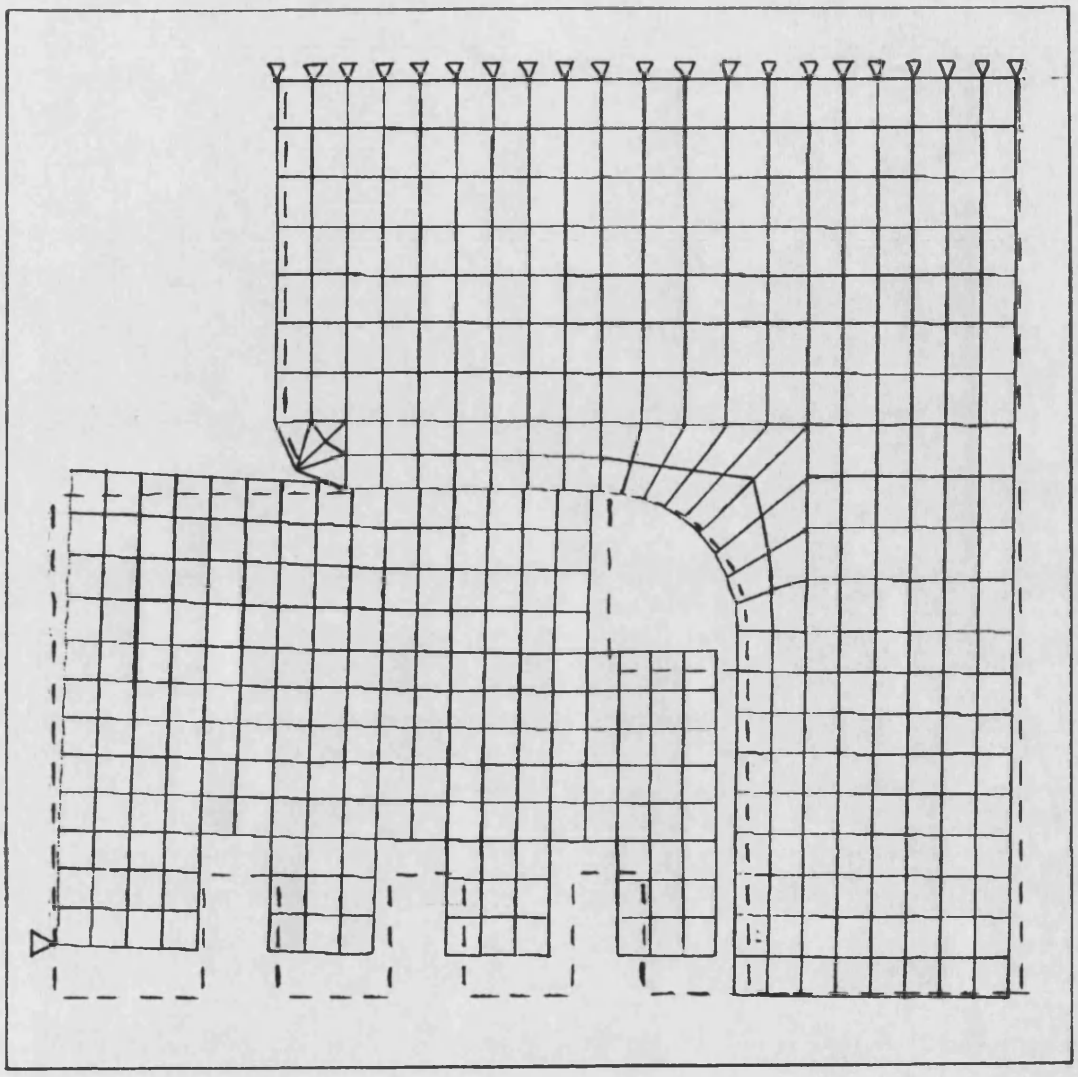

Pinning Points shown thus Δ

Shrink Fit Analysis for 390□C
drop from zero stress fit

Figure 6.13 - Thermal Displacement Plot from Shrink Fit Analysis - Single axial pin

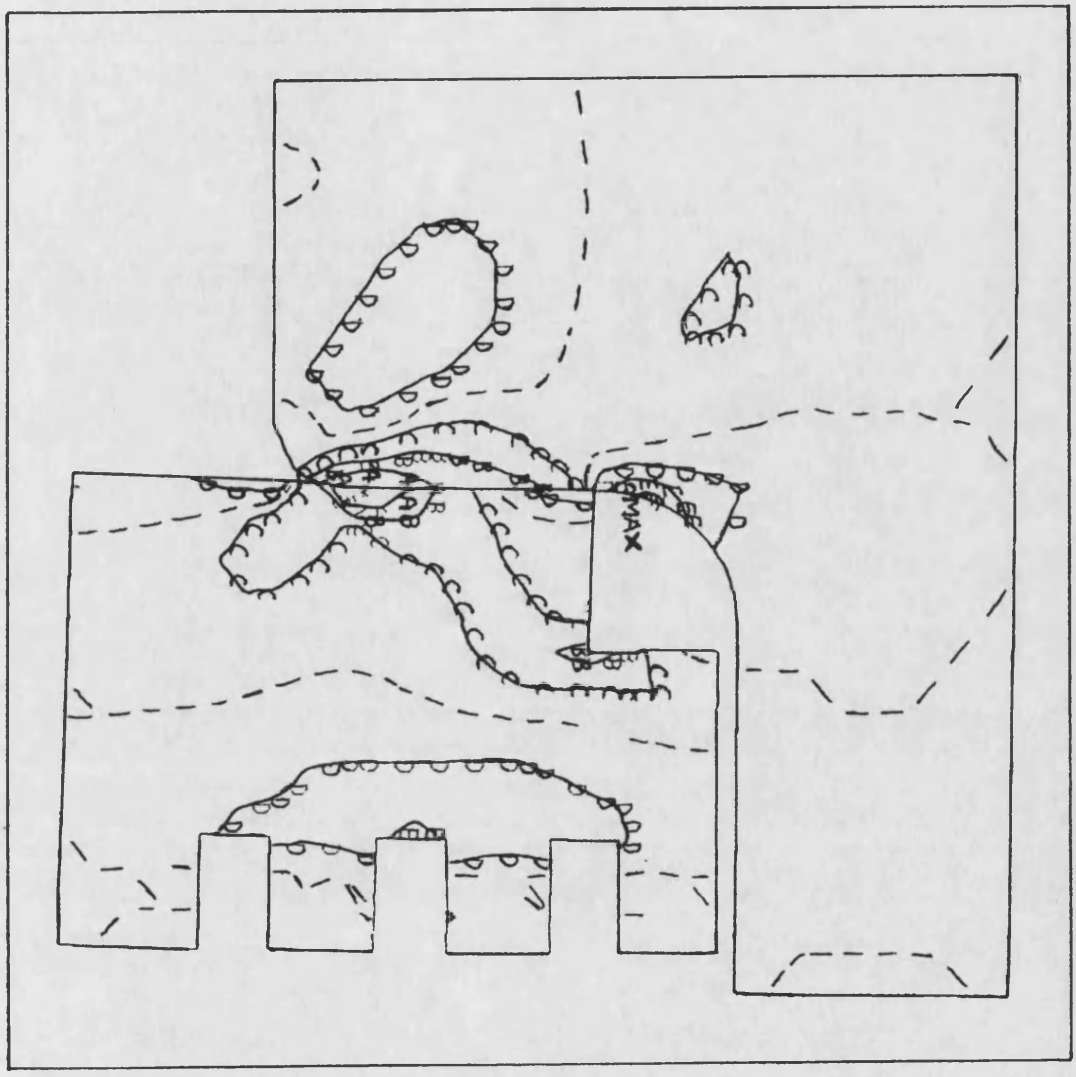

Figure 6.14 - **Thermal Stress Plot from Shrink Fit Analysis - Single axial pin**

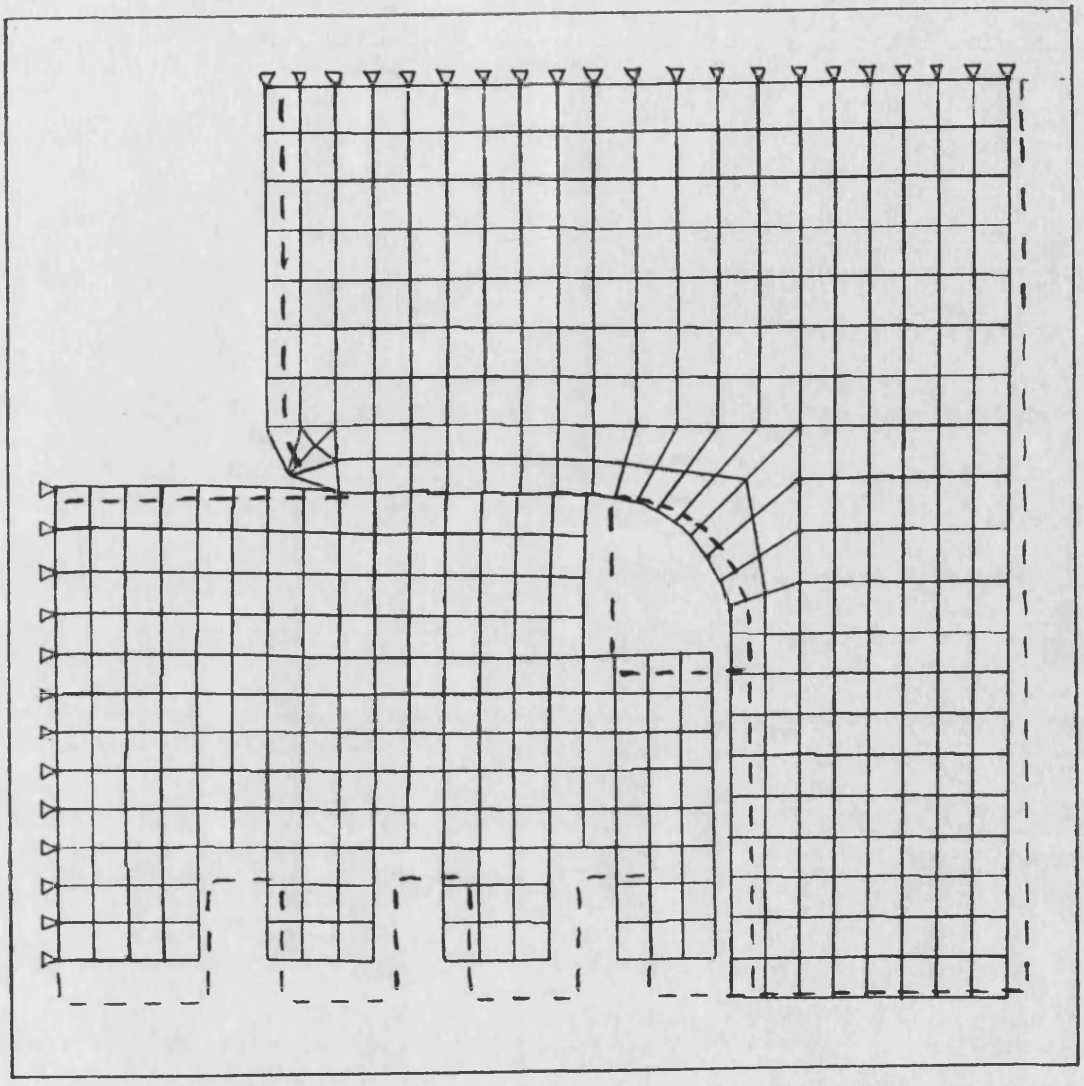

Pinning Points shown thus Δ

Shrink Fit Analysis for 390□C
drop from zero stress fit

Figure 6.15 - Thermal Displacement Plot from Shrink Fit Analysis - Multiple axial pinning

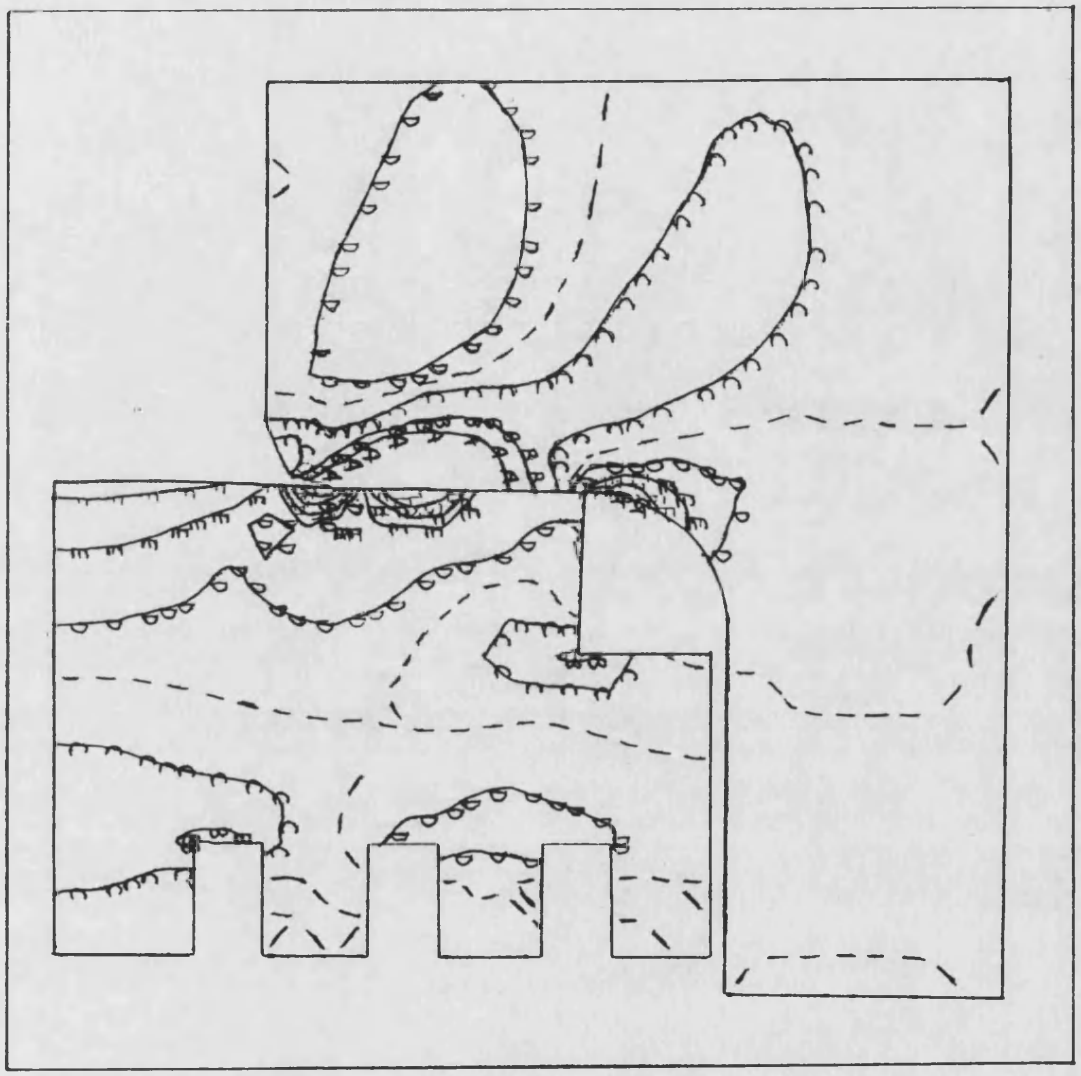

Figure 6.16 - **Thermal Stress Plot from Shrink Fit Analysis - Multiple axial pinning**

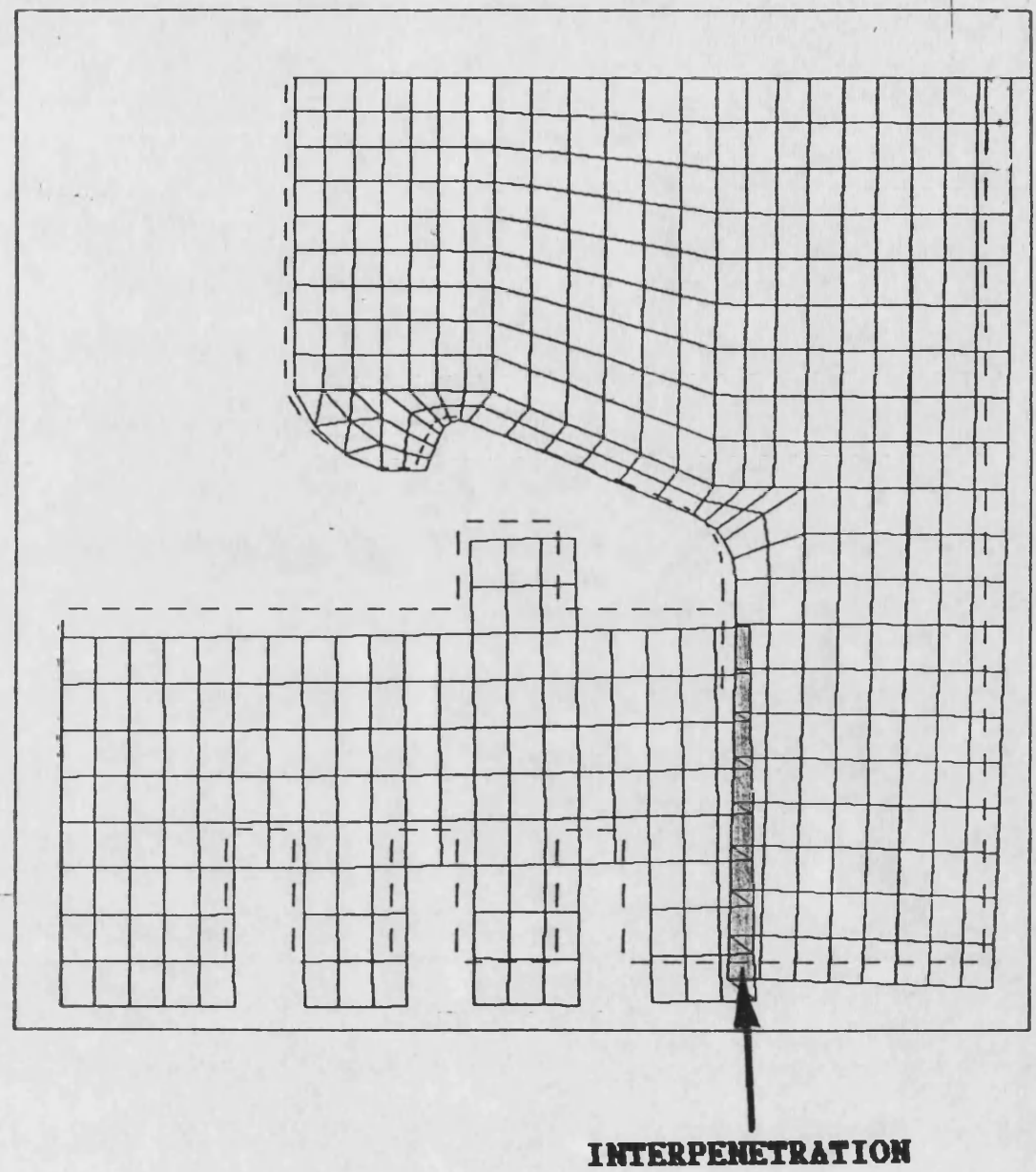

Figure 6.17 - Thermal Displacement Plot showing Mesh Interpenetration

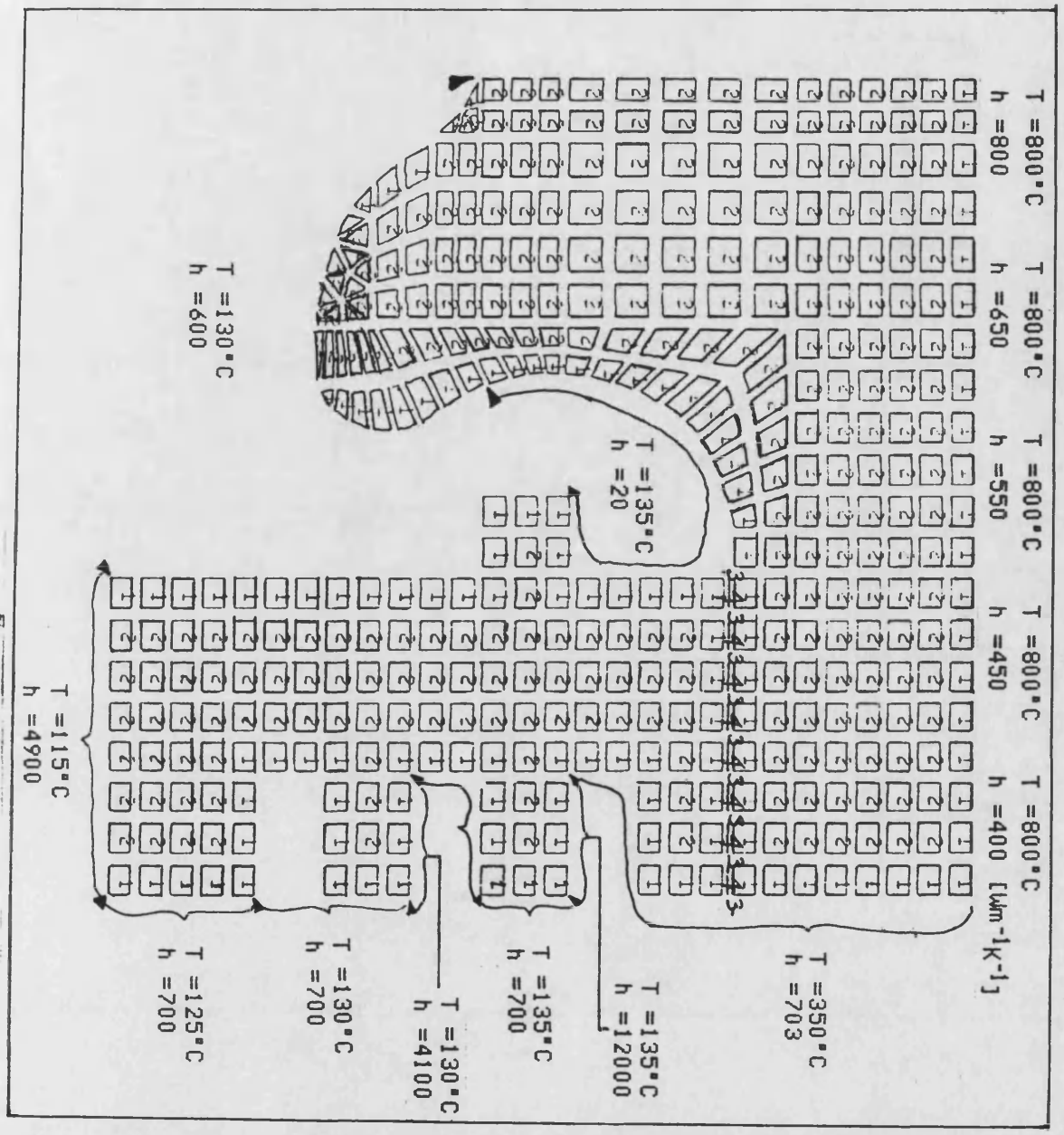

Figure 6.18 - Petter Crown Analysis
Thermal Boundary Conditions

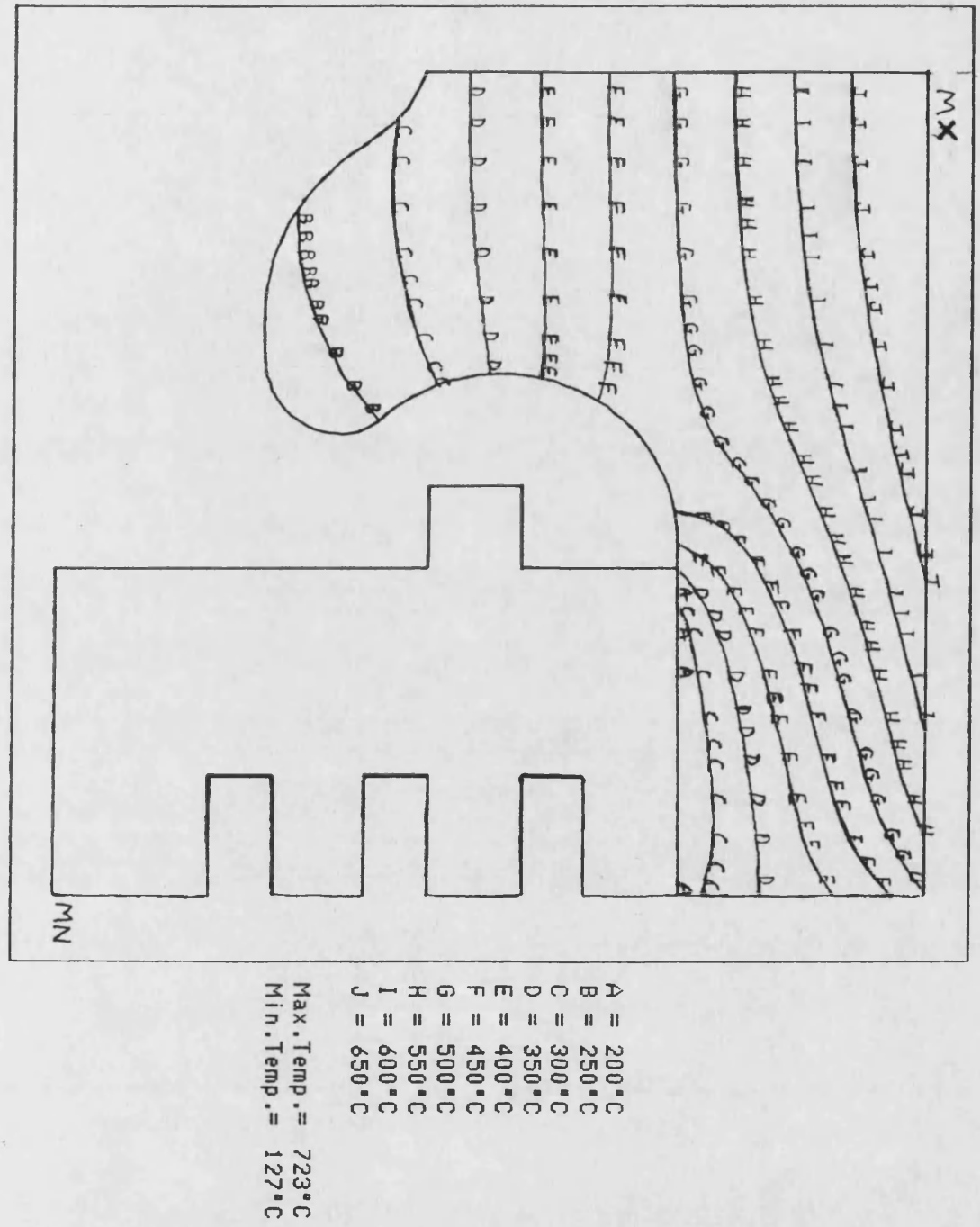

Figure 6.19 - Petter Crown Analysis
Temperature Distribution

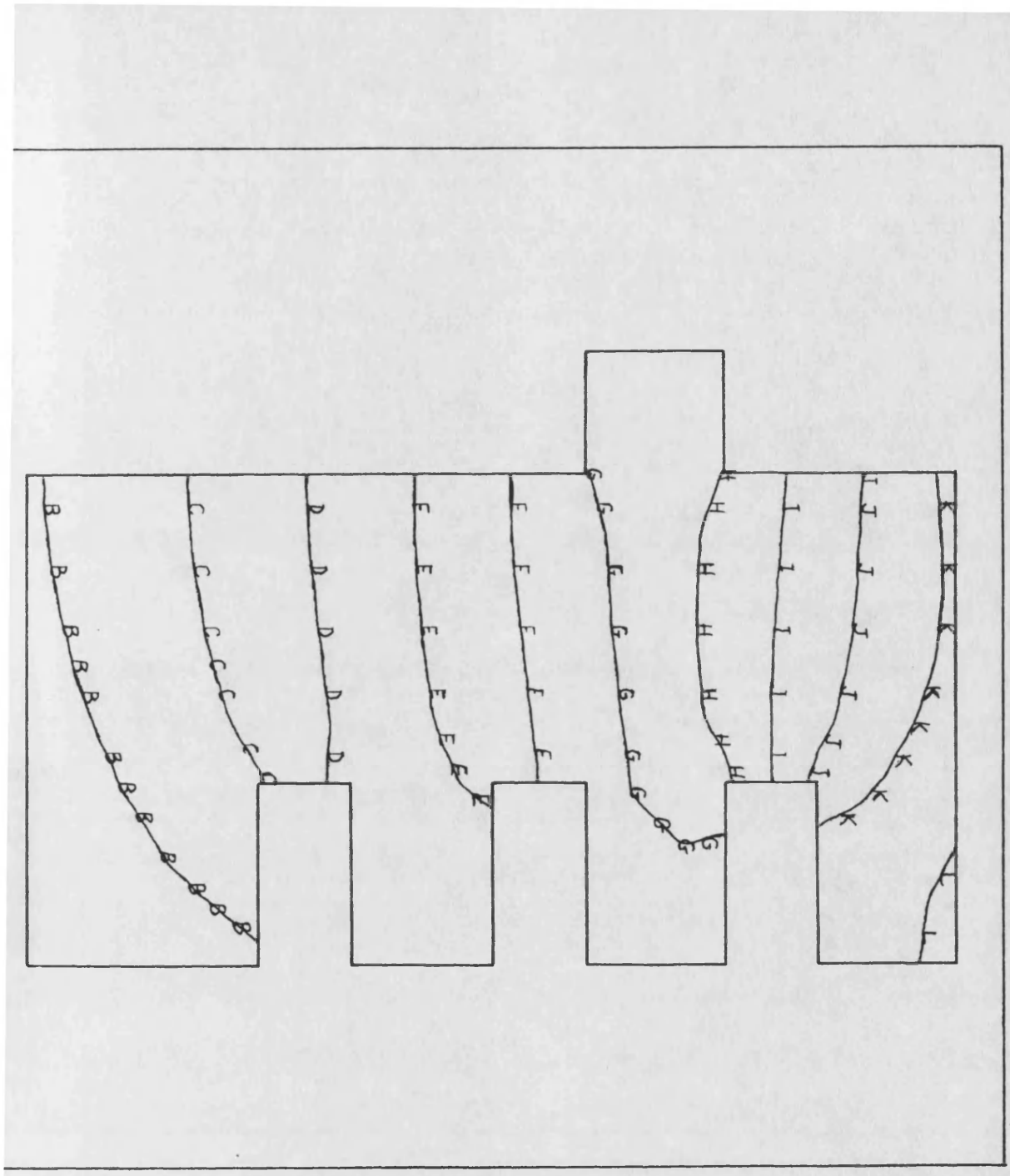

Figure 6.20 - Petter Crown Analysis
Temperature Distribution
around Ring Belt

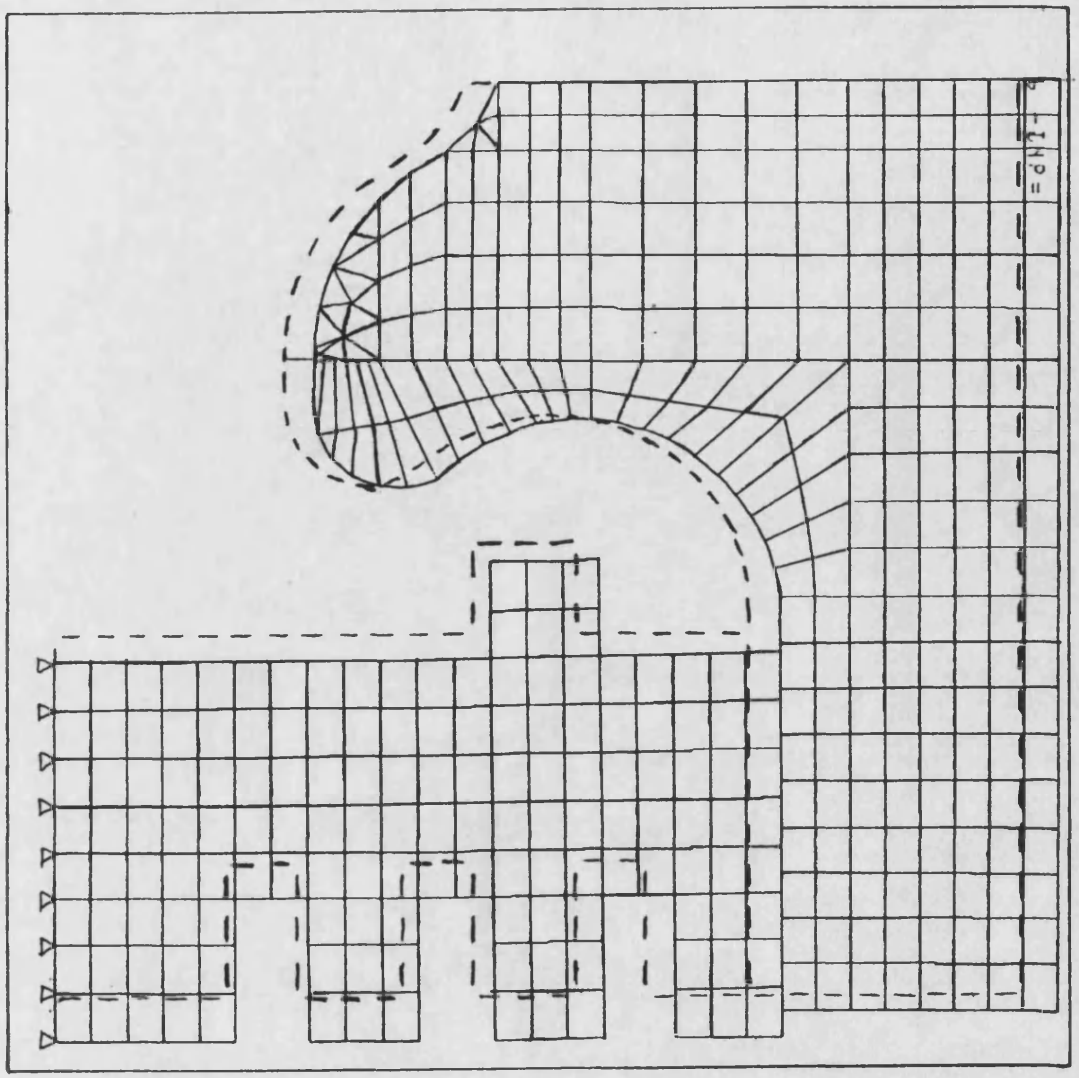

Figure 6.21 - Petter Crown Analysis
Thermal Displacement

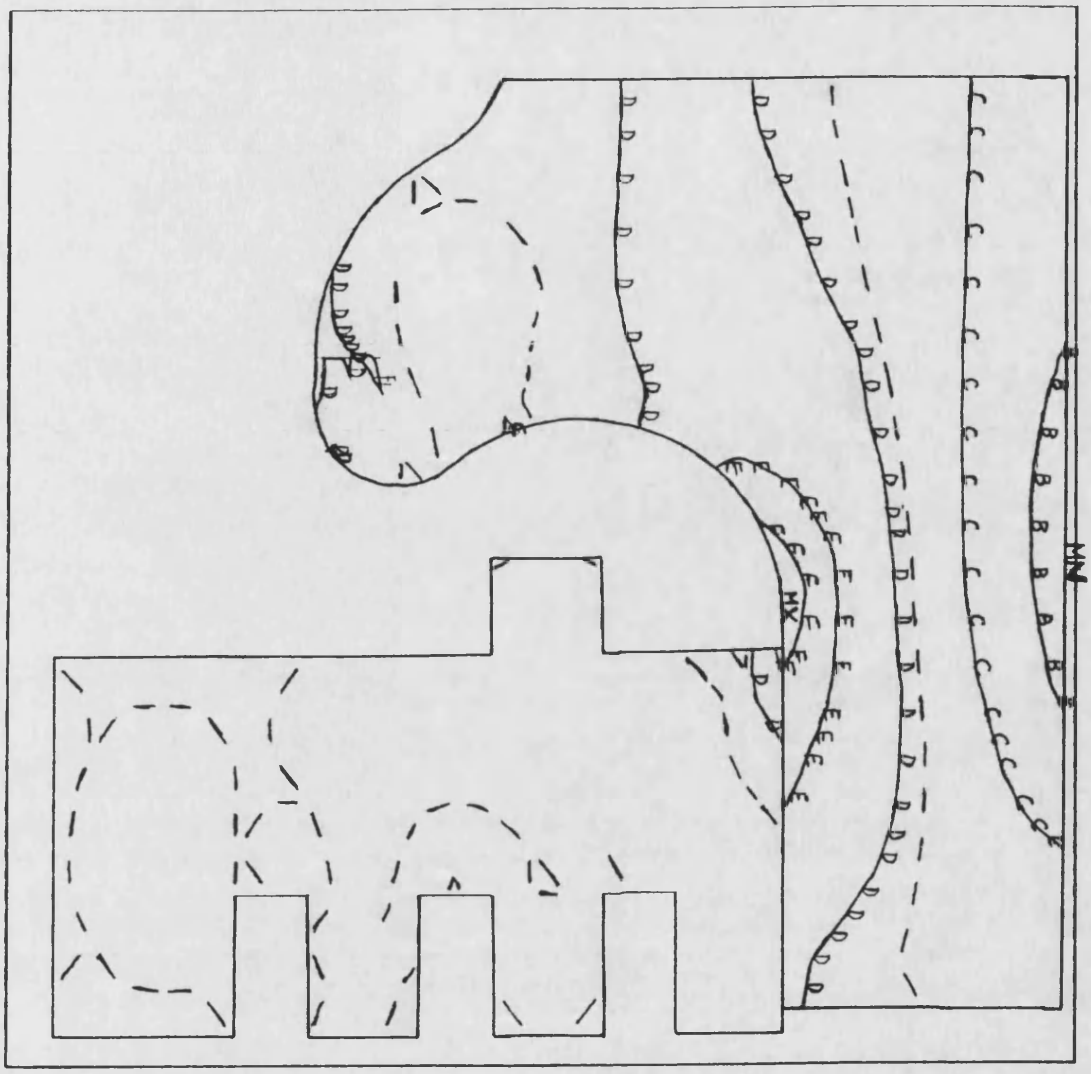

Figure 6.22 - Petter Crown Analysis
Radial Stress Distribution

Axial Stress σ_y

B = -90 MPa
C = -50 MPa
D = -10 MPa
E = +30 MPa

Max. Stress +51 MPa
Min. Stress -118 MPa

Figure 6.23 - Retter Crom Analysis
Axial Stress Distribution

Hoop Stress σ_z

A = -60 MPa
B = -20 MPa
C = +20 MPa
D = +60 MPa
E = +100 MPa

Max. Stress +135 MPa
Min. Stress -66 MPa

Figure 6.24 - Petter Crown Analysis
Hoop Stress Distribution

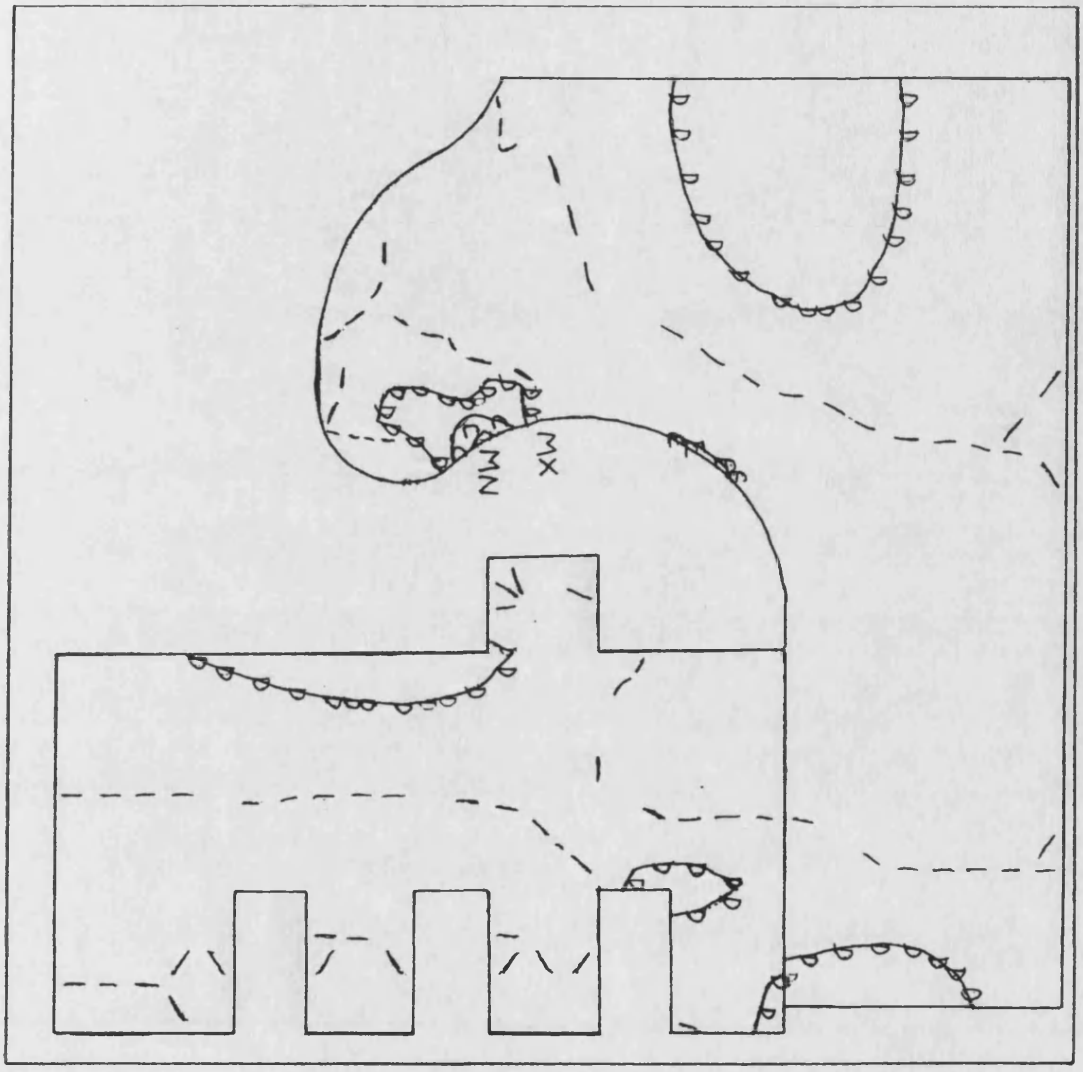

Figure 6.25 - Petter Crown Analysis
Axial Stress Distribution
with Insulating Layer present

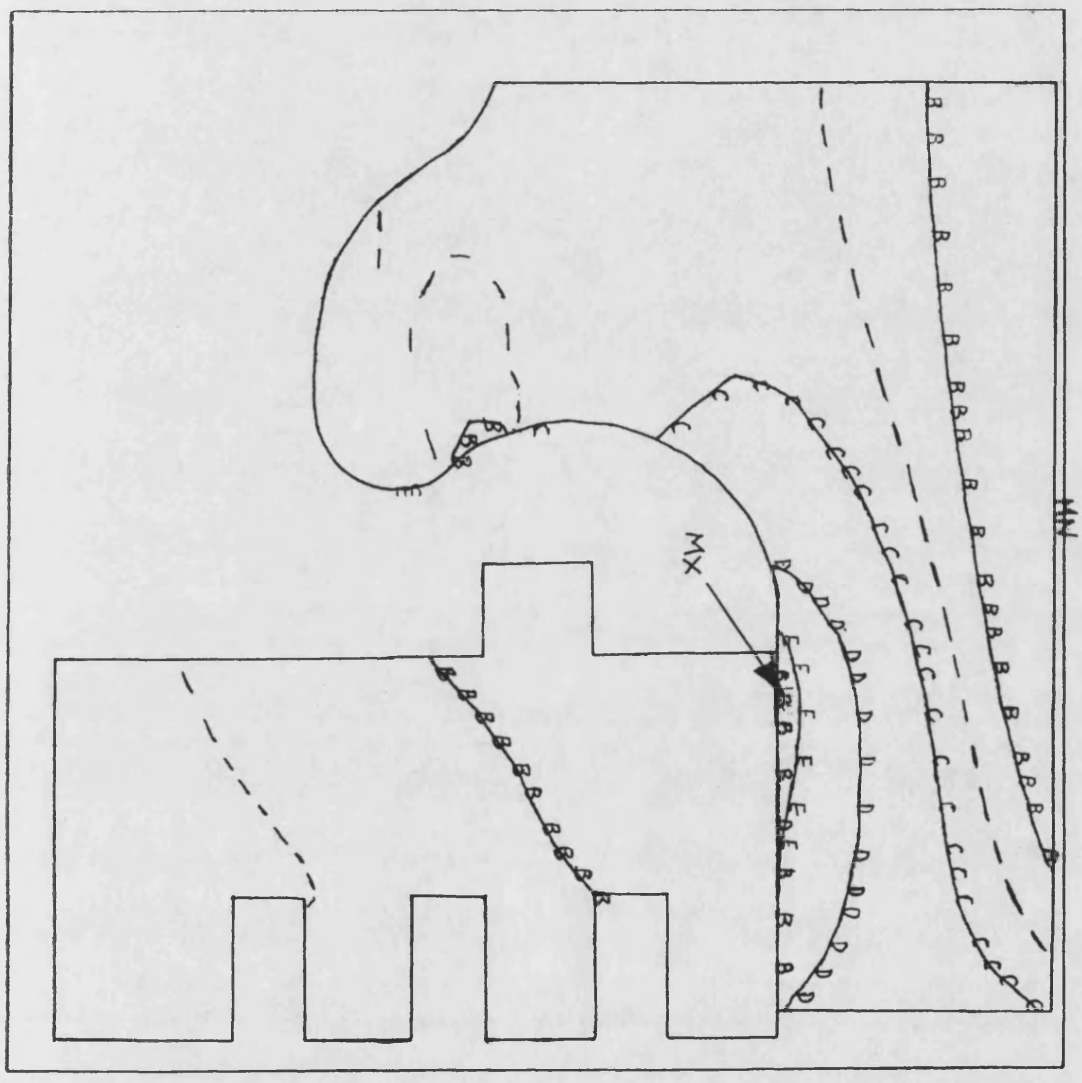

Figure 6.26 - **Petter Crown Analysis**
Hoop Stress Distribution
with Insulating Layer present

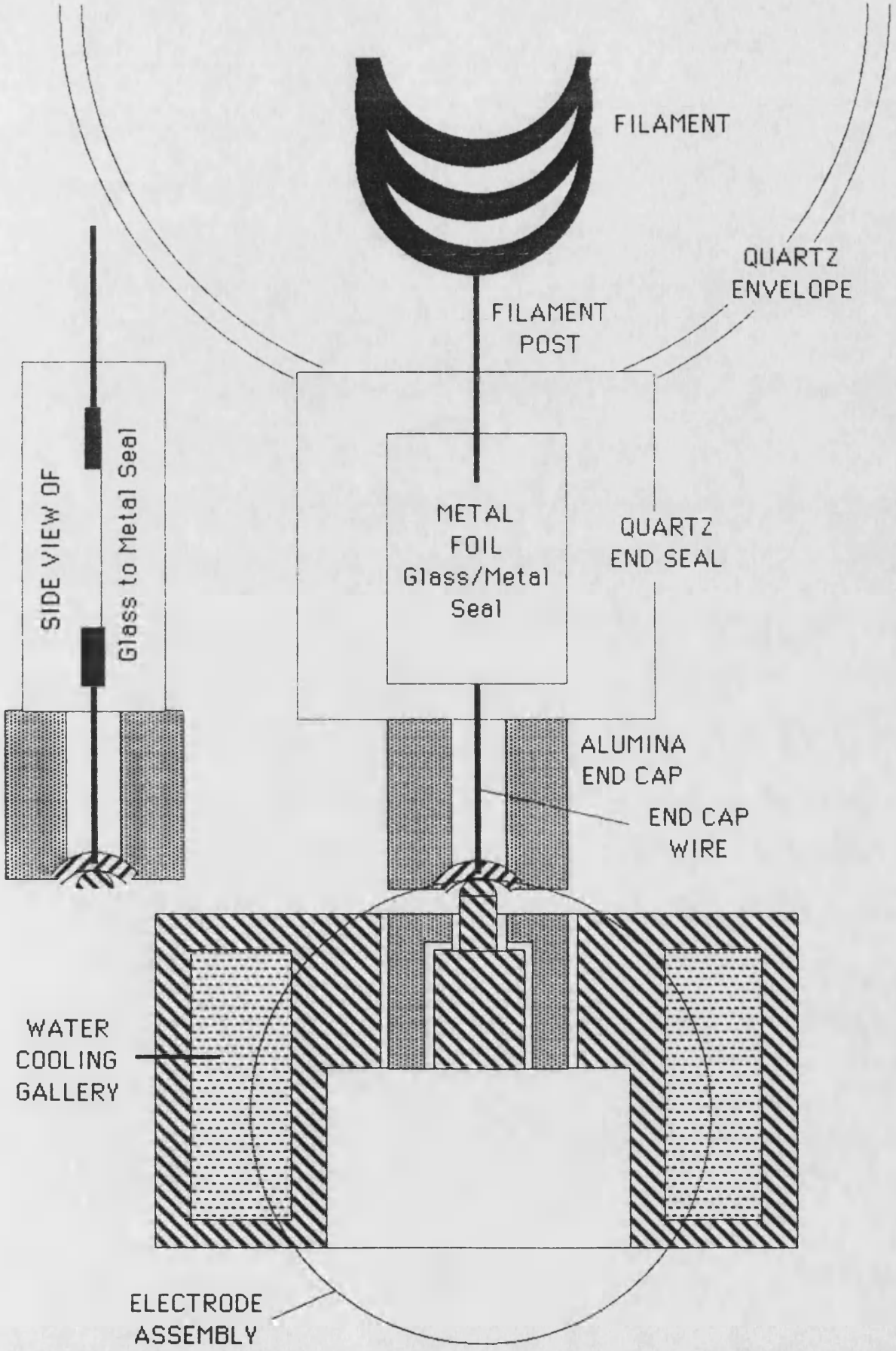

Figure 6.27 - Quartz-Halogen Lamp Geometry

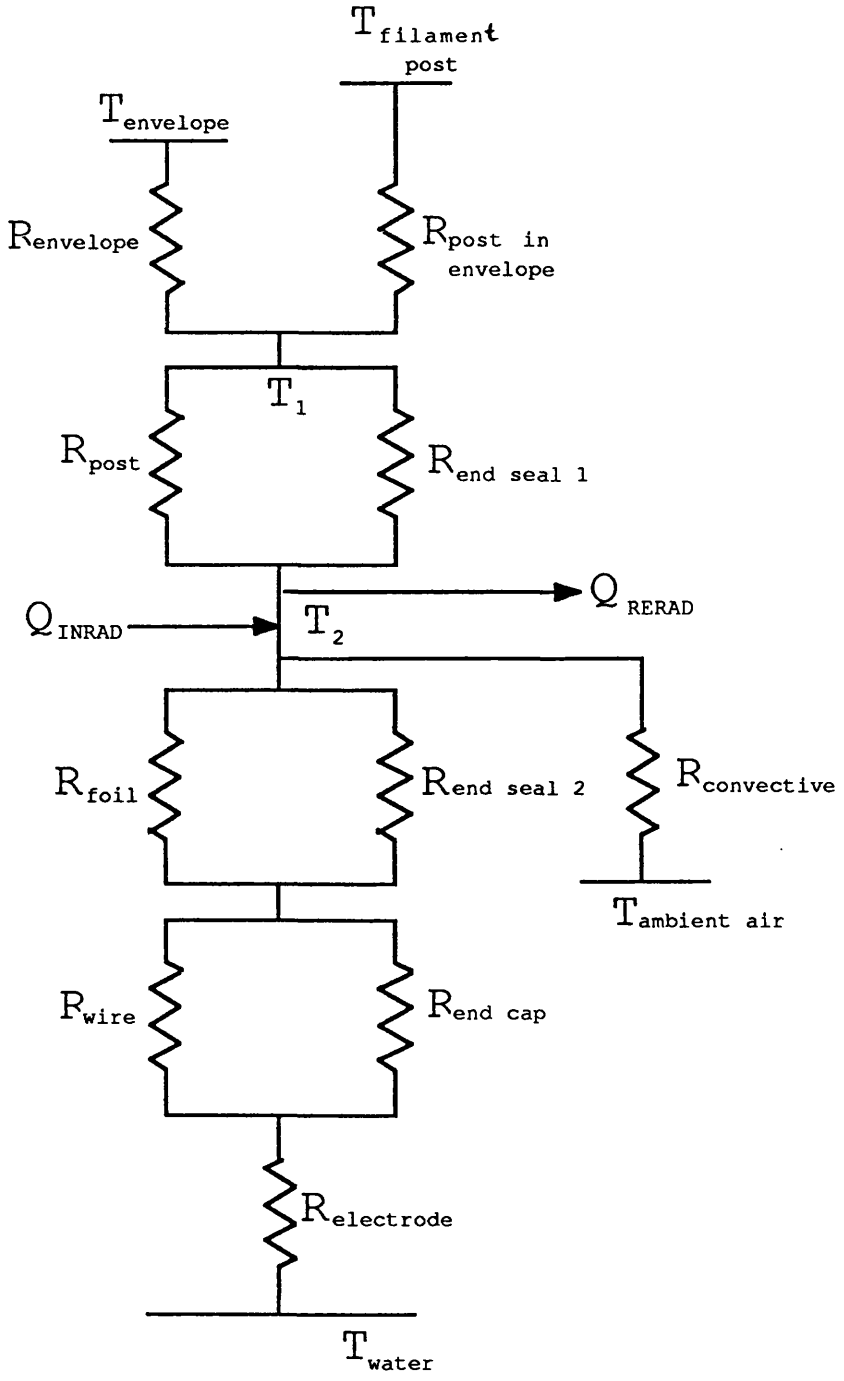

Figure 6.28 - Lamp Resistance Model

The resistance shown in Figure 6.28 may be broken down into several sections as shown below : -

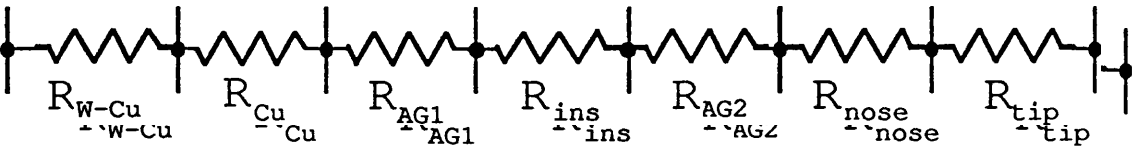

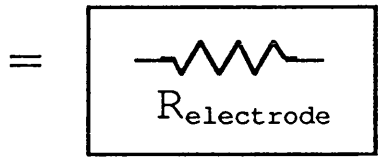

R_{W-Cu} is the resistance from the copper block to the water in the cooling gallery

R_{Cu} is the resistance of the conduction path from the electrode assembly to the water gallery

R_{AG1} is the resistance of the gap between the insulator and the copper block

R_{ins} is the resistance of the electrical insulating section which surrounds the actual electrode and electrically isolates it from the water cooled copper block

R_{AG2} is the resistance of the gap between the insulator and the electrode

R_{nose} is the resistance of the electrode itself, not including the contact resistance

R_{tip} is the estimated contact resistance between the nose tip of the electrode and the lamp end cap electrode.

The estimated values for each of the resistances are as follows : -

$$R_{W-Cu} = \frac{1}{2000 \times 5.66 \times 10^{-4}} = 0.884 \ [°CW^{-1}]$$

$$R_{Cu} = \frac{2 \times 10^{-3}}{385 \times 9.02 \times 10^{-4}} = 0.058$$

$$R_{AG1} = \frac{0.185 \times 10^{-3}}{0.03 \times 9.02 \times 10^{-4}} = 6.837$$

$$R_{ins} = \frac{3.78 \times 10^{-3}}{1.25 \times 6 \times 10^{-4}} = 5.04$$

Figure 6.29a - Electrode Resistance Breakdown

$$R_{AG2} = \frac{0.127 \times 10^{-3}}{0.03 \times 3.13 \times 10^{-4}} = 13.53$$

$$R_{nose} = \frac{15 \times 10^{-3}}{380 \times 7.92 \times 10^{-6}} = 4.98$$

$$R_{tip} = \frac{10^{-3}}{150 \times 1.77 \times 10^{-6}} = 3.77$$

The above values are only estimates of the thermal resistances, and rather crude approximations have been made in order to arrive at a solution in a short period of time. R_{nose} may indeed be out by a factor of two, while the degree of uncertainty in the value of R_{tip} is still higher.

It was noted that the air gap thermal resistances were rather high and that by the introduction of a more thermally conductive medium into the spaces, lower temperatures at the tip of the electrode would result.Further reductions in thermal resistance were also considered possible by : -

a). changing the insulator material to alumina (k = 25 $Wm^{-1}K^{-1}$) from the existing pyrophyllite (k = 1.25 $Wm^{-1}K^{-1}$)

b). remachining the nose of the electrode to increase the cross sectional area for heat transfer away from the tip region

c). introduction of heat transfer medium into the region around the tip of the electrode.

The effect which these changes have on the resistance values for this section are shown in the following table : -

	R_{W-Cu}	R_{Cu}	R_{AG1}	R_{ins}	R_{AG2}	R_{nose}	R_{tip}	R_{total}
Original	0.884	0.058	6.837	5.040	13.530	4.980	4	~ 35.3
Greased air gaps	0.884	0.058	0.075	5.040	0.181	4.980	3.5	~ 14.7
All mods included	0.884	0.058	0.075	0.399	0.181	0.500	2	~ 4.1

Figure 6.29b - Electrode Resistance Breakdown (contd.)

Table 6.2 - Listing of Program to Calculate the Lamp End Seal Temperature

```
REM this is  a program  to calculate  the end seal  temperature  in a high
REM intensity  quartz  halogen  lamp
REM the estimated  lamp envelope  temperature  Te
        Te = 750+273
REM the estimated  filament  temperature  at the internal  post
        Tf = 1500+273
REM the lamp envelope  resistance  R1
        R1 = 40
REM the filament  post resistance  within  the lamp  R2
        R2 = 170
REM the filament  post resistance  within  the end seal  first  section  R3
        R3 = 42.4
REM the resistance  of the first  section  of the end seal  R4
        R4 = 12
REM the absorbed  radiant  heat on the end seal  section  Qr
        Qr = 8.8
REM  the resistance  due to convective  losses  from the end seal  R5
REM this resistance  will depend  on whether  the fixed or free electrode  is
REM being considered,  free - 47 , fixed - 355
        R5 = 47
REM the ambient  temperature  for convective  heat loss calculations  Ta
REM this value  is dependent  on whether  the fixed or free electrode  end is
REM being considered,  free - 40 , fixed 150
        Ta = 40+273
REM the temperature  of the surrounds  for radiative  loss calculations  Ts
        Ts = 70+273
REM a combined  value for radiative  loss calculation  E
        E = 7.144E-11
REM the resistance  of the foil leadthrough  in the second  section  of the end
seal  R6
        R6 = 40
REM the resistance  of the second  section  of the end seal  R7
        R7 = 12
REM the resistance  of the wire leadthrough  R8
        R8 = 340
REM the resistance  of the ceramic  end cap  R9
        R9 = 7.7
```

```
REM the total resistance of the electrode assembly mating with the lamp R10
REM this is affected by whether or not the assembly is greased, or not,
REM ungreased - 35 , greased - 15
      R10 = 15
REM the temperature of the water in the reflector coolant galleries Tw
      Tw = 40+273
REM first calculate the coefficients of the quartic equation which describes
REM the model
      rx=R2*(R3+R4)
      ry=R1*(R3+R4)
      rz=R1*R2*R3*R4
      rt=ry+rx+rz
      X = ((Te*rx)+(Tf*ry))/(rx+ry+rz)
      Y = rz/rt
      rb=((R6*R7)/(R6+R7))+((R8*R9)/(R8+R9))+R10
REM the constant coefficient C
      C = Qr+X*((R3*R4)/(R3+R4))+(E*Ts^4)+Ta/R5+Tw/rb
REM the linear term in T2 - L
      L =((R3*R4)/(R3+R4))+(1/rb)+(1/R5)-(Y*(R3*R4)/(R3+R4))
REM the quartic term is simply E
REM the equation to be solved is E*T2^4 + L*T2 - C = 0 , a Newton-Raphson
REM iterative method is used to solve for T2
REM the derivative equation used is 4*E*T2^3 + L = 0
REM the first estimate for T21 will be Tf/2
      T21 = Tf/2
10    T2 = T21-((E*T21^4)+(L*T21)-C)/((4*E*T21^3)+L)
      IF (ABS(T21-T2)(.1)  GOTO 20
      T21=T2
      GOTO 10
20    PRINT T21-273,T2-273
      END
```

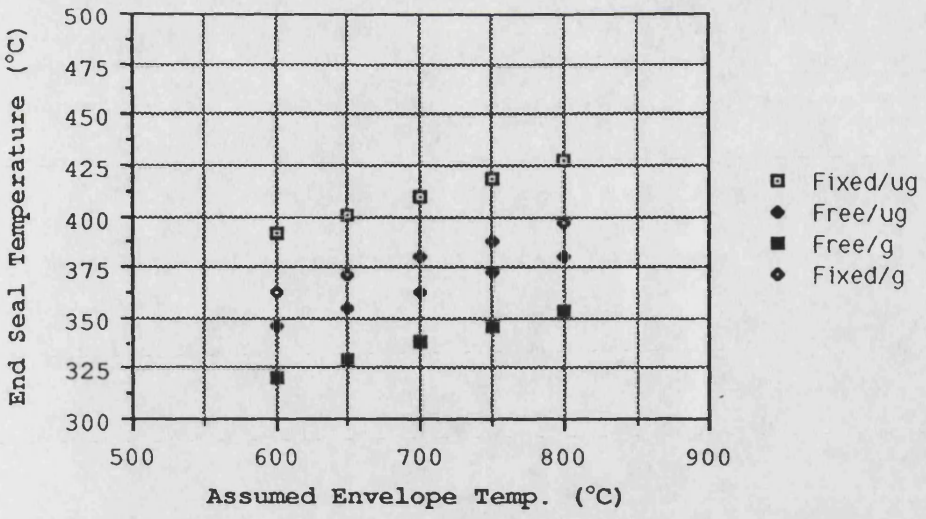

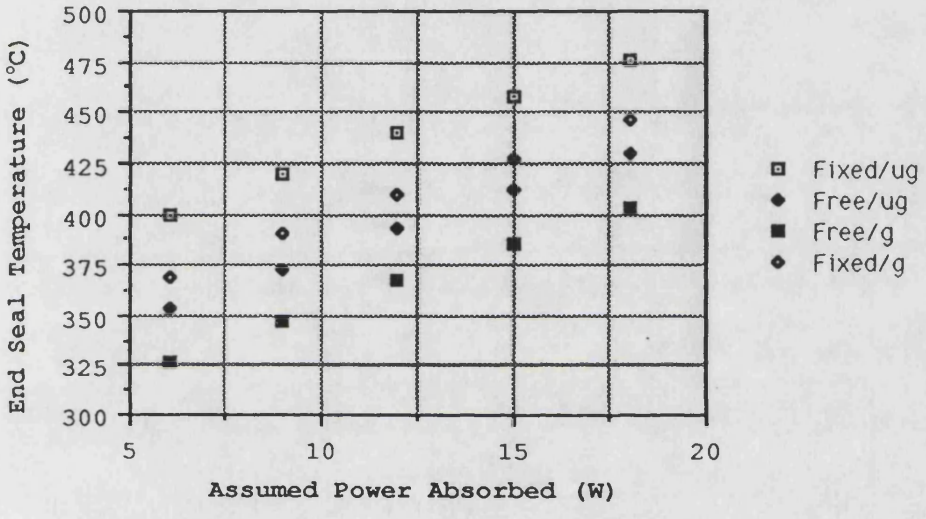

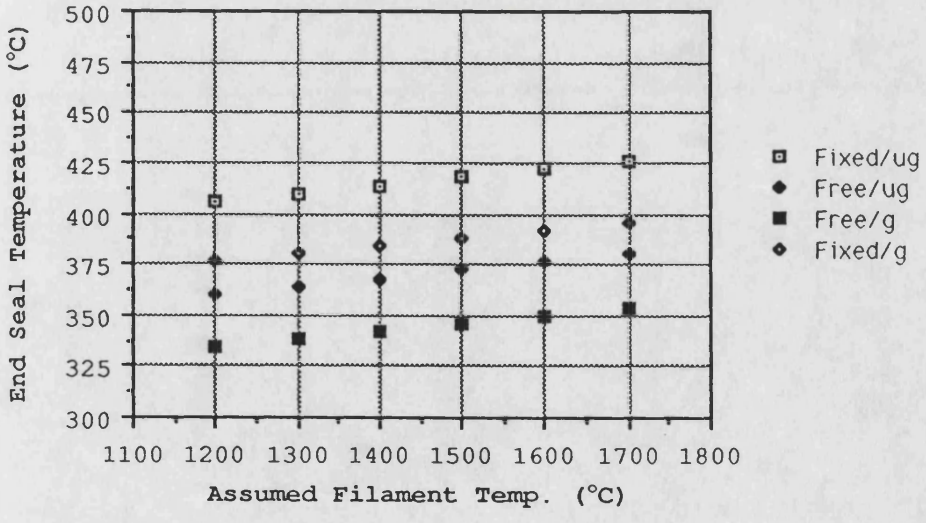

Figure 6.30 - Effect of Varying Program Parameters on End Seal Temperature

CHAPTER 7 - EXPERIMENTAL RESULTS

7.1 Thermal Shock Test Results

The design work for this test facility was carried out under a SERC supported programme between 1985 and 1987. The full realisation of the concept was brought about under the current D.T.I. sponsored work already mentioned.

The thermal shock rig has been used extensively in the School of Materials Science for thermal fatigue and thermal shock testing of both monolithic ceramics and plasma spray coatings. The testing has been accompanied by acoustic emission data collection. Monolithic disc samples of lithium aluminium silicate (LAS) and cordierite have been subjected to thermal cycling. The front face thermocouples used to date, have been platinum - gold pairs. **Fig. 7.1** shows aluminium disc specimens plasma spray coated with zirconia (8% yttria), one of these is "as sprayed", and the other has had gold/platinum thermocouples deposited on the ceramic. The cycle period for both monolithic and coated specimens has been adjusted to around 100 seconds, with approximately 40-50 seconds heating times and 50-60 seconds cooling times. Each sample is subjected to 1000 thermal cycles. Operation of the test rig is usually limited to working hours, although the automatic shutdown system is capable of handling fault conditions, should they arise. **Fig. 7.2** shows a typical chart recorder trace of specimen front face temperature versus time. Strictly speaking this trace is of thermal e.m.f. generated versus time, for more accurate results of temperature against time **Fig. 7.3** and **Fig. 7.4** show single cycles of temperature versus time for cordierite and LAS respectively. A curve fit of the oven calibration data obtained from gold-platinum thin film couples, was used to convert the thermal e.m.f.'s to temperatures. A comparison of these two figures shows the effect on the rates of rise and decay of the front face temperature, for two materials with different densities and thermal conductivities. LAS has lower density and thermal conductivity and thus shows a more rapid rise of front face temperature under the same front face

thermal conditions.

In the early stages of commissioning, a number of early lamp failures (only 2 to 6 hours) were experienced. The source of the lamp failures was attributed to overheating of the lamp end caps, and the lamp envelope. **Fig. 7.5** shows typical lamp envelope and end seal failures. These points were addressed by the application of cooling air around the end caps and over the envelopes, together with some modification of the end sections of the reflector. A resistance model of the lamp was developed which gave appropriate guidleines on the degree of forced convective cooling required. The life expectancy of the lamps has been increased to around 30 to 40 hours, which is sufficient for an entire 1000 cycle test.

Of the monolithic samples tested, only three have failed, all in cordierite. This is a little surprising on two counts. The first is that the finite element model predicted thermal stresses below those which would cause failure. The second point is that the LAS material survived under very similar conditions to those which failed the cordierite samples. Regarding the first point, the thermal stress field predictions are based on an axisymmetric model. This situation does not pertain at the front face of the specimen, with two distinct "hot spots" being present either side of the specimen centreline. A full three dimensional analysis is currently being undertaken to examine the effects of these asymmetrical thermal boundary conditions. The second point, regarding the survival of the LAS specimens under almost identical thermal boundary conditions, to those applied to the cordierite specimens, is not so simple to explain. Finite element analysis of piston crowns in cordierite and LAS show that indeed the thermally generated streeses are less for the LAS than for the cordierite, however, the LAS material is a considerably weaker material. The actual values of the thermal stresses are not in direct relationship to the strength of the material and so, it would appear, that if the cordierite body failed then the LAS body should also fail, if subjected to the same thermal boundary conditions. Two possible explanations could be put forward. The first of these is that the LAS

material is less susceptable to surface damage than the cordierite. It is certainly the case that tests on a number of cordierite samples showed a mean breaking strength well below the quoted figure. This was later corrected by ensuring a finer surface finish on the specimens. The second explanation is that the mechanical constraints/boundary conditions applied to the finite element model were not correct. The LAS has a lower thermal expansion coefficient than the cordierite, and this would induce higher stresses than expected if the mechanical clamping constraint had been underestimated. It should be remarked that one of three specimens which failed did not fail right through. The crack had only moved through about half of the specimen diameter, this behaviour is typical of thermal stress failure.

A wealth of acoustic emission data has been produced for the plasma spray coated specimens, as a result of using this test rig. A sample of this is shown in **Fig. 7.6,** but the reader is directed to the detailed reports available on this subject from the School of Materials Science (see **Ref. 46**) .

The radiant flux present at the surface of the specimen has been monitored and **Fig. 7.7** shows a normalised map from one set of data. It should be remarked that this data was collected from relatively cool lamps, as there were operating limitations on the mean flux which the fibre optic could handle. However, as stated elsewhere in this thesis, unless the filaments change shape appreciably, the flux map should remain reasonably constant over the lamp power output range, even though the mean flux level increases with increasing lamp power. The mean flux level has been monitored using the calorimeter described in the experimental section. This simple device has performed well and the output plots of temperature versus time show good linearity up to over 150°C, which allows the mean flux to be easily calculated from a strip recorder output. A typical strip recorder output plot was shown earlier in Chapter 2 , **Fig. 2.15** .

7.2 Thermal Conductivity Test Results

The thermal conductivity facility has so far been

used for the determination of thermal conductivity versus temperature for three materials, namely : - cordierite , LAS , and plasma sprayed zirconia. The results for each of these is given in **Figures 7.8, 7.9** and **7.10** . The results would appear to show that the thermal conductivity of each one of these materials is largely independent of temperature. However, the following points should be made, regarding the accuracy of the results. The first is that the flux field on the front face of the specimen is far from being flat and uniform (note **Fig. 7.7**). This implies that the heat flux through the specimen is not one dimensional. The original intention was to use the lower power lamps as a source for the thermal conductivity experiments, and thus obtain a more uniform flux field. The results given in the figures mentioned above, should therefore be taken only as preliminary. The other point is that no check on the absolute values of flux distribution at the higher lamp powers has yet been made, to ensure that the flux distribution is the same at high powers as it is at low powers. This latter point will be addressed when the heat flux probes are completed and tested, as it should be possible to calibrate these absolutely using calorimetry of the cooling supply to the probes.

7.3 Results from the Thin Film Heat Flux Probes

Production of these probes is still being undertaken and, as yet, no results are available. However, in due course, these probes will first be calibrated under equilibrium conditions, and then subjected to transient thermal conditions. The transient will be arranged such that a simple theoretical model may be used to validate the operation of the probes under such conditions. The final test for the probe will be a test of its integrity under engine firing conditions.

7.4 Component Temperature Field Results

7.4.a Piston Temperature Fields

Although the writer was involved from the outset with the specification of the temperature sensing

instrumentation for both the standard and insulated airgap piston, this work together with the results obtained are reported by Cole (**Ref. 3**). This thesis will confine itself to reporting the results from the liner thermocouples, already described in **Chapter 4 , section 4.6.b.**

7.4.b Liner Temperature Fields

Installation details for the liner thermocouples have already been given in **Chapter 4** as above , and analyses related to thermocouples in liner walls in **Chapter 6 , section 6.1.b** . In terms of reliability the liner thermocouples performed well and provided some useful information relating to the axial temperature distribution within the liner. However, these results should be viewed in the light of the comments made earlier in **Chapter 6** with regard to the large errors which can arise to the construction of the thermocouples. A comparison of the liner temperatures for a standard and insulated piston engine build is given with reference to **Figures 7.11** and **7.12** . The main feature which was found in all of the temperature plots was that of a reasonably isothermal region occupying a considerable portion of the liner. This allowed simplifications to be made in the resistance modelling of the liner section of the resistance network, which was incorporated in the cycle simulation program C.S.P. Further details of this are to be found in Cole's PhD thesis (**Ref. 3**). Data collected from the liner thermocouples were later used by Rasihan (**Ref. 23**) to set up appropriate resistances for more advanced transient wall modelling which was in turn incorporated by him in the SPICE cycle simulation program. Another feature which the thermocouples showed, was the large, axial temperature gradient which exists at the head deck end of the liner. A comparison of **Figures 7.11** and **7.12** would seem to suggest that the top of liner temperatures were higher for the barrier piston build over those for the standard build. It should be remarked, however, that the two plots which show much higher temperatures at the top end of the liner, are both for low air fuel ratio cases. Once again, a direct comparison is difficult because of the changes in combustion and engine condition

between the standard and the barrier piston cases.

7.4.c Injector Fouling

The injector used in the insulated piston tests showed varying degrees of fouling depending upon the engine load. **Figure 7.13** shows examples of such injector tip fouling. Although the injector was not instrumented for temperature monitoring it was considered that overheating of the injector was taking place. The engine performance data, together with the general smoke levels monitored, indicated that poor combustion resulted when operating with the insulated piston. The carbon which was encrusted around the nozzle holes of the injector seemed to suggest that the injector body was overheating, which in turn was causing pyrolysis of the fuel in this region. A finite element study of the injector was carried out under the supervision of the author to look further into the problem (see **Ref. 45**). The results of this study showed that a considerable amount of experimental validation of the model was required before any definite conclusions could be arrived at. However, the study did show the importance of heat transfer between the fuel and the injector body. The analyses assumed equilibrium conditions of heat transfer as a simplification, whereas in reality the problem is markedly transient in nature, as is the fuel flow through the injector/nozzle assembly.

7.5 Engine Simulation Test Rig Results

This investigation is part of the D.T.I. supported research programme concerned with monolithic ceramic pistons crowns.

The running of this test rig may be divided into two parts :-

i). test runs with the special head which contained a stationary ceramic specimen and

ii). test runs which were carried out with the I.D.I. head with instrumented plug.

7.5.a Initial Running of the Simulation Test Facility

The special head which was designed to enable testing of large (80mm diameter) test specimens, had a number

of problems associated with its operation. Although initially this head was designed to allow easy access to the specimen for instrumentation , this proved to be far from simple. The position of the specimen relative to the rest of the head, only allowed access for instrumentation through the side of the head. This situation made fixing of instrument wires to the thin film surface thermocouples extremely difficult. The sealing operation which was necessary for correct test rig operation, comprised ceramic and silicone rubber composite seals, the assembly of which was also frought with problems. Further difficulties arose from the main, head to block gaskets, and as the head was of split design, from the gaskets internal to the head. These latter points meant that frequent test rig stripdowns were necessary for the replacement, or refurbishment of the gaskets, in order that successful running of the rig took place. However, breakdown of the gaskets were commonplace and a great deal of time and effort was devoted to attempts to solve this problem.

In spite of the gasket and other sealing problems a number of the design features on the test rig functioned as required. The unidirectional air flow system incorporating the reed valve assemblies in conjunction with the single poppet valve worked well, as did the double acting valve actuation mechanism. The air preheater circuit and air inlet pressure control also functioned well.

Uninstrumented running of the test rig with silicon nitride test specimens was carried out and over 50 hours of problem free running were accumulated. The test specimen showed no signs of fracture, although this had rather been expected as the thermal load on the specimen was rather low. Instrumented running was attempted at a later stage, but as indicated above, this proved to present insurmountable problems with the special head design. Thin foil thermocouples were adhesively bonded to the surafce of a silicon nitride disc and a few minutes of running were achieved before failure of the adhesive bond occured. One of the problems with the adhesively bonded, thin foil thermocouples was the need to accurately set the thickness of the adhesive layer, under the

thin foil gauge. This was required in order that this dimension, together with the thermal properties of the adhesive layer,could be correctly used as data input for the finite difference program. **(Ref. 23)**. The adhesive obtained, was rather coarse and unfortunately, bonded poorly to both the thermocouple alloys and to the silicon nitride. Alternative grades of ceramic adhesive, from the same supplier, proved to be only slightly better in terms of adhesion. A more detailed account of the adhesively bonded thin foil thermocouples, together with the attempts to produce surface thermocouples using wire and thin film techniques, are given by Rasihan in his thesis **(Ref. 23)**.

7.5.b Conversion of Test Rig for Operation with I.D.I. Pistons

The "catalogue of disasters" which accompanied the running of this test rig, was finally brought to a halt when the test rig was converted to operating with a modified I.D.I. head. The main reason for doing this was that the firing engine test rig was to be likewise converted from direct injection to indirect injection operation, and this involved a bore size change. It was decided that the simulation test rig would become a proof test rig for pistons to be operated in the firing engine test rig. Of major importance was the need to test experimental piston designs under inertial and pressure loading conditions, similar to those in the firing engine test rig, while at the same time applying some degree of thermal loading.

Thus far only one ceramic capped piston has been tested in this rig. The design of piston, which incorporates a cast in spring section, ran successfully for 50 hours at speeds between 1000 and 2000 r.p.m. A cross section of this piston, showing the method of construction has already been shown in **Fig. 5.14**

7.6 I.D.I. Engine Test Results

This investigation, also, is part of the current D.T.I. supported research programme concerned with monolithic ceramic piston crowns.

The piston mentioned in the preceding subsection was tested in the I.D.I. form of the firing engine test rig and failed after about 13 minutes. The operation of the engine appeared to be satisfactory for the quarter and half load conditions. Failure occurred after a period of about two to three minutes of operation at the three quarter load level. The satisfactory performance of this piston in the simulation test rig did, however, prove useful. The fact that the piston survived the inertial and pressure loading in the simulation test rig would seem to suggest that the cause of the piston failure was thermal in origin. As might be expected, little could be inferred from the collection of ceramic pieces which was all that remained after the failure. **Figures 7.14a, 7.14b, 7.15a,** and **7.15b** show details of the damage which resulted. Three possible explanations may be put forward to explain the early demise of the piston. The assembly of the ceramic crown and stainless steel retaining ring, into the top of the piston body, involved the use of a rather crude casting technique. The intention of the design was to provide compliance between the ceramic and the piston body, by use of the stainles steel ring. It is possible that the quantity of aluminium alloy melt, which was used, was excessive. Inspection of the sectioned piston revealed that, indeed, excessive quantities of aluminium filler metal had been used, and that this had completely filled the region around the stainless steel ring instead of only partially filling this region. **Figure 7.16** shows photographs of the sectioned piston in this region, and clearly show the extent of the metal filling. In view of this, and the difficulties involved in accurately metering the quantity of alloy melt used, an alternative method of fixing was sought. However, although it would seem likely that the explanation given for failure, is reasonable, two further alternative explanations are put forward. The cap had been extensively chipped around the crown top section as a direct result of the casting technique, and although this was largely removed by careful grinding of the crown, this portion of the ceramic may have been considerably weakened by the penetration of cracks beneath the original

surface, and which were not removed on grinding. Examination of the crown for such cracks, using dye penetrant, did not reveal any substantial damage, but it is feasible that potentially fatal flaws were overlooked. The remaining explanation concerns the nature of the thermal boundary conditions on the uppermost surface of the ceramic crown. The finite element modelling carried out was purely axisymmetric. This did not take into account the highly asymmetric thermal conditions which exist around the prechamber throat. This matter is currently receiving attention, with respect to the asymmetric loading of the thermal shock specimens.

After the piston failure, the engine was stripped down to the crankcase and fully examined to judge the extent of the damage. The cylinder liner had been marked, as had both of the valves. The connecting rod had been bent, but the crankshaft was unharmed. One valve guide had been damaged and was replaced, together with the damaged valves. After draining the oil sump and cleaning out, the engine was rebuilt with a new cylinder liner, connecting rod and piston. A baseline test of the engine was carried out to check performance.

Further piston crown failures have been experienced but one design, similar to that in **Fig. 5.12**, has been successfully run at modest load and speed levels for over 50 hours. Further running of this design is currently being undertaken to establish the limits of operation.

7.7 Mechanical Test Results

The only mechanical test which the pistons were subjected to was a simple tensile test. This test was comprised of adhesively bonding an adaptor to the crown of the piston, and attaching a pulling arm to the underside of the piston via the gudgeon pin. The assembly was then placed in a standard tensile testing machine and subjected to loads somewhat higher than the inertial loads expected to occur in the running engine.The adaptor was later removed from the piston crown by heating the whole assembly to around 180°C in an oven. **Fig. 7.17** show the adaptor and puller arms used to fit the piston/ceramic crown assembly into the tensile test

machine. **Fig. 7.18** shows a chart recorder output of load versus extension for one of the ceramic crown piston assemblies tested.

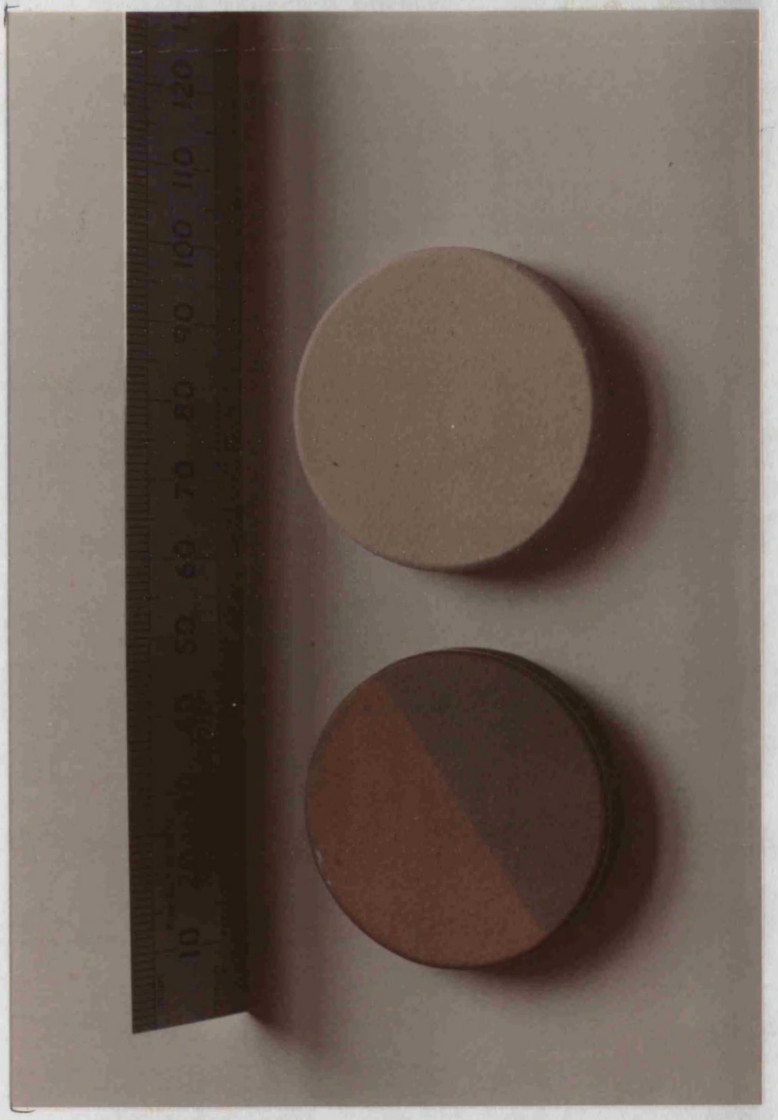

Figure 7.1 - Plasma Sprayed Thermal Shock Disc Specimens (one with Au/Pt thin film T/C)

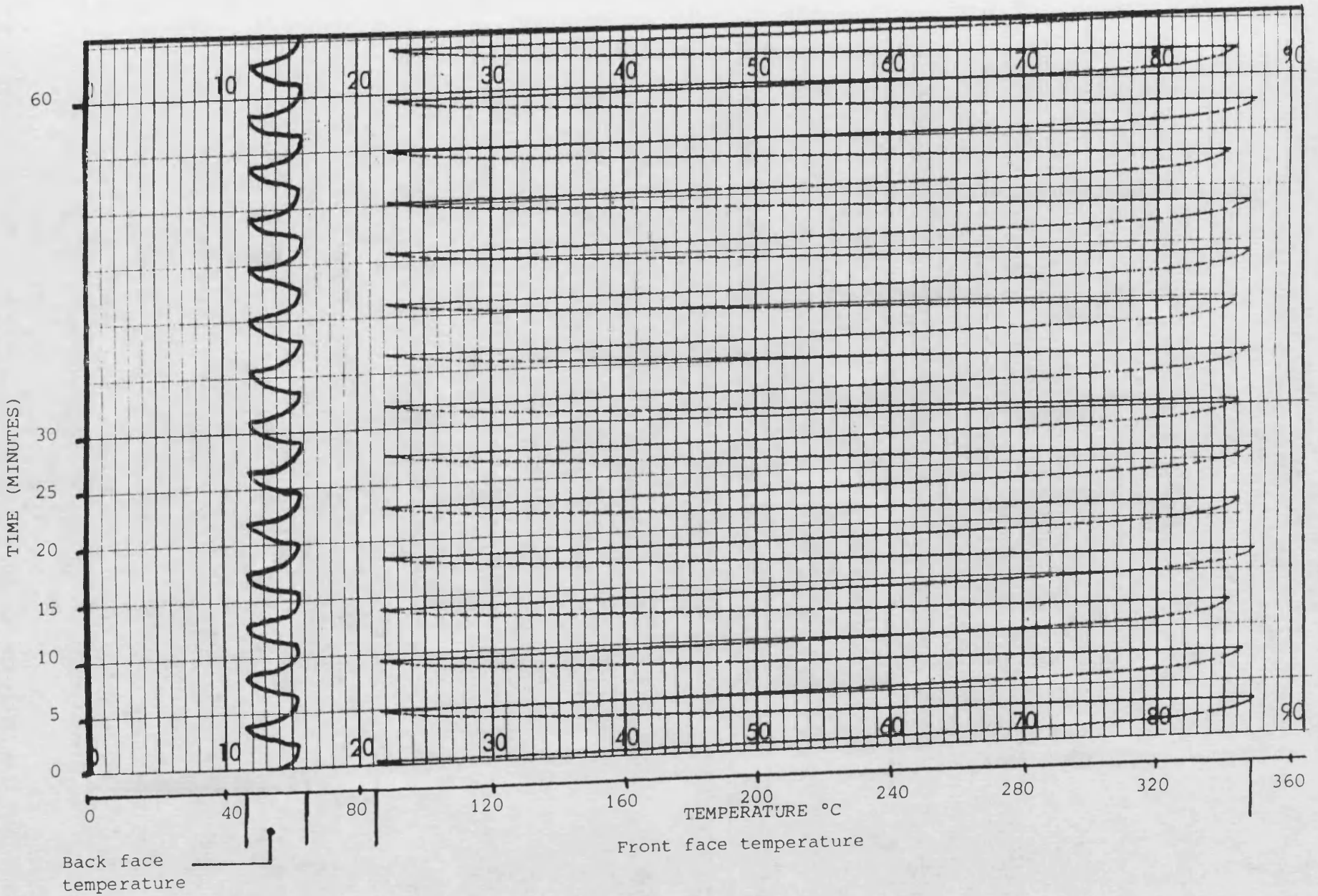

Figure 7.2 - Specimen Surface Temp. vs. Time

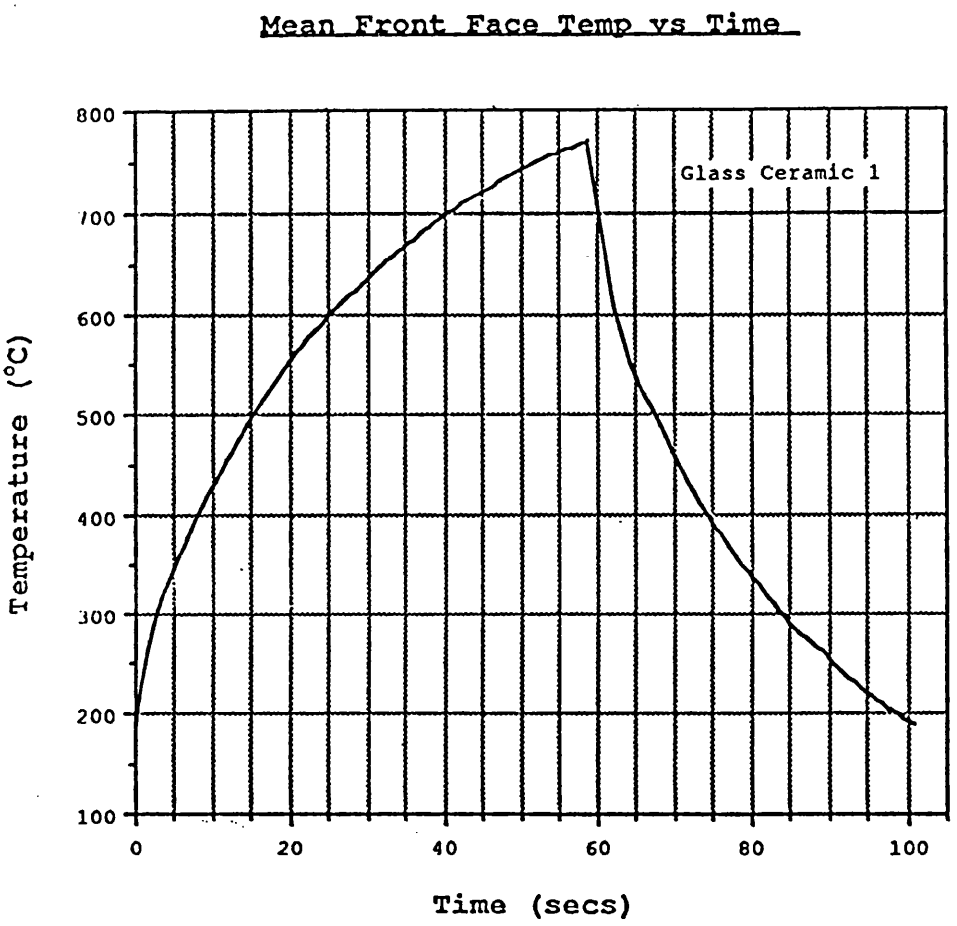

Figure 7.3 - Mean Front Face Temperature of Specimen Versus Time (Cordierite)

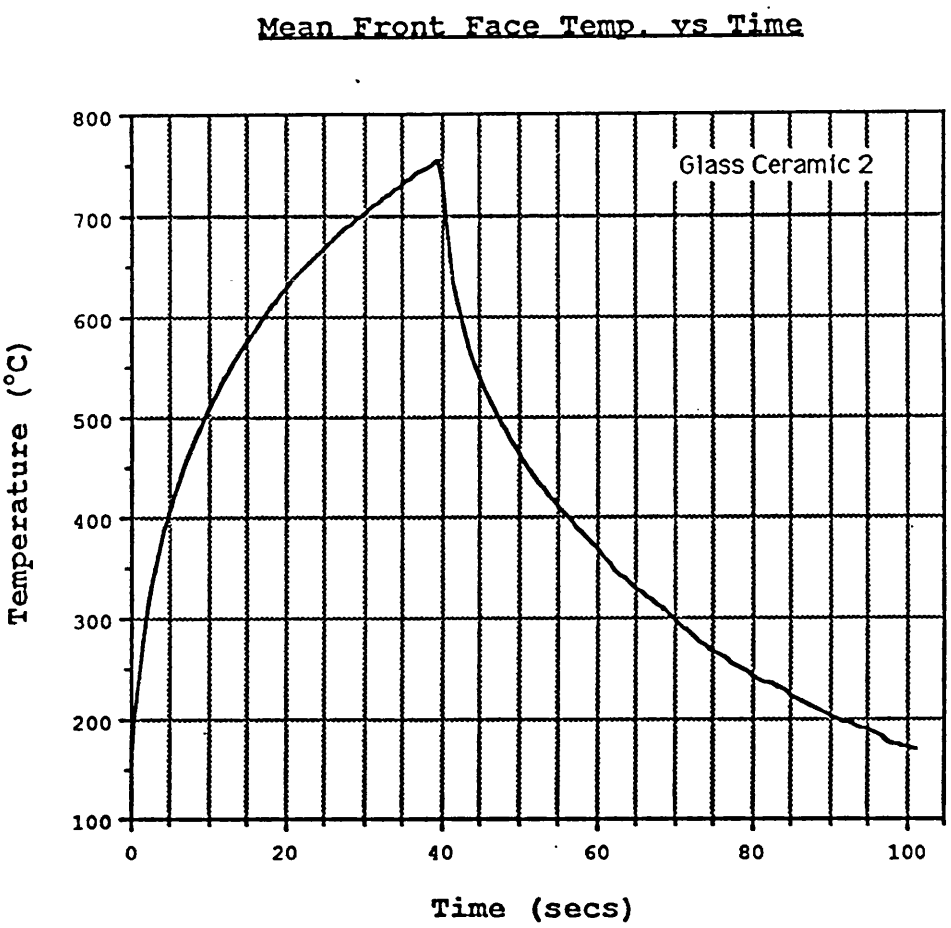

Figure 7.4 - Mean Front Face Temperature of Specimen Versus Time (LAS)

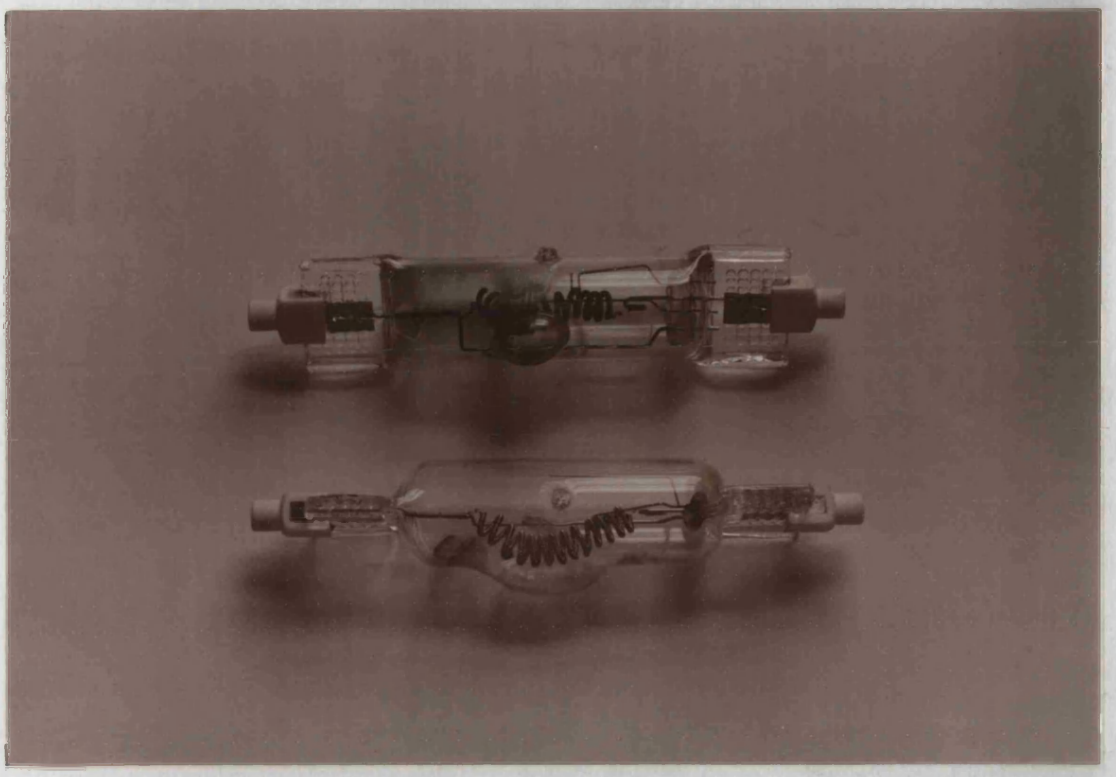

Figure 7.5 - Typical Lamp Failures

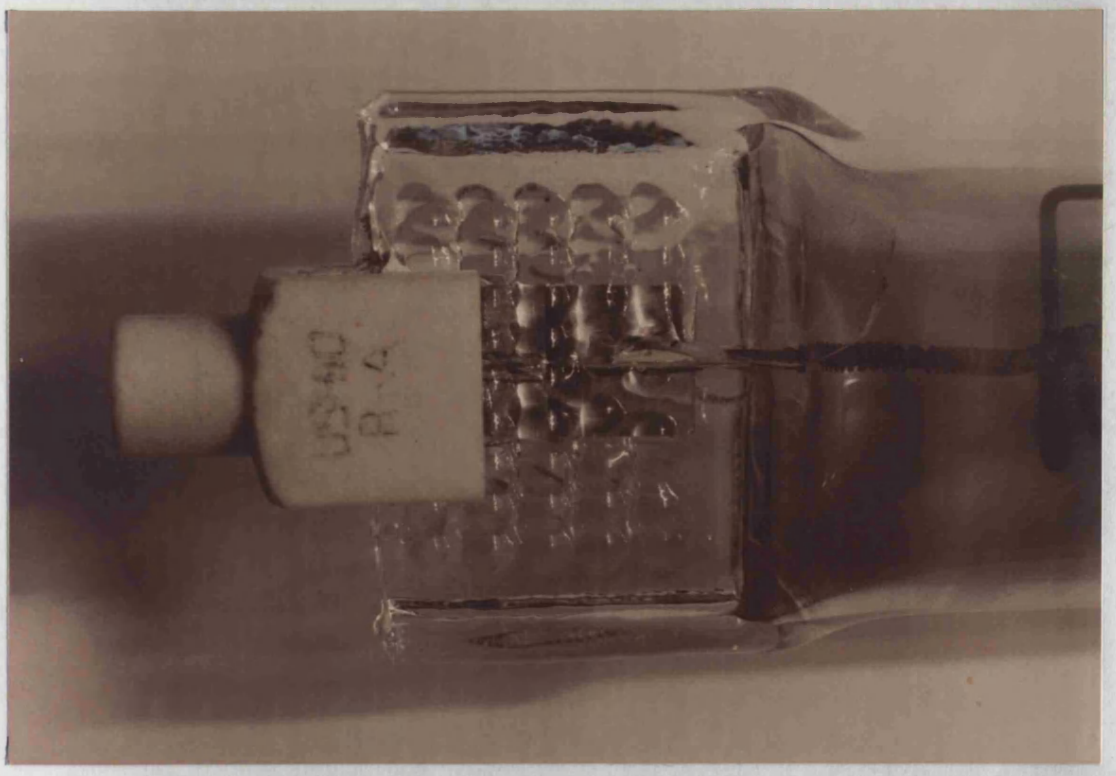

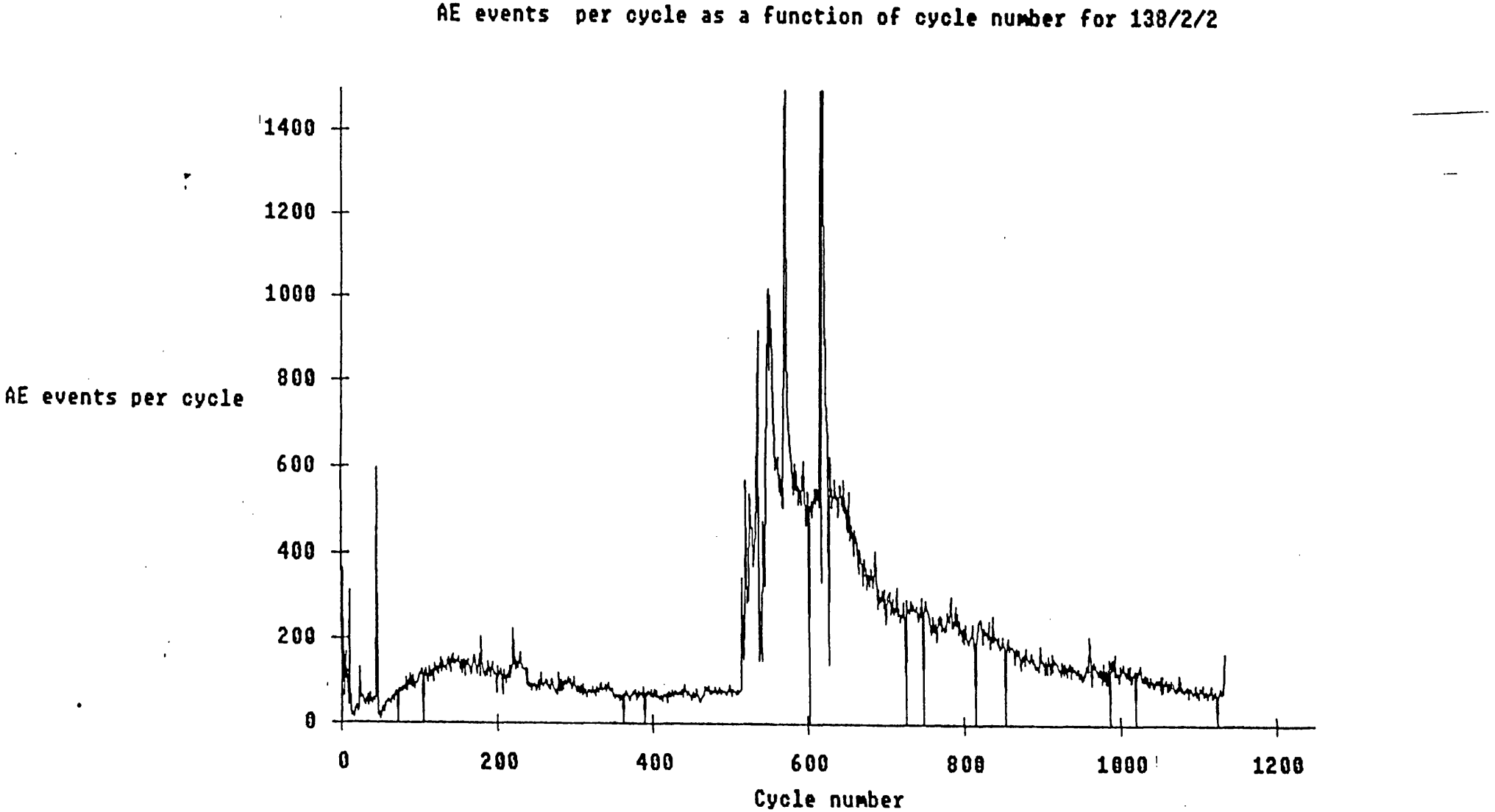

Figure 7.6 - Typical Acoustic Emission Records from Thermal Shock Specimens

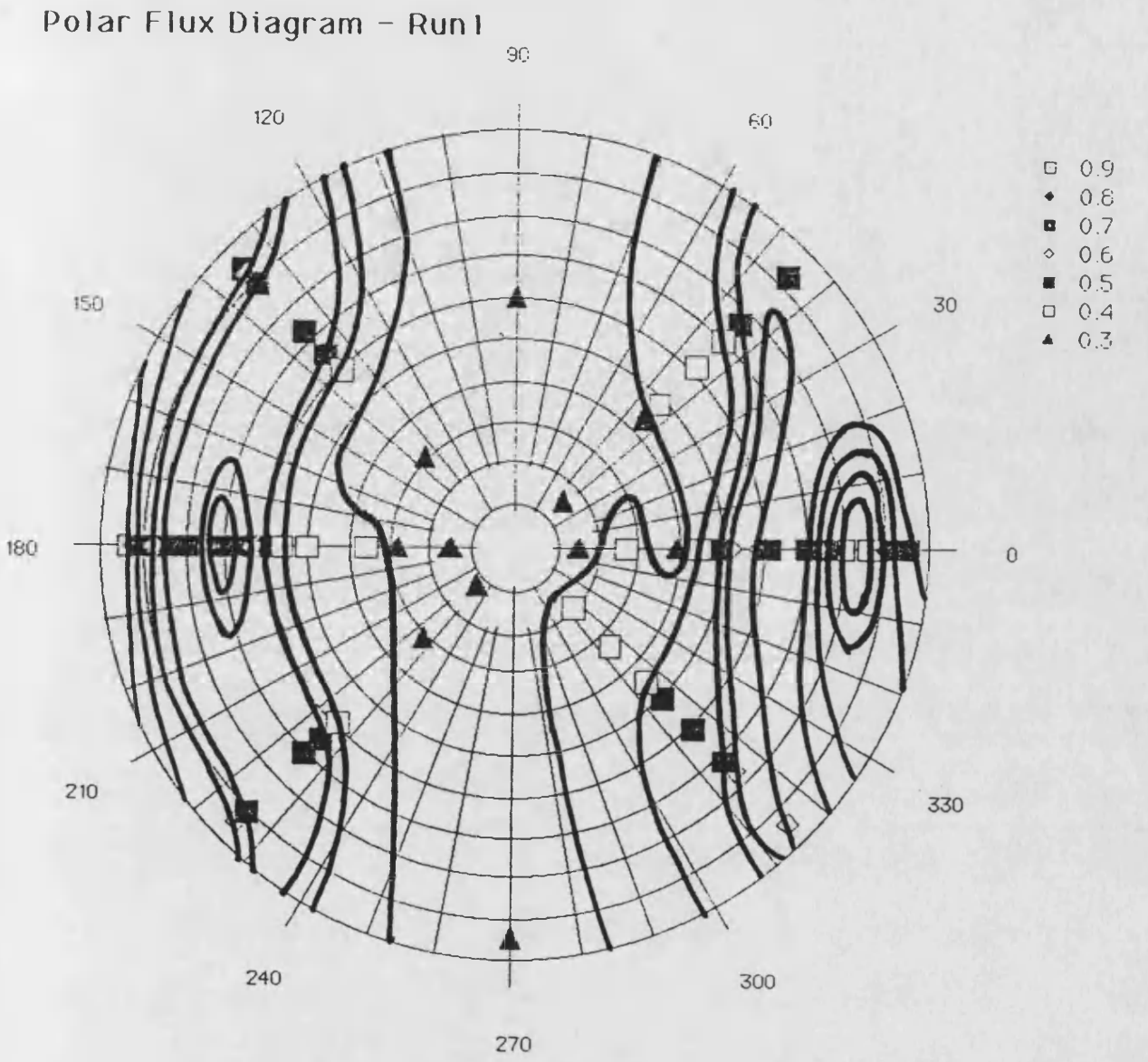

Figure 7.7 - Normalised Polar Flux Diagram for the Second Reflector (at the specimen plane)

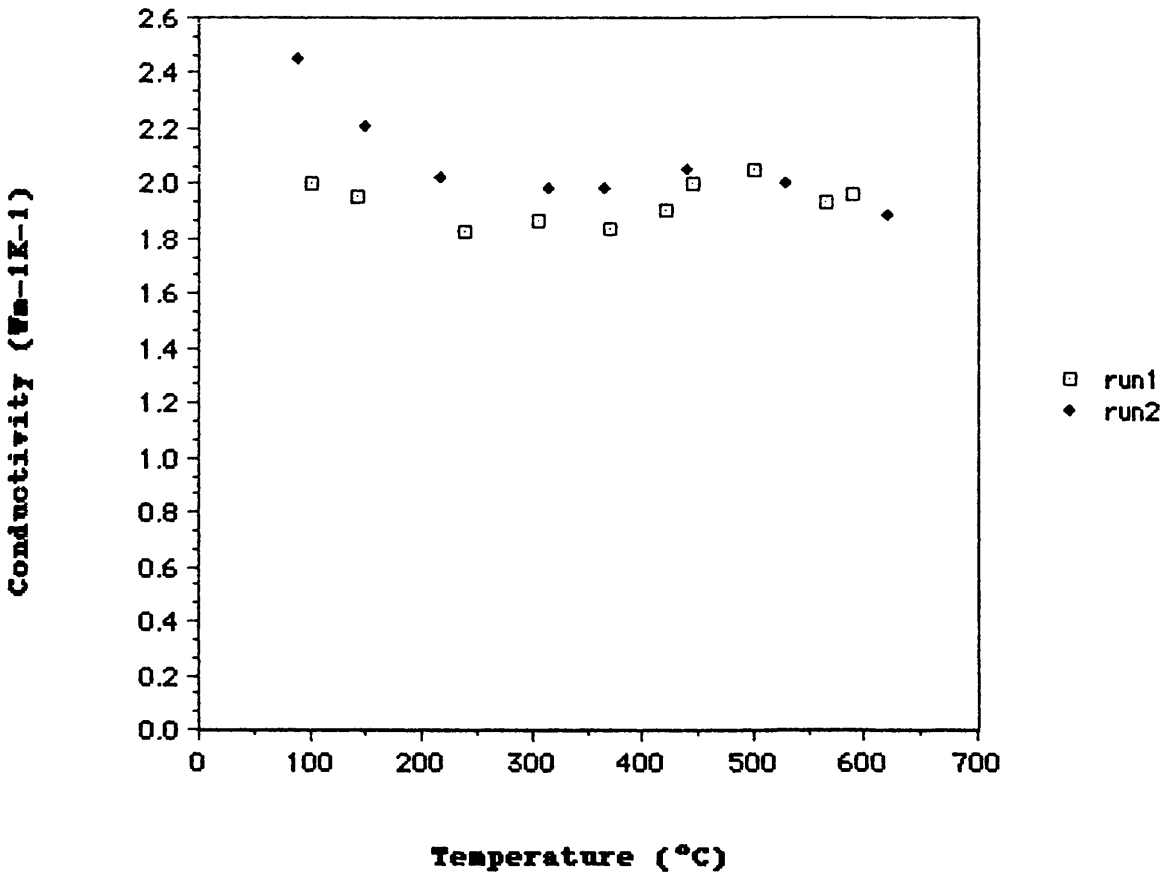
Thermal Conductivity vs Temp. for Cordierite
Conductivity (Wm-1K-1)
2.6
2.4
2.2
2.0
1.8
1.6
1.4
1.2
1.0
0.8
0.6
0.4
0.2
0.0
0
100
200
300
400
500
600
700
Temperature (°C)
run1
run2

Figure 7.8

Thermal Conductivity vs Temp. for LAS 693

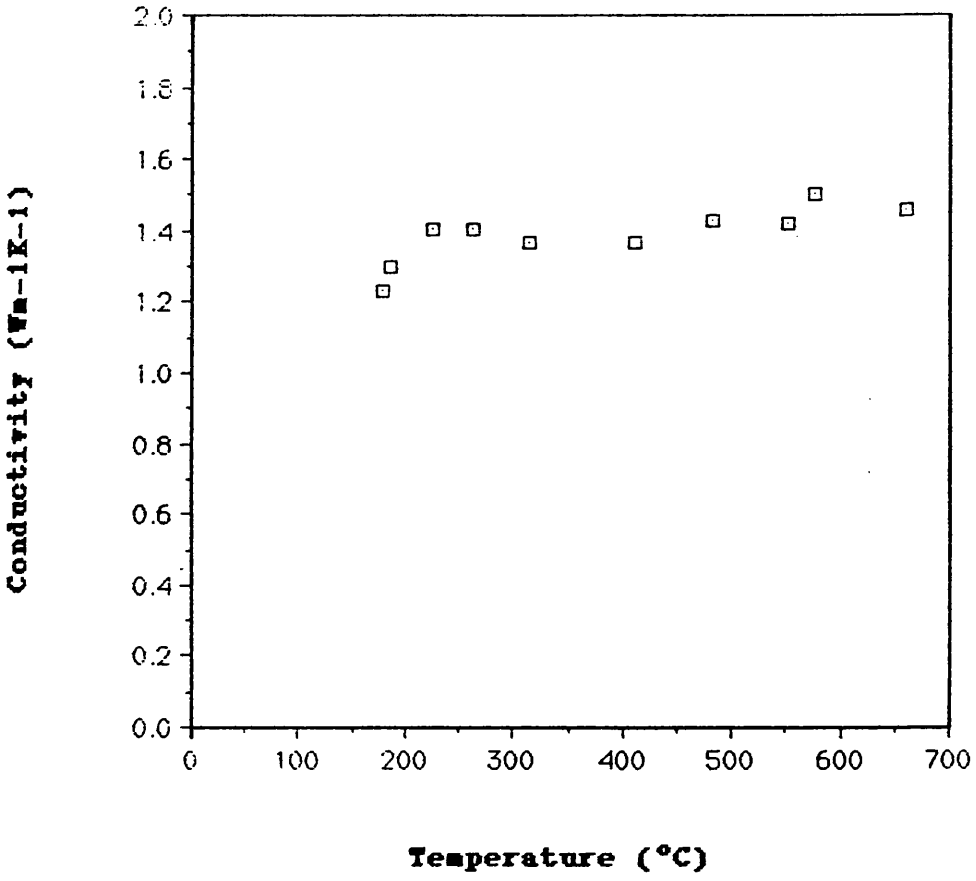

Figure 7.9

Thermal Conductivity vs Temp. for PSZ

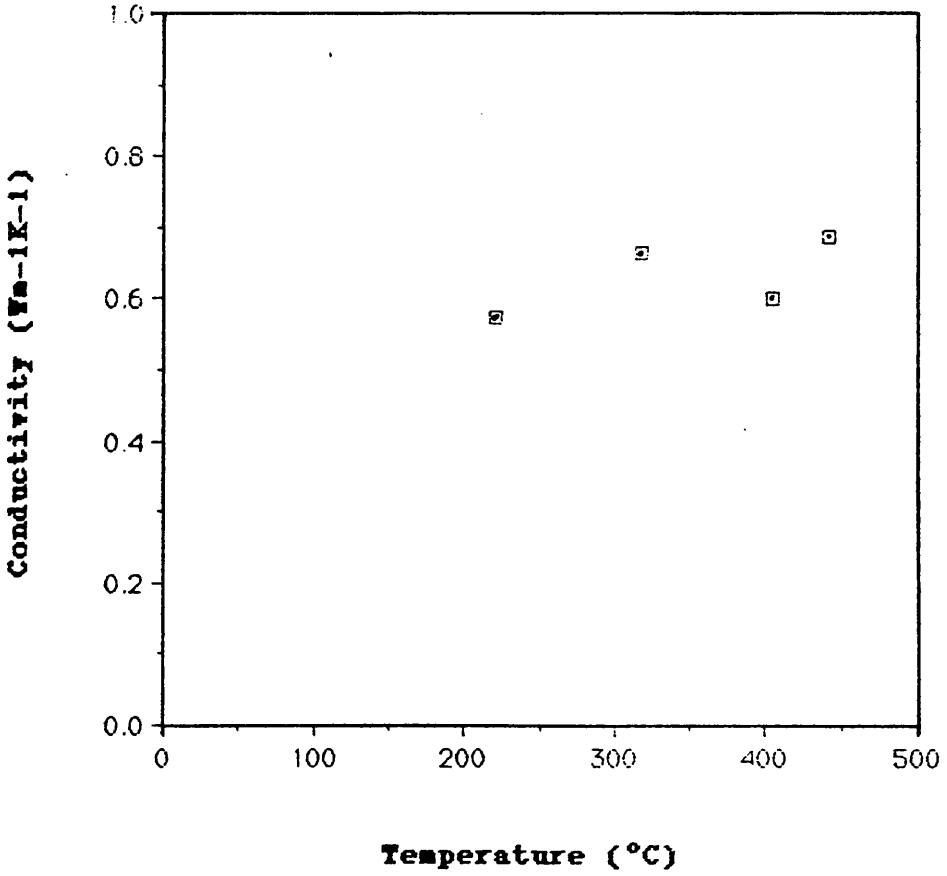

Figure 7.10

LINER TEMPERATURE vs. POSITION

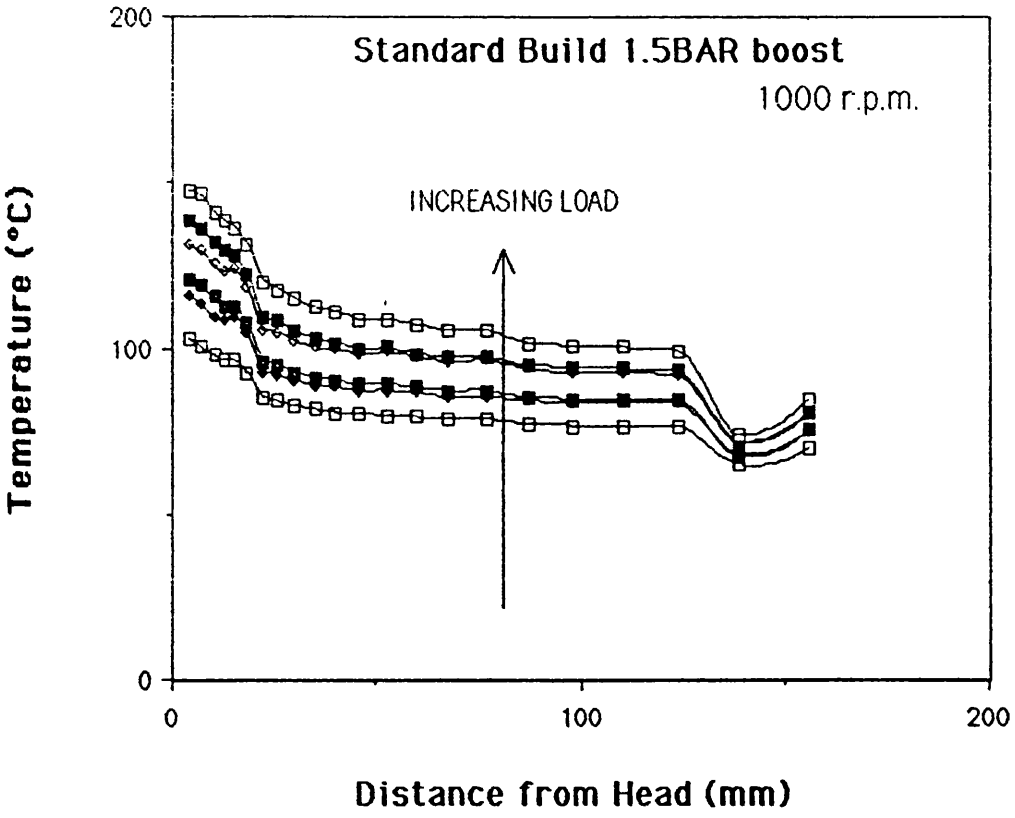

Figure 7.11

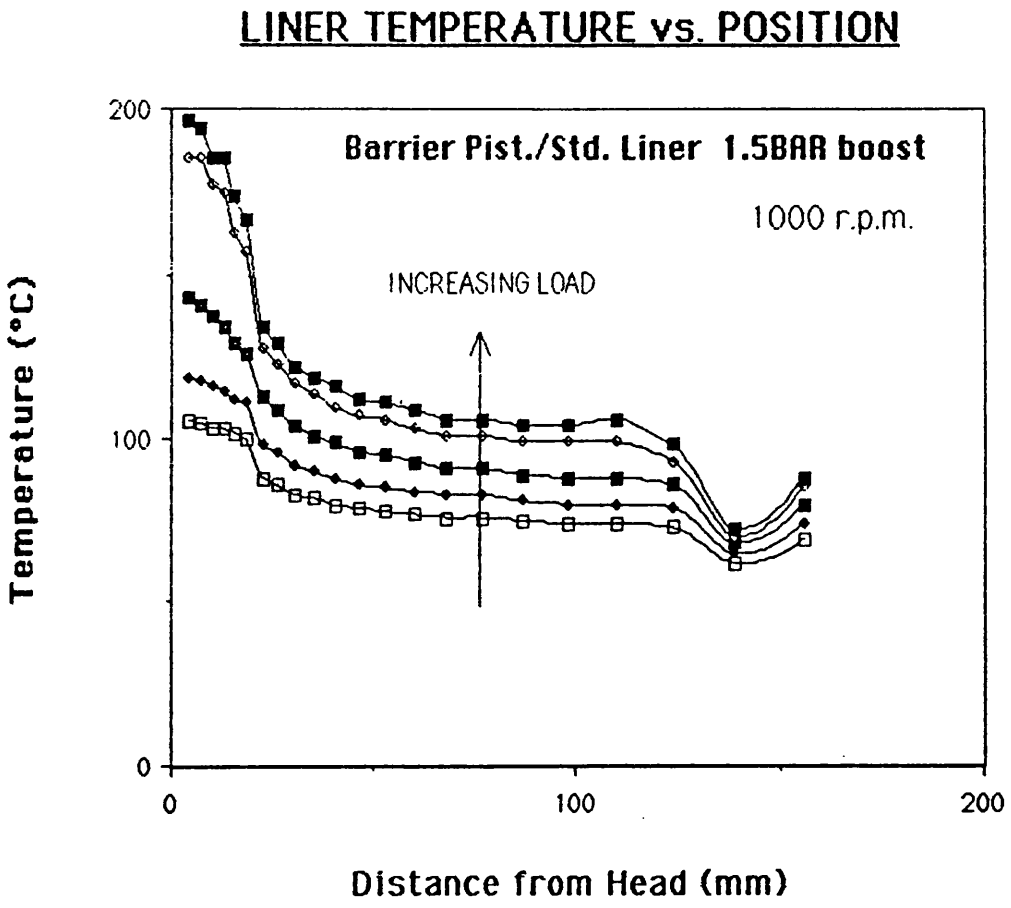
LINER TEMPERATURE vs. POSITION
Barrier Pist./Std. Liner 1.5BAR boost
1000 r.p.m.
INCREASING LOAD
Temperature (°C)
200
100
0
0
100
200
Distance from Head (mm)

Figure 7.12

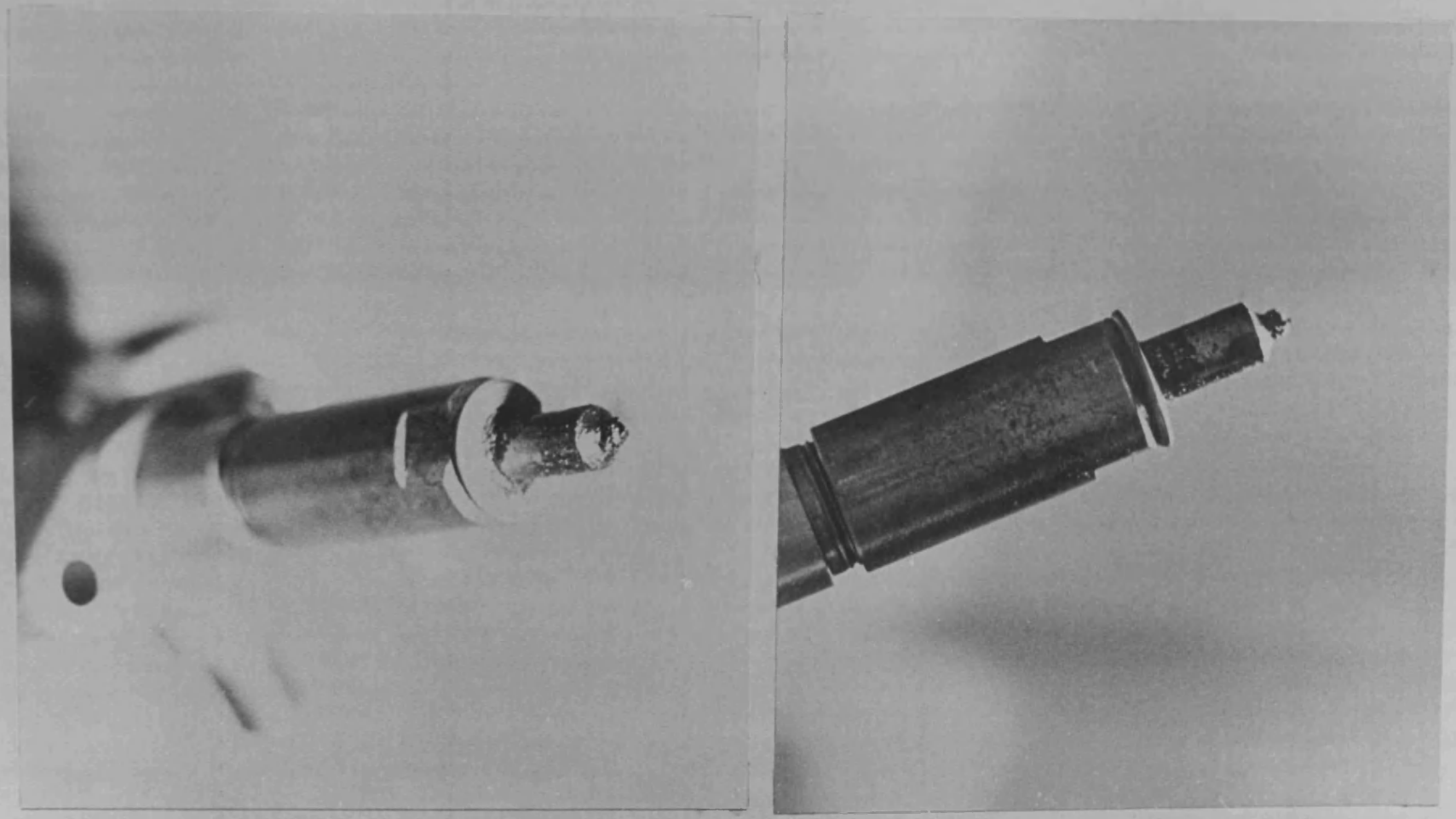

Figure 7.13 - Examples of Injector Fouling

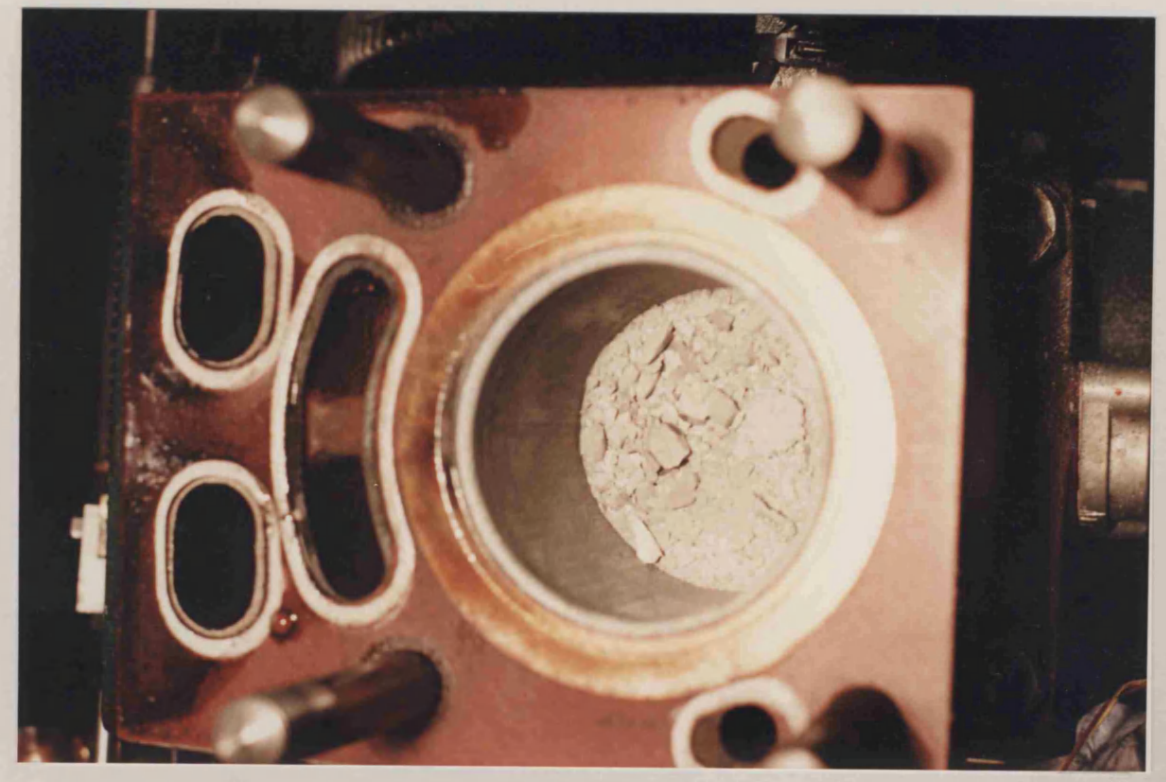

Figure 7.14a - View of Failed Crown

(looking into bore)

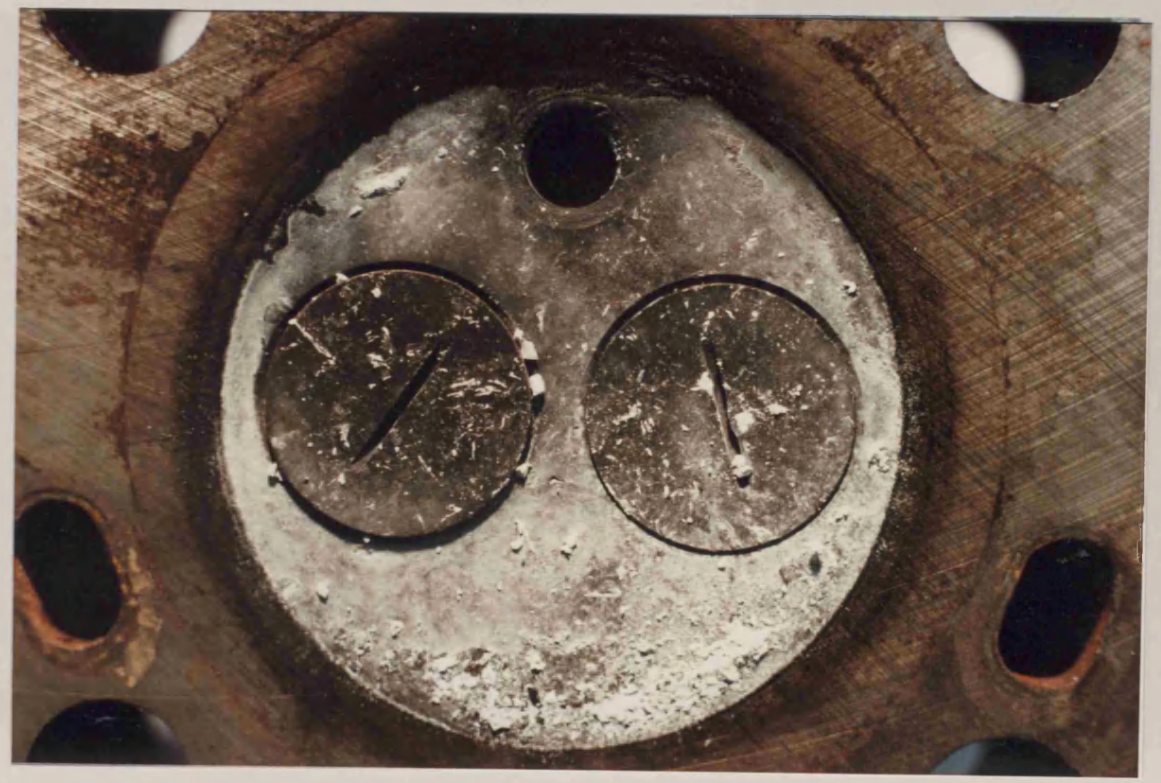

Figure 7.14b - View of Head & Valves after Failure

Figure 7.15a - Side View of Failed Piston

Figure 7.15b - View of Failed Crown

(in situ after removal of debris)

Figure 7.16 - Sections of Failed Piston (Cast in Ring Type)

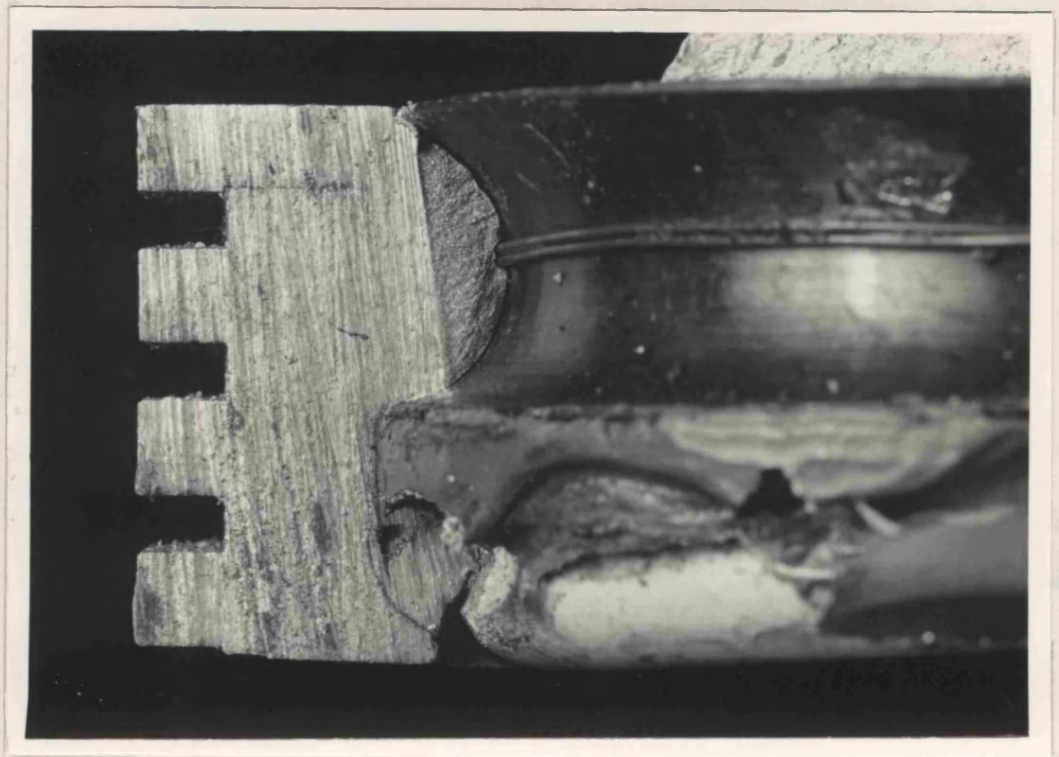

Figure 7.17 - **Tensile Test Adaptors fitted to Ceramic Capped Piston Assembly**

Tensile Test on Petter Piston with Ford style Ceramic Crown

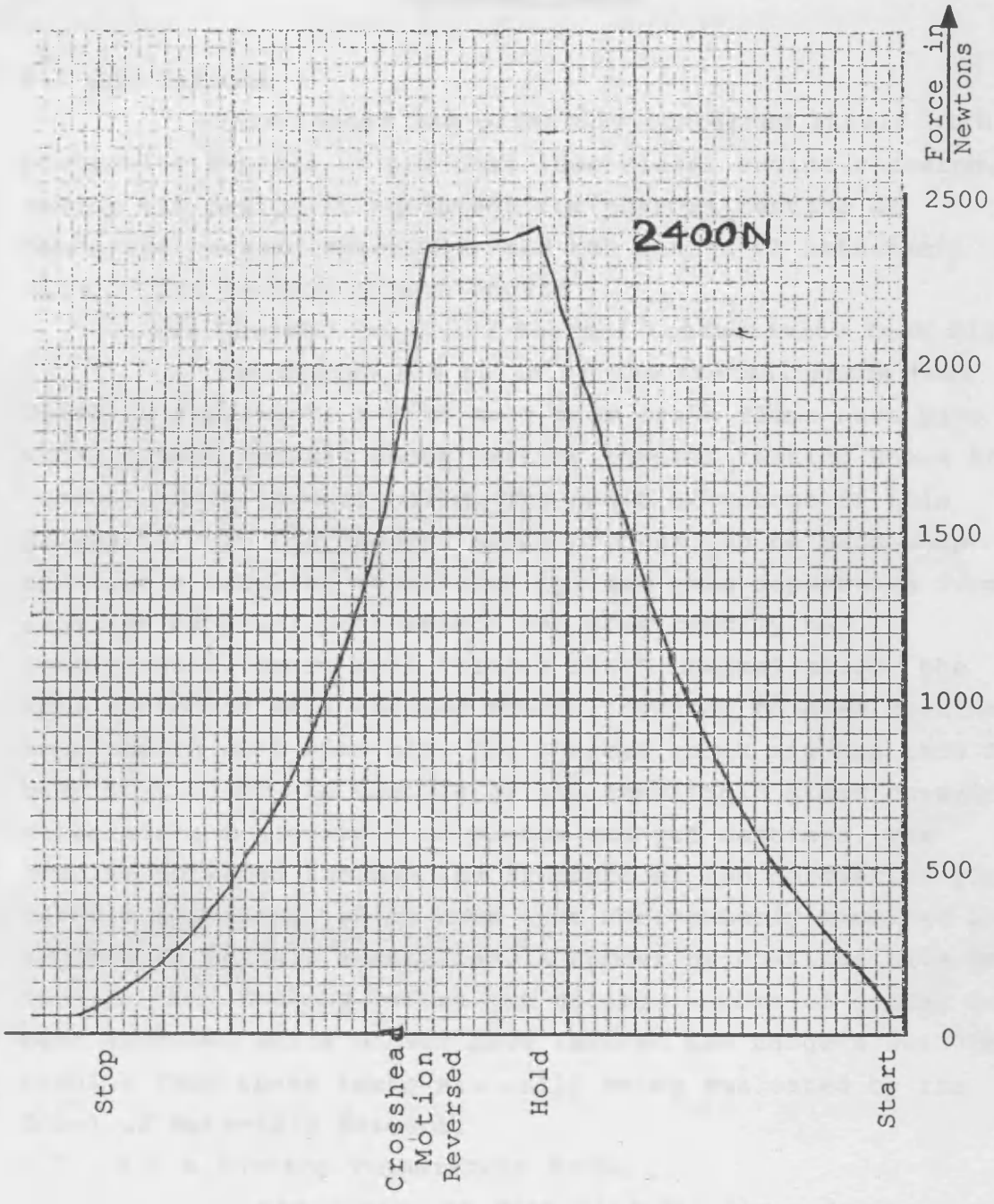

Crosshead speed fixed at 0.5 mm/min
Chart Recorder speed 50 mm/min
500 kgf load cell used

Figure 7.18

CHAPTER 8 - CONCLUSIONS AND SUGGESTIONS FOR FURTHER WORK

8.1 Conclusions

This thesis has primarily concerned itself with two particular aspects of low heat loss diesel engine research, namely the design of equipment for thermal testing of candidate ceramic materials, and the design of attachment methods for ceramic piston crowns.

8.1.a Thermal Shock and Thermal Conductivity Test Rig

The design and build of the thermal shock test facility represents a move away from crude flame heat plus water quench thermal shock testing towards testing where the thermal shock is controlled. The great advantage of this scheme is that the thermal shock process can be much more accurately modelled theoretically, and thus departures from expected material performance can more readily be investigated. Apart from "single shot" thermal shock, the application of well defined thermal cycling to disc specimens is possible with this rig. The thermal shock rig has thus far been applied to the testing of two monolithic glass ceramic materials and a variety of plasma sprayed coatings. The results obtained include the fracture of two cordierite glass ceramic specimens, which have been subsequently examined and sources of failure identified. A number of coatings have been tested, some failing before the desired number of cycles had been executed while others have reached the targets set. The results from these tests are still being evaluated by the School of Materials Science.

8.1.b Surface Temperature Probe

In the course of designing the thermal shock test rig a method of obtaining specimen front face temperatures was developed, which in turn led to the design and production of a surface temperature probe. This has yet to be tested but it is hoped that it will provide an additional tool for examining short duration heat transfer phenomena.

8.1.c Ceramic Piston Crowns and Attachment Schemes

The writer has developed "from scratch" novel methods of attaching ceramic piston crowns to standard piston bodies. These developments have been followed through from initial design sketches through to working prototypes and have involved extensive finite element design work for both the Petter engine and the Ford engine. While the results have generally been disappointing in terms of the piston crown failures which have occurred, there is evidence that improvements in material properties coupled with further detailed design work could yield satisfactory performance from piston designs incorporating such attachment schemes. The basis for this optimistic view is the fact that succesful running of one of the piston crowns for over 50 hours has recently been achieved. However, it should be remarked that this period of running has been at relatively light load and speed combinations, and that further work has yet to be undertaken to establish the integrity of the crown/piston assembly at all load and speed levels.

In spite of the failures which occurred, the production of the glass ceramic piston crowns yielded much valuable information both to the research teams at Bath University and to those working at Pilkington Brothers p.l.c.

At the present moment in time it would appear unlikely that ceramic piston crowns will be in production engines within the next five to ten years, longer term it is harder to say. It is possible that high thermal conductivity, high strength ceramic piston crowns will appear in highly rated engines but there are still a number of problems associated with higher in cylinder temperatures to be solved before the low heat loss Diesel engine can be accepted for future prime mover applications.

8.2 Suggestions for Further Work

8.2.a Improvements in Materials

The two candidate glass ceramic materials, LAS and cordierite, were originally chosen for their low thermal conductivity coupled with low density together with reasonable levels of strength. Additional reasons were the low thermal

expansion coefficients of the two materials and their formability. However, particularily with regard to surface damage and flaws, it is evident that these materials are far more susceptible than had been expected, with considerable reductions in breaking strength resulting from such crack starters. This behaviour is characteristic of most ceramics, although recent advances with transformation and fibre toughening mechanisms have been succesfully applied. The limits of this project did not allow for investigations into thermal, chemical, fibre or transformation toughening, and thus there is considerable scope for development along these lines.

8.2.b Design Techniques

The finite element techniques have been an essential part of the design process, but a number of important aspects still remain to be explored. Fully three dimensional modelling with improved thermal and mechanical boundary conditions would certainly be needed for future piston crown designs. Plastic flow studies would be essential if shrink fitting techniques were to be applied, as it is evident that the stresses involved are generally far beyond the elastic limit for the standard aluminium alloy piston alloys. However, although presently available finite element programs can solve both three dimensional and plastic flow problems, the computational times involved are lengthy, and consideration should be given to alternative solutions. This is particularily the case during the early stages of design when finite element methods are of little use. Although electrolytic tank and photoelastic models are hardly state of the art technology, they still offer considerable advantages over F.E. methods during these stages.

REFERENCES

1. Kao, T.K.
"Prediction of Heat Flow and Temperature Distribution in Adiabatic Engine Components"
MSc Thesis, University of Bath, 1981

2. Kao, T.K.
"Prediction of Heat Flow, Temperature and Stress in Diesel Engine Pistons Incorporating Thermal Barriers"
PhD Thesis, University of Bath, 1983

3. Cole, A.C.
"Diesel Engine Thermal Insulation"
PhD Thesis, University of Bath, 1986

4. Manton, S.M.
"Assessment of Ceramic Materials - Thermally Insulated Reciprocating Engines"
PhD Thesis, University of Bath, 1986

5. Hobbs, M.
"The Structure and Properties of Plasma Sprayed 8% Yttria-Zirconia Thermal Barrier Coatings"
PhD Thesis, University of Bath, 1989

6. Kamo, R. and Bryzik,W.
"Adiabatic Turbocompound Engine Performance Prediction"
SAE 780068 , 1978

7. Wallace, F.J., Vollmert, H., Way, R.J.B.
"Effect of Partial Suppression of Coolant on the High Output Diesel Engine Cycle"
SAE 790823 , 1979

8. Valland, H. and Wyspianski, G.
"A Theoretical Analysis of Thermal Barriers in Diesel Engine Cylinders"

Norwegian Maritime Research, Vol. 10, Pt. 2, 1982

9. Griffiths, W.
"Thermodynamic Simulation of the Diesel Engine Cycle to Show the Effect of Increasing Combustion Chamber Wall Temperatures on Thermal Efficiency and Heat Rejection"
Wellworthy Topics No. 63, p.7-10, 1976

10. Pappas, P.
"Thermal Conductivity Determination of Thin, Low Thermal Conductivity Ceramic Materials"
MSc Thesis, University of Bath, 1984

11. Woodside, W.
"Analysis of Errors due to Edge Heat Loss in Guarded Hot Plates"
Symp. Thermal Conductivity Measurement and Applications of Thermal Insulations", Philadelphia
ASTM Special Tech. Pub. No. 217, p49 - 64, 1957

12. Huang, J.C. and Borman, G.L.
"Measurements of Instantaneous Heat Flux to Metal and Ceramic Surfaces in a Diesel Engine"
SAE 870155 , (also in SAE pub. SP700) , 1987

13. Morel, T. and Keribar, R.
"Heat Radiation in D.I. Diesel Engines"
SAE 860445 , 1986

14. Wahiduzzaman, S., Morel, T., Timar, J. and DeWitt, D.P.
"Experimental and Analytical Study of Heat Radiation in a Diesel Engine"
SAE 870571 , 1987

15. ASTM
"Steady State Thermal Transmission by means of the Guarded Hot Plate"
Annual book of ASTM Standards, C177, Pt.18, 1976

16. Thorn Lighting Limited
"Photographic Lamps"
Publication No. 586 , Feb. 1979

17. Somers, E.V. and Cyphers, J.A.
"Analysis of Errors in Measuring Thermal Conductivities of Insulating Materials"
Rev. Sci. Instr., Vol.22, No.8, p 583 - 585, 1951

18. Overbye, V.D., Bennethum, J.E., Uhehara, O.A. and Myers, P.S.
"Unsteady Heat Transfer in Engines"
SAE Trans. Vol.69, p 461 -494 , 1961

19. Kamel, M. and Watson, N.
"Heat Transfer in the Indirect Injection Diesel Engine"
SAE 790826 , 1979

20. Sihling, K. and Woschni, G.
"Experimental Investigation of the Instantaneous Heat Transfer in the Cylinder of a High Speed Diesel Engine"
SAE 790833 , 1979

21. Enomoto, Y. and Furuhama, S.
"Study on Thin Film Thermocouple for Measuring Instantaneous Temperature on Surafec of Combustion Chamber Wall in Internal Combustion Engine"
Bull. JSME , Vol. 28, No. 235, p 108 - 116, Jan. 1985

22. Jackson, N.S. and Sandford, M.H.
"An Experimental Assessment of Instantaneous Heat Transfer within a Highly Rated D.I. Truck Engine"
I.Mech.E. Seminar "Experimental Methods in Engine Research and Development" I.Mech.E. London, 10th. March 1989

23. Rasihan, Y.
"Further Developments in Performance Predictions of Adiabatic Diesel Engines"
PhD Thesis, University of Bath, 1989

24. Partridge, J.H.
"Glass to Metal Seals"
The Society of Glass Technology 1949 (1962 reprint)

25. Kastner, L.J.
"An Investigation of the Airbox Method of Measuring Air Consumption of Internal Combustion Engines"
Proc. I. Mech. E. 1946

26. Woolman, J. and Mottram, R.A.
"The Mechanical and Physical Properties of the British Standard En Steels - Volume 1, En1 to En20"
The British Iron and Steel Research Association
Pergamon Press, 1964

27. British Standards BS 1042 pt.1 and 2, 1964

28. Taylor, C. F.
"The Internal Combustion Engine in Theory and Practice"
Vol.1 and 2, 2nd. Ed., M.I.T. Press, 1976
ISBN 0 262 70015 8

29. Moffat, R.J.
"Temperature, its Measurement and Control in Science and Industry - Gas Temperature Measurement"
Rheinhold, 1962

30. Caton, J.A.
Comparisons of Thermocouple, Time-Averaged and Mass-Averaged Exhaust Gas Temperatures for a Spark Ignited Engine"
SAE 820050 , 1982

31. Caton and Heywood
"An Experimental and Analytical Study of Heat Transfer in an Engine Exhaust Port"
Inst. Heat and Mass Transfer, Vol.24, No.4, 1981

32. Amman, C.A.
"Classical Combustion Diagnostics for Engine Research"
SAE 850395 (Also SAE P-156), 1985

33. Brown
"Methods for Evaluating Requirements and Errors in Cylinder Pressure Measurements"
SAE 670008, 1967

34. Lyn, Stockwell and Wang
"Accuracy in Cylinder Pressure Measurement"
Proc. I. Mech. E., Vol.180, Pt.36, 1965-66

35. Way, R.J.B.
"Heat Release and Thermal Loading in Pressure Charged Automotive Type Diesel Engines"
PhD Thesis, University of Bath, 1974

36. Wiebe, I.
"Habempirische Formel für die Verbrennungsgeschrivindigkeit"
Verlag der Akademie der Wissenschaften der VdSSR
Moscow 1956

37. Marzouk, M., Watson, N. and Pilley, A.D.
"A Combustion Correlation for Diesel Engine Simulation"
SAE 800029 , 1980

38. Barker, D., Prest, P. and Packer, J.P.
"High Speed Control and Data Acquisition System for a

Novel Combustion Rig"
Proc. 3rd. Int. Conf. on Eng. Software, 3, p666 -678, April 1983

39. Barker, D. and Prest, P.
"Internal Report on a Slow Speed Data Acquisition System for the Adiabatic Diesel Engine Test Rig"
Instrumentation Section, Sch. of Mech. Eng., University of Bath, 1987

40. Alexander, W.D., Wallace, F.J., Kao, T.K.
"Improvements Relating to Pistons"
U.K. Patent Application 8226331 1982

41. Alexander, W.D.
"Corrugated Piston Insert"
U.K. Patent GB 2172084 B , Filed Mar. 1985, Granted May 1988

42. Rentsch, R.
"Design and Development of a Ceramic Piston Crown for a Four Stroke Indirect Injection Diesel Engine"
Student Report, Sch. of Mech. Eng., University of Bath, October 1987

43. Kassens, I.
"Design of a Glass-Ceramic Piston Cap for a Low Heat Loss Engine"
Student Report, Sch. of Mech. Eng., University of Bath, June 1988

44. Wilson, M.
"Study of Gap Elements within the ANSYS suite of Programs"
Internal Report, Sch. of Mech. Eng., University of Bath, February 1989

45. Brouzakis, A.
"Thermal Analysis of Diesel Engine Injector Assembly"
MSc Thesis, University of Bath, 1985

46. Russell-Floyd, R. and Reiter, H.
"Acoustic Emission in Thermally Shocked Plasma Sprayed Coatings" , to be published.

47. Shams, O.M.A.
PhD Thesis, University of Bath, to be published

48. Cornwell, K.
"The Flow of Heat" p.54
Van Nostrand Rheinhold, 1977 ISBN 0 442 30168 5

49. Wong, H.Y.
Handbook of Essential Formulae and Data on
"Heat Transfer for Engineers" p.29
Longman, 1977, ISBN 0 582 46050 6

APPENDIX 1 - THERMAL CONDUCTIVITY VERSUS TEMPERATURE DATA FOR THIN SPECIMENS OF INSULATING MATERIAL

This appendix shows how the temperature dependency of thermal conductivity for insulating materials may be obtained from relatively simple measurements. It also indicates how the through thickness homogeneity of coatings may be ascertained from the same measurements if the temperature dependency of thermal conductivity is already known.

Thermal Conductivity Testing of Thin Insulating Specimens

The disc specimen, of known thickness, is first subjected to a known temperature difference between its front and rear faces. The temperature difference should, for convenience, be an integral subdivision of the temperature range over which the thermal conductivity is to be determined. For example if the thermal conductivity is to be found between 20°C and 820°C, then this is an 800°C range which could be simply subdivided into 100°C sections as below : -

Front face	Rear face
20°C	120°C
20°C	220°C
20°C	320°C
20°C	420°C
20°C	520°C
20°C	620°C
20°C	720°C
20°C	820°C

The heat flow into the calorimeter is found for each of the above.
The following will explain the principles behind the method.
Consider a disc of material of known thickness and with uniform front and rear face temperatures

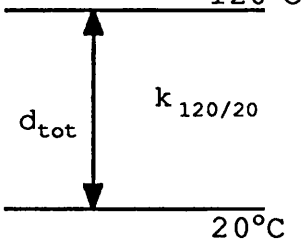

[1]

$$\dot{q}_{120/20} = \frac{k_{120/20}\,(120-20)}{d_{tot}} \Rightarrow k_{120/20} = \frac{d_{tot}\ \dot{q}_{120/20}}{(120-20)}$$

The mean value of "k" for the temperature range 20°C to 120°C has now been found.

Raise the front face temperature to 220°C

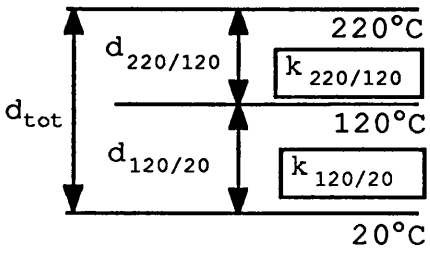

With the higher heat flux the thickness of material bounded by the 120°C and 20°C isotherms has shrunk, exactly in proportion to the ratio of the old heat flux to the new.

The thickness bounded by any pair of isotherms is dependent on the heat flux through the region, and so some form of denoting this must be given. The thicknesses will be fully described using a subscript to denote which isotherms bound the thickness, and a superscript which will define the heat flux at which this thickness exists. For example to denote the thickness of the region bounded by the 250°C and 200°C isotherms, when the region experiences that flux which exists when the whole body thickness is exposed to say 350°C and 50°C the following is used : -

$$d_{250/200}^{q350/50}$$

It is also evident that the thickness bounded by the 220°C and 120°C isotherms must be the total thickness minus the thickness bounded by the 120°C and 20°C isotherms.This may be expressed mathematically by the following expressions :-

$$d_{tot} = d^{q220/20}_{220/120} + d^{q220/20}_{120/20} \Rightarrow d^{q220/20}_{220/120} = d_{tot} - d^{q220/20}_{120/20} \quad [2]$$

Know that thickness decreases in ratio to flux :-

$$d^{q220/20}_{120/20} = d^{q120/20}_{120/20} \frac{q_{120/20}}{q_{220/20}} \quad [3]$$

$$d^{q220/20}_{220/120} = d_{tot} - d^{q120/20}_{120/20} \frac{q_{120/20}}{q_{220/20}} \qquad \text{but } d^{q120/20}_{120/20} = d_{tot}$$

$$\Rightarrow d_{220/120} = d_{tot} - d_{tot} \frac{q_{120/20}}{q_{220/120}} \quad [4]$$

Now the value of "k" for the temperature interval 120°C to 220°C can be found.

$$\text{Generally : -} \qquad d = \frac{k\,\Delta T}{\dot{q}} \quad [5]$$

Which implies that : -

$$d^{q220/20}_{220/120} = \frac{k_{220/120}(220-120)}{\dot{q}_{220/20}} \quad [6]$$

Eliminating the 220°/120° thickness from equations [4] and [6] gives : -

$$\frac{k_{220/120}(220-120)}{\dot{q}_{220/120}} = d_{tot} - d_{tot} \frac{q_{120/20}}{q_{220/20}}$$

$$k_{220/120} = \frac{d_{tot}}{(220-120)}\left(\dot{q}_{220/20} - \dot{q}_{120/20}\right)$$

The temperature on the front face of the specimen is now raised to 320°C

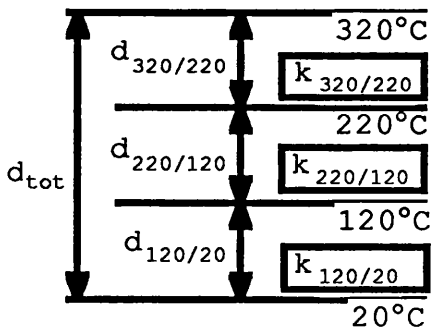

As for the previous increase in the front face temperature of the specimen, the total thickness may be subdivided as shown on the left.

The derivation of the expression for the thickness between the 220°C and 320°C isotherms is given next.

$$d_{tot} = d^{q320/20}_{320/220} + d^{q320/20}_{220/120} + d^{q320/20}_{120/20}$$

$$d^{q320/20}_{120/20} = d_{tot}\,\frac{q_{120/20}}{q_{320/20}} \qquad (A)$$

$$d^{q320/20}_{220/120} = d^{q220/20}_{220/120}\,\frac{q_{220/20}}{q_{320/20}} \qquad (B)$$

But $$d^{q220/20}_{220/120} = d_{tot} - d_{tot}\,\frac{q_{120/20}}{q_{220/20}} \qquad (C)$$

Substituting (C) in (B) gives

$$d^{q320/20}_{220/120} = \left\{d_{tot} - d_{tot}\,\frac{q_{120/20}}{q_{220/20}}\right\}\frac{q_{220/20}}{q_{320/20}}$$

This in turn gives the following : -

$$d^{q320/20}_{220/120} = d_{tot}\,\frac{q_{220/20}}{q_{320/20}} - d_{tot}\,\frac{q_{120/20}}{q_{320/20}} \qquad (D)$$

Substitution in the equation which heads the page : -

$$d^{q320/20}_{320/220} = d_{tot} - d_{tot}\,\frac{q_{120/20}}{q_{320/20}} - d_{tot}\,\frac{q_{220/20}}{q_{320/20}} + d_{tot}\,\frac{q_{120/20}}{q_{320/20}}$$

$$\Rightarrow d^{q320/20}_{320/220} = d_{tot} - d_{tot}\,\frac{q_{220/20}}{q_{320/20}}$$

But also : -

$$d^{q320/20}_{320/220} = \frac{k_{320/220}(320-220)}{q_{320/20}}$$

Eliminating $d^{q320/20}_{320/220}$ gives : -

$$d_{tot} - d_{tot}\frac{q_{220/20}}{q_{320/20}} = \frac{k_{320/220}(320-220)}{q_{320/20}}$$

From which the thermal conductivity for the range 220°C - 320°C is : -

$$k_{320/220} = \frac{d_{tot}}{(320-220)}(q_{320/20} - q_{220/20})$$

It may be seen that the assumption that the specimen is homogeneous through its thickness is essential for this approach to be correct. As the temperature difference across the specimen is increased the regions which are bounded by particular isotherms actually change their dimensions, within the specimen. This approach to the determination of thermal conductivity for thin insulating specimens could therefore be applied to determine their homogeneity.

APPENDIX 2 - GENERAL NOTES ON THE APPLICATION OF THERMOCOUPLES

The first section of this appendix deals with the general application of thermocouples, as temperature measuring devices. A simplified approach to the analysis of different thermocouple configurations is given.

The second section of the appendix applies a thermal resistance model to the situation arising when calibrating a thin film thermocouple in a furnace. This analysis shows the importance of taking care when calibrating thin film thermocouples.

Temperature Measurement using Thermocouples

Generally speaking thermocouple temperature sensors offer the advantage over many other types of temperature sensor in that they are capable of monitoring point temperatures, and owing to their mode of construction are capable of very fast response rates to changes in temperature. The basis of thermocouple operation is that when two dissimilar, electrically conductive materials are brought into intimate contact a potential difference will result which is dependent upon the temperature of that junction. This is an oversimplification of the situation but will serve to explain the steps which must be taken when using thermocouples if accurate results are to be obtained.

Thermocouple materials with good linearity of output e.m.f. versus temperature have been developed over many years. An ideal thermocouple would have the following characteristics : -

i/. wide operating temperature range
ii/. good linearity of e.m.f. generated versus temperature
iii/. excellent resistance to corrosion and negligible change of characteristics in harsh environments be they oxidising or reducing
iv/. long term stability
v/. large output e.m.f.
vi/. mechanical strength and absence of brittlenesss
vii/. manufactured from low cost materials
viii/. ease of forming the junction

As with most engineering solutions some compromises have to be made in the selection of a particular couple, as there is no single material combination which covers all situations. These materials have been developed over many years to provide as many of the above characteristics as possible but with particular combinations being favoured for certain applications. However, a number of standard material pairs are available which cover most situations. Standard thermocouple materials are most commonly found in wire form although strip is sometimes available. The material compositions are covered by standards around the world and a potential user may be confident that thermocouples made from certified material will conform to

these standards if the specified operating conditions are adhered to.

If obtained in wire form the user may construct the junction by a number of recognised jointing techniques, such as :- welding, brazing, and soldering. It is permissible to have an intermediate conducting medium between the two thermocouple materials in order that a junction be formed, but care must be exercised if this is to be done. Brazing or soldering alloys will have a melting point lower than that of the thermocouple materials and so the operating temperature limit of the thermocouple formed will be lower than that normally quoted for the thermocouple type. Embrittlement of the junction, caused by diffusion of the brazing alloy into the thermocouple materials may take place, making the junction more susceptible to mechanical damage, particularly if the junction is operated close to the brazing alloy's maximum temperature limit. Regardless of jointing technique, there may exist a shift in calibration due to residual strains in the thermocouple materials. Ideally this should be annealed out before the thermocouple is put into service.

It is strongly advised to run thermocouple material all the way from the junction to the measuring instrument, if this is at all possible. However, this may not always be case, particularly for the case of noble metal thermocouples where the cost of long runs of thermocouple material may be prohibitive. Another example is the situation where flexing of the wires is likely to take place, this may require the use of a different material which has better fatigue resistance.

The introduction of connecting cables which are not of the same material(s) as the thermocouple introduces secondary junctions to the measuring system and unless account is taken of this, erroneous readings will result.

Generally speaking there is some degree of confusion surrounding the use of thermocouples and thermocouple systems. The following explanation seeks to remedy this. First a generalised thermocouple system will be considered, followed by some examples of typical systems.

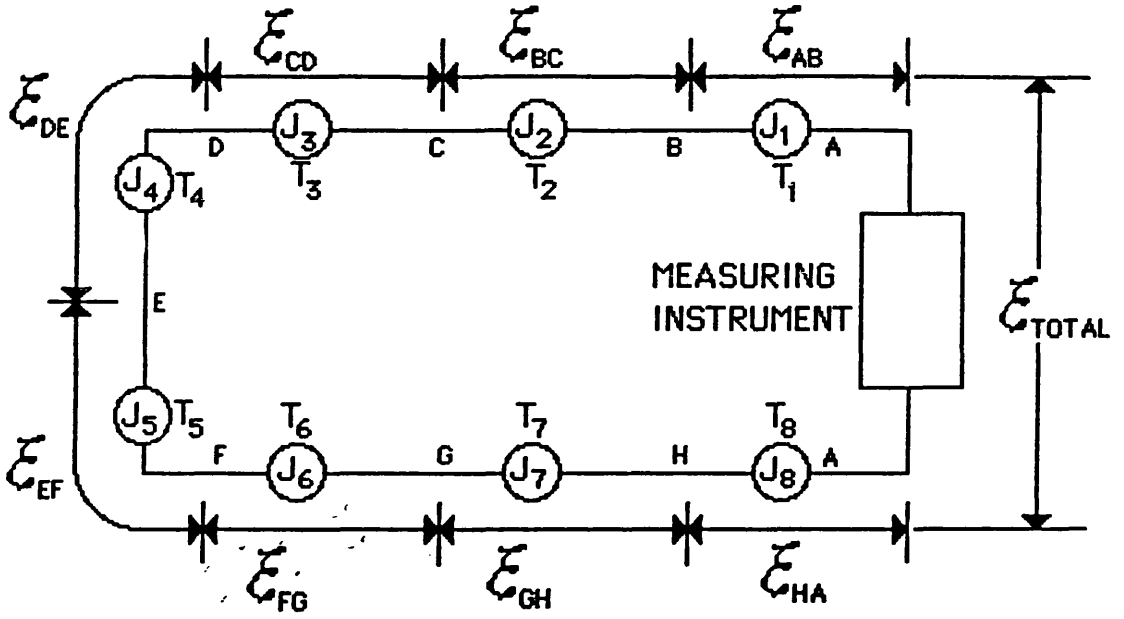

The net output from the thermocouple system may be found by summing the contributions from each of the individual junctions, taking care that each of the e.m.f.s is taken in the right sense. For the above case the following will result :-

$$\mathcal{E}_{TOT} = \mathcal{E}_{AB} + \mathcal{E}_{BC} + \mathcal{E}_{CD} + \mathcal{E}_{DE} + \mathcal{E}_{EF} + \mathcal{E}_{FG} + \mathcal{E}_{GH} + \mathcal{E}_{HA}$$

Now each of these e.m.f.s is temperature dependent and so more correctly the above expression should be written as follows :-

$$\mathcal{E}_{TOT}\{f(T)\} = \mathcal{E}_{AB}(T_1) + \mathcal{E}_{BC}(T_2) + \mathcal{E}_{CD}(T_3) + \mathcal{E}_{DE}(T_4) + \mathcal{E}_{EF}(T_5) + \mathcal{E}_{FG}(T_6) + \mathcal{E}_{GH}(T_7) + \mathcal{E}_{HA}(T_8)$$

where $\mathcal{E}_{xy}(T_z)$ is the e.m.f. generated by the junction of the two metals x and y at temperature Tz.
The above expression is for the general case and without resorting to having special calibrations for each of the dissimilar metal junctions, some simpification must be made if the system is to be of any practical use. Taking first the junction itself, most thermocouple junctions are physically small and thus there is normally negligible temperature difference across the junction, temperatures T4 and T5 may thus be said to be identical.

$$\mathcal{E}_{DE}[T_4] + \mathcal{E}_{EF}[T_5] = \mathcal{E}_{DE}[T4] + \mathcal{E}_{EF}[T4]$$

As the two materials D and F form junctions at the same temperature T4, with the material E then it may be said that material E has no effect upon the junction. This fact allows the construction of thermocouples by joining the principal materials with a third material of different composition, provided that there is no temperature difference across this jointing material. This is the case with all non-welded junctions such as those produced by either brazing or soldering. Thus it may be said that the following holds :-

$$\mathcal{E}_{DE}[T4] + \mathcal{E}_{EF}[T4] = \mathcal{E}_{DF}[T4]$$

More generally it may be stated that if two connected junctions are at the same temperature, the following holds :-

$$\mathcal{E}_{MN}[T] + \mathcal{E}_{NO}[T] = \mathcal{E}_{MO}[T]$$

A further more obvious rule which may be applied is that regardless of the temperature, the e.m.f. generated when two identical composition wires are joined, is zero :-

$$\mathcal{E}_{PP}[T] = 0$$

Now from these two basic rules most situations regarding thermocouples may be simply treated.
Four common situations will now be treated as examples.

i/. simple T/C, thermocouple wires brought straight back to the measuring instrument.

ii/. remote T/C plus copper leads to the measuring instrument.

iii/. possible configuration for calibration of an unknown pair of materials.

iv/. alternative configuration for calibration of unknown pair of materials.

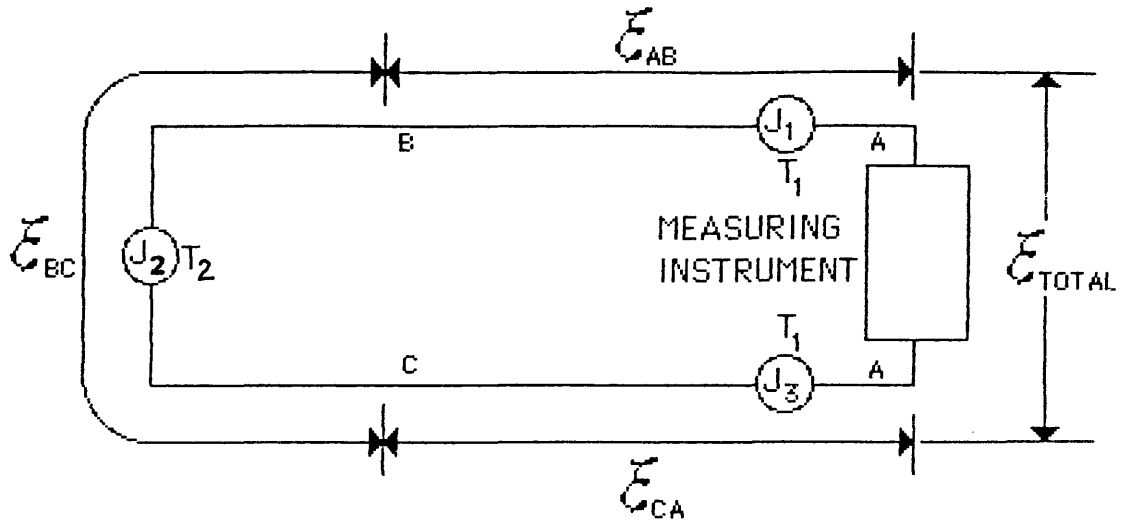

Example 1 :-

This is probably the simplest of the cases possible with one thermocouple junction, the output of which is brought back to the measuring instrument with the same materials as used for the junction. The expression written down earlier for the general case may be reduced to :-

$$\mathcal{E}_{TOT} = \mathcal{E}_{AB}(T1) + \mathcal{E}_{BC}(T2) + \mathcal{E}_{CA}(T1)$$

Now $\mathcal{E}_{AB}(T1) = -\mathcal{E}_{BA}(T1)$ and $\mathcal{E}_{CA}(T1) = -\mathcal{E}_{AC}(T1)$

$$\Rightarrow \mathcal{E}_{AB}(T1) + \mathcal{E}_{CA}(T1) = -\{\mathcal{E}_{BA}(T1) + \mathcal{E}_{AC}(T1)\}$$

$$= -\mathcal{E}_{BC}(T1)$$

The full equation now reduces to :-

$$\mathcal{E}_{TOT} = \mathcal{E}_{BC}(T2) - \mathcal{E}_{BC}(T1) = \mathcal{E}_{BC}(T2-T1)$$

This simply states that if the temperature at the measuring instrument is known, then the temperature of the sensing junction can also be found. In modern instruments the temperature of the measuring instrument is sensed internally by an absolute temperature sensor such as a platinum resistance sensor or by a semiconductor sensor. This internal temperature is then added to that produced by the thermocouple system.

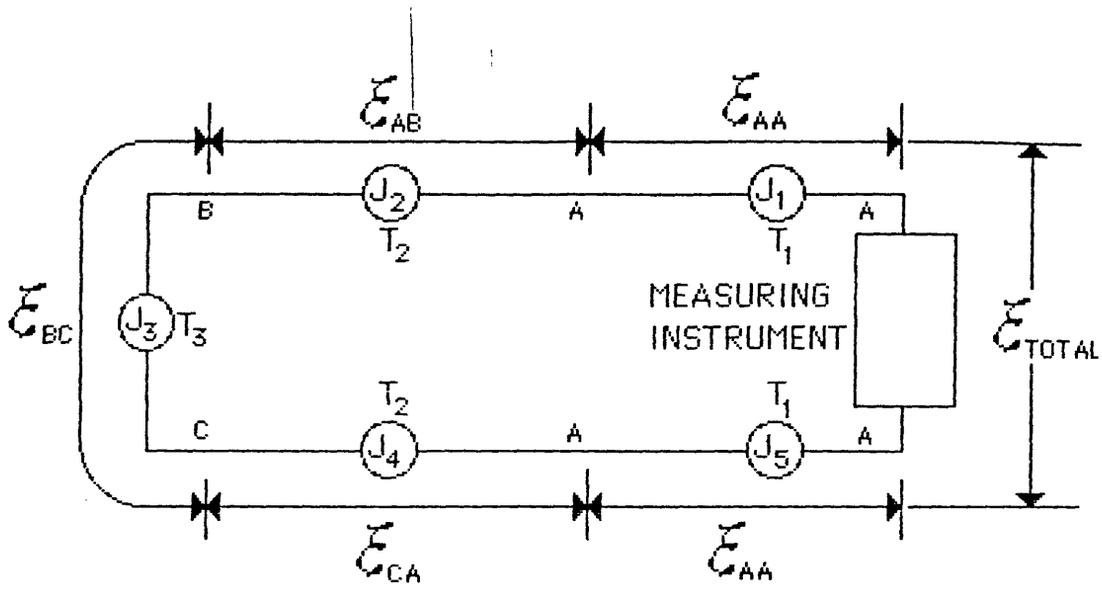

Example 2 :-

This is a thermocouple configuration which is used in certain situations where the use of thermocouple material might cause premature failure, such as where the output of the thermocouple has to be taken from a moving object (e.g. a piston) to a stationary point. In this situation the use of copper conductors can reduce the possibility of fatigue failure, due to bending or twisting of the leadout wires. The expression for this case may be written thus :-

$$\mathcal{E}_{TOT} = \mathcal{E}_{AA}(T1) + \mathcal{E}_{AB}(T2) + \mathcal{E}_{BC}(T3) + \mathcal{E}_{CA}(T4) + \mathcal{E}_{AA}(T1)$$

This reduces to :- $\mathcal{E}_{TOT} = \mathcal{E}_{AB}(T2) + \mathcal{E}_{BC}(T3) + \mathcal{E}_{CA}(T4)$

If T2 = T4 $\Rightarrow$ $\mathcal{E}_{TOT} = \mathcal{E}_{AB}(T2) + \mathcal{E}_{BC}(T3) + \mathcal{E}_{CA}(T2)$

As before $\mathcal{E}_{AB}(T2) = -\mathcal{E}_{BA}(T2)$ and $\mathcal{E}_{CA}(T2) = -\mathcal{E}_{AC}(T2)$

$$\Rightarrow \mathcal{E}_{AB}(T2) + \mathcal{E}_{CA}(T2) = -\{\mathcal{E}_{BA}(T2) + \mathcal{E}_{AC}(T2)\}$$

$$= -\mathcal{E}_{BC}(T2)$$

Which gives :- $\mathcal{E}_{TOT} = \mathcal{E}_{BC}(T3) - \mathcal{E}_{BC}(T2) = \mathcal{E}_{BC}(T3 - T2)$

This shows that for this situation it is essential to monitor the temperature of the junctions J2 and J4, that is temperature T2. For the case of the piston a thermistor bead sensor is placed at

this junction to give an absolute temperature measurement at this point. This temperature is then added to that which is equivalent to the e.m.f. generated by the thermocouple junction at T3. For high accuracy work it should be noted that strictly speaking the equivalence

$$\mathcal{E}_{XY}(T1) - \mathcal{E}_{XY}(T2) = \mathcal{E}_{XY}(T1 - T2)$$

is only true if the e.m.f. generated is truly linear with temperature. However, the commonly used thermocouple combinations are of good linearity and an error of less than 5°C is likely to be incurred as a result of this approximation. If it is essential to reduce the error below this level then the e.m.f. generated by the junction must be compared with a standard calibration table of the thermocouple pair at the temperature registered by the additional sensor.

Example 3 :-

This situation shows one possible configuration for the calibration of an unknown thermocouple pair. In this case the

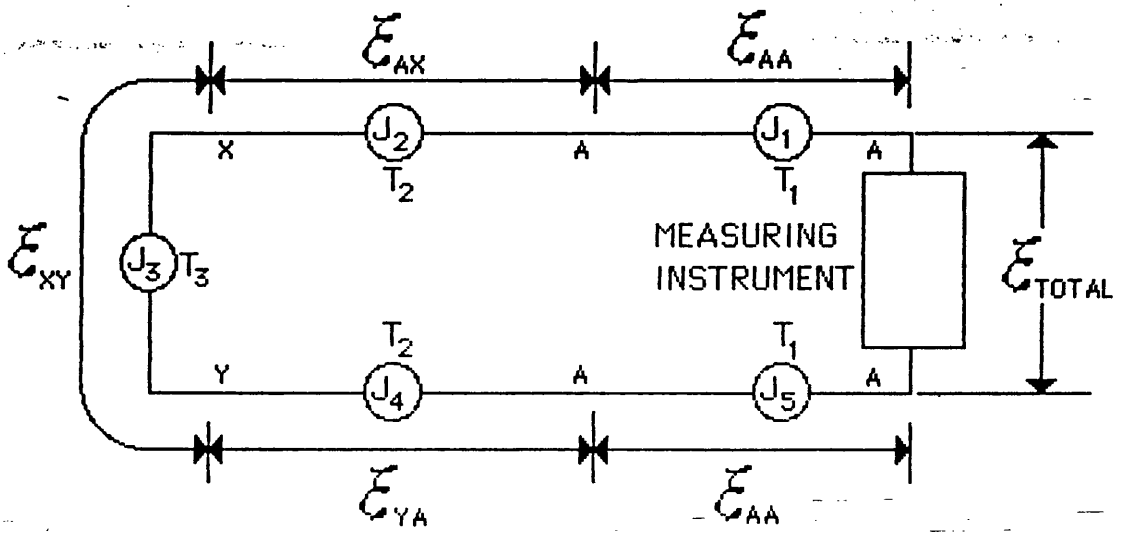

output of the thermocouple pair is brought back to the measuring instrument using identical leadout wires (e.g. copper).
This is identical to the previous case but with unknown materials in place of the known thermocouple materials. The expression for this setup is therefore :-

$$\mathcal{E}_{TOT} = \mathcal{E}_{XY}(T3) - \mathcal{E}_{XY}(T2) \simeq \mathcal{E}_{XY}(T3 - T2)$$

For calibration purposes it is therefore essential to know both the temperatures T2 and T3. If the calibration is carried out in a salt bath the temperature of the salt bath is usually known to a reasonable degree of accuracy, as these baths are nearly always temperature controlled. For the case of calibrations carried out in a furnace the temperature controllers tend to be of lower accuracy and so it is wise to place a reference thermocouple in good thermal contact with the junction to give T3 to high accuracy. In either case, it is important that the two secondary junctions are thermally isolated from the primary junction under test, otherwise the temperature difference T3 - T2 will be too small to register any reasonable signal. In the extreme case of T3 - T2 = 0 for the example above, then the e.m.f. generated drops to zero.

Summing up for the example above, it is essential that junctions J2 and J4 are thermally isolated and that both the temperatures T3 and T2 are monitored if accurate calibration is to be performed.

Example4 :-

This is the last example and gives an alternative system for the calibration of unknown thermocouple materials. In this case the output from the unknown thermocouple pair is

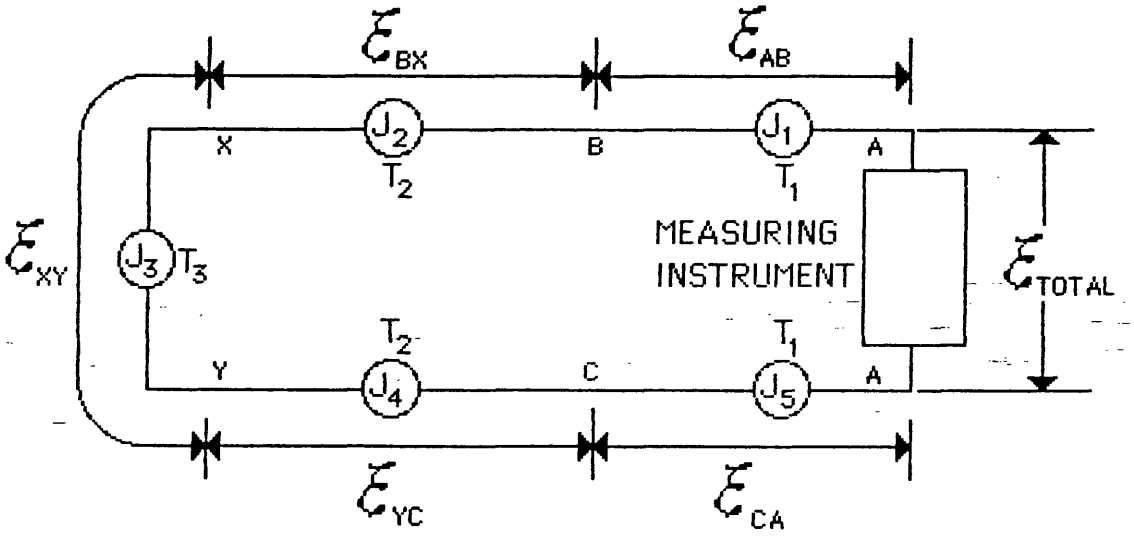

returned to the instrument via a pair of thermocouple wires of known calibration. The expression for this case will now be given.

$$\mathcal{E}_{TOT} = \mathcal{E}_{AB}(T1) + \mathcal{E}_{BX}(T2) + \mathcal{E}_{XY}(T3) + \mathcal{E}_{YC}(T2) + \mathcal{E}_{CA}(T1)$$

Now $\mathcal{E}_{AB}(T1) = -\mathcal{E}_{BA}(T1)$ and $\mathcal{E}_{CA}(T1) = -\mathcal{E}_{AC}(T1)$

$$\Rightarrow \mathcal{E}_{AB}(T1) + \mathcal{E}_{CA}(T1) = -\{\mathcal{E}_{BA}(T1) + \mathcal{E}_{AC}(T1)\} = -\mathcal{E}_{BC}(T1)$$

Also $\mathcal{E}_{BX}(T2) + \mathcal{E}_{YC}(T2) = \mathcal{E}_{BC}(T2)$

Which gives :-

$$\mathcal{E}_{TOT} = \mathcal{E}_{XY}(T3) + \mathcal{E}_{BC}(T2) - \mathcal{E}_{BC}(T1) \simeq \mathcal{E}_{XY}(T3) + \mathcal{E}_{BC}(T2 - T1)$$

This expression shows that it is not sufficient to know only T3 and T2 , but that it is also required that the instrument temperature T1 be known as well. If materials X and B are the same and materials Y and C are the same then the expression reduces to

$$\mathcal{E}_{TOT} = \mathcal{E}_{BC}(T3) + \mathcal{E}_{CC}(T2) - \mathcal{E}_{BC}(T1) = \mathcal{E}_{BC}(T3) - \mathcal{E}_{BC}(T1)$$

$$\propto \mathcal{E}_{BC}(T3 - T1)$$

which is the expression which was obtained for the first example. It could be argued that this is a method which might indicate whether or not a thermocouple pair conformed to the required specification. Although this is true it is not a calibration method unless all three temperatures are monitored, and in this sense it is easier to use the first of the calibration systems analysed.

APPENDIX 3 - PROGRAM LISTING FOR THE CALCULATION OF FLUX LEVELS ARISING FROM MULTIPLE SOURCES

This appendix covers the programs which were used in the design of the first lamp/reflector assembly for the THERMAL SHOCK TEST RIG.

THERMSHOCK2000DOC is a documented BASIC program, and was the development program for the later FORTRAN program paraRUNS9.fortran. The BASIC program has been thoroughly documented with explanatory statements. **Figure A3.1,** shows the layout which is to be analysed by the program. The user sets the number of lamps, the position of the reflectors and their critical dimensions and positions. It should be remarked that the program assumes simple two dimensional geometry. The actual values of flux should thus be considered in relative, rather than absolute terms, even though the values shown are in absolute units.

THERMSHOCK2000DOC Program Listing

```
100 REM**********************************
110 REM**DOCUMENTED VERSION OF
120 REM*THERMSHOCK2000---SAVED ON TAPE
130 REM*AS "THERMSHOCK2000DOC"  ******
140 REM**********************************
150 DIM A(100),B(100),OB(100),W(100),NT(100),WU(100),NO(100),OW(10
160 DIM HM(100,10),PH(100,10),TD(100),PT(100),OM(100)
170 OPEN1,4,1
180 PRINT#1,"CALCULATION OF INCIDENT POWER VARIATION ACROSS"
190 PRINT#1,"SURFACE OF SPECIMEN IN THERMAL SHOCK TEST RIG"
200 PRINT#1,"USING A PARABOLIC REFLECTOR AND LINE SOURCE"
210 PRINT#1," "
220 INPUT"NUMBER OF LAMPS(MAX.10)=";NL
230 INPUT"FIELD WIDTH OF INTEREST =";FW
240 INPUT"NUMBER OF POINTS IN MAIN BEAM =";N
250 INPUT"NUMBER OF OUTPUT POINTS =";N1
260 PRINT#1,NL;"LAMPS"
270 PRINT#1,"FIELD WIDTH OF INTEREST ="FW;"METRES"
280 PRINT#1,"NO. OF OUTPUT POINTS ="N1
290 REM**POWER NORMALIZING CONSTANT**
300 NP=1.0E+06
310 OPEN2,4,2
320 REM**OUTER LAMP LOOP**
330 FOR S=1TONL
340 REM**SCREEN PRINT LAMP NUMBER**
350 PRINT"LAMP";S"DATA"
360 REM**INDIVIDUAL LAMP INPUT DATA**
370 INPUT" FOCAL LENGTH OF REFLECTOR (M)=";F
380 INPUT"REFLECTOR HALF APERTURE SIZE (M)=";YA
390 INPUT"FOCAL POINT TO SPECIMEN PLANE DISTANCE =";FS
400 INPUT"REFLECTOR AXIS TO SPECIMEN PLANE ANGLE =";AL
410 INPUT"LAMP DISTANCE FROM ORIGIN=";OL
420 PRINT#1," "
430 REM**PRINT LAMP INPUT DATA**
440 PRINT#1,"LAMP NUMBER";S
450 PRINT#1,"FOCAL LENGTH OF PARABOLIC REFLECTOR ="F;"METRES"
460 PRINT#1,"PARABOLIC REFLECTOR HALF APERTURE SIZE ="YA;"METRES"
470 PRINT#1,"FOCAL POINT TO SPECIMEN PLANE DISTANCE ="FS;"METRES"
480 PRINT#1,"REFLECTOR AXIS TO SPECIMEN PLANE ANGLE ="AL;"RADIANS"
490 PRINT#1,"LAMP DISTANCE FROM ORIGIN =";OL;"METRES"
500 PRINT#1," "
510 REM*CALCULATE FOCUS/APERTURE ANGLE*
520 AZ=ATN(YA/(((YA↑2)/(4*F))-F))
530 REM**FIX DELTA ANGLE**
540 EL=1.0E-05
550 E2=EL
560 REM**INITIALIZE I FOR MAIN BEAM
570 REM*CALCULATIONS**
580 I=1
590 REM**SET FIRST ANGLE IN MAIN BEAM**
600 A(I)=AZ
610 REM**CALCULATE ANGLE INCREMENT**
620 DA=2*(π-AZ)/N
```

```
630 REM**START OF MAIN BEAM LOOP**
640 REM**FIRST CALCULATE INDIRECT/
650 REM*REFLECTED POWER**
660 Y1=4*F*SIN(A(I))/(2*(1-COS(A(I))))/COS(AL)+FS*TAN(AL)
670 Y2=4*F*SIN(A(I)+E2)/(2*(1-COS(A(I)+E2)))/COS(AL)+FS*TAN(AL)
680 X=ABS(Y1-Y2)
690 W(I)=(Y1+Y2)/2
700 PI=(1/X)*0.9
710 REM**DIRECT POWER CALCS. IN MAIN*
720 REM*BEAM**
730 DB=ATN(Y1/FS)-ATN(Y2/FS)
740 PD=DB/(E2*X)
750 REM**TOTAL POWER IN MAIN BEAM**
760 TP=PI+PD
770 REM**NORMALIZE TOTAL MAIN BEAM
780 REM*POWER**
790 NT(I)=TP/NP
800 REM**INCREMENT ANGLE**
810 I=I+1
820 A(I)=A(I-1)+DA
830 REM*DELTA SIGN CHANGE FOR SYMMETRY*
840 IFA(I)>πTHENE2=-EL
850 REM**CHECK ON ANGLE**
860 IF(A(I)-EL)>(2*π-AZ)GOTO890
870 REM**END OF MAIN BEAM LOOP**
880 GOTO 660
890 C1=I
900 REM**INITIALIZE J FOR FORWARD BEAM
910 REM*CALCULATIONS**
920 J=1
930 REM*SET FIRST ANGLE IN FORWARD BEAM*
940 B(J)=ATN((FS*TAN(AL)+YA/COS(AL))/FS)+(DA/10)
950 REM**START OF FORWARD BEAM LOOP**
960 Y1=FS*TAN(B(J))
970 Y2=FS*TAN(B(J)+EL)
980 X=Y2-Y1
990 WO(J)=(Y2+Y1)/2
1000 REM**FORWARD BEAM POWER**
1010 PO=1/X
1020 REM**NORMALIZE FORWARD BEAM POWER**
1030 NO(J)=PO/NP
1040 REM**INCREMENT ANGLE**
1050 J=J+1
1060 B(J)=B(J-1)+DA
1070 REM**CHECK ANGLE WITH FORWARD BEAM
1080 REM*LIMIT**
1090 IF B(J)>(AZ+AL)ORB(J)>(π/2)GOTO1120
1100 REM**END OF FORWARD BEAM LOOP**
1110 GOTO960
1120 C2=J
```

```
1130 REM**INITIALIZE M FOR REVERSE BEAM
1140 REM*CALCULATIONS**
1150 M=1
1160 REM*SET FIRST ANGLE IN REVERSE BEAM*
1170 OB(M)=ATN((FS*TAN(AL)-YA/COS(AL))/FS)-(DA/10)
1180 REM**START OF REVERSE BEAM LOOP**
1190 Y1=FS*TAN(OB(M))
1200 Y2=FS*TAN(OB(M)-EL)
1210 X=Y1-Y2
1220 OW(M)=(Y2+Y1)/2
1230 REM**REVERSE BEAM POWER**
1240 OP=1/X
1250 REM**NORMALIZE REVERSE BEAM POWER**
1260 OM(M)=OP/NP
1270 REM**INCREMENT ANGLE**
1280 M=M+1
1290 OB(M)=OB(M-1)-DA
1300 REM**CHECK ANGLE WITH REVERSE BEAM
1310 REM*LIMIT**
1320 IF OB(M)<(-AZ+AL)OROB(M)<(-π/2)GOTO1350
1330 REM**END OF REVERSE BEAM LOOP**
1340 GOTO 1190
1350 C3=M
1360 REM**REARRANGE POWER AND DISTANCE
1370 REM*OUTPUTS IN ASCENDING ORDER**
1380 K=1
1390 FOR M=(C3-1)TO1STEP-1
1400 HM(K,S)=OW(M)+OL
1410 PH(K,S)=OM(M)
1420 K=K+1
1430 NEXTM
1440 FOR I=(C1-1)TO1STEP-1
1450 HM(K,S)=W(I)+OL
1460 PH(K,S)=NT(I)
1470 K=K+1
1480 NEXTI
1490 FOR J=1TO(C2-1)
1500 HM(K,S)=WO(J)+OL
1510 PH(K,S)=NO(J)
1520 K=K+1
1530 NEXTJ
1540 C4=K
1550 REM**END OUTPUT REARRANGEMENT**
1560 IFNM<<C4-1)THENNM=(C4-1)
1570 NEXT S
1580 REM**END OF OUTER LOOP**
1590 REM**SET POSITION INCREMENT**
1600 DX=FW/N1
1610 REM**INITIALIZE I FOR POSITION
1620 REM*STEPPING**
1630 I=1
1640 REM**CALCULATE START POSITION**
1650 T?(I)=-(FW/2)
```

```
1660 REM**START OF POSITION STEPPING
1670 REM*LOOP**
1680 I=I+1
1690 REM**INCREMENT POSITION**
1700 TD(I)=TD(I-1)+DX
1710 REM**CHECK POSITION WITH LIMIT**
1720 IFTD(I)>(FW/2)GOTO2030
1730 REM**LIMIT FOR PRINT PURPOSES**
1740 IM=I
1750 REM**LAMP LOOP FOR POWER
1760 REM*INTERPOLATION SECTION**
1770 FORS=1TONL
1780 REM**INITIALIZE K**
1790 K=0
1800 REM**INCREMENT K AND CHECK IF
1810 REM*BEYOND ARRAY LIMIT**
1820 K=K+1:IFK>NMGOTO2000
1830 REM**CHECK IF BEYOND ARRAY**
1840 IFPH(K,S)=0GOTO2000
1850 REM**CHECK IF POSITION VALUE
1860 REM*BELOW LOWER ARRAY LIMIT**
1870 IF TD(I)<HM(1,S)GOTO2000
1880 REM**BRANCH TO INTERPOLATION IF
1890 REM*CHECK TRUE**
1900 IFTD(I)<HM(K,S)GOTO1940
1910 REM**END OF ARRAY LOOP**
1920 GOTO1820
1930 REM**INTERPOLATION CALCULATIONS**
1940 V1=(PH(K,S)-PH((K-1),S))/(HM(K,S)-HM((K-1),S))
1950 V2=TD(I)-HM((K-1),S)
1960 V3=(V1*V2)+PH((K-1),S)
1970 REM**SUM LAMP CONTRIBUTION**
1980 PT(I)=PT(I)+V3
1990 REM**END OF LAMP LOOP**
2000 NEXTS
2010 REM**END OF POSITION STEPPING LOOP*
2020 GOTO1680
2030 PRINT#1," "
2040 REM**PRINT OUTPUT TITLES**
2050 PRINT#1," HEIGHT FROM            NORMALISED"
2060 PRINT#1,"CENTRELINE (M)       INCIDENT POWER"
2070 REM**OUTPUT PRINT LOOP**
2080 FOR I=1TOIM
2090 PRINT#2
2100 PRINT#2,"    S9.9999              S99.9999
2110 PRINT#1,TD(I),PT(I)
2120 REM**END OUTPUT PRINT LOOP**
2130 NEXTI
2140 CLOSE1:CLOSE2
2150 END
```

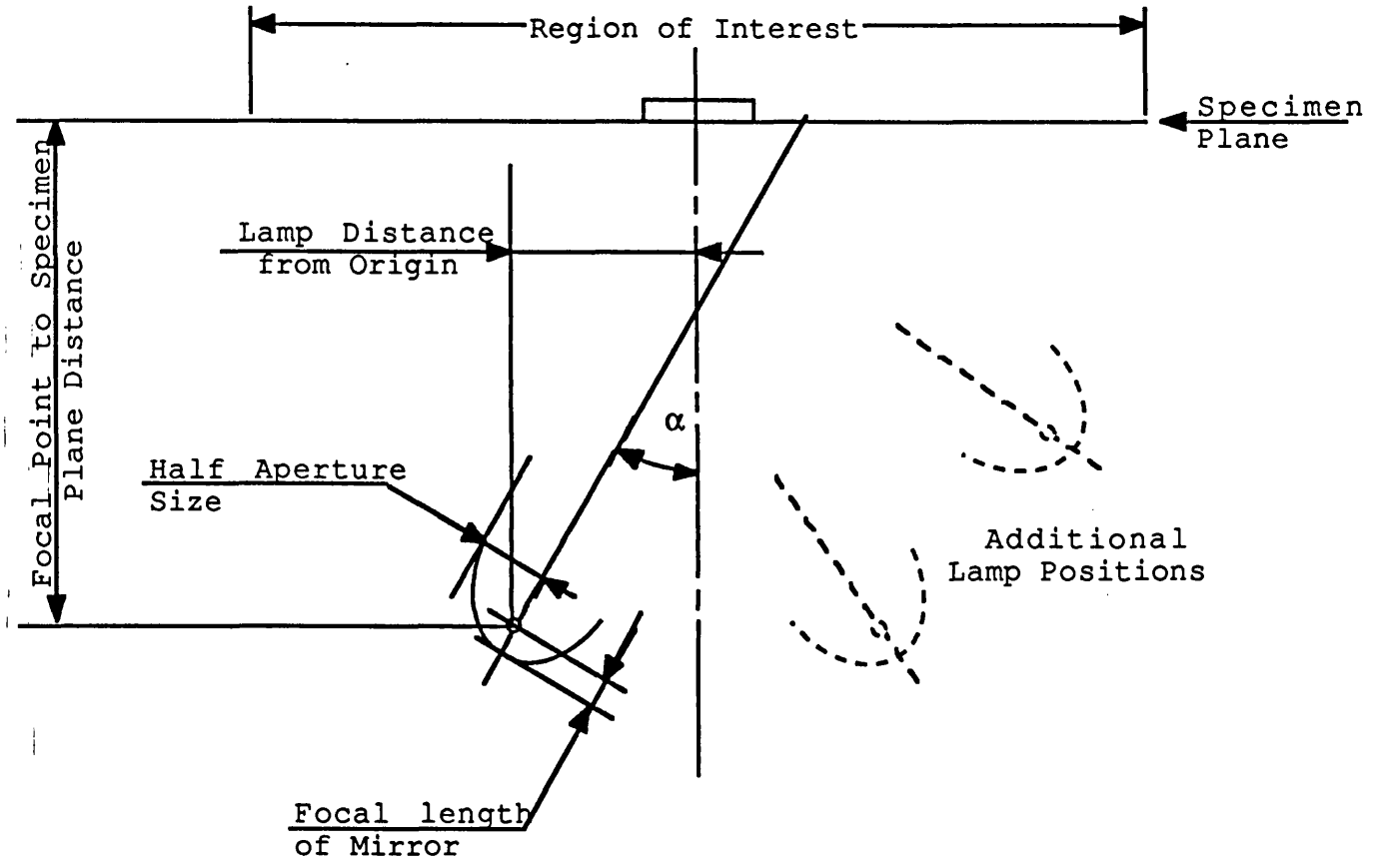

Figure A3.1 - Layout of Model used to Calculate the Flux at the Specimen Plane of the Thermal Shock Test Rig

The major assumptions which are made by this model are that the lamps behave as point sources, and radiate equally around their envelope. The mirrors are all assumed to be perfect parabolas and that the lamps sit at the focal points of the mirrors.

INPUT DATA FOR SERIES OF RUNS WITH PARARUNS9 RUNNING ON MULTICS

LAMP CONFIGURATION

HELD CONSTANT DURING SERIES OF RUNS
NUMBER OF LAMPS =2
FIELD WIDTH OF INTEREST =0.2 METRES
NUMBER OF CALCULATED POINTS =80
NUMBER OF OUTPUTTED POINTS =80
SOURCE LENGTH =0.1250 METRES
INDIVIDUAL LAMP POWER =1250 WATTS
HALF APERTURE SIZE =0.040 METRES
REFLECTOR FOCAL LENGTHS =0.010 METRES

INPUT FOR PLOT5A
0.5 0.2544 -0.130
0.5 -0.2544 0.130

INPUT FOR PLOT5B
0.5 0.2450 -0.130
0.5 -0.2450 0.130

INPUT FOR PLOT5C
0.5 0.2356 -0.130
0.5 -0.2356 0.130

INPUT FOR PLOT5D
0.5 0.2261 -0.130
0.5 -0.2261 0.130

INPUT FOR PLOT5E
0.5 0.2166 -0.130
0.5 -0.2166 0.130

INPUT FOR PLOT5F
0.5 0.2070 -0.130
0.5 -0.2070 0.130

INPUT FOR PLOT5G
0.5 0.1974 -0.130
0.5 -0.1974 0.130

INPUT FOR PLOT5H
0.5 0.1878 -0.130
0.5 -0.1878 0.130

INPUT FOR PLOT5I
0.5 0.1781 -0.130
0.5 -0.1781 0.130

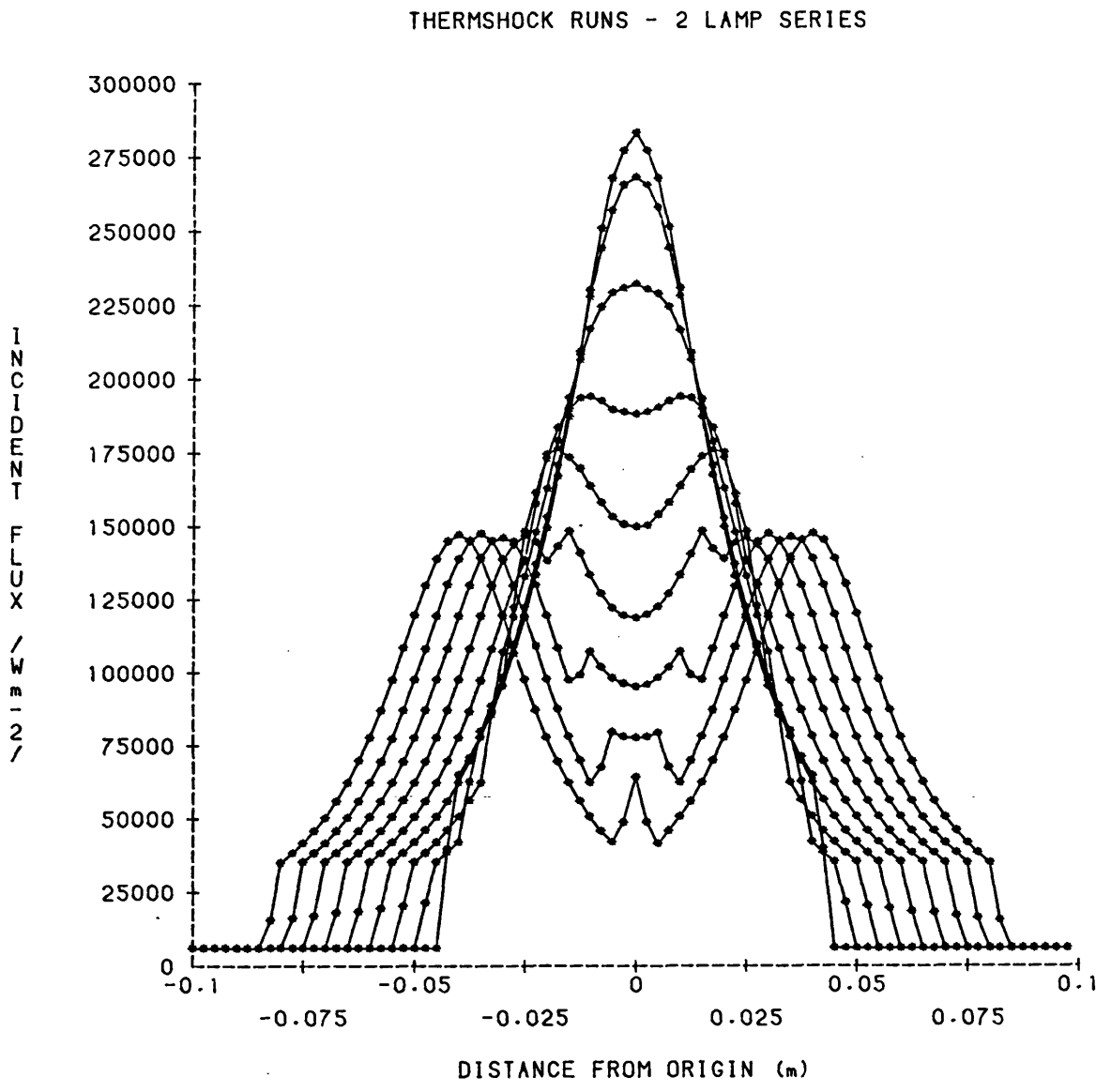
THERMSHOCK RUNS - 2 LAMP SERIES
INCIDENT FLUX /Wm-2/
300000
275000
250000
225000
200000
175000
150000
125000
100000
75000
50000
25000
0
-0.1
-0.075
-0.05
-0.025
0
0.025
0.05
0.075
0.1
DISTANCE FROM ORIGIN (m)

INPUT DATA FOR SERIES OF RUNS WITH PARARUNS9 RUNNING ON MULTICS

FOUR LAMP CONFIGURATION

HELD CONSTANT DURING SERIES OF RUNS
NUMBER OF LAMPS =4
FIELD WIDTH OF INTEREST =0.2 METRES
NUMBER OF CALCULATED POINTS =80
NUMBER OF OUTPUTTED POINTS =80
SOURCE LENGTH =0.1250 METRES
INDIVIDUAL LAMP POWER =1250 WATTS
HALF APERTURE SIZE =0.040 METRES
REFLECTOR FOCAL LENGTH =0.010 METRES

INPUT FOR PLOT2A

0.5	0.3719	-0.195
0.5	0.1293	-0.065
0.5	-0.1293	0.065
0.5	-0.3719	0.195

INPUT FOR PLOT2B

0.5	0.3632	-0.195
0.5	0.1194	-0.065
0.5	-0.1194	0.065
0.5	-0.3632	0.195

INPUT FOR PLOT2C

0.5	0.3544	-0.195
0.5	0.1096	-0.065
0.5	-0.1096	0.065
0.5	-0.3544	0.195

INPUT FOR PLOT2D

0.5	0.3456	-0.195
0.5	0.0997	-0.065
0.5	-0.0997	0.065
0.5	-0.3456	0.195

INPUT FOR PLOT2E

0.5	0.3367	-0.195
0.5	0.0898	-0.065
0.5	-0.0898	0.065
0.5	-0.3367	0.195

INPUT FOR PLOT2F

0.5	0.3277	-0,195
0.5	0.0798	-0.065
0.5	-0.0798	0.065
0.5	-0.3277	0.195

INPUT FOR PLOT2G

```
0.5  0.3188  -0.195
0.5  0.0699  -0.065
0.5 -0.0699   0.065
0.5 -0.3188   0.195
```

INPUT FOR PLOT2H

```
0.5  0.3097  -0.195
0.5  0.0599  -0.065
0.5 -0.0599   0.065
0.5 -0.3097   0.195
```

INPUT FOR PLOT2I

```
0.5  0.3006  -0.195
0.5  0.0500  -0.065
0.5 -0.0500   0.065
0.5 -0.3006   0.195
```

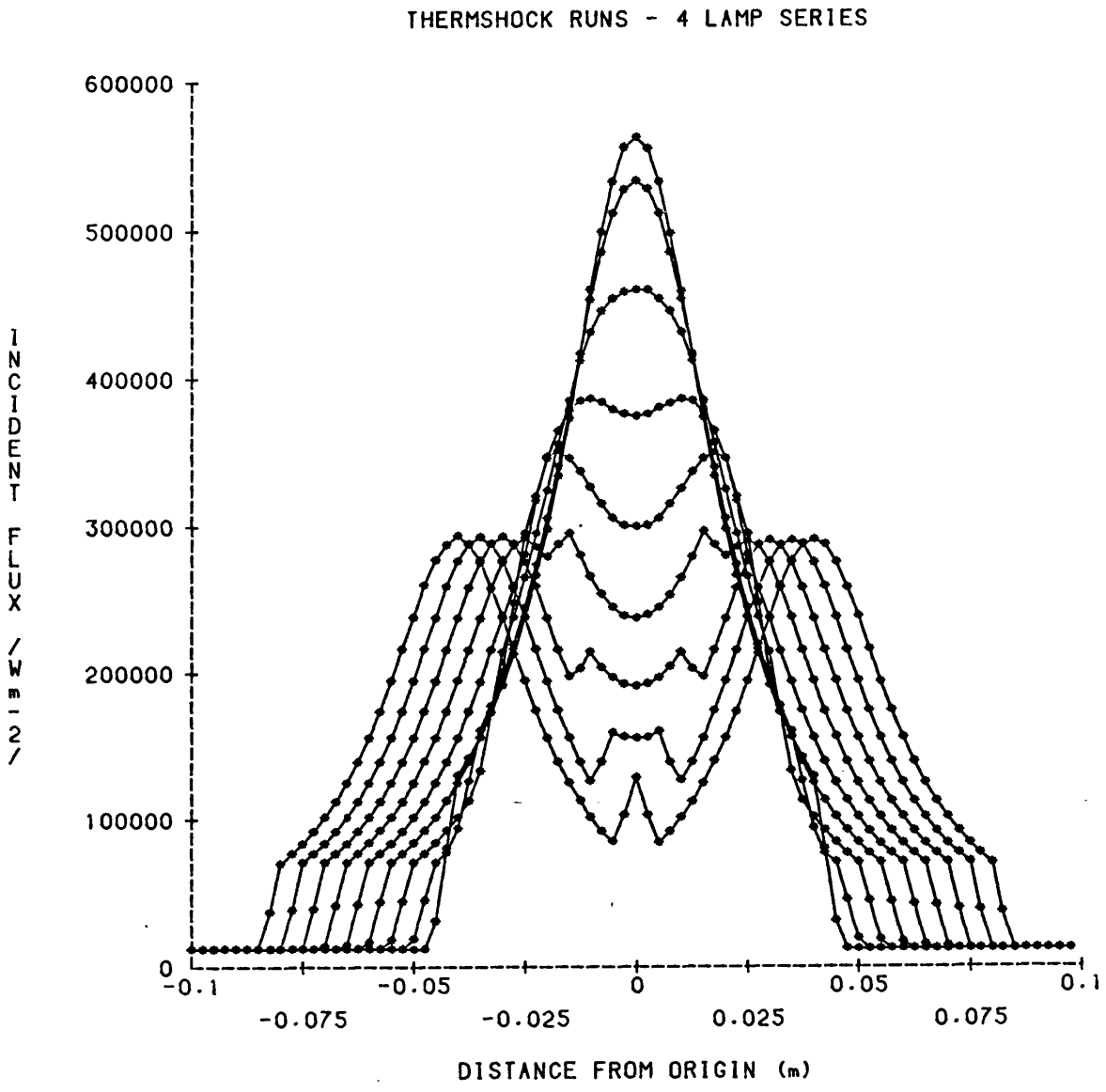
THERMSHOCK RUNS - 4 LAMP SERIES
INCIDENT FLUX /Wm-2/
600000
500000
400000
300000
200000
100000
0
-0.1
-0.075
-0.05
-0.025
0
0.025
0.05
0.075
0.1
DISTANCE FROM ORIGIN (m)

INPUT DATA FOR SERIES OF RUNS WITH PARARUNS9 RUNNING ON MULTICS

TWO LAMP CONFIGURATION

HELD CONSTANT DURING SERIES OF RUNS
NUMBER OF LAMPS =2
FIELD WIDTH OF INTEREST =0.2 METRES
NUMBER OF CALCULATED POINTS =80
NUMBER OF OUTPUTTED POINTS =80
SOURCE LENGTH =0.1250 METRES
INDIVIDUAL LAMP POWER =1250 WATTS
HALF APERTURE SIZE =0.040 METRES
REFLECTOR FOCAL LENGTHS =0.010 METRES

INPUT FOR PLOT4A
0.5 0.2261 -0.115
0.5 -0.2261 0.115

INPUT FOR PLOT4B
0.5 0.2166 -0.115
0.5 -0.2166 0.115

INPUT FOR PLOT 4C
0.5 0.2070 -0.115
0.5 -0.2070 0.115

INPUT FOR PLOT4D
0.5 0.1974 -0.115
0.5 -0.1974 0.115

INPUT FOR PLOT4E
0.5 0.1878 -0.115
0.5 -0.1878 0.115

INPUT FOR PLOT4F
0.5 0.1781 -0.115
0.5 -0.1781 0.115

INPUT FOR PLOT4G
0.5 0.1648 -0.115
0.5 -0.1684 0.115

```
INPUT FOR PLOT4H
          0.5  0.1587  -0.115
          0.5 -0.1587   0.115

INPUT FOR PLOT4I
          0.5  0.1489  -0.115
          0.5 -0.1489   0.115
```

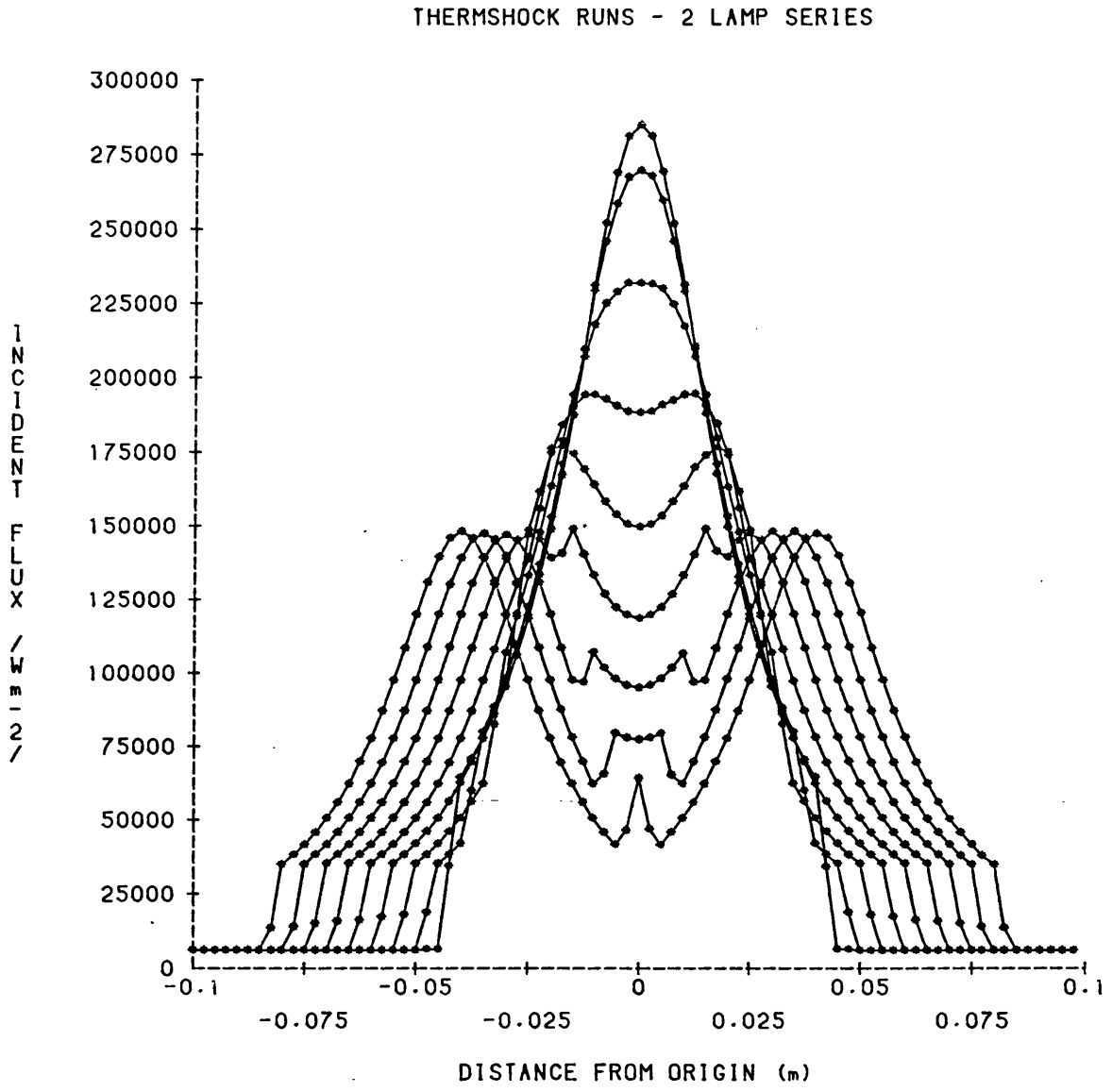
THERMSHOCK RUNS - 2 LAMP SERIES
INCIDENT FLUX /Wm-2/
300000
275000
250000
225000
200000
175000
150000
125000
100000
75000
50000
25000
0
-0.1
-0.075
-0.05
-0.025
0
0.025
0.05
0.075
0.1
DISTANCE FROM ORIGIN (m)

APPENDIX 4 - ANALYSIS OF FUEL FLOW ERROR DUE TO DAMPER

This appendix outlines an analysis which was instigated after doubts arose, regarding the repeatability of fuel flow measurements on the firing engine test rig. The problem was traced to a damper which had been inserted in the fuel line to enable reliable reading of volumetric fuel flow using a burette. Prior to the insertion of the damper, considerable difficulties had been experienced in taking readings from the burette due to :-

i). violent oscillations of the fuel column

ii). frothing of the fuel in the burette as a result of the oscillations.

The analysis shows that the error in fuel flow measurement can be substantial. However, if care is taken to minimise the volume of air in the damper, then the error becomes negligible. Alternatively, if the volume of air in the damper is known, then the error may be compensated for.

Basically the origin of the error brought about by the inclusion of the damper arises as follows :-

Initially, on charging the system with fuel, the tapped vent is open to atmosphere to allow fuel into the damper. At some point the vent is closed, and fuel ceases to flow into the damper when the pressure in the gas space equals the pressure head developed by the day tank (which is vented to atmosphere, but which resides some distance above the damper. Let this initial condition in the damper be defined by P_1, V_1. P_1 is simply calculated from the mean tank head, the fuel density and gravitational acceleration.

$$P_1 = \rho_f g h_t + P_{atmospheric}$$

V_1 is also well defined, which fully defines the starting product $P_1 V_1$.

By using the simple equation - $P_1 V_1 = P_2 V_2$ all subsequent pressure - volume conditions for the damper may be calculated. and thus the quantity of fuel flowing out of the damper in addition to that from the burette.

Just prior to a fuel flow measurement being made, the stop valve is closed and the level in the burette allowed to drop into the graduated zone. Let the point at which timing commences be designated by a head h_2 and the point at which timing ceases be designated by a head h_3, as in the preceding figure. Then using the above equation we see that :-

$$P_1 V_1 = P_2 V_2 = P_3 V_3 = K \text{ (say)}$$

$$\Rightarrow \quad V_2 = \frac{K}{\rho_{fuel} g h_2 + P_{atmos.}} \quad \& \quad V_3 = \frac{K}{\rho_{fuel} g h_3 + P_{atmos.}}$$

$$\Rightarrow \quad V_{diff} = K \left\{ \frac{1}{\rho_{fuel} g h_2 + P_{atmos.}} - \frac{1}{\rho_{fuel} g h_3 + P_{atmos.}} \right\}$$

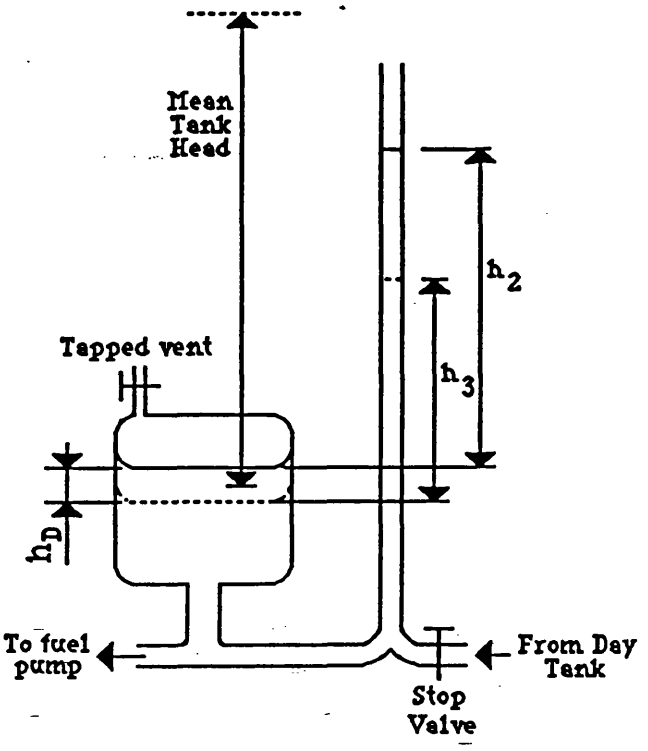
Mean
Tank
Head
h_2
h_3
Tapped vent
h_D
To fuel
pump
From Day
Tank
Stop
Valve

Figure A4.1

Assume that the burette cross-sectional area is A_B and that of the damper A_D. The level drop in the damper will be :-

$$h_D = \frac{V_{diff}}{A_D} \qquad \text{and that in the burette} \qquad h_B = h_2 + h_D - h_3$$

Then the volume flow from the burette is :-

$$V_{FB} = A_B h_B$$

While the volume flow from the damper is :-

$$V_{FD} = A_D h_D$$

The percentage error in flow is therefore :-

$$\% \text{ error} = \frac{A_D h_D}{A_B h_B} \times 100$$

Substituting as much as possible this gives :-

$$\% \text{ error} = \frac{K\left\{\dfrac{1}{\rho_{fuel} g h_2 + P_{atmos.}} - \dfrac{1}{\rho_{fuel} g h_3 + P_{atmos.}}\right\} \times 100}{A_B\left[(h_2 - h_3) + \dfrac{K\left\{\dfrac{1}{\rho_{fuel} g h_2 + P_{atmos.}} - \dfrac{1}{\rho_{fuel} g h_3 + P_{atmos.}}\right\}}{A_D}\right]}$$

Example of Fuel Flow Error Calculation

First calculate "K" = P_1V_1 $\quad P_1 = \rho_f gh_t + P_{atmospheric}$

Typical value of h_t is 1.5m this gives a value of "K" : -

$P_1 = 840 \times 9.81 \times 1.5 + 1.013 \times 10^5 = 1.1366 \times 10^5$

If the cross sectional area of the damper is assumed to be 1.257×10^{-3} m^2 and if the length of air space is 20mm then $V_1 = 2.514 \times 10^{-5}$ m^2 $\Rightarrow P_1V_1 = 2.8574$

$\rho_{fuel} gh_2 + P_{atmos} = 840 \times 9.81 \times 0.71 + 1.013 \times 10^5$

$= 1.0715 \times 10^5$

$\rho_{fuel} gh_3 + P_{atmos} = 840 \times 9.81 \times 0.51 + 1.013 \times 10^5$

$= 1.0550 \times 10^5$

$$\text{Now } \left(\frac{1}{\rho_{fuel} gh_2 + P_{atmos}}\right) = 9.3327 \times 10^{-6}$$

$$\text{and } \left(\frac{1}{\rho_{fuel} gh_3 + P_{atmos}}\right) = 9.4787 \times 10^{-6}$$

the difference between the terms being 1.46×10^{-7}

multiplying by "K" gives 4.172×10^{-7}

Further multiplication by 100 gives the numerator of the expression namely 4.172×10^{-5}

$$\frac{K\left(\frac{1}{\rho_{fuel} gh_2 + P_{atmos}} - \frac{1}{\rho_{fuel} gh_3 + P_{atmos}}\right)}{A_D} = \frac{4.172 \times 10^{-7}}{1.257 \times 10^{-3}} = 3.319 \times 10^{-4}$$

Adding this to the burette column height change and multiplying by the burette cross sectional area gives : -

$10^{-4} \times (0.2 + 3.319 \times 10^{-4}) = 2.003 \times 10^{-5}$

The percentage error under these circumstances is therefore $= \dfrac{4.172 \times 10^{-5}}{2.003 \times 10^{-5}} = 2.08$ % error

APPENDIX 5 - EXHAUST DUCT HEAT FLOW LOSS ANALYSIS

This appendix considers the heat loss from a typical engine exhaust duct, both for the case of an uncooled duct and for the case of a cooled duct. The reduction in temperature which is predicted, from a simply cooled cylindrical exhaust duct, is sufficient to dramatically reduce the duty of exhaust components downstream from the cooled section. This allows for safer operation of exhaust components such as receivers.

An analysis similar to the one shown may be readily adapted for the design of exhaust gas calorimeters, to be used for exhaust gas enthalpy measurements. The simple cylindrical form of duct, which has been analysed, affords low pressure drop, and good transfer of heat from the exhaust stream. The use of an exhaust gas calorimeter system is suggested earlier in this thesis to improve the measurement of exhaust gas enthalpy, for the purposes of improving the accuracy of the engine heat balances. Although no exhaust gas calorimeter can extract and monitor all of the heat in an exhaust duct it can extract a large percentage. The remaining percentage can still be measured to the same accuracy as before, but any errors in this measurement, now represent a lower fraction of the total than before, thus improving the accurracy.

HEAT LOSSES FROM EXHAUST DUCT

One of the methods of determining exhaust gas enthalpy requires that the exhaust gas stream be conveyed to a damping tank, where the exhaust gas temperature and pressure may be monitored under constant flow conditions. To determine whether or not this particular method is feasible, it is required to determine the losses which would result if the exhaust duct were insulated. The heat transfer coefficients on the internal and external surfaces must first be calculated.

Internal Heat Transfer Coefficient :-

First consideration is whether the flow is laminar or turbulent. This requires calculation of the Reynolds number, which in turn is dependent on the mass flow.

$$Re = \frac{\rho U d}{\mu} = \frac{\dot{m} d}{A_c \mu} = \frac{4\dot{m}}{\Pi d \mu}$$

The mass flow rate is calculated for a number of engine operating conditions both naturally aspirated and boosted, and from this the Reynolds number for each case is determined. Next the Prandtl number is calculated.

$$Pr = \frac{c_p \mu}{k}$$

Finally we determine the heat transfer coefficient using the Nusselt equation and the equation due to Dittus and Boelter assuming turbulent flow

$$Nu = \frac{hd}{k} = 0.023 Re^{0.8} Pr^{n}$$

n = 0.4 for heating fluid

$$h = \frac{0.023 Re^{0.8} Pr^{0.4} k}{d}$$

Values calculated for the heat transfer coefficient for a number of cases are tabulated on the next page.

Variation in Exhaust Duct Heat Transfer Coefficient with Operating Condition

	ENGINE CONDITIONS	$\dot{m}$	Re	Pr	k/d	h
NATURALLY ASPIRATED	1000 H.L.	5.165E-03	3120	0.680	1.374	17.12
	1000 L.L.	5.165E-03	4765	0.703	0.840	14.50
	2000 H.L.	1.033E-02	6241	0.680	1.374	29.81
	2000 L.L.	1.033E-02	9531	0.703	0.840	25.25
2 BAR BOOST	1000 H.L.	1.033E-02	6241	0.680	1.374	29.81
	1000 L.L.	1.033E-02	9531	0.703	0.840	25.25
	2000 H.L.	2.066E-02	12482	0.680	1.374	51.91
	2000 L.L.	2.066E-02	19062	0.703	0.840	43.97

H.L. — High load condition L.L. — Low load condition

The above table shows approximate values for the heat transfer coefficient inside the exhaust duct. To calculate approximate losses from the duct the external heat transfer coefficient is also required. This is calculated using a simplified expression for the heat transfer coefficient of an horizontal tube in air at approximately atmospheric temperature and pressure (Cornwell Ref. 48). It is first necessary to calculate the Rayleigh number :-

$$Ra = Gr * Pr$$

$$= \frac{g \beta \Delta T d^3 c_p \rho^2}{\mu k}$$

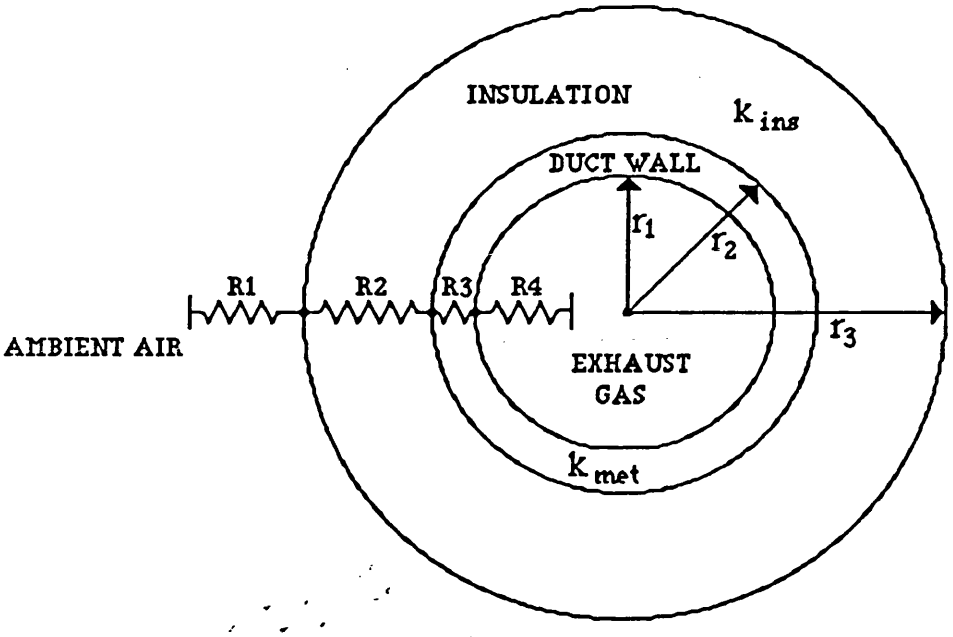

Heat loss from the insulated exhaust duct may be modelled as in the figure above. R1 represents the resistance to heat flow from the exterior of the insulation surrounding the exhaust duct, to the atmosphere. R2 represents the resistance to heat flow from the metal wall of the duct through the insulation. R3 represents the resistance to heat flow through the metal wall of the duct, and R4 that from the exhaust gas to the duct wall. The radii of the respective components are shown as r_1 , r_2 , and r_3 .
The resistances are as follows :-

$R1 = \dfrac{1}{h_{amb}\, A_{amb}} = \dfrac{1}{h_{amb} 2\Pi r_3 1}$	$R2 = \dfrac{\ln(r_3 / r_2)}{2\Pi k_{ins.} 1}$
$R3 = \dfrac{(r_2 - r_1)}{2\Pi r_2 1 k_{met.}}$	$R4 = \dfrac{1}{h_{exh.} 2\Pi r_1 1}$

The total resistance is the simple summation of the above resistances :- $R1 + R2 + R3 + R4 = R_{tot.}$
Appropriate values for each of the parameters pertaining to the insulated exhaust duct are given overleaf, together with the calculated resistances.

Resistance Calculation for Insulated Exhaust Duct

The following values were taken in calculating the resistances for the determination of the heat losses from an insulated exhaust duct.

r_1 = 25 mm
r_2 = 26 mm
r_3 = 50 mm
$k_{met.}$ = 20 $Wm^{-1}K^{-1}$
$k_{ins.}$ = 0.15 $Wm^{-1}K^{-1}$
l = 2 m

These values together with the values already obtained for the internal and external heat transfer coefficients are combined in the formulae on the previous page to give the resistances necessary for calculating the heat losses.
The resistances calculated are :-

R1 = 0.1592
R2 = 0.3469
R3 = 0.0003
R4 = 0.2122 for the low load 1000r.p.m. case.
0.0612 for the high load 2000r.p.m. case.
This gives R_{tot} values of 0.7186 (1000r.p.m. L.L.) and 0.5676 (2000r.p.m. H.L.).

The E-NTU method (as used in heat exchanger design) is used to provide a solution to finding both duct heat loss and duct outlet temperature, rather than using the log mean temperature difference and iterating, see Cornwell (Ref.48) or Ref. 49
First the capacity rate ratio, C, is determined :-

$$C = \frac{(\dot{m}\,c)_{min}}{(\dot{m}\,c)_{max}}$$

Now for the case in hand, although the effective thermal resistances of exhaust gas to duct wall and external free convective air to insulation are similar, the external air flow is not constrained and is at the same temperature at all points along the exterior of the duct. In this case let C = 0. Next it is necessary to consider the Number of Transfer Units NTU, which is defined as :-

$$NTU = \frac{1}{R_{tot}\,(\dot{m}\,c)_{min}}$$

After the NTU is set it remains for the effectiveness, E , to be found. With C = 0 the expression for E reduces to :-

$$E = 1 - \exp(-NTU) \qquad \text{now also :-}$$

$$E = \frac{T_{gas1} - T_{gas2}}{T_{gas1} - T_{ext2}} \qquad \text{or} \qquad T_{gas2} = T_{gas1} - (T_{gas1} - T_{ext2})E$$

Once the outlet gas temperature, T_{gas2} , the corresponding exhaust duct loss may also be found. The values corresponding to the insulated exhaust duct are now given, first for the low load 1000 r.p.m. case :-

$$C = 0 \qquad NTU = \frac{1}{5.165E\text{-}03 * 1035 * 0.7186}$$

$$= 0.2603$$

$$E = 1 - \exp(-0.2603) = 0.2292$$

$$T_{gas2} = 525 - (525-293)*0.2292 = 471.8\ K$$

Heat flow rate = 5.165E-03 * 1035 * 53.2 = 284.4 W

Total heat flow rate into duct = 5.165E-03 * 1035 * (525-293)
= 1240.2 W

Now, the high load, 2000 r.p.m. case :-

$$C = 0 \qquad NTU = \frac{1}{2.066E\text{-}02 * 1146 * 0.5676}$$

$$= 0.0744$$

$$E = 1 - \exp(-0.0744) = 0.0717$$

$$T_{gas2} = 1025 - (1025-293)*0.0717 = 972.5\ K$$

Heat flow rate = 2.066E-02 * 1146 * 52.48 = 1242.5 W

Total heat flow rate into duct = 2.066E-02 * 1146 * (1025-293)
= 17331 W

The respective % losses are therefore 23% for the low load 1000 r.p.m. case and 7% for the high load 2000 r.p.m. case (% of total exhaust heat flow)

Resistance Calculation for Cooled Exhaust Duct

Heat loss to the coolant water surrounding the exhaust duct may be modelled as in the figure below. R1 represents the resistance to heat flow from the external surface of the duct to the coolant. R2 is the resistance due to the metal duct wall, and R3 is the resistance to heat flow from the exhaust gas to the internal surface of the duct wall.

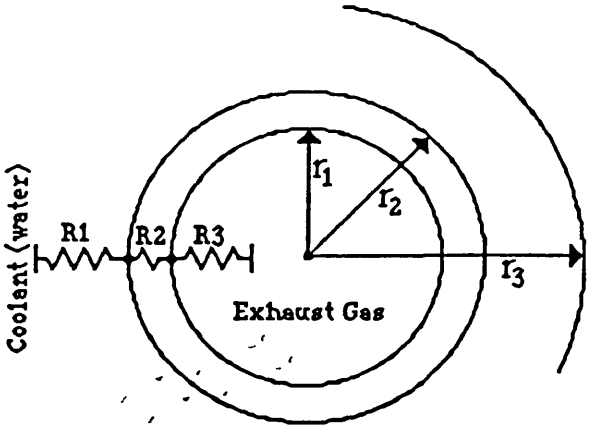

r_1 = 25 mm
r_2 = 26 mm
r_3 = 30 mm
$k_{met.}$ = 20 $Wm^{-1}K^{-1}$

The resistances are as follows :-

$$R1 = \frac{1}{h_{cool}\ A_{cool}} = \frac{1}{h_{cool}\ 2\Pi r_2\ 1}$$

$$R3 = \frac{1}{h_{exh.} 2\Pi\ r_1\ 1}$$

$$R2 = \frac{(r_2 - r_1)}{2\Pi r_2\ k_{met.}\ 1}$$

As for the insulated case the total resistance is the simple summation of the above resistances :-

$$R1 + R2 + R3 = R_{tot.}$$

For R1 the heat transfer coefficient of the coolant to duct must be calculated, appropriate correlations are found in Wong (Ref. 49). First the Reynolds number for the water flowing in the coolant channel must be found. With a water flow rate of 4.0E-02 kg/s, the Reynolds number is found to be 1010, which suggests laminar flow conditions. More than one correlation appeared to suit the situation. The result of using each of these gave different heat transfer coefficients, as might be expected. The Nusselt number for the situation of two parallel plates with one being insulated, is given overleaf.

$Nu = 4.86$ with the characteristic dimension 'D' as four times the width of the channel, gives $h = 180\ Wm^{-2}K^{-1}$

The mean Nusselt number for flow over a plane surface with pure laminar flow is :-

$$\overline{Nu} = 0.664\, Re_x^{1/2}\, Pr^{1/3}$$

This gives a mean heat transfer coefficient of $h = 23\ Wm^{-2}K^{-1}$

There is therefore a wide variation in the predicted heat transfer coefficients for this situation. Taking as a very approximate estimate for the heat transfer coefficient a value of $100\ Wm^{-2}K^{-1}$ then $R1 = 0.0306$. The other resistances are respectively $R2 = 0.0003$ and $R3 = 0.2122$ at low load 1000 r.p.m. and 0.0612 at high load 2000 r.p.m.

This gives values of $R_{tot.}$ of 0.2431 for 1000 r.p.m. low load and 0.0921 for 2000 r.p.m. high load.

The E-NTU method is used again for the calculation of the heat removed from the exhaust duct by the water cooled walls.

For the 1000 r.p.m. low load case :-

$$C = \frac{5.165E\text{-}03 * 1035}{4.0E\text{-}02 * 4180} = 0.0320$$

$$NTU = \frac{1}{5.165E\text{-}03 * 1035 * 0.2431} = 0.7696$$

$$E = \frac{1 - \exp(-NTU(1-C))}{1 - C\exp(-NTU(1-C))} = 0.5334$$

$$T_{gas2} = 525 - (525-293) * 0.5334 = 401.3$$

and heat loss to coolant = 5.165E-03 * 1035 * 123.7 = 662 W

Total heat flow into duct = 5.165E-03 * 1035 * (525-293)
= 1240.2 W

Now the high load, 2000 r.p.m. case :-

$$C = \frac{(\dot{m}\, c)_{min.}}{(\dot{m}\, c)_{max.}} = \frac{2.066E\text{-}02 * 1146}{4.0E\text{-}02 * 4180} = 0.1416$$

$$NTU = \frac{1}{(\dot{m}\, c)_{min.} R_{tot.}} = \frac{1}{2.066E\text{-}02 * 1146 * 0.0921}$$

$$= 0.4586$$

$$E = \frac{1 - \exp(- 0.4586 * (1 - 0.1416))}{1 - 0.1416 * \exp(- 0.4586 * (1 - 0.1416))} = 0.3598$$

$$T_{gas2} = 1025 - (1025 - 293) * 0.3598 = 761.6 \text{ K}$$

Heat flow rate = 2.066E-02 * 1146 * 263.4 = 6236 W

Total heat flow rate into duct = 2.066E-02 * 1146 * (1025-293)
= 17331 W

The respective % losses are therefore 53% for the low load 1000 r.p.m. case and 36% for the high load 2000 r.p.m. case (% of total exhaust heat flow).

The results of the above calculations are to be considered as estimates only, as a number of assumptions have been made in order to model the system. Immediate improvements in the predictions would arise from :-

i). a more accurate correlation for the heat transfer coefficient between the external surface of the exhaust duct and the coolant water.

ii). account taken of the temperature dependence of the fluid properties.

The calculations have been estimates of exhaust duct heat loss alone and do not take into account changes in enthalpy which result from pressure loss due to pipe friction. However, for the duct size in question these losses would be small and the loss in pressure would appear in the overall heat balance due to the monitoring of heat loss to the duct coolant, by conservation of energy.

An advantage of the cooled duct is easily seen from the resultant exit gas temperatures, which put much less severe demands on the design of the exhaust receiver.

APPENDIX 6 - ANALYSIS OF CHARGE AMPLIFIER DRIFT

This appendix explains the "drift" in the output waveform of a charge amplifier. A square wave pressure signal is assumed to be input to the piezoelectric pressure transducer. This is done to simplify the mathematical treatment. Two figures showing the performance of a piezoelectric pressure transducer/charge amplifier, are shown, when exposed to real engine signals. The first of these shows the effect of the charge amplifier time constant on the output voltage waveform droop, and thus the effect on the accuracy of the signal monitored. The second of the figures shows the drift in charge amplifier output voltage over a period of engine cycles after the charge amplifier grounding link is removed.

It is apparent from the treatment that a compromise in time constant is an inevitable consequence of using this form of instrumentation. The use of too long a time constant, while being limited to a large extent by the cable and connector resistances, produces very lengthy settling times. The use of shorter time constants, while producing short settling times, may result in peak pressure reading errors. Generally, a charge amplifier time constant of around 10 seconds would be chosen for engines operating in the 1000 to 3000 r.p.m. speed range.

Apparent "Drift" of Charge Amplifier Output with Time

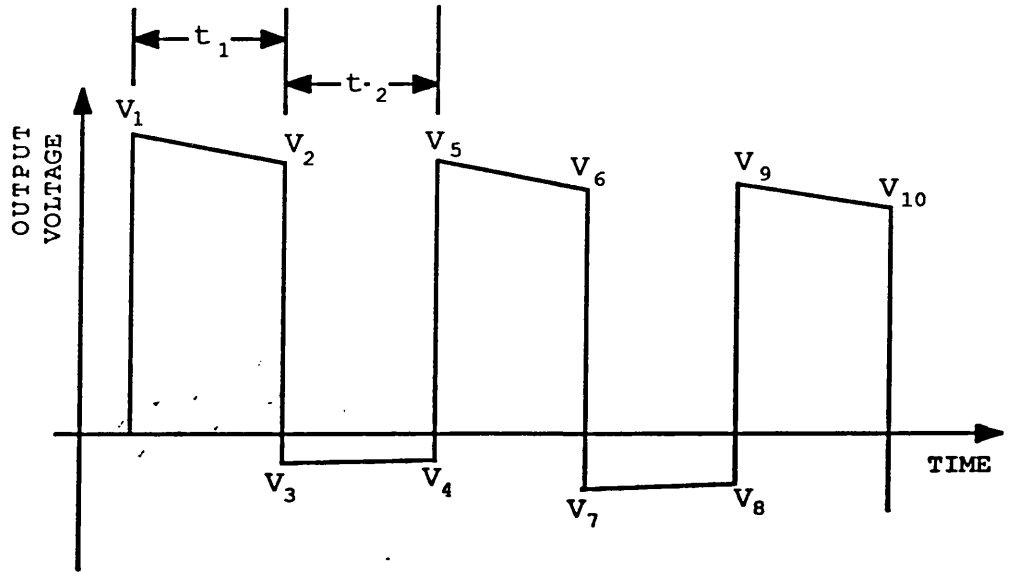

The above waveform is typical of the output from a charge amplifier. The figure shows the decay of the waveform, brought about by the time constant of the amplifier. For the purposes of this explanation, the waveform droop is exagerrated. A square wave is used in this case to simplify the analysis, which is shown on the accompanying pages. A series solution is found for only one of the points on the waveform, although obviously similar series could be derived for the other points on the wave. Of particular interest, is the number of cycles which are executed bfore the waveform settles to a fixed position, either side of the zero voltage line. An expression which calculates this is given.

Assuming a square wave pressure input to the pressure transducer/charge amplifier the following equations describe the voltages at different points on the output waveform.

$$V_1 = V_0$$

$$V_2 = V_0 e^{-\frac{t_1}{\tau}}$$

$$V_3 = V_0 e^{-\frac{t_1}{\tau}} - V_0$$

$$V_4 = \left(V_0 e^{-\frac{t_1}{\tau}} - V_0 \right) e^{-\frac{t_2}{\tau}}$$

$$V_5 = \left(V_0 e^{-\frac{t_1}{\tau}} - V_0 \right) e^{-\frac{t_2}{\tau}} + V_0$$

$$V_6 = \left[\left(V_0 e^{-\frac{t_1}{\tau}} - V_0 \right) e^{-\frac{t_2}{\tau}} + V_0 \right] e^{-\frac{t_1}{\tau}}$$

$$V_7 = \left[\left(V_0 e^{-\frac{t_1}{\tau}} - V_0 \right) e^{-\frac{t_2}{\tau}} + V_0 \right] e^{-\frac{t_1}{\tau}} - V_0$$

$$V_8 = \left\{ \left[\left(V_0 e^{-\frac{t_1}{\tau}} - V_0 \right) e^{-\frac{t_2}{\tau}} + V_0 \right] e^{-\frac{t_1}{\tau}} - V_0 \right\} e^{-\frac{t_2}{\tau}}$$

$$V_9 = \left\{ \left[\left(V_0 e^{-\frac{t_1}{\tau}} - V_0 \right) e^{-\frac{t_2}{\tau}} + V_0 \right] e^{-\frac{t_1}{\tau}} - V_0 \right\} e^{-\frac{t_2}{\tau}} + V_0$$

If t_1 and t_2 as well as τ are fixed then it can be stated that : -

$n = e^{-\frac{t_1}{\tau}}$ and $m = e^{-\frac{t_2}{\tau}}$ which leads to the simplified formulae : -

$V_1 = V_0$	1
$V_2 = nV_0$	n
$V_3 = nV_0 - V_0$	n-1
$V_4 = (nV_0 - V_0)m$	(n-1)m
$V_5 = (nV_0 - V_0)m + V_0$	(n-1)m + 1
$V_6 = ((nV_0 - V_0)m + V_0)n$	((n-1)m + 1)n
$V_7 = ((nV_0 - V_0)m + V_0)n - V_0$	((n-1)m + 1)n -1
$V_8 = (((nV_0 - V_0)m + V_0)n - V_0)m$	(((n-1)m + 1)n - 1)m
$V_9 = (((nV_0 - V_0)m + V_0)n - V_0)m + V_0$	(((n-1)m + 1)n - 1)m + 1

The column of equations on the right hand side are a further simplification by simply dividing through by V_0.

The points on the output which are in the same place on the waveform are now compared and appropriate series solutions found, which describe the magnitude of each of these points with respect to the zero voltage line.

The voltage at points 5, 9, 13, etc. of the waveform, i.e. the peak voltage at the leading edge of the pulses, may be expressed by the series : -

$$V_{lead} = V_0\{1 + (mn-m)[1 + mn + (mn)^2 + (mn)^3 + (mn)^4 + \ldots\ldots + (mn)^z]\}$$

The geometric series on the right hand side of the above equation may be written as below, for the sum to the "a"th term : -

$$V_{lead} = V_0\left\{1 + (mn-m)\left(\frac{1-(mn)^{a+1}}{1-mn}\right)\right\}$$

One point of interest is the number of pulses which occur before the change in consecutive peak values is less than 0.1% . Consideration of the values for the "a"th and the "a+ 1"th pulse gives the following : -

$$V_{lead(a)} = V_0\left\{1 + (mn-m)\left(\frac{1-(mn)^{a+1}}{1-mn}\right)\right\}$$

$$V_{lead(a+1)} = V_0\left\{1 + (mn-m)\left(\frac{1-(mn)^{a+2}}{1-mn}\right)\right\}$$

For a 0.1% change the following holds : -

$$\frac{V_{lead(a)} - V_{lead(a+1)}}{V_{lead(a)}} < 0.001$$

Working through the manipulation of the equations gives the solution : -

$$a = \frac{\log\left[\left(\frac{0.001}{mn-0.999}\right)\left(\frac{1-mn}{mn-m} + 1\right)\right]}{\log(mn)} - 1$$

A further point is the disposition of the waveform about the zero voltage line. Considering the areas of the pulse, above and below the zero voltage line, the following may be stated : -

$$A_1 = V_0\left\{\frac{1-m}{1-mn}\right\} t_1 \quad \text{and} \quad A_2 = V_0\left\{\frac{n-1}{1-mn}\right\} t_2$$

If the mark space ratio is 1 : 1 then the above equations reduce to :-

$$A_1 = V_0\, t \left\{\frac{1-m}{1-m^2}\right\} \quad \text{and} \quad A_2 = V_0\, t \left\{\frac{m-1}{1-m^2}\right\}$$

Adding the two areas gives :-

$$A_1 + A_2 = \frac{V_0\, t}{(1-m^2)}\left[(1-m)+(m-1)\right] = 0$$

This shows that a waveform with equal mark space ratio will tend, in the limit to a position, such that there are equal areas either side of the zero voltage line. However, this is a special case.

Generally, the position of the zero voltage line with respect to the signal, will depend upon the waveform which is presented to the charge amplifier. It is theoretically possible that automatic compensation for the so-called "drift" in the ouput of the charge amplifier could be provided. This feature would remove the need for a datum pressure point on the engine pressure signal, however, the task of providing a sufficiently accurate compensating signal is by no means simple.

A remaining point is that, in most cases no compensating signal is provided. A compromise time constant is usually chosen which produces acceptably small levels of signal decay within the engine cycle, but at the same time provides relatively short periods of time before the signal has settled down, with respect to the zero voltage line. This latter point is necessary for data acquisition and further analysis, particularily if cycle averaging is to carried out.

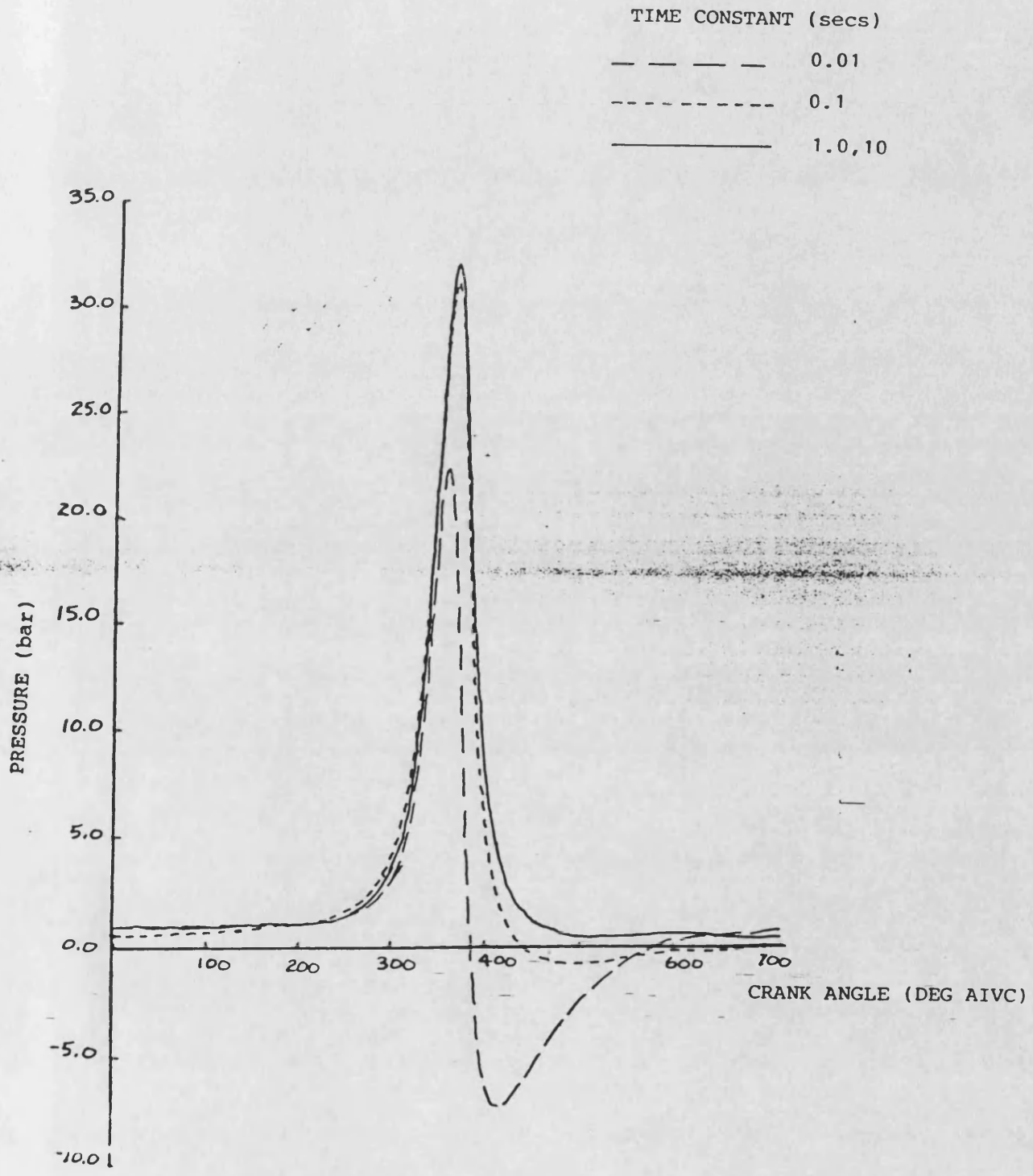

FIGURE A 6.1 EFFECT OF SIGNAL CONDITIONING TIME CONSTANT ON RECORDED CYLINDER PRESSURE
(1000 rev/min: N.A.: 25:1 AFR)

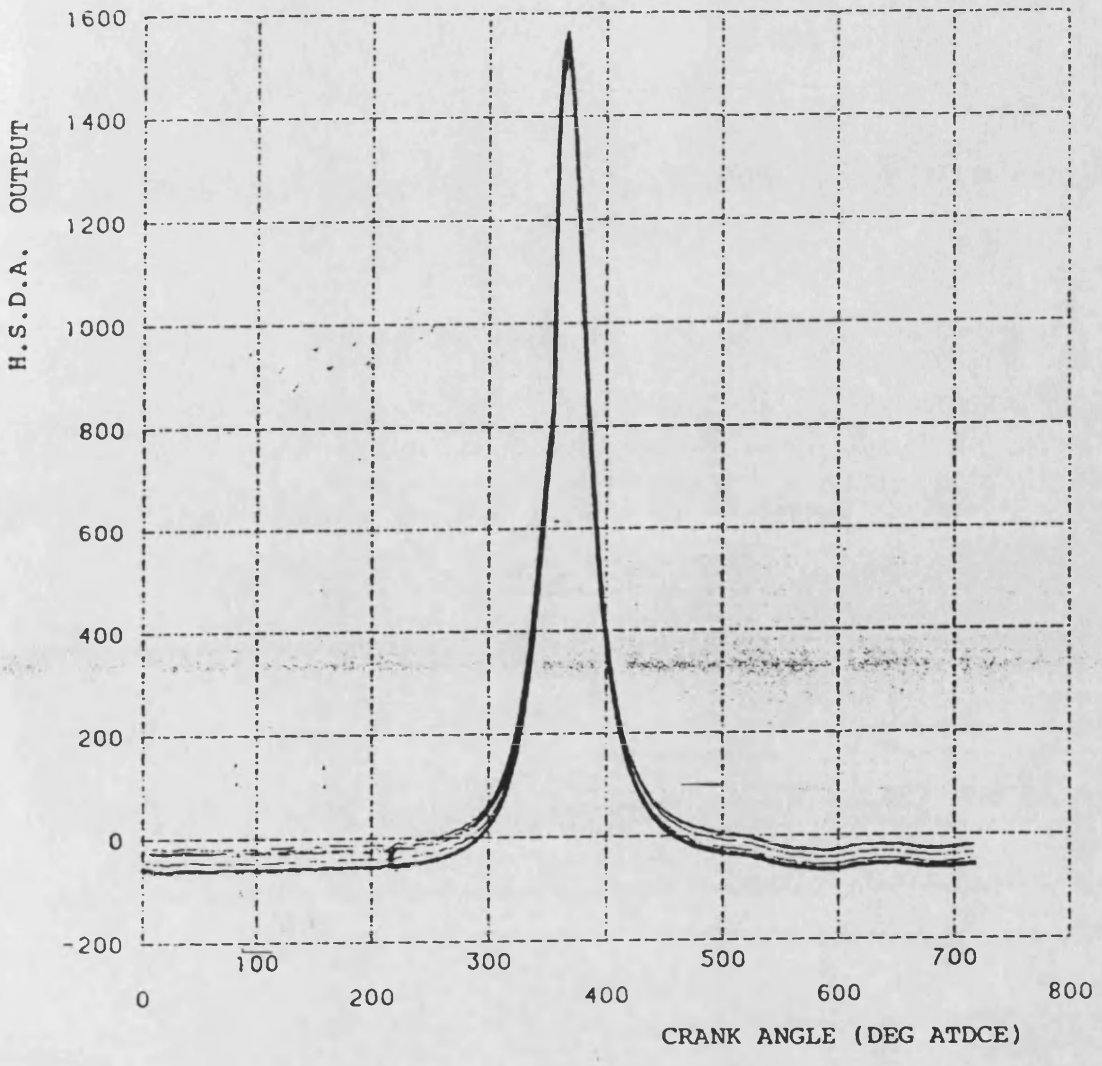

FIGURE A.6.2 EFFECT OF SIGNAL DRIFT ON 40 SUCCESSIVE ENGINE CYCLES OF MEASURED CYLINDER PRESSURE (1000 rev/min: N.A.: 40:1 AFR)